INFORMATION TO USERS

This manuscript has been reproduced from the microfilm master. UMI films the text directly from the original or copy submitted. Thus, some thesis and dissertation copies are in typewriter face, while others may be from any type of computer printer.

The quality of this reproduction is dependent upon the quality of the copy submitted. Broken or indistinct print, colored or poor quality illustrations and photographs, print bleedthrough, substandard margins, and improper alignment can adversely affect reproduction.

In the unlikely event that the author did not send UMI a complete manuscript and there are missing pages, these will be noted. Also, if unauthorized copyright material had to be removed, a note will indicate the deletion.

Oversize materials (e.g., maps, drawings, charts) are reproduced by sectioning the original, beginning at the upper left-hand corner and continuing from left to right in equal sections with small overlaps.

ProQuest Information and Learning
300 North Zeeb Road, Ann Arbor, MI 48106-1346 USA
800-521-0600

Université d'Ottawa · University of Ottawa

LAYERED DOUBLE HYDROXIDES AS ELECTRODE MATERIALS FOR Ni BASED BATTERIES AND AS NOVEL INORGANIC/ORGANIC HYBRID MATERIALS

Gianni Caravaggio

Thesis submitted to the Faculty of Graduate and Postdoctoral Studies

University of Ottawa

In partial fulfillment of the requirements for the

Ph.D. degree in the

Ottawa-Carleton Chemistry Institute

Thèse soumise à la

Faculté des études supérieures et postdoctorales

Université d'Ottawa

En vue de l'obtention du doctorat à

L'institut de chimie d'Ottawa-Carleton

ACKNOWLEDGMENTS

I would like to thank my supervisor Christian Detellier for allowing me to work under his supervision to accomplish my thesis. His support, time, council, suggestions and comments during my studies were all greatly appreciated.

I would also like to thank my co-supervisor Zbigniew Wronski who initiated me to my graduate research and allowed collaborative work between the University of Ottawa and Canmet. His critical suggestions and comments in addition to his time taken for productive discussions have been very valued.

My thanks also go to my working colleagues: Arvin Moser, Sophie Quevillon, Mark Weir, Yaël Israeli, Richard Leblanc, Marcel Beaudoin, Nidia Villalva, Wen-Xing Kuang, Harouna Drame, for their help, friendship and fruitful discussions throughout my studies.

I would like to thank all the people who have dedicated part of their time to help me with the instrumentation needed to complete my thesis: Glenn Facey (NMR, chemistry department, University of Ottawa), Daniel Martineau (multichannel potentiostat, Canmet), Ron Hartree (XRD, Geology department, University of Ottawa), John Loop (ICP, Geology department)

A very, very special thanks goes to my wife Julie for all the support, time and patience she has given me to accomplish my thesis. I am not sure I would have attained my goal without her help. I would also like to especially thank my family for all the support and times they have endured me throughout my studies.

This thesis has been made possible in part due to the financial support from the Ontario Graduate Scholarship in Science and technology (OGSST)

Thank you God for many answered prayers.

ABSTRACT

Layered double hydroxides (LDH) containing NiAl or NiV of varying M(II):M(III) (2:1, 5:1, 9:1 for NiAl and 2:1, 5:1 for NiV) ratios have been prepared by coprecipitation and characterized by XRD, elemental analysis, and FT-IR. The LDHs electrochemical properties were investigated in half-cells to determine their potential application as positive electrode in Ni-Cd and NiMH batteries. The Ni_2Al LDH exchanges the most electrons (up to 1.6) and is the most stable during discharging in the KOH electrolyte. The large quantity of electrons and accrued stability was attributed to the aluminium in the layers acting in a two fold manner: High charge to radius ratio increased the electrostatic interaction between the anions and the metal layers increasing the stability of the LDHs and the increase in Brønsted acidity of the hydroxyl groups was accredited for the high exchange of electrons. Notwithstanding the high exchange of electrons of the NiAl LDHs the powders exhibit lower discharge capacity compared to commercial electrode material (β-$Ni(OH)_2$) due to their low density.

The NiV LDHs only exchanged up to 1.2 electrons (Ni_2V) and were found only stable up to a maximum of 14 days in electrolytic solutions of the cells.

In the second part of the study ZnAl LDHs were synthesized and intercalated with phenyl phosphonic acid (PPA) or 1,4-phenylene bis phosphonic acid (B-PPA) in order to create microporous materials. The compounds were characterized by XRD, chemical, IR and solid state NMR analysis in addition to being tested for microporosity. The ZnAl LDHs

treated with phenyl phosphonic acid gave rise to materials with a d spacing of 14.7Å and when treated to B-PPA resulted in materials with a d spacing of 9.6 Å. The results showed that the grafting of both phosphonates to the metal layers had occurred. The d spacing of 14.7 Å was interpreted as being due to a bilayer of PPA molecules in head to head configuration in the layers. The d spacing of 9.6 Å was consistent with a monolayer of B-PPA molecules cross-linking the metal layers of the material. Both materials exhibited little or no microporosity due to the "packing" of the phosphonate moieties in the layers.

The last section of the thesis consisted of attempting to synthesize MCM or FSM type molecular sieves by the treatment of ZnAl LDH with hexadecane sulfonic acid or sodium dodecyl sulfate used as templates under different reaction conditions. The materials were characterized by XRD, chemical analysis and IR analysis. The results were consistent with LDHs intercalated with either a monolayer or a bilayer arrangement of surfactant molecules and therefore did not exhibit MCM or FSM mesoporous frameworks.

TABLE OF CONTENT

LIST OF FIGURES

LIST OF TABLES

CHAPTER 1

1.1 INTRODUCTION

1.1.1 Historical

Clays have been an integral part of everyday life throughout the ages. Because of their availability and malleability, clays have commonly been used for making pottery items for daily use, have been used in construction materials but have also been used to make objects of expression of arts and culture. A wonderful example of this expression of art is the ancient ceramic technique known as Nerikomi.

> *"This technique was known to Roman and early French potters in Europe and became an art form during the T'ang Dynasty in 7th century China. To create Nerikomi, the clays are mixed with ceramic stains and metal oxides. Then the slabs of colored clays are stacked, folded and pressed to form a log. Slices of the log are cut, stretched, twisted and arranged in a mold to form a vessel or plate. Nerikomi is a true thief of time. Of all ceramic vessel techniques, it is perhaps the most time consuming. Yet it offers the artist limitless opportunities to create distinctive colored designs and patterns within the very body of the work. The patterns are identical on both the interior and exterior; patterns that range from the most orderly and structured to the completely abstract."* [a]
>
> [a]http://gingerbreadsquaregallery.com/ArtGlass/Thivo/Thivo-bio/thivo-bio.html

Below is a picture of a bowl fabricated using the Nerikomi technique by the artist Thivô entitled: " Phoenix Rising"

PHOENIX RISING

In addition to the traditional uses of clays, in present times, clays are used in a much wider spectrum of application such as drilling, paint additives, paper production, catalysts and lately have also caught the interest of the scientific community. Chemists are now modifying clays to obtain useful new materials in a wide range of fields of innovative nanotechnology.

There are two main families of clay minerals: cationic and anionic. Cationic clays are part of the phyllosilicate family, which is a subclass of the silicate minerals. The main building blocks of the phyllosilicates are Si,AlO_4 tetrahedra and SiO_8 octahedra. The tetrahedra are linked together by sharing oxygens that form two-dimensional sheets. These sheets are bound to cations containing octahedral layers. When one octahedral layer is bound to a tetrahedral sheet the clay has a 1:1 structure. When one octahedral sheet is bound to two tetrahedral sheets, one on each side, the clay has a 2:1 structure. There are six groups of cationic clay minerals differentiated by their structural type, charge and basal spacing:[1]

1. kaolinite-serpentine: uncharged 1:1 layers, 7 Å basal spacing in the absence of water and 10 Å with sorbed interlayer water.
2. pyrophilite-talc: uncharged 2:1 layers.
3. micas : negatively charged 2:1 layers, 10 Å basal spacing.
4. chlorite : negatively charged 2:1 layers, 14 Å basal spacing.
5. smectite/vermiculite: negatively charged 2:1 layers, variable thickness.
6. fibrous palygorskite/sepiolite: narrow ribbons of 2:1 layers.

These minerals are very abundant in nature and are classified as cationic clays, given that they adsorb cations due to their predominantly negatively charged layers. On the other hand, anionic clays, which are not as abundant in nature, can be considered the mirror image of the

cationic clays if charges are considered. They have positively charged metal layers and adsorb anions in their interlayers. Layered double hydroxides are part of the anionic clay family and will be the subject of this study. These types of minerals were discovered approximately 150 years ago and the first layered double hydroxides that have been discovered were:

- Hydrotalcite: a magnesium-aluminum hydroxycarbonate
- Pyroaurite: a magnesium-iron hydroxycarbonate
- Stichtite: a magnesium-chromium hydroxycarbonate.

Hydrotalcite was discovered in Sweden around 1842.[2] "Its name comes from the fact that it can easily be crushed into a white powder similar to talc".[3] Pyroaurite (named pyroaurite because when it is heated it resembles gold)[2;3] was discovered in Sweden in 1865 and Stichtite in 1910 in Tasmania. "The composition and structure of these compounds were unclear for many years because of the lack of understanding of their crystal data, their non-stochiometric nature, the lack of satisfactory chemical analysis of the time and the lack of correlation of knowledge between the many published articles on the topic."[2;4]

Many considered Hydrotalcite as a mixture of minerals such as aluminate, gibbsite, magnesite or an admixed basic magnesium carbonate because of the constant and large amount of carbonate found in the mineral. It wasn't until 1915 that Manasse, a professor of mineralogy of the university of Florence ranked, the mineral as a species. He proved that CO_3^{2-} was a constitutional part of the structure and derived the following formula:

$Mg_6Al_2(OH)_{16}CO_3 \bullet 4H_2O$

Pyroaurite was also considered a mixture of minerals and was initially thought to be a mixture of magnesium and iron hydroxides with large amounts of carbonates as being an alteration of the compound. Once again, Manasse reexamined the composition of the mineral and concluded that CO_3^{2-} was a constitutional part of pyroaurite and derived the following formula for this mineral:

$Mg_6Fe_2(OH)_{16}CO_3 \bullet 4H_2O$

He also therefore showed that hydrotalcite was the aluminum analogue of pyroaurite.

Stichtite was originally described by Petterd and he considered it to be the chromium analogue of pyroaurite. This mineral was analyzed by many researchers, and in 1920, Foshag similarly concluded that CO_3^{2-} was a component of stichtite. He also suggested that pyroaurite, hydrotalcite and stichtite had all the same general formula as shown below.[4]

$Mg_6R_2(OH)_{16}CO_3 \bullet 4H_2O$

Where R = Cr, Fe or Al

More data was being gathered on these minerals and in 1930, Broomé and Aminoff found that pyroaurite had two polytypes: rhombohedral and hexagonal.[4] However, a great deal of confusion still existed about the composition and structure of these minerals. In 1941, Frondel, in addition to his own research, carried out an extensive review of the available data on layered double hydroxides. He concluded that pyroaurite, hydrotalcite and stichtite were

in fact isostructural. He also proved the existence of the two polytypes of pyroaurite suggested by Broomé and Amminoff, and showed that these polytypes also extended to stichtite and hydrotalcite. He arbitrarily assigned the following names to the different polytypes of the MgFe, MgAl and MgCr layered double hydroxides, which are still in use today:

Pyroaurite: rhombohedral MgFe

Sjögrenite: hexagonal MgFe

Hydrotalcite: rhombohedral MgAl

Manasseite: hexagonal MgAl

Stichtite: rhombohedral MgCr

Barbetnite: hexagonal MgCr

"In 1942 Feitknecht synthesized a large number of hydrotalcite analogues and named them "doppelschichstrukturen" which means double sheet structure. He suggested that these compounds were formed of a layer of M(II) hydroxides intercalated with a layer of M(III)OOH oxyhydroxides."[5:6] In 1967, Gastuche and Brown[7] proposed, based on infrared, chemical and powder X-ray analysis, another structure for the synthetic Mg-Al hydroxides. The proposed structure of the synthetic hydrotalcite was one where Al substituted Mg in the positively charged brucite layers. Feiknecht's structure was finally refuted by Almman[8] in 1968 and Taylor in 1969.[9] By studying single crystal data on sjögrenite and pyroaurite, they concluded that both M(II) and M(III) cations are located in the same sheets and that the anions and water molecules are found in between the layers.

1.1.2 Structure

The general structure of a layered double hydroxides (LDH) is similar to that of brucite $Mg(OH)_2$.(Figure 1.1) Brucite is a mineral composed of magnesium hydroxide where edge sharing octahedral of hydroxyl groups surround magnesium and form infinite two-dimensional sheets.

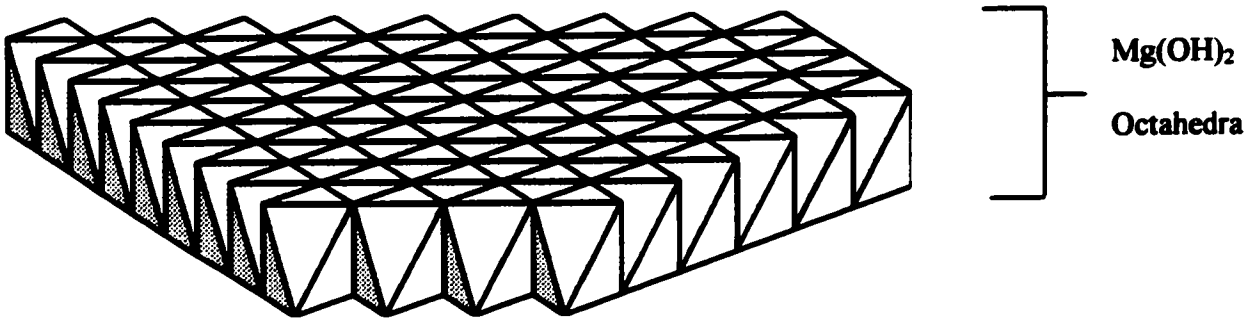

Figure 1.1 Structure of brucite $Mg(OH)_2$

"Brucite crystallizes in layers because of the presence of positively charged divalent cations in close proximity to the non spherosymmetrical and highly polarizable hydroxyl anions. These layers stack on top of each other and are held by weak interactions through hydrogen atoms."[3]

In a layered double hydroxide, (Figure 1.2) the M(II) atom is replaced isomorphously by a M(III) atom of similar radius which generates a positive charge inside the metal layer. The brucite like sheets are neutralized by anions found in between the layers and water molecules are also located in between these sheets. LDHs can be formed with a wide variety of

M(II)/M(III) combinations of atoms and ratios, as well as a large variety of anions, carbonate being the predominant one in nature.

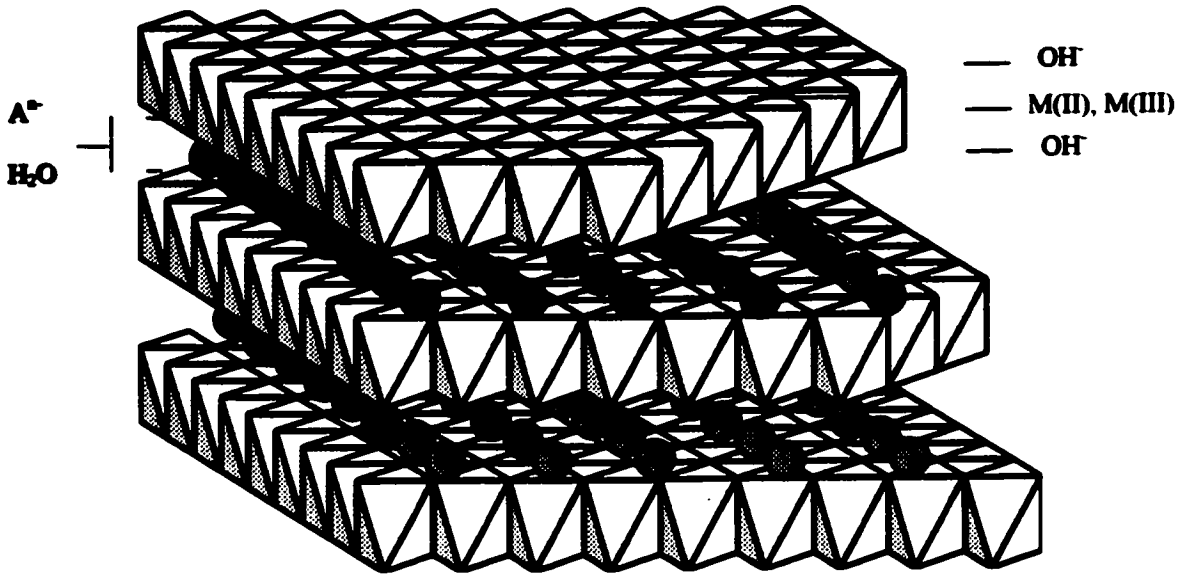

Figure 1.2 Structure of a layered double hydroxide

The structure of layered double hydroxides has predominantly been determined by the study of the single crystals of sjögrenite and pyroaurite, which was accomplished by Allmann[8;10], Ingram and Taylor,[11] in addition to the study of the crystal structure of hydrotalcite carried out by Allmann.[12]

According to Taylor, "the metal hydroxide sheets stack onto each other so that the hydroxyl groups on the lower surface of one layer are positioned directly above those on the upper surface of the one below as in gibbsite and not as in brucite. The rombohedral (3R) and the hexagonal (2H) conformations represent the simplest sequence satisfying this condition."[13] "If ABC designates the 3 fold axis in x,y = (0,0;2/3,1/3;1/3,2/3) of the OH groups in the

brucite like sheets, the stacking sequence may have the order -BC-CA-AB-BC- for the rombohedral symmetry with 3 sheets and 2 interlayers in the unit cell and -BC-CB-BC- for the hexagonal symmetry with 2 sheets and 1 interlayer in the unit cell." [2;8] The parameters of the unit cell for the rhombohedral symmetry are: a, which corresponds to the cation-cation distance in the metal hydroxide layers[14] and c = 3c' (where c' is the thickness of one layer which includes one brucite sheet and one interlayer). The parameters for the hexagonal symmetry are a and c = 2c'.

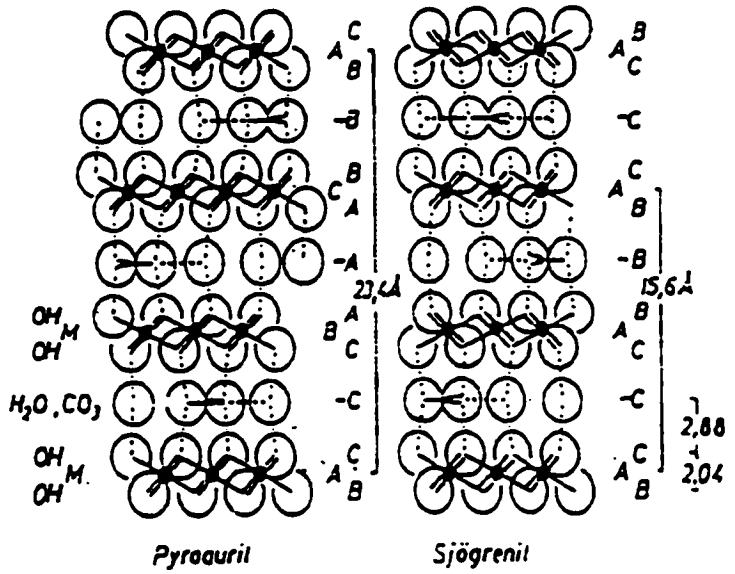

Figure 1.3 Stacking sequence of layered double hydroxides with different symmetries. [2]

"Layered double hydroxides having the rhombohedral symmetry have mostly been found in nature, however it has been noted that certain natural layered double hydroxide minerals, such as pyroaurite, contain the hexagonal stacking sequence in the interior of the crystallites and the rhombohedral sequence in the exterior."[2] According to Allmann; "this was an indication of the crystal growth starting with the hexagonal sequence followed by the growth of the rhombohedral one. This phenomenon was explained by assuming that the temperature of the mineral decreased during its formation and that the hexagonal phase was formed at

higher temperatures. Once the hexagonal symmetry was attained it would not revert to the rhombohedral phase due to a presumably larger energy barrier between the 2 phases and of the very small gain in lattice energy." [2;8]

The anions and the water molecules of layered double hydroxides are found in the interlayer spaces of these materials. In the article titled: "The Crystal Structure of Pyroaurite" written by Allmann[8], it is stated; " the interlayer can best be visualized as being in permanent motion, the H_2O and CO_3^{2-} changing their places by forming new hydrogen bonds and disconnecting old ones just as water molecules do in the liquid states." "The oxygen atoms of the water molecules and of the carbonates groups are distributed approximately closely around the symmetry axis that passes through the hydroxyl groups (0.56 Å apart) of the adjacent sheets metal hydroxide sheets." [2]

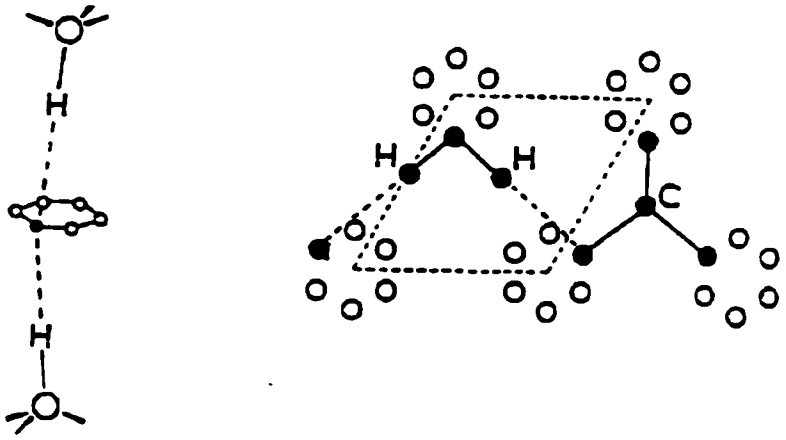

Figure 1.4 Position of interlayer anions and water[2]

The CO_3^{2-} anions directly link the hydroxyls groups or link them through intermediate H_2O with hydrogen bonds in the following manner: $OH\text{-}CO_3\text{-}OH$ or $OH\text{-}H_2O\text{-}CO_3\text{-}OH$.[15] Because

of the small interlayer space (2.9 Å), carbonate can only be in a horizontal position in this area.[8]

1.1.3 Chemical composition

The general molecular formula of a layered double hydroxide is

$$M(II)_{1-x}M(III)_x(OH)_2A^{n-}_{x/n}\bullet mH_2O$$

Layered double hydroxides having the formula below also exist but this type of LDH can only be synthesized with lithium. [2]

$$M(I)_{1-x}M(III)_x(OH)_2A^{n-}_{(2x-1/n)}\bullet mH_2O$$

Each of the components of the LDH will be discussed separately in the following text. However, only the LDHs containing M(II) cations will be described in further detail.

1.1.3.1 M(II)/M(III) Cations

Layered double hydroxide can be formed from a wide variety of M(II))/M(III) combinations in addition to combinations of three or more cations normally having a radius similar to that of Mg^{2+}. The cations must also fit in the octahedral sites of the closed packed configurations of the hydroxyl sheets of the material. Table 1.1 and 1.2 shows many different existing types

of natural and synthetic layered double hydroxides. Table 1.1 shows a list and composition of some of the most studied natural layered double hydroxides and table 1.2 shows a list and general composition of many synthetic layered double hydroxides.

Table 1.1: Name symmetry and composition of several natural layered double hydroxides

Name	Chemical composition	Symmetry	References
Hydrotalcite	$Mg_6Al_2(OH)_{16}CO_3 \bullet 4H_2O$	3R	12
Manasseite	$Mg_6Fe_2(OH)_{16}CO_3 \bullet 4H_2O$	2H	13
Pyroaurite	$Mg_6Fe_2(OH)_{16}CO_3 \bullet 4.5H_2O$	3R	15
Sjrögrenite	$Mg_6Fe_2(OH)_{16}CO_3 \bullet 4.5H_2O$	2H	15
Stichtite	$Mg_6Cr_2(OH)_{16}CO_3 \bullet 4H_2O$	3R	4;13
Barbetonite	$Mg_6Cr_2(OH)_{16}CO_3 \bullet 4H_2O$	2H	4;13
Takovite	$Ni_6Al_2(OH)_{16}CO_3 \bullet 4H_2O$	3R	16

Note: table adapted from ref. [2]

Table 1.2: Synthetic layered double hydroxides

General Composition of Metals	Anions	References
MgAl	CO_3	5;6;17-20
	OH	5;21
	NO_3	5;6;22;23
NiAl	CO_3	19;24-28
	NO_3	29;30
NiV	CO_3	29;31
LiAl	CO_3	25;27;32-35
CuAl	CO_3	36
CuZnAl	CO_3	37-40
CuCoZnAl	CO_3	41
CuZnCr	CO_3	42;43
ZnAl	CO_3	24;36;41;44
	Cl	18
	NO_3	45;46
MnAl	CO_3	36
ZnCr	CO_3	36
	Cl	47;48
	NO_3	47;48
CdCr	Cl	49
CaAl	CO_3	50
MgGaAl	CO_3 NO_3	51
MgAlSn	CO_3	14
MgAlY	CO_3	52
MgGa	CO_3	53

Note: Table adapted from ref. (2)

Table 1.3: Cations coordination number and radius in angstroms[54]

Metal (II)	Radius Å		Metal (III)	Radius Å		Other metals	Radius Å	
	CN (6)	CN (8)		CN (6)	CN (8)		CN (6)	CN (8)
Mg^{2+}	0.72	0.89	Al^{3+}	0.54	NA	Li^{+}	0.76	0.98
Ni^{2+}	0.69	0.69	Co^{3+}	0.55	NA	Sn^{4+}	0.69	0.81
Zn^{2+}	0.74	0.90	Cr^{3+}	0.62	NA			
Fe^{2+}	0.61	0.72	Ga^{3+}	0.62	NA			
Co^{2+}	0.65	0.90	Sn^{3+}	0.69	0.81			
Cu^{2+}	0.73	0.73	V^{3+}	0.64	NA			
Mn^{2+}	0.83	0.96	In^{3+}	0.80	NA			
Cd^{2+}	0.95	1.10	Y^{3+}	0.90	1.02			
Ca^{2+}	1.00	1.12						

Note: NA: indicates not available

The radii of the cations used to form the LDHs are shown in table 1.3. Most of the cations shown in this table have a similar radius to Mg^{2+} however a few do not, namely Cd^{2+}, Ca^{2+}, Y^{3+}. It was thought that cadmium and calcium were too large to form layered double hydroxides and would form other phases.[2] However, the synthesis of LDH using these cations has been recently reported. Vichi *et al.* synthesized a layered double hydroxide containing cadmium and aluminum prepared by the coprecipitation of a mixed metal nitrate

solution.[55] A calcium containing LDH was prepared by Aramendia *et al.*[50] and was calcined to be used as a basic catalyst for the catalytic transfer hydrogenation of citral with 2 propanol. Furthermore, the synthesis of a LDH with yttrium was achieved despite its large radius.[52]

The metals that produce a Jahn Teller effect such as $Cu^{2+}(d^9)$, Ni^{3+} (d^7 low spin) and Mn^{3+} (d^4 high spin)[3] do not normally form layered double hydroxides. For example, copper normally forms malachite like phases, because this structure is preferred when copper is in a distorted octahedral configuration, which is adopted due to the Jahn-Teller effect. However, it is stated that: "when the ratio of Cu^{2+}/M^{2+} is ≤ 1 the copper atoms are separate from one another and therefore adopt an undistorted octahedral shape and can arrange in brucite like structures."[2]

All the trivalent cations in the radius range of 0.5 to 0.8 Å can form LDHs.[2] The synthesis of LDHS using non air stable cations such as V^{3+} is more difficult, nevertheless LDHs containing this metal have been successfully synthesized.[31;56] However, to date, no layered double hydroxides has been formed with Ti^{3+}.

1.1.3.2 M(III)/M(II) ratio (Value of x)

Many studies have been done to determine the range of the x value that give pure layered double hydroxides. Much of the research has been done on Mg/Al and Ni/Al LDHs. The value of x has also been studied using other layered double hydroxides such as: Zn/Al, ZnCr,[57] CuCr, CoFe.[37;58;59]

Table 1.4: Optimal value of x to obtain layered double hydroxides

Range of x	Layered double hydroxide	References
0.25-0.44	MgAlOH	21
0.23-0.33	MgAlOH	23
0.20-0.33	$MgAlClO_4$	19
0.17-0.33	$MgAlCO_3$	17
0.20-0.337	$MgAlCO_3$	20
0.17-0.33	$NiAlCO_3$	19

Note: Table adapted from ref. [2]

The research found in the literature on this topic, indicates that the range of x to obtain pure LDHs is between 0.1 and 0.5. However, according to Trifirò *et al.*[2] "the optimal range to obtain pure layered double hydroxides seems to be in the range of $0.2 \leq x \geq 0.33$". For Mg/Al and Ni/Al LDHs the upper limit is apparently controlled because of the repulsion between aluminum containing octahedra.[19] When the value of x is larger than 0.33 there is formation of $Al(OH)_3$ due to the increased number of neighboring Al^{3+} octahedra. Low values of x (e.g. $x < 0.1$) lead to a large number of neighboring Mg^{2+} atoms and form $Mg(OH)_2$. It has however been shown that it is possible to obtain Mg/Al layered double hydroxides with a higher content of aluminum ($x = 0.44$). Pausch *et al.*[21] have managed to synthesize using higher pressure, a magnesium and aluminum containing layered double hydroxide with an aluminum content of $x = 0.44$. The successful synthesis of this compound

was explained by $Al(OH)_6$ octahedra being adjacent to each other, and the electrostatic repulsion was compensated by the smaller radius of Al^{3+}. Other layered double hydroxides with values of x larger than 0.33 have also been obtained. Pure ZnAl LDHs with x =0.44 has been synthesized by Thevenot *et al.*[44]

Studies have also shown that the a parameter is related to the value of x and it has been demonstrated that the parameter a decreases with an increase of x. The a parameter gives the cation–cation distance in the brucite layer and can also be taken as an index of the non-stochiometry with respect to the formation of pure layered double hydroxides.[2] According to Kikkawa *et al.* [19] the change of a with x can be considered as follows; for an ideal octahedral layer the a parameter equals $2^{1/2}$ (M-O) where M-O is the metal ion-oxygen distance. The mean metal ion radius r is given by:

$$R = (1-x)\, r(M) + x\, r(Al)$$

Where M = Mg or Ni

The negative slope of a with x is given by

$$\Delta a/\Delta x = -2^{1/2}[r(M) - r(Al)]$$

This can then be transformed into more general terms by changing M to M(II) and Al to M(III) to give the mean ionic radius R:

$$R = (1-x)r\, M(II) + x\, r\, M(III)$$

And the relationship between a and x is the slope of the line: [2]

$$-2^{1/2}[r\ M(II) - r\ M(III))]$$

The value of x versus a for many synthetic and natural Mg/Al LDHS were plotted and gave a straight line.[21] When x was extrapolated to zero, (i.e. no aluminum) it was found that a was equal to 3.14 Å which is near the value of pure $Mg(OH)_2$ (brucite with a = 3.147).[19:21] For values of x higher than 0.33, the value a, stayed constant at approximately 3.05 Å.

1.1.3.3 Anions (A^{n-})

Almost any type of anion can be found between the layers of layered double hydroxides. Inorganic as well as organic anions can neutralize the excess positive charge of the hydroxide sheets. Below is a listing of the different types of anions that can be found in layered double hydroxides and, in the following text, a few of the effects of the different types of anions on LDHs will be described.

Inorganic:

- Simple anions: CO_3^{2-}, NO_3^-, OH^-, F^-, Cl^-, Br^-, I^-
- Isopolyanions: $V_{10}O_{28}^{6-}$, $Mo_7O_{24}^{6-}$ etc.
- Heteropolyanions : $PMo_{12}O_{40}^{3-}$, $PW_{12}O_{40}^{3-}$ etc.
- Complex anions: $Fe(CN)_6^{3-}$, $Fe(CN)_6^{4-}$

Organic anions:

- Terephthalate, benzoates, aliphatic carboxylates, phosphonates, polymeric anions, alkyl sulfates and sulfonates.

A study on the anion exchange properties and the effect of the basal spacing of LDHs as a function of the type of simple anions was done by Miyata.[22] It was determined that the size, charge, position and quantity of anions inside the layer determine the interlayer spacing of layered double hydroxides. Table 1.5 shows the basal spacing of Mg/Al LDHs containing inorganic anions.

Table 1.5: Basal spacing of LDH containing simple inorganic anions.

Anions	Basal Spacing (Å)
OH^-	7.55
F^-	7.66
Cl^-	7.86
Br^-	7.95
NO_3^-	8.79
I^-	8.16
CO_3^{2-}	7.65

Note: Table adapted from ref. [22]

The basal spacing of the LDHs containing halogens increase from F^- (d spacing: 7.66 Å) to I^- (d spacing: 8.16 Å) which is consistent with the increase in radius from F^- to I^-. For these cases, it is the size of the anion that dictates the interlayer spacing. The LDH containing the hydroxide ion has the smallest basal spacing and according to Miyata this is because the OH^-

can form strong H bonds with the layers. The hydroxide ion has a diameter similar to that of H_2O. This allows for a structure with the closest possible packing arrangement in the 001 direction hence the smallest basal spacing. Carbonate also has a small basal spacing and this is because its divalent charge allows stronger electrostatic interaction between the layers.

The correlation between the basal spacing and the M(II)/M(III) ratio (value of x) was also studied. It was found that the basal spacing decreased with an increase of x (i.e. an increase in the M(III) ratio) except for LDHs containing nitrate. An increase in the M(III) ratio increased the positive charge density of the LDH, allowing more anions in the layers. This in turn increased the electrostatic interactions between the layers thus reducing the basal spacing. However, for nitrate containing LDHs the trend was reversed. As x increased, the interlayer spacing also increased. For this case, since nitrate is a large monovalent anion, the repulsion between the anions changed the orientation of nitrate from a flat to a non-parallel position as the density of NO_3^- between the layers increased.[22]

LDHs containing many different types of organic anions were also studied in the literature. The basal spacing of LDHs containing organic anions is more dependent on the structure of the organic moiety, its position inside the layers and hydration level of the layered double hydroxide. It is less dependent on the charge of the anion. For example, it has been shown that the terephthalate anion adopts a perpendicular position in the layers of many different LDHs increasing their basal spacing up to ~14 Å. [60] Furthermore, it has also been shown that depending on the M(II) and M(III) ratio, in addition to the hydration level of the LDH, terephthalate can adopt either a vertical or horizontal position between the layers consequently altering the basal spacing of the materials.[61;62] Similarly for the benzoate

molecule, it has been presumed that this anion adopts two possible arrangements in the layers: a bilayer arrangement of molecules in the horizontal position[61;62] with a 35° angle[63] or a vertical position in which a water molecule is kept in between the aromatic ring and the brucite like layers.[64] A different basal spacing was obtained for each of the different positions adopted by the benzoate molecule. As for aliphatic carboxylates, dicarboxylates, sulfates and sulfonates, they generally adopt a perpendicular or near perpendicular position to the hydroxide layers and sometimes form bilayer arrangements between the sheets. Hence, there is generally a direct relationship with the increase of the interlayer spacing of the layered doubles hydroxides and the length of the aliphatic chains. For example, Miyata and Kumura[24] synthesized a series of LDHs containing terminal linear aliphatic dicarboxilic acids of varying lengths and found a direct correlation between the interlayer spacing and the length of the aliphatic chains. The interlayer spacing increased from 9.4 Å for the oxalate $(CO_2^-)_2$ containing LDH up to 18-19 Å for the sebacate ($CO_2^-C_8H_{16}CO_2^-$) LDH. In addition, Raki *et al.* [65] have reported the same trend for the intercalation of dicarboxilic aliphatic anions inside ZnAl LDH. It was found that the d spacing increased linearly with the number of carbons in the aliphatic chain of the anion. Figure 1.5 below shows the plot of the interlayer spacing versus the number of carbons in the aliphatic chain for calculated and experimental results.

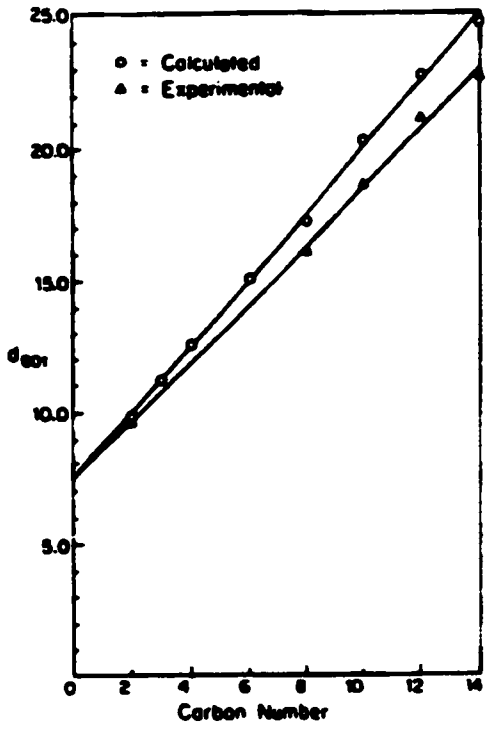

Figure 1.5 Interlayer spacing versus the number of carbons in the dicarboxilic aliphatic anion[65]

The basal spacing could be predicted by adding the length of the brucite layer (4.8Å) to the length of the anion showing that the molecules were intercalated in an almost perpendicular fashion between the layers of the LDH. Furthermore, solid state ^{13}C NMR showed that the carbon chains were all in a trans conformation.[65] Finally, other similar trends have also been noted in the literature for these types of systems.[64] Systems containing alkyl sulfates have been studied by Kopka *et al.*[66] It was proposed that the alkyl sulfates adopted a perpendicular position to the hydroxide sheets and after washing and drying, the interlayer spacing decreased. This was attributed to the chains adopting a 56° angle inside the sheets. Clearfield *et al.* [67] synthesized layered double hydroxides of NiAl, MgAl and ZnAl of varying M(II) and M(III) ratio and inserted sodium dodecyl sulfate in between the layers using two

different methods: coprecipitation and anion exchange. Materials having three different interlayer spaces were discovered and attributed to three different types of dodecyl sulfate layer arrangements. The first one had a layer spacing of 26 Å corresponding to a monolayer arrangement of dodecyl sulfate molecules. The second, with a layer spacing of 36 Å was determined to be dodecyl sulfates molecules in a bilayer arrangement with a 40° tilt and finally, the third at 47 Å was attributed to the anions being in an end to end ordering inside the layers. Similar results from other researchers studying LDHs intercalated with sodium dodecyl sulfate were also obtained.[68;69] Phosphonates and polymers have also been intercalated in the layers of LDHs. Studies in which a MgAl layered double hydroxides were treated with benzenediphosphonate anions ($[O_3P\text{-}(C_6H_4)_n\text{-}PO_3]^{4-}$, with n=1,2,3) , have shown that the depending on the temperature of reaction, the phosphonates groups can either be intercalated or grafted to the metal layers. At relatively low temperatures, (ca 0°C) intercalation takes place, and at higher temperatures, grafting of the phosphonate moieties directly to the metal layers with the elimination of the hydroxyl group occurs.[70] Research on polymers intercalated in LDHs has also been reported in the literature. Tanaka *et al.*[71] reported the intercalation of acrylate in nitrate and chloride containing MgAl LDHs but they noted that it was unsuccessful with the MgAl LDHs containing CO_3^{2-}. The acrylate intercalated in the MgAl LDH was subsequently polymerized by heat treatment at 80°C with the help of potassium peroxodisulfate as an initiator. Aniline has been intercalated in CuCr LDHs containing either the terephthalate anion or the hexacyannoferrate(II) ions as pillars, and subsequently polymerized to polyaniline by the oxidant character of the copper.[72] Polyacrylate, polyvinylsulfonate, polystyrenesulfonate have been incorporated in the layers of a variety of LDHs (MgAl, ZnAl, CaAl CoAl and ZnCr)[73] Other polymers such as

polyacrylonitrile,[74] and polyaspartate[75] have also been intercalated in layered double hydroxides.

1.1.3.4 Water content in layered double hydroxides

Interlayer water molecules in layered double hydroxides occupy the sites that are without anions. The amount of water contained in LDHs can be determined by thermal gravimetric analysis (TGA). There are however formulae in the literature that have been devised to determine the maximum amount of water found in LDHs. These are based on assuming a closed packed configuration of oxygen atoms, subtracting the sites occupied by anions and the remainder of the sites are left for water molecules. Miyata, Taylor and Mascolo *et al.* have all devised their own formula to determine the maximum amount of water that can be found in LDHs.

Miyata[18]: $m = 1 - N\,x/n$

Where m is the amount of water, N the number of sites occupied by the anions, n the charge of the anion, $x = M(III)/(M(II) + M(III))$

Taylor[13]: $m = 1 - 3x/2 + d$ where $x = M(III)/(M(II) + M(III))$ and $d = 0.125$ (for pyroaurite and sjögrenite)

Mascolo *et al.* [23] : $m = 0.81 - x$ where $x = M(III)/(M(II) + M(III))$

According to Roy *et al.*[76] "the hydration state of a LDH is given at once by its temperature and the water vapor pressure with which it is in equilibrium." By studying the variation in hydration of ZnCr and ZnAl LDH in relation to the relative humidity and the ambient atmosphere, Roy *et al.*[76]determined the presence of intracrystalline water, which is found in the interlayer of the LDH, and extracrystalline water adsorbed on the surface of the microcrystallites of the LDHs. These both take part in the global hydration state of the sample

The water molecules adsorbed on the surface of the microcrystallites were designated as extrinsic water and the ones found in the intralayers were designated as intrinsic water. The following formula was determined taking into account extrinsic and intrinsic water in a layered double hydroxide.

$$[M^{II}_{1-x}M^{III}_{x}(OH)_2]^{x+}[x^{m-}_{x/m}nH_2O]^{x-}n^{'}H_2O$$

Where n is the amount of intrinsic water and n" is the amount of extrinsic water.

1.1.4 Synthesis of layered double hydroxides

Several techniques can be used to synthesize layered double hydroxide depending on the type of material needed. Nevertheless, coprecipitation is the technique that is the most widely used to make large batches of materials because of its relatively simple ease of use. Shown below is a listing of the many other different types of techniques that may be adopted to synthesize LDHs:

- Anion exchange
- Structure reconstruction
- Electrochemical synthesis
- Hydrothermal synthesis
- Sol gel synthesis
- Hydrolysis

All the methods used to synthesize LDHs with anions other than carbonate have the common problem of CO_3^{2-} contamination. Carbonate is readily incorporated and held tenaciously in the layers. To obtain LDHs without the carbonate anion, the water must be decarbonated and all the reactions must be carried out in a nitrogen environment. In addition, exposure to the atmosphere must be kept at a minimum. Notwithstanding, any precautions taken to eliminate CO_3^{2-}, small quantities of carbonate are always incorporated when synthesizing LDHs.[18]

1.1.4.1 Precipitation

When using the precipitation methods, it is necessary to carry out the reactions under conditions of supersaturation. Three methods of precipitation exist: 1) Precipitation at variable pH, 2) Precipitation at constant pH at low supersaturation (coprecipitation) and 3) Precipitation at constant pH at high supersaturation.

1.1.4.1.1 Precipitation at variable pH

Precipitation at variable pH involves the titration of a solution containing the required metal salts with an alkali hydroxide or a carbonate solution. Titration with a basic solution normally induces sequential precipitation of ions. It is therefore not possible to directly precipitate a pure LDH and inhomogeneities of the LDH phase may be expected. It has been hypothesized that precipitation at low pH of the trivalent hydroxide occurs first followed by its reaction with the other ions in solution. The first synthetic layered double hydroxide was prepared using the titration method.[5-7] Diluted solutions of Mg and Al were titrated up to a pH of 10. The precipitate was placed in a dialysis bag, immersed in water and the Cl^- and sodium ions were replaced by carbonates from the atmosphere.

1.1.1.4.2 Coprecipitation at constant pH and low supersaturation

Coprecipitation at constant pH and low supersaturation is the most commonly used method to synthesize LDHs. This technique requires the preparation of two solutions that are kept separate: one containing the metal salts and one containing the alkali hydroxide. Concentrations of the solutions are normally in the range of 0.5 M to 2 M. The pH is kept constant by slowly adding the alkali and the salts solutions together into a single flask. The pH is generally kept in a range of 7 to 10, as this is the range that most metal hydroxides precipitate to form LDHs.[2] Temperatures are kept between 298-353 K and washing is carried out with water. Finally, drying is performed at temperatures lower than 393 °K.

At low supersaturating conditions, precipitates with more crystallinity are obtained with respect to materials obtained from coprecipitation at high supersaturation because in the latter case, the rate of nucleation is greater than the rate of crystal growth.

1.1.1.4.3 Coprecipitation at constant pH and high supersaturation

Synthesis of LDHs using the coprecipitation method at high supersaturation can be achieved using a similar procedure as described above. "However, high supersaturation conditions are achieved by increasing the concentration of solutions and/or increasing the addition rates."[3] This procedure generally gives rise to a material of lower crystallinity due to the higher quantity of crystallization nuclei. Prolonged washing of the material is usually required to reduce the amount of alkali due to the low solubility of the alkali hydrogen carbonate.

1.1.4.2 Anionic exchange

The anionic exchange method is usually employed to prepare LDHs with anions that are difficult to intercalate directly. Large anions such as isopolyanions and heteropolyanions[46;77-81] as well as long chains organic anions[64;68;82-84] have been intercalated in LDHs using this procedure. Exposing the LDH to an excess of the salt of the anion to be intercalated carries out the exchange reaction. The selectivity of the anion is an important factor for the exchange reaction. Given that the selectivity of divalent anions are higher than monovalent ones, LDHs containing monovalent anions such as nitrates or chlorides are preferred as precursors for

these types of reactions. The pH must also be in the range to favor the exchange and in the range of stability of the starting layered double hydroxide.

1.1.4.3 Reconstruction

The reconstruction method is another technique that is used when it is difficult to intercalate anions directly into LDHs. This ability is a peculiarity of layered double hydroxides and is based on the "memory effect". When a layered double hydroxide is thermally decomposed it is possible to reconstitute the original structure upon adsorption of anions [85] or upon exposure to air.[18] The temperature of decomposition is very important such that it must be high enough to obtain decomposition of the LDH phase in order to obtain mixed oxides but low enough so as not to form stable spinnels.[12;85] The temperature of decomposition depends significantly on the composition of the LDH but principally on the nature of the trivalent cation. Wide ranges of anions have been intercalated using this technique such as inorganic[85-87]organic[88-90] and polyoxoanions.[91-93]

1.1.4.4 Electrosynthesis

Electrosynthesis of layered double hydroxide is of special interest in the field of electrochemistry especially for the fabrication of electrode material. In this procedure, LDHs are electrodeposited from a metal nitrate solution onto a cathode. This method is also used to prepare positive nickel hydroxide electrodes for nickel metal hydride batteries and has shown

better results in cycling than electrodes prepared from the conventional chemical impregnation techniques.[94] The layered double hydroxides are normally prepared by a deposition process by cathodic reduction of nitrate ions from a mixed-metal nitrate bath. A divided electrochemical cell having Pt foil as the cathode and a Pt wire as the anode is utilized to carry out the process. A current is applied to the cell (~ 65 mA/cm^2) and the material is deposited on the cathode. The process involves two possible reactions that generate hydroxyl ions:

1) Nitrate reduction at the cathode:

$$NO_3^- + H_2O + 2e^- \rightarrow NO_2^- + 2OH^-; \quad E^0 = 0.01\ V$$

Or 2) hydrogen evolution:

$$2H_2O + 2e^- \rightarrow H_2 + 2OH^-$$

According to Indira *et al.*[95] both reactions can possibly lead to the formation of metal hydroxides by causing a steep local increase in the pH close to the cathode as shown by the reaction below:

$$M^{z+} + z(OH)^- \rightarrow M(OH)_z\downarrow$$

This method has been used to successfully synthesize NiAl, NiCr, NiMn, NiFe,[96] MgAl and MgCr LDHs.[95]

The methods described above give a general overview of the many different types of possible synthesis that can be used to produce layered double hydroxides.

1.1.5 Applications

Layered double hydroxides are materials used in wide range of applications such as, anion exchanger, adsorption media, electrochemistry, however, they are more prominently used in the field of catalysis. The interest of LDHs as catalyst arises from the easily controllable chemical composition of the metal layer, as well as the interlayer and the thermal stability of the materials. Cavani *et al.* have reviewed catalytic applications of layered double hydroxides for the following reactions:[2]

1) Basic catalysts

2) Reforming of hydrocarbons

3) Hydrogenation reactions

4) Oxidation reactions

5) Support for Zieggler-Natta catalysts

Layered double hydroxides acquire basic catalytic properties when activated by thermal treatment (calcination). When calcined at the correct temperature, LDHs form mixed oxides that show an increase in surface area and reactivity. The increase in reactivity comes from the formation of catalytically active basic sites.[97] The basic character of the oxides has largely been studied on the $MgAlCO_3^{2-}$ system and 3 different basic sites have been demonstrated:[98-101] Strongly basic sites of O^{2-} present at the surface of the material, medium basic O^- sites located beside the hydroxyl groups and sites of weak basicity represented by the OH groups.

"Calcined LDHs have been used for polymerization of ethylene and propylene oxide to form polymers such polyethylenene oxide and polypropylene glycols. These polymers are important in the epoxide industry because polyethylenene oxide is used as water-soluble lubricants for rubber mould, textile fibers, and components in cosmetic and pharmaceuticals. Polypropylene glycols are important materials for the production of urethane rubbers."[2]

Aldol condensation is another reaction that uses basic catalysts. Four chemicals that are synthesized from aldol condensation using calcined layered double hydroxides and are interesting from an industrial point of view are: mesityloxide, acetone alcohol, isophorone and 2-ethylhexenal. When hydrogenated, they yield solvents or lubricants, or are used as intermediates for the production of insecticides.[2]

Coprecipitated NiAl precursors were being used for steam reforming synthesis of methane even before people using them for this purpose realized that they were actually forming layered double hydroxide precursors.[102]

Layered double hydroxide as precursors were used for hydrogenation reactions in the production of higher alcohols,[38;39;103] CH_4, methanol, paraffins, olefins from syngas and hydrogenation of nitro benzene.[2]

Polyoxometalate intercalated LDHs were used for the photoxidation preparation of acetone from isopropyl alcool.[80] Furthermore, there are patents of various types of layered double hydroxides prepared as precursors for the support of Zieggler-Natta catalysts that are used in the polymerization of olefins.[104]

1.1.6 Other properties and applications

1.1.6.1 Adsorption

The large variety of exchangeable anions of layered double hydroxide allows them to be used as anion exchangers. They must however be prepared carbonate free because this anion is preferentially sorbed above other anions.[105] This property has allowed them to be used for purification of waste waters [106] and as sorbents for organic substances from water. [107-109] In addition, the adsorption properties of calcined LDHs could possibly be used to save heritage buildings around the world. Granite and sandstone materials are widely found in heritage buildings around the world and the crystallization of salts such as sulphates inside the pore networks of stone materials is one of most widely occurring processes for the stone decay of buildings. Trujillano *et al.* [110] have shown that calcined hydrotalcite (MgAl LDH) can extract sulphate from granite and sandstone. This could therefore be used as a method to selectively extract sulphate from buildings and ceramic materials in order to preserve them. The adsorption properties of LDHs have also allowed the preparation of new materials. Novel membrane like-materials are formed upon intercalation of certain organic anions. For example a LiAl LDH intercalated with myristate or hexanoate has been shown to partition pyrene from a methanol water solution[2].

1.1.6.2 .Electrochemistry

Layered double hydroxides also have the potential for use in applications of electrochemistry. NiAl [29;30] and NiCo [111] have shown promising results as the replacement

materials for use in the positive electrode in rechargeable nickel cadmium (Ni/Cd) and nickel metal hydride (NiMH) batteries.

CHAPTER 2

Layered Double Hydroxides for Use as Electrode Material for the Positive Electrode in Rechargeable Nickel Metal Hydride and Nickel Cadmium batteries

2.1 INTRODUCTION

A battery is a device that converts chemical energy into electricity by means of an electrochemical oxidation-reduction reaction. It is believed that batteries may have been fabricated as early as 2000 years ago. In the late 1930s', curious objects of unknown purpose were discovered in the excavation site of Khuyut Rabbouà, the remains of a Parthian town in the outskirts of Baghdad (Iraq) (the Parthians dominated the Baghdad region between 250 B.C. and 224 A.D.). The objects were composed of a clay jar with a stopper made of asphalt. Sticking through the asphalt was an iron rod surrounded by a copper cylinder. Wilhelm König, a German archeologist studied the objects to determine their purpose and in 1938 he published a paper referring to the devices as possibly being galvanic cells. The results of his research were compiled in his book "Lost Paradise of Iraq".[112;113] Strong support for this hypothesis came from Willard F.M. Gray of General Electric who successfully made working replicas of these objects.[114] Other scientists were also able to reproduce working replicas; namely, John B Piercing of the University of North Carolina was able to obtain a current of 0.5 V for 18 days by adding a 5% vinegar or wine solution to the units.[115] In 1978

a German Egyptologist demonstrated that an electrical current of 0.5 volts could also be obtained by adding freshly squeezed grape juice to the device. In addition, he was able to plate a small silver figurine with gold using the battery. Additional research from other scientists showed that it was also possible to use replicas of the batteries for the purpose of electroplating.[116-118] Some of the artwork of the Parthians such as drinking horns were selectively gold plated which would be in line with the idea that the vase like objects were used as batteries for this purpose.

Approximately 2000 years later, in 1798 to 1800 Alessandro Volta[119] while trying to refute Luigi Galvani's hypothesis of "bioelelectrogenesis"[120] (where muscle tissue can generate electricity on their own) discovered that 2 different metals in an acidic solution that are in proximity to each other could produce an electrical current. He produced the first voltaic pile, which consisted of a series of zinc, and silver disks separated from each other by a porous nonmetallic material, soaked with salt water. Later, in 1836, J.F. Daniel developed a cell using zinc and copper as the electrodes. These were immersed in a zinc sulfate sulfuric acid electrolyte and copper sulfate electrolyte respectively with a porous barrier between the solutions to prevent extensive mixing. The innovation of this battery was that it contained a *depolarizing agent*, "a material which reduces the accumulation of hydrogen on the electrode" and increased the life of the cell.[114] In 1859, Planté developed the lead-sulfuric acid storage battery. However, this chemical battery used a liquid electrolyte and was not easily transportable. The development of the dry cell resolved the problem of maneuverability of the earlier batteries given that the electrolyte of the dry cell was composed of a damp paste that prevented leakage during transport. Between 1886 and 1888, Dr. Carl Gassner developed the first true dry cell, which consisted of a zinc oxide, ammoniac

and water electrolyte paste. It contained a zinc negative electrode that was also the container of the cell and a carbon rod as a positive electrode. The cell was practical and portable, which allowed for production on a commercial scale. The common alkaline batteries that are used today were developed by T.A. Edison in 1914. They are so called because the electrolyte is basic (alkaline) instead of being acidic. Since then, significant progress has been achieved in battery technology. In the current era, the advent of many devices needing lighter and more powerful batteries as well as environmental concerns has prompted the research for better performing and longer lasting non-rechargeable and rechargeable batteries.

2.1.2 Types of batteries

There are two main classifications of batteries: primary (non rechargeable) batteries and secondary (rechargeable) batteries. Primary batteries are not easily rechargeable and therefore are only good for one use and then they are discarded. However, it is know that virtually all electrochemical processes are in theory reversible and that there are many primary cells that may be developed as rechargeable cells in the future. The most common anode material for primary batteries is zinc because of its good electrochemical behavior, its stability with electrolytes, high electrochemical equivalence, low cost and availability. The most widely used primary battery is the zinc carbon dry cell because of its low cost, reliable performance and its availability. This battery uses a zinc anode, a manganese dioxide cathode and an electrolyte of ammonium chloride or zinc chloride dissolved in water. Powdered carbon is mixed with the manganese dioxide to improve the conductivity of the electrode. They are used in everyday devices such as flashlights, portable radios and toys. These types of batteries are however being replaced by Zn/alkaline/MnO_2 (commonly called alkaline

batteries) despite their higher cost per unit, because of their higher performance. Other primary batteries include magnesium cells (Mg/MnO_2), alkaline-manganese dioxide cells, mercuric oxide cells (Zn/HgO), silver oxide cells (Zn/AgO_2), zinc/air cells (Zn/O_2) and lithium cells which use lithium as the anode and a wide variety of materials for the cathode. These batteries are used for a variety of applications for instance in military devices, hearing aids, pace makers, as well as many other electronic devices.

Secondary batteries, on the other hand, are rechargeable batteries. They can be recharged to their original state after being discharged, by applying an electrical current in the reverse direction of the discharge current. These batteries can be used in two major types of applications:

They can function as energy storage devices that are constantly being charged by a primary source of energy and giving electricity only on demand when the primary source is not available or is inadequate to handle the energy demand. Examples are batteries used in vehicles to start engines or in emergency no-fail and standby power sources.

They can also be used similarly to primary batteries where the application requires a complete discharge of the battery and then must be recharged for further use. Examples are batteries used in electric vehicles, remote control toys, and most consumer electronic devices.

Lead acid batteries are the most widely used rechargeable batteries. The lead acid battery uses lead dioxide as the material for the positive electrode and metallic lead for the negative electrode. These batteries have relatively good performance at low cost. Their charge discharge process is essentially completely reversible; it is reliable over a wide temperature

range and has a long lifetime. This type of battery has many applications such as in the automotive industry (to start the engines), aircraft industry, emergency power applications and small appliances.

Most of the other secondary batteries are based on alkaline (KOH or NaOH) electrolyte. The alkaline electrolyte has the advantage of being less corrosive to the electrode materials. In addition, the electrolyte concentration does not change during the normal operation of the cell, because it is used only for the transport of oxygen or hydroxyl ions from one electrode to another. The most popular alkaline batteries are the nickel cadmium secondary batteries. There are three different types of these cells: vented industrial, vented sintered-plate, sealed nickel-cadmium. The vented industrial battery uses β-nickel hydroxide with graphite for increased conductivity for the positive electrode, and additives such as cobalt or barium for increased life. The negative electrode is prepared from cadmium hydroxide. Vented sintered-plate batteries use sintered nickel plates in which either β-nickel hydroxide or cadmium hydroxide is impregnated for their positive and negative electrodes respectively. The sealed Ni-Cd batteries also use nickel hydroxide for the positive electrode and cadmium for the negative electrode. The Ni-Cd type batteries are very reliable, sturdy and have long lifetimes. They come in a variety of shapes and sizes and are used in many different types of applications. For example, the vented industrial types are used in heavy industry, military applications and railroad service. The vented sintered plate has up to 50% higher energy density than the vented industrial battery and is therefore used in high power demand applications such as in aircraft engine turbine and diesel engine starting. The sealed Ni-Cd battery has features stopping the buildup of pressure during usage, which allows it to be

sealed. It can therefore be used in applications where lightweight portable power is needed such as in portable computers, toys, telephones etc...

The sealed nickel metal hydride (NiMH) batteries are relatively new technology (~1990)[121] and are very similar to Ni-Cd batteries. The NiMH batteries also use β-nickel hydroxide for the positive electrode material however they use hydrogen adsorbed on metal for the negative electrode. The metal hydride electrode has approximately 50% more energy density than the cadmium negative electrode of the Ni-Cd battery. It therefore requires less material to obtain the same power. Furthermore, NiMH batteries are environmentally friendly compared to Ni-Cd batteries because they are free of cadmium. The negative electrodes are normally made with what are called AB_5 or AB_2 alloys. The AB_5 alloy is based on lanthanum and nickel ($LaNi_5$). In this alloy, rare earth metal atoms and transition metal atoms are stacked in layers. In many cases, other atoms can replace La or Ni. The replacement of La by other rare earth metals such as Nd and Ce enhanced the longevity of the electrode by forming a protective surface film. Therefore, lanthanum was often replaced by a mixture of naturally occurring rare earth metals formed mostly of La, Ce, Pr and Nd, which is called Misch metal (Mm). Nickel is also often substituted by Al, Si Fe, Mn and Sn. In both cases, the substitution of lanthanum or nickel is done either to optimize hydrogen storage, stabilize the alloy or lowering the cost of the alloy. The AB_2 alloys are produced from either zirconium or titanium and other transition elements such as V, Cr, Mn, Fe Co, Ni. "The initial interest in these alloys was the binary crystalline and glassy alloys however this switched to multi-element pseudo binary intermetallics having a stochiometry near AB_2 were A = Zr and Ti and B = V, Cr, Mn, Fe Co, Ni."[121] The AB_2 alloys have approximately 25% higher capacity than the AB_5 alloys however, the trend is to use the AB_5 alloys due to the latter's better charge retention

and accrued stability. Other alkaline secondary batteries that are being used currently or are being presently researched are: Nickel-Iron, Nickel-Zinc, Silver-Zinc and Silver-Cadmium batteries.

2.1.3 Basic components of a cell and batteries

The basic electrochemical unit of a battery is a cell. The cell is composed of three main components; two electrodes, and an electrolyte solution. The anode during a discharge process is considered the negative electrode by definition. At this electrode, anions are oxidized and electrons are given to the external circuit. A cathode is the positive electrode by definition during a discharge process. This electrode accepts electrons and at this location, the cations are reduced.[122] The electrolyte is the ionic conductor. Typically, a liquid such as water with dissolved salts, acid or base to provide ionic conductivity is used as the electrolyte.

2.1.4 General requirements of batteries

The ideal performance requirements for any batteries are to have high energy density, high power density, low cost, long life, and a wide operating temperature range and should be environmentally friendly. The energy density is defined as the power density times the hours of usage:

Energy density = Power density x hours of usage.

The power density is given by:

Power density = V x A /kg

Where V is the voltage and A is the current in amperes. If we take a battery system to power an electric vehicle for example, the power density could be seen as the attribute needed for quick acceleration. On the other hand, the energy density could be seen as the attribute needed for the range of travel of the vehicle. The secondary batteries of today cannot fulfill simultaneously all of the requirements mentioned above, however, there are many types of batteries available each having their advantages and disadvantages making them suitable for specific applications. This therefore makes the improvement of batteries an active field of research. Below are a few examples of the advantages and disadvantages of some of the most common systems available today and some potential systems.

Lead acid batteries are a very well researched system and the most advanced lead acid batteries are relatively low cost, almost completely recyclable, have a large operating temperature range, high power density (~400 w/kg) but have the drawback of low energy density (~10-35 Wh/kg). This gives them the ability to give large outputs in a short period of time (for example in starting a car engines) but does not allow for long continuous discharge. Furthermore, the toxicity of lead is an environmental concern to consider for any part of the electrodes that might not be recyclable.

The nickel zinc battery that uses zinc as the negative electrode and $Ni(OH)_2$ as the positive electrode is a system that has been researched extensively in the past years[123] because of its

relatively high power and energy density (~60 Wh/kg) and low cost. However, this system is plagued by short life, which has been attributed to two main problems:

1. Material dissolution and uneven redistribution resulting in loss of usable active material
2. The formation of Zn dendrites which causes loss of porosity and short-circuiting, as the dendrites can travel to the other electrode and short-circuit the system. [121]

Zn silver oxide cells are noted for their high energy and power density however have limited cycle life and are only used in special applications because of their expensive cost due to the silver oxide electrode.

Nickel cadmium batteries are rugged and have long lifetimes. They have high power density however they have low energy densities in the range of 30-35 Wh/kg. They also have the disadvantage of containing cadmium, a poisonous metal, in the negative electrode and are therefore not environmentally friendly. On the other hand, nickel metal hydride (NiMH, where MH is the hydride of the inter-metallic alloy used for the negative electrode e.g. $LaNi_5H_{6.6}$) batteries, which also use Ni hydroxide for the positive electrode, have power densities in the same range as the Ni-Cd batteries. They however have higher energy densities (50 Wh/kg) and because they do not contain cadmium are considered environmentally friendly. Their cycle life is however shorter than the Ni-Cd system. The negative electrode of the NiMH battery has allowed this battery to obtain a higher energy density. Improvements are therefore needed for the positive electrode if more gains are to be obtained in this area. This is definitely an active field of research as many scientists are trying to improve on the positive electrodes performance and it's longevity. There is however a strong competition appearing from the rapid development of lithium batteries because they offer longer lifetimes and higher energy densities than NiMH batteries. However, the

reactivity of lithium in these batteries increases as the discharge and charging cycling progresses occur, making them a safety hazard as their use increases. Until there is a solution to this problem, NiMH batteries still have a very useful future for many years to come.

2.1.5 Operation of a cell

The general charge and discharge process of cells will be reviewed with the emphasis on the NiMH and Ni-Cd batteries.

2.1.5.1 Discharge process

The discharge process occurs when the cell is connected to an external load and chemical energy of the cell is transformed into useful electrical energy. When this occurs, the anode is oxidized, giving of electrons to the load and the cathode, which is reduced, accepts the electrons. The circuit is completed by the ions found in the electrolyte. The anions travel to the anode and the cations travel to the cathode. This process is illustrated in the diagram below (Figure 2.1)

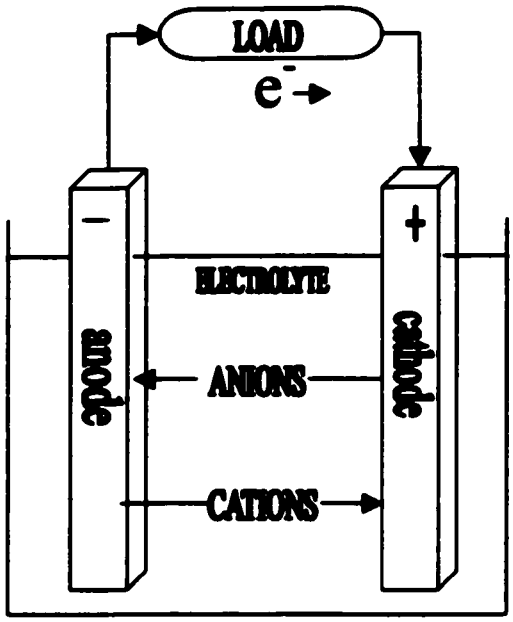

Figure 2.1 Discharge process

In nickel-cadmium and nickel metal hydride batteries the discharge process is the same at the cathode (positive electrode) because they both contain β-$Ni(OH)_2$ as the active material and the simplified process is shown in the equations below:

Nickel oxyhydroxide is reduced to β-nickel hydroxide:

$$Ni(OOH) + H_2O + e^- \rightarrow \beta\text{-}Ni(OH)_2 + OH^- \qquad E^0 = 0.52\ V$$

At the negative electrode, the process involves different materials:

In the nickel metal hydride battery, the metal hydride (MH) electrode is oxidized to the metal alloy (M):

$$MH + OH^- \rightarrow M + H_2O + e^- \qquad E^0 = 0.83\ V$$

In the nickel-cadmium battery cadmium is oxidized to cadmium hydroxide

$$Cd + OH^- \rightarrow Cd(OH)_2 + 2e^- \qquad E^0 = 0.81\ V$$

The overall discharge process is represented as:

NiMH battery

$$Ni(OOH) + MH \rightarrow M + \beta\text{-}Ni(OH)_2 \qquad E^0 = 1.35\ V$$

Ni-Cd battery

$$2Ni(OOH) + Cd + 2H_2O \rightarrow 2\ \beta\text{-}Ni(OH)_2 + Cd(OH)_2 \qquad E^0 = 1.33\ V$$

2.1.5.2 Charge process

A charging process takes place when the current in the cell is reversed and the electrical energy is transformed back into chemical energy. In this process, the oxidation occurs at the anode, which is now the positive electrode and reduction occurs at the cathode that is now the negative electrode.

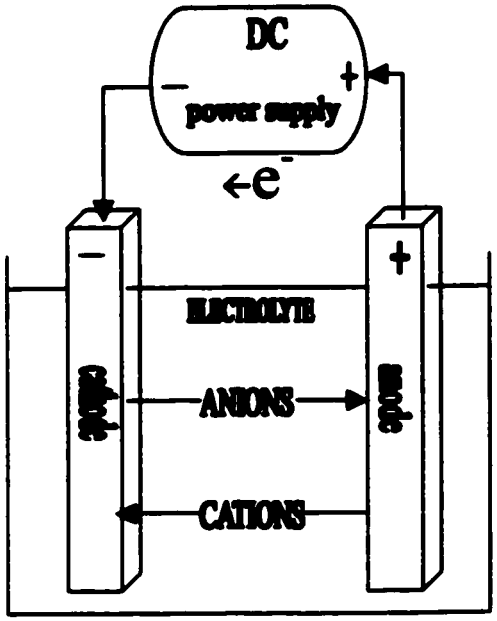

Figure 2.2 Charge process

For the Ni-Cd and nickel metal hydride batteries the reverse reaction of the discharge process occurs at the anode (now the positive electrode):

$$\beta\text{-}Ni(OH)_2 + OH^- \rightarrow Ni(OOH) + H_2O + e^-$$

At the cathode (now the negative electrode) the following process occurs:

NiMH battery

$$M + H_2O + e^- \rightarrow MH + OH^-$$

Ni-Cd battery

$$Cd(OH)_2 + 2e^- \rightarrow Cd + 2OH^-$$

The overall charge process is described as:

NiMH battery

$$M + \beta\text{-}Ni(OH)_2 \rightarrow Ni(OOH) + MH$$

Ni-Cd battery

$$2\beta\text{-}Ni(OH)_2 + Cd(OH)_2 \rightarrow 2\ Ni(OOH) + Cd + 2\ H_2O$$

The overall charge and discharge process of a NiMH cell can also be described by the diagram shown below in which the positive and negative electrodes can be seen as layered materials with intercalation and deintercalation of protons occurring during these processes. (Figure 2.3)

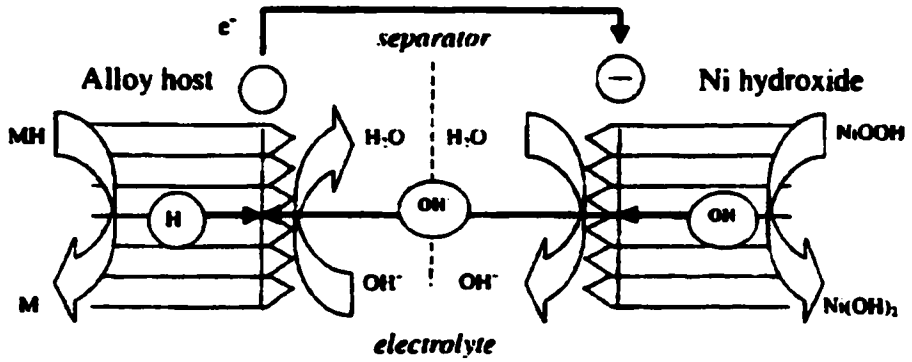

Figure 2.3 Overall discharge and charge process of NiMH battery[121]

2.1.6 Cell Voltage, Free Energy of a cell, Discharge Voltage and Discharge Capacity

2.1.6.1 Theoretical cell voltage

The theoretical voltage or standard potential of a cell depends on the material of the electrodes and can be calculated from free energy data or can be obtained experimentally. Many electrode potentials have already been experimentally determined and the standard cell potential can be calculated by the difference between the potential of the cathode and the anode. It should be noted that the potential of a single electrode is practically impossible to measure and potentials are measured against a standard reference electrode. By convention, the hydrogen electrode is considered the standard electrode and has been arbitrarily assigned a potential of zero. Therefore, the given potential of an electrode is the difference in potential between the hydrogen electrode and the electrode in question.

2.1.6.2 Free Energy

The reactions that occur at the electrodes in a cell can be represented by:

The reduction reaction at the cathode

$$aA + ne^- \rightarrow cC$$

where a is the number of moles of A, n the number of moles of electrons and c the number of moles of C that are formed.

The oxidation at the anode

$$bB \rightarrow ne^- + dD$$

where b is the number of moles of B, n the number of moles of electrons and d the number of moles of D that are formed

The overall reaction is given by:

$$aA + bB \rightarrow cC + dD$$

The relationship that relates the change in free energy of the redox reactions that occur at the electrodes and the standard potential of the cell is given by:

$$\Delta G^\circ = -nFE^\circ \qquad (2.1)$$

Where F is the Faraday constant (96485 C/mole), n is the number of electrons involved in the oxidation-reduction reaction, and E° is the standard potential in Volts. The maximum electrical energy (in the standard state: 25°C and 1 atm. of pressure) that can be provided by the chemicals in the electrodes of a cell depends on the change in free energy ΔG° of the electrochemical reaction. The change in the standard free energy is the driving force enabling the battery to give electricity.

When a cell is operating in conditions that are different from the standard state, the Nernst equation can be used to determine the theoretical potential of a cell that is represented by equation 2.3:

$$E = E^\circ + (RT/nF)\ln(a_C^c a_D^d / a_A^a a_B^b) \quad (2.3)$$

Where a are the activity coefficients of the species in question, R is the gas constant, and T is the absolute temperature.

2.1.6.3 Discharge Voltage

When a cell is discharged, the voltage is lower than the theoretical voltage because of three main factors:

- Activation polarization: Property associated with the loss of energy during the charge transfer from the reactants to the electrode.
- Concentration polarization: Property associated with the loss of energy due to the diffusion process of the reactants being transported to the electrode surface from the bulk of the electrolyte and the reverse transport of products.
- Ohmic polarization (or the Internal impedance of the cell): Property associated with the loss of energy due to the internal resistance of the cell (IR drop), which is proportional to the current drawn from the cell. "The total internal impedance of a cell is the sum of the ionic resistance of the electrolyte, the electronic resistance of the active mass, and the contact resistance between the active mass and the current collectors." [122]

All of these factors consume part of the energy, which is wasted as heat. The actual voltage of the cell (E) must take these factors into account an can be expressed as:

$$E = E^0 - [(n_{ct})_a + (n_{ct})_c] - [(n_c)_a + (n_c)_c] - iR_i$$

Where E° is the theoretical voltage of the cell (or electromotive force), $(n_{ct})_a$ and $(n_{ct})_c$ are the activation polarization at the anode and the cathode respectively, $(n_c)_a$ and $(n_c)_c$ are the

concentrations polarization at the anode and cathode, i is the operating current and R_i is the internal resistance of the cell.

The plot of the variation of the voltage as a function of time or increasing gravimetric capacity is called a discharge curve. A theoretical discharge curve would give a straight line at the maximum voltage of the cell until the reactants are fully utilized. The voltage would then drop to zero. However, under actual conditions, the initial voltage of the discharge curve has a lower potential than the theoretical voltage due to the IR drop. The voltage also drops during discharge as the cell resistance increases, due to the accumulation of discharge products, polarization and related factors. A theoretical discharge curve as well as a discharge curve under real conditions are shown in Figure 2.4

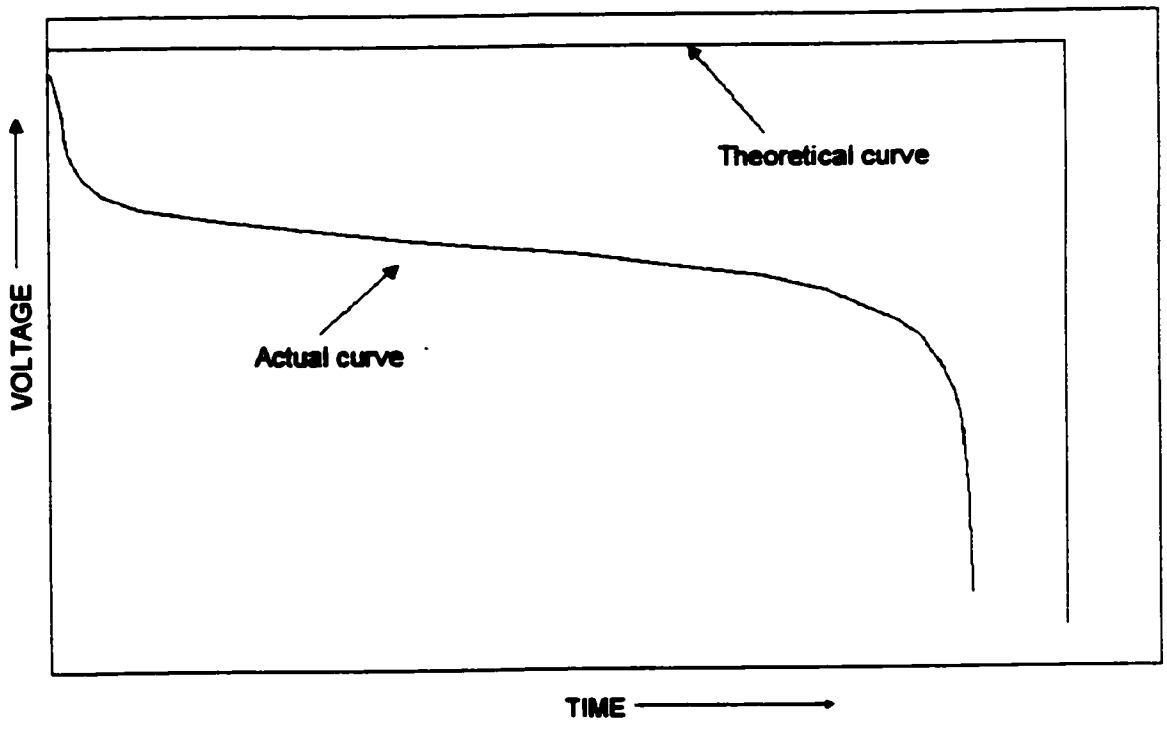

Figure 2.4 Characteristic discharge curves

2.1.6.4 Discharge Capacity

The discharge capacity can be expressed as the maximum quantity of electrons (or current) that can be provided per hour by the electrochemically active material in the electrode. It can be defined in terms of ampere-hour per gram of material (Ah/g) or in milli ampere-hour per gram (mAh/g). For example an electrode containing 1 g of $Ni(OH)_2$ gives a maximum capacity of 289 mAh/g (assuming a one electron process).

2.1.7 Review of the literature on the positive electrode of Ni Based batteries

This review will first focus on the current knowledge of the structure of the polymorphs of nickel hydroxide that occur during the cycling of the nickel hydroxide electrode, then the focus will be on LDHs that have been used to improve on the nickel hydroxide electrode.

2.1.7.1 Layered Nickel Hydroxides

The material that is found in the positive electrode of Ni based batteries is nickel hydroxide. During the cycling of a cell, nickel hydroxide transforms into different types of polymorphs. All of the polymorphs can conveniently be described as having the structural composition of slabs of NiO_2 made of NiO_6 edge sharing octahedra with protons and sometimes water or other ions intercalated in the interslab. This description is convenient because during the discharge and charge process of nickel hydroxide, there is either the gain or a loss of protons.

The Bode diagram[124] shown below (Figure 2.5) describes the different types of polymorphs that are obtained during the cycling of a positive electrode containing nickel hydroxide. During cycling, β(II)–$Ni(OH)_2$ is transformed reversibly into β(III)–Ni(OOH) during the charging process. On prolonged charging or on overcharge, β(III)–Ni(OOH) material is transformed into γ(III+)-Ni(OOH) where III+ denotes a valence higher than 3, typically 3.6. On discharge, γ(III+)-Ni(OOH) becomes α(II)-$Ni(OH)_2$, which is unstable in strong alkali and reverts back to β(II)–$Ni(OH)_2$.

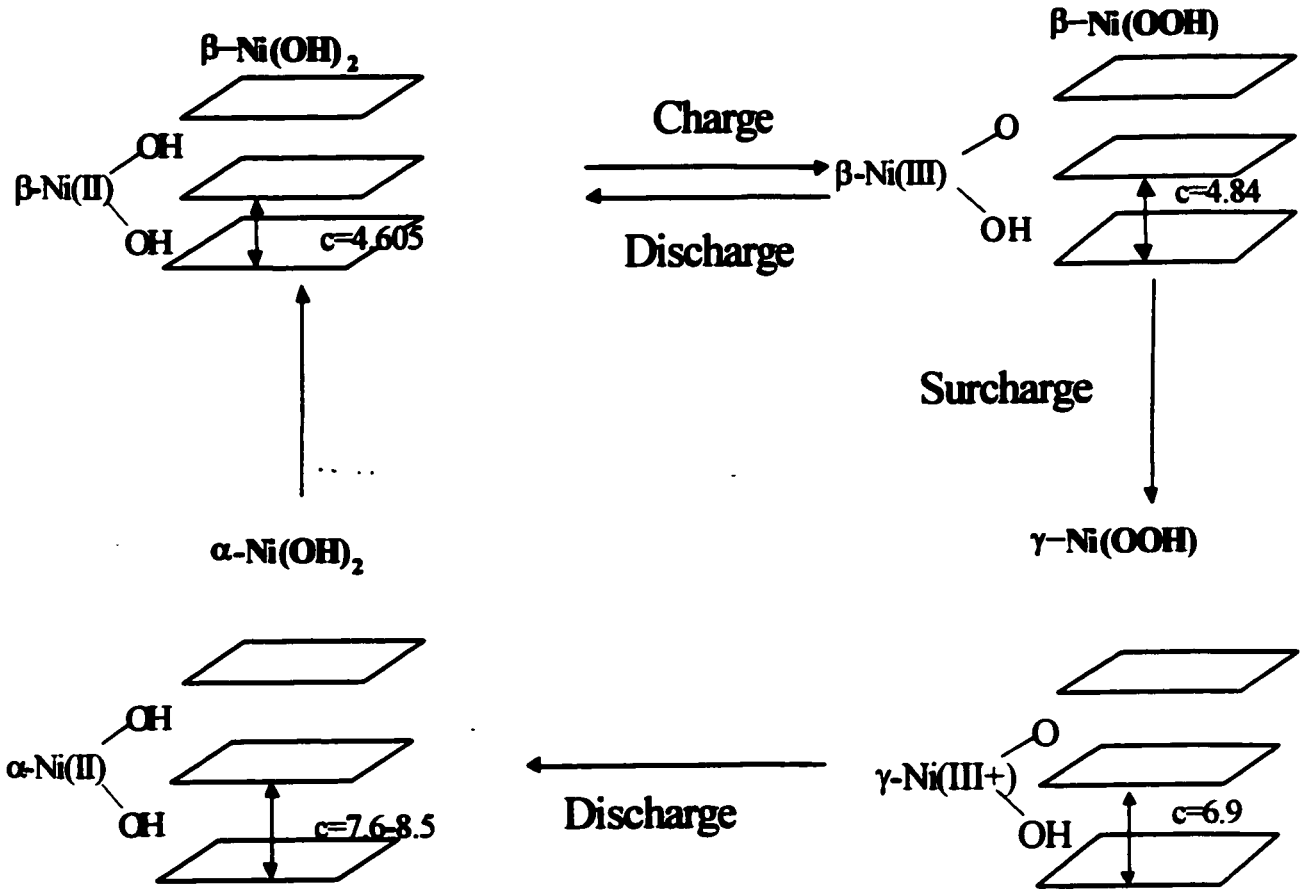

Figure 2.5 Bode diagram; Polymorphs obtained when cycling β-$Ni(OH)_2$

β-$Ni(OH)_2$ is considered to be isostructural to brucite [$Mg(OH)_2$].[125] and has a hexagonal unit cell as shown in the Figure 2.6 below:

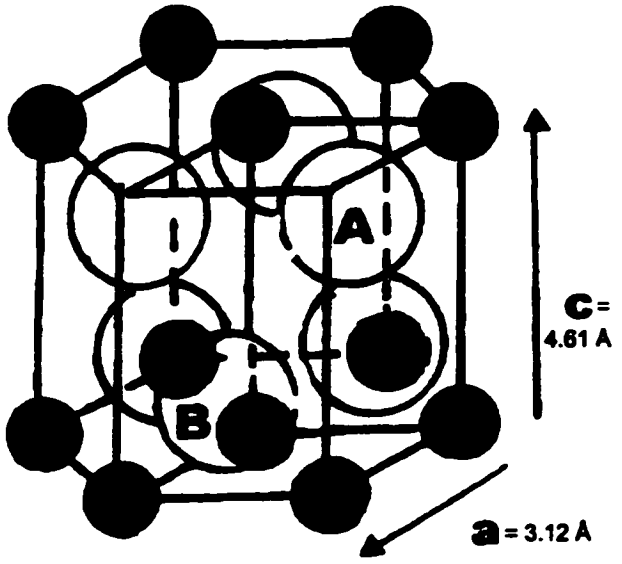

Figure 2.6 Unit Cell of β-$Ni(OH)_2$

Dark circles: Nickel,. white circles: oxygens, hydrogen atoms are not shown.[121]

Brucite is made of sheets of magnesium containing edge sharing octahedrally coordinated hydroxyl groups that form two-dimensional infinite sheets. Alternatively, other authors have described β-$Ni(OH)_2$ as slabs of NiO_2 formed of edge sharing oxygen atoms with hydrogen atoms intercalated between the sheets of the material.[126] Neutron diffraction studies have shown the compound to have the CdI_2 structure with the P3m1 space group.[127;128] Inelastic neutron scattering spectroscopy revealed the same information.[129] The authors, however, still consider the structure to be of the brucite type (trigonal, space group P3m1) and still consider the material to be formed of layered edge sharing NiO_6 octahedra with H atoms found

between the layers bound to the oxygen atoms with the OH bond parallel to the c axis. Figure 2.7 shows a representation of the structure of β-$Ni(OH)_2$ along the c axis.[129]

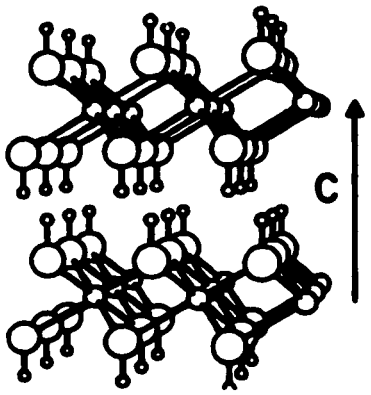

Figure 2.7 Structure of β-$Ni(OH)_2$

Large circles: Oxygen, small circles: nickel, smallest circles: hydrogen.[129]

The nickel in β-$Ni(OH)_2$ is found in the divalent state and has the $T_{2g}^6e_g^2$ electronic configuration.[130] The lattice parameters of the material are a = 3.12 Å (which gives the interatomic Ni distance in the layers) and c = 4.605 Å which gives the interlayer spacing.[131;132] This phase has no hydrogen bonding between the OH groups of adjacent layers.[125] Furthermore, the relatively simple structure of nickel hydroxide is more complicated than expected. Wronski *et al.*[133-135] recently proposed that $Ni(OH)_2$ contained structural defects that were considered to be stacking faults, on the grounds of the study of the broadening observed in certain peaks in the XRD pattern of $Ni(OH)_2$. The amount of so called stacking fault disorder was correlated with the improvement of discharge capacity and durability of the nickel hydroxide material.[135] In following studies, Delmas *et al.*[136;137] confirmed the structural defects proposed by Wronski *et al.*[135]The XRD patterns of nickel

hydroxide powders were simulated by considering two types of faults in the material: growth and deformation faults. In nickel hydroxide the oxygen packing is considered to be ABAB type packing where the oxygen layers tend to be exactly above or below each other. Growth faults are defects that lead to the formation of face centered cubic blocks, which leads to an ABC type packing within the normal ABAB oxygen packing. Deformation faults lead to the growth of face centered cubic and non-close packing (AA) blocks. By adding certain percentages of deformation and stacking faults to their XRD simulation program, they were able to reproduce a pattern similar to the experimental ones. [136;137]

When nickel hydroxide is charged β(III)-Ni(OOH) is formed. This material resembles β-$Ni(OH)_2$ with the disintercalation of one proton and the loss of one electron. β(III)-Ni(OOH) crystallizes in the hexagonal system having lattice parameters of a = 2.82 Å and c = 4.85 Å.[132] The oxidation state of nickel in this material is +3. During conditions of overcharge, high charge or discharge rates, γ-Ni(OOH) is formed. During this process, alkaline ions and water molecules are intercalated between the layers and the interslab spacing increases to 6.9 Å. The lamellar layers are of the same composition as β(III)-Ni(OOH).[132] Nickel is found in the +3 and + 4 oxidation state[138] and the general formula can be considered as γ-$H_xK_yNiO_2 \cdot zH_2O$. The lattice parameters of the gamma phase are a = 2.82 Å, and c = 21 Å (having a triple unit cell with each layer having an interlammelar spacing of 7 Å).[132]

Upon discharging the gamma phase, the α-$Ni(OH)_2$ phase is formed. This material has been described as having equally distant layers of nickel hydroxide that are parallel but randomly oriented in the a and b plane (turbostratic) with water molecules found in the interlayer

region.[131;132] This phase has the following lattice parameters: c = 7.6-8.5 Å and a = 3.08Å. α-Ni(OH) and is known to be unstable in alkali becoming β-$Ni(OH)_2$.

The materials that are formed during the cycling of nickel hydroxide are difficult to characterize because there is often more than one phase present during cycling, the phases are often nearly amorphous, and because of the harsh conditions found in the cells due to the electrolyte (often KOH $\geq$ 6M). In consequence increasing the performance of the material is also a difficult task. Furthermore, to understand the phenomena involving nickel hydroxide during cycling, researchers often synthesize similar materials separately outside the cells and frequently the obtained materials are similar but not exactly the same as the ones formed during cycling of the cells. There has been extensive research performed on the understanding and the optimization of the nickel hydroxide electrode. Much of the work focused on the structural characterization of the different polymorphs obtained during cycling of the nickel hydroxide using a panoply of characterization techniques such as: XRD,[132;139] IR,[132;137;139;140] Inelastic Neutron Scattering Spectroscopy,[129] EXAFS[130] and X-ray Absorption Spectroscopy.[138] Engineering aspects of the active material such as particle size and shape of the nickel hydroxide,[141] adding defects to β-$Ni(OH)_2$ by milling[135] in addition to the method in which the active material is inserted in the electrode support[94;142-144] have also been studied. The following review of the literature will mostly focus on the uses of layered double hydroxides as the active material for the positive electrode.

2.1.7.2 Layered Double Hydroxides as Battery Material

Cobalt was the first transition metal considered for doping nickel hydroxide and has been known to enhance the properties of the nickel hydroxide electrode since the beginning of the century. In the late 80s' and early 90s', the addition of Co to the nickel hydroxide electrode has been studied extensively. Much of the earlier work dealt with the influence of Co on the β(II) phase[145;146] however, later work dealt with the formation of a stable alpha phase due to the addition of cobalt. The goal of the work was not only to stabilize the alpha phase but also to synthesize a material with smaller particle size, which has better electrochemical properties. Delmas *et al.*[147] synthesized what he denominated $\alpha^{\bullet}$, α and $\alpha^{\cdot}$ phases and considered them as LDHs. The denomination used by Delmas *et al.* will therefore be kept in the following text to minimize confusion and to differentiate between the different types of materials. The $\alpha^{\bullet}$ phase was prepared by so called "chimie douce" techniques and exhibited large particle sizes. The "chimie douce" technique involves the oxidizing hydrolysis of a sodium nickelate ($NaM_xNi_{1-x}O_2$ where $M=Co^{3+}$ or Fe^{3+}) phase into the gamma phase followed by the reduction of the latter phase to form the $\alpha^{\bullet}$ phase. Delmas defines the reaction as "chimie douce" because of the low temperature reactions that are involved (room temperature) and the structure of the final product resembles the structure of the starting material.[148] The $\alpha^{\cdot}$ was prepared by coprecipitation of the β(II) phase, followed by the oxidation to the gamma phase and reduction to the $\alpha^{\cdot}$, which exhibited small particle size and was a very crystalline material. The α phase was obtained from coprecipitation and gave a turbostratic material with very small particles. All of these materials were characterized by IR, chemical analysis and were cycled in a battery. One of the initial studies involved the synthesis of an $\alpha^{\bullet}$ hydrated phase that showed stability in KOH when at least 20% of cobalt

was substituted for nickel.[149;150] However, this material had large particle sizes (D = 10^4 Å and H = 10^3 Å: where D is the diameter and H the height of the particle along the a and c axis respectively[147]). Later, cobalt substituted α phases with different anions (carbonate and sulfate) were synthesized with cobalt substitution in the 20% to 55% ranges.[151] The research revealed that the material having cobalt in the +3 valence was stable in 5 N KOH when at least 20% of the nickel was substituted by cobalt. However, alpha-Co^{2+} phases that were synthesized were unstable in KOH regardless of the concentration of cobalt. They also determined by iodometric titration that the oxidation state of Ni varied with the cobalt content of the material in the range of 2+x, where x is the weight % of cobalt. Furthermore, during long exposure to 5N KOH the sulfate anions were replaced by carbonates in any of the sulfate containing alpha phases. They were able to determine the particle size of the α phase only after long-term exposure to the alkali solution, given that the particles increased in size when immersed in KOH (via a dissolution recrystalization process).[151] The size of the particles were determined to be D = 80 Å and H = 50 Å. The α phases were then tested as electrode material and a maximum of 1.3 electrons per (Ni+Co) atom was exchanged (NEE) when 20% of cobalt was substituted for nickel.[111] The theoretical number of exchanged electrons was reported to be [3.5-(2+x)] e^- per (Ni+Co), where 3.5 was the oxidation state of nickel in the γ phase at the end of the charge process (as determined in an earlier study [152]), 2+x was the oxidation state in the alpha phase and x was the % of cobalt in the material. The material also exhibited a lower discharge potential than the regular β(II)-$Ni(OH)_2$. However, on long-term cycling, the NEE decreased for all the alpha materials tested. Preliminary experiments showed that this was due to the low discharge voltage used during discharging which reduced the cobalt from the +3 valence to the + 2 valence. Once in the +2 state the alpha Co^{2+} would then revert to β(II)-$Ni(OH)_2$ and lower the capacity of electrode.

Nickel iron LDHs have also been studied. Delmas *et al.*[148] have synthesized α–$Ni(OH)_2$ with iron substituting the nickel atoms. This was done since the Fe^{3+} oxidation state was more stable than the Co^{3+}. They hoped to stabilize the α–γ cycle using iron instead of cobalt. The NiFe materials exhibited lower capacities than the homologous nickel cobalt α phases and higher charge and discharge potentials. The lower capacities were attributed to the higher charge potential of the NiFe LDH. The potential was in the range of oxygen evolution. Therefore, during charging, the current was used to hydrolyze water instead of charging the material. They explained that the higher potential was due to the change in Fermi level of the positive electrode. The potential of a cell is equal to the difference between the Fermi levels of the electrodes (highest occupied molecular orbital). The Fermi level of the positive electrode was affected by the decrease of the energy of the Madelung constant (which is one of its' main affecting parameters) due to the larger size of the iron cation.[153] Other studies on nickel iron LDHs have shown the same results. A study on NiFe LDHs prepared by electrosynthesis, reported by Kamath *et al.*[96] showed that these materials catalyzed the oxygen evolution reaction and could possibly be used as electrodes for water hydrolysis.

Cobalt aluminum and cobalt iron LDHs are other examples of LDHs that have been studied in the literature.[154] Cobalt hydroxide was not normally used as an electrode material because of its irreversibility when used as a positive electrode. Bauer *et al.*[154] reported the synthesis of β-$Co(OH)_2$ doped with Al and Fe (with a 4:1 $Co:M^{3+}$ ratio) that formed LDHs. These LDHs were synthesized with either carbonates or sulfates as the interlayer anions and were then cycled. The CoAl sulfate containing LDH obtained the highest capacity having a maximum capacity of 85 mAh/g. This translated into having only a maximum of 1.1

electrons exchanged per cobalt atom. The reversibility was associated to the change of symmetry of cobalt due to the doping of the M^{3+} atom allowing forbidden electronic transition of Co to occur.

The electrochemical behaviors of manganese substituted nickel hydroxides, which are strongly related to LDHs, were also studied.[155] The long-term stability (up to 120 cycles) of these materials was associated to the small difference in the interlayer distance between the gamma and so-called I_E phase. The I_E phase was identified as being a mixture of α and γ phases, which developed as a result of the formation of the Mn^{4+} when the NiMn material was aged in KOH. The Mn^{4+} preferred remaining in the γ type structure. The maximum number of exchanged electrons (~1.1 electrons/(Ni+Mn) atoms) for this material was obtained when the concentration of manganese was at $x = 0.05$ and 0.1 (i.e. 5% and 10% substitution of manganese for nickel).

NiAl LDHs have also been studied as possible electrode material for the positive electrode of NiCd and NiMH batteries. Ehlsissen *et al.*[30] was one of the first to report the testing of the NiAl LDHs. They reported the stability of a series of NiAl LDHs with varying Ni:Al ratios in 8 M KOH in view of their potential application for electrode material. They showed that at least 20% Al substitution of nickel was needed to stabilize the LDH for long-term stability in the alkali solution. Furthermore, they showed that the material became more crystalline when exposed to the 8M KOH (via a dissolution recrystallization process) and that the original anions were replaced with carbonate. However, no electrochemical results of materials were reported. An electrochemistry study by Kamath *et al.*[156] on NiAl LDHs also showed similar stability results. In this study, they tested a NiAl LDH containing 20% aluminum and

obtained a specific capacity of 240 mAh/g but only 20 cycles were reported. These results were higher than the capacity of β-$Ni(OH)_2$ and a cobalt doped β-$Ni(OH)_2$ prepared in the same fashion. Recently, the study of a nickel aluminum LDH with 20% Al has been reported in which they obtained a capacity of 340 mAh/g and showed with a cyclic voltametry study that the material is easier to charge.[157] Another recent study has shown that a crystalline NiAl LDH attained a higher capacity than a poorly crystallized one. In this article, a capacity of 381 mAh/g was obtained for the most crystalline material. The lower capacity of the poorly crystallized material was attributed to its large polarization (i.e high charge potential and low discharge potential). It was proposed that this polarization was caused by the hindrance of the diffusion of protons due to an excess of anions in the interlayers. The excess quantity of anions was a result of OH deficiencies in the material.[158]

2.1.8 Basis for research

The main impetus for using LDHs containing nickel as electrode material is that they are isostructural to α-$Ni(OH)_2$ (both materials contain layers of nickel hydroxide with edge sharing hydroxide octahedra, they also contain interlayer water molecules and have approximately the same interlayer spacing) and should allow cycling between the alpha and gamma phase. The advantage of cycling between the alpha and the gamma phase, is the possibility of exchanging up to 1.6 electrons as compared to only one electron when cycling in between the β(II) and β(III) phases. Furthermore, cycling between the alpha and gamma phase would diminish the deformation and irreversible damage that is caused to the electrode upon the transformation from the β(III) to the γ(III) to the α and back to the β(II) phase.

In this study, LDHs of nickel aluminum and LDHs of nickel vanadium of varying M(II) to M(III) ratios have been investigated. NiAl was chosen because previous work has shown it to be a promising candidate for the positive electrode in Ni-Cd and NiMH[30;96;157] batteries. NiV LDH was chosen because vanadium is known to have high oxidation states; therefore, it might be possible to access these oxidation states to increase the number of exchanged electrons during the cycling process.

2.2 EXPERIMENTAL

2.2.1. Synthesis of the NiAl and the NiV LDHs

The preparation of the LDHs was performed under a nitrogen atmosphere to minimize carbonate contamination. Distilled water was deionised to 18.3 MΩ/cm in resistivity through a Barnstead B-pure deioniser and then was boiled (refluxed) under nitrogen for at least a day before being used for the LDHs synthesis. The pH values for the LDH synthesis were measured with a VWR scientific model 2000 pH meter fitted with a VWR low maintenance Triode pH electrode with Ag/AgCl internal reference system, sealed reference and built in thermistor for automatic temperature compensation. The pH meter was always calibrated with a pH 7 and pH 10 buffer prior to any measurements. Reagents used were from commercial sources. Two types of LDHs, NiAl and NiV, were synthesized with three different M(II):M(III) ratios for the NiAl LDH and two different ratios for the NiV LDH which are shown below:

NiAl = 2:1, 5:1, 9:1

NiV = 2:1, 5:1

The synthesis of NiV LDH with a 9:1 ratio was attempted but $Ni(OH)_2$ was obtained. Ni_2Al and Ni_5Al LDHs were synthesized using the method of Wang *et al.*[81] A mixture consisting of $Ni(NO_3)_2 \cdot 6H_2O$ (58.16 g, 0.20 moles, Aldrich 99.1 %) and of $Al(NO_3)_3 \cdot 9H_2O$ (37.51 g, 0.10 moles, Aldrich 98+ %) in 300 ml of freshly boiled deionised water was added together with a 2 M NaOH (BDH 98 %) solution (~200 ml), to a flask containing 150 ml of deionised water. Rapid stirring was kept throughout the addition and the rate of addition was such that the pH was kept at 10±0.5. After the addition was completed, the mixture was heated at ~75-80°C for 16 hrs under N_2. It was then filtered, washed with water then dried at 70°C for 24hrs. Ni_5Al was prepared in the same fashion but the nickel and aluminum nitrates were weighed to obtain the appropriate molecular ratios.

The Ni_9Al LDH was prepared using the method of Kamath *et al.*[156] as it was impossible to obtain such a low aluminum ratio using the Wang *et al.*[81] method. A mixed metal nitrate solution (210 mL) of $Ni(NO_3)_2.6H_2O$ (21.99 g, 0.076 moles, Aldrich 99.1%) and of $Al(NO_3)_3 \cdot 9H_2O$ (3.15g, 0.0084 moles, Aldrich 98+ %) was added drop-wise (~3 mL/min) to 210 mL solution of NaOH (8.4 g, 0.21 moles, BDH 98.0 %) containing sodium carbonate (3.00 g, 0.28 moles, Aldrich 99.5+ %) at 35°C. The mixture was heated at 65°C for ~16 hrs and was filtered with large amounts of water until a neutral pH was obtained. The sample was dried at 65°C for 24 hrs. All the samples were ground in a mortar and pestle until a fine powder was obtained.

Ni_2V and Ni_5V LDHs were obtained using a modified version of the Rives method.[56] Preparation was performed under a nitrogen atmosphere. A 200 mL solution containing $NiCl_2 \cdot 6H_2O$ (47.54g, 0.20 moles, Aldrich 97.2 %) and VCl_3 (15.79g, 0.10 moles, Aldrich

98.1 %) was added drop wise to 250 mL of a Na_2CO_3 (21.19g, 0.20 moles, Aldrich 99.5+ %) and NaOH (28g, 0.7 moles, BDH 98.0 %) solution at room temperature. The solution was stirred for ~2 hrs then the volume was reduced to ca. 50%. It was filtered hot and washed with water until no Cl^- was detected. The samples were dried in air at room temperature (20-25°C).

2.2.2 Characterization

2.2.2.1 Powder X-ray diffraction

The powder X-ray diffraction patterns reported in Chapter 2 were obtained using a Philips PW3710 diffractometer with Cu-Kα radiation at a wavelength of $\lambda = 1.54059$ Å. A voltage of 45 kV and a current of 40 mA were used to record the patterns. The samples were run in a range from 2θ : 8° to 72°. The samples were prepared in the following fashion unless stated otherwise: 50 mg of the sample was added to 1 mL of acetone. The mixture was sonicated for ~ 30 seconds to form a slurry and was transferred, using a Pasteur pipette, on a zero background silicon disk and left to dry. The disk was mounted in the diffractometer and analysed. This technique gave samples that were in a preferred orientation.

2.2.2.2 Elemental Analysis

Elemental analyses of the samples were carried out on a Jarrell Ash Atom Scan model inductively coupled plasma emission spectrometer (ICPES) after dissolution in a 2:5 V/V mixture of nitric and hydrochloric acid.

HNO_3 (2 mL conc.) was added to 0.1000 to 0.2000 grams of sample. The mixture was swirled and heated at 90°C for ~ 10 minutes. HCl (5 mL conc.) was then added in 3 portions of 2,2 and 1 mL. The samples were heated for an extra 20 minutes and 5 mL of deionised water was added followed by a dilution in a 50 mL volumetric flask with deionised water.

2.2.2.3 Carbon, Hydrogen, and Nitrogen elemental analysis

Carbon, Hydrogen, and Nitrogen elemental analysis were done on a Perkin Elmer Series II CHNS/O 2400 elemental analyser (EA). 1.5 to 2.5 mg of sample is weighed accurately in a small tin capsule, using a microbalance. The capsule is introduced in the analyser's furnace (combustion tube), and oxidized in a pure oxygen environment at a temperature of 950°C. At this temperature, the tin capsule combusts and forms tin oxide. This combustion elevates the temperature to well above 1800°C. The sample is vaporised and undergoes complete combustion, to form CO_2, N_2, N_xO_y, H_2O and other by-products. Undesirable by-products such as halogens, sulphur, and phosphorus, etc. are removed by 'scrubbing' chemicals inside the combustion tube. After combustion, the sample gases flow through a reduction tube, which removes any unused oxygen, and converts oxides of nitrogen to N_2. These gases are then homogenised at a precise temperature, pressure and volume in the mixing area. A small

portion of this mixture, from the sample volume, then flows through a series of thermal conductivity cells (the detector), where the quantity of each gas, CO_2, H_2O, N_2 and He carrier gas, is recorded. From these readings, and the weight of sample used it is possible to calculate %C, %H, %N.

2.2.2.4 Infrared spectra

Infrared spectra were recorded using a Bomem MB-100 model Fourier Transform-infrared spectrometer (FT-IR). Specimens were tested in the form of KBr pellets. The samples (1 mg) were added to dry KBr (100 mg) in a mortar and pestle. The mixture was ground for a short period of time until thoroughly mixed. The mixture (50 mg) was pressed into a KBr pellet. The pellet was inserted in an IR holder and analysed.

2.2.2.5 Density measurements

The densities of the materials were determined with a Micromeritics multivolume model 1305 pycnometer. "The sample chamber with the sample present is first charged to a gas pressure of about 20 psig. Subsequent expansion of this gas charge into a second precisely measured volume, which previously was at the same temperature and at zero psig results in a second pressure, which becomes progressively smaller for larger samples. Application of mass balance equations for the gas permits easy computation of the sample volume when the sample volumes of the empty sample chamber and expansion chamber are known and the pressure drop ratio upon expansion is known." [159]

2.2.2.5.1 Volume and density calculation

To calculate the volume of a sample the following equation is used:

$$V_{samp} = V_{cell} - V_{exp}/[(P_1/P_2) - 1] \quad (1)$$

Where

V_{samp} = The volume to be found.

V_{cell} = The empty volume of the sample cell with the empty cup in place.

V_{exp} = The volume of the expansion cell.

P_1 = The measured initial pressure.

P_2 = The final measured pressure when the valve is opened an the gas has expanded into the expansion cell.

The density of the sample is calculated by dividing the weight of the sample by the volume obtained with (1).

2.2.3 Stability testing of the LDHs in 6M KOH

LDHs were immersed in 6 M KOH at room temperature and were analyzed by XRD and IR over a period of time up to a maximum of one and a half months. For these tests, 0.5g of material was immersed in 50 mL of 6 M KOH. The samples were removed at predetermined

intervals rinsed with water until neutral pH, dried, and portions of them were analyzed by XRD and IR. The materials were then reimmersed into a freshly prepared solution of 6N KOH after the analysis.

2.2.4 Electrode Testing

2.2.4.1 Half Cell Fabrication

In this study, pasted electrodes were fabricated from the NiAl, NiV LDHs and the commercial battery grade $Ni(OH)_2$ powder and tested in half-cells with a nickel counter electrode used as the negative electrode. Half-cell preparation is as follows. For each electrode the LDH or $Ni(OH)_2$ powder was mixed with Ni extra fine filamentary powder, (Inco, type 210), Co powder, water and polyvinyl alcohol (used as a binder), and then mixed to create a paste. (The cobalt and nickel filamentary powder were added to increase the conductivity of the electrode.) A porous nickel foam (INCOFOAM 98% porosity) substrate, cut to dimensions of 4 by 12 cm and 8 mm thick, was manually filled with the current conducting paste using a spatula and dried at 100°C for 1 h. This method of incorporation of the active material is based on the latest technology of pasted electrodes and is used in the laboratories of Mines and Resources Canada (CANMET).[160] The pasted foam was rolled (calendered) into a 0.75 mm thick strip from which three circular electrodes were punched. Nickel wires were then spot-welded on the electrodes. The newly prepared electrodes were inserted into a polypropylene battery grade material felt pocket that serves as a membrane. The felt pocket also diminishes the loss of material when the electrode is immersed in the electrolyte. The main insulator/spacer between the positive and negative electrodes are two

square grid nylon plastics inserted between the positive electrode and the counter electrode. This is accomplished to eliminate the possibility of a short circuit during the cycling process. The nylon grid also helps in the release of gases that would form during the cycling of the batteries. Finally, the cell's electrodes are held tightly in place using paper clamps and are then introduced into a beaker to which 100 ml solution of KOH (30%) and LiOH(1%) is added as electrolyte. The cell is connected to a computer controlled multichannel galvanostat/potentiostat cycling unit (Arbin Instruments, College station TX.) by attaching the alligator clips of the power cables from the cycling unit to the electrode's wires. The cycling is then performed at room temperature (20-25°C)

2.2.4.2 Description of the Canmet multi-channel potentiostat /galvanostat cycling unit

The electrochemical testing of the electrodes (cycling; charging and discharging of electrodes) is accomplished by using an Arbin Multi-channel/multi-electrode galvanostat/ potentiostat cycling apparatus. (Arbin instruments, College station, Texas). This unit is designed to perform low power tests on single cells or small batteries with a voltage range of –4 to +5 volts and 3 current ranges of 2 amps, 100 milliamps and 10 milliamps. This unit has 36 channels that can be used simultaneously allowing 36 independent cells to be tested at the same time. Each channel is monitored and controlled through a 16-bit A/D converter, yielding a very good accuracy. An IBM-compatible computer controls the cycling unit. Software that contains "schedules" provides the required instructions and parameters to perform a test of a cell on each individual channel. Schedules are modular programs with subroutines that are called steps. The steps are complete sets of instructions that direct the

charging and discharging processes. They can be programmed to charge or discharge a cell by controlling the current, the voltage, the load or the power, and measure several parameters at once.

2.2.4.3 Cycling profile

The tables 2.1 to 2.4 give the cycling conditions used for testing the NiAl, NiV LDHs and the reference β-$Ni(OH)_2$ powders. All the electrodes were soaked 24 hrs in the KOH before the activation charge and discharge steps. These steps consist of charging the material for 35.6 hours at a rate that is 20 times less than the regular discharge and discharged for 8.1 hours at a rate that is 10 times less than a regular discharge. The electrodes were then charged (regular charge) at the rates shown in the tables below for 4.0 hrs followed by a regular discharge for 45 minutes. There was always a one-minute rest period between a charge and a discharge cycle. In addition, every ten cycles the electrodes were discharged at a slower rate (slow discharge = 5 times less than a regular discharge). The commercial nickel hydroxide had its first slow discharge at cycle 17 and then every following ten cycles. The LDHs had their first slow discharge at cycle 10 and then every following ten cycles. It has been recognized that this profile was used because it was an optimized cycling profile for the commercial nickel hydroxide. However, the optimal cycling profile for testing LDHs may require different charging or discharging routes

Table 2.1: Loading of the active material in the electrodes

Electrode #	Material	Loading(g LDH/β-$Ni(OH)_2$)
OH030A	$Ni(OH)_2$ commercial	1.2354
OH030C	$Ni(OH)_2$ commercial	1.2200
OH175A	Ni_2Al LDH	0.6234
OH175C	Ni_2Al LDH	0.6469
OH169A	Ni_5Al LDH	0.8609
OH169B	Ni_5Al LDH	0.7747
OH176A	Ni_9Al LDH	0.9185
OH176C	Ni_9Al LDH	0.9100
OH178A	Ni_2V LDH	0.7134
OH178C	Ni_2V LDH	0.6933
OH168A	Ni_5V LDH	0.8394
OH168B	Ni_5V LDH	0.8400

Table 2.2: Charge and discharge rates (Ah) of the commercial nickel hydroxide

Electrode name	OH030A	OH030C
Activation charge (C/20)	0.0179	0.0176
Activation discharge (C/10)	0.0357	0.0353
Regular charge (C/4)	0.0893	0.0881
Regular discharge (C)	0.357	0.353
Slow discharge (C/5)	0.0714	0.0705

Table 2.3: Charge and discharge rates (Ah) of the NiAl LDHs

Electrode name/ LDH	OH175A Ni_2Al	OH175C Ni_2Al	OH169A Ni_5Al	OH169B Ni_5Al	OH176A Ni_9Al	OH176C Ni_9Al
Activation charge	0.00901	0.00935	0.0118	0.0124	0.0133	0.0132
Activation discharge	0.0180	0.0187	0.0236	0.0249	0.0265	0.0263
Regular charge	0.0450	0.0467	0.0590	0.0622	0.0664	0.0658
Regular discharge	0.180	0.187	0.236	0.249	0.265	0.263
Slow discharge	0.0360	0.0374	0.0472	0.0498	0.0531	0.0526

Table 2.4: Charge and discharge rates (Ah) of the NiV LDHs

Electrode name/ LDH	OH168A Ni_2V	OH168B Ni_2V	OH178A Ni_5V	OH178B Ni_5V
Activation Charge	0.0103	0.0100	0.0121	0.0121
Activation discharge	0.0206	0.0200	0.0243	0.0243
Regular charge	0.0515	0.0501	0.0606	0.0607
Regular discharge	0.206	0.200	0.243	0.243
Slow discharge	0.0412	0.0401	0.0485	0.0486

2.3 RESULTS AND DISCUSSION

2.3.1 Elemental and ICP analysis of the LDHs

Table 2.5: Elemental analysis and ICPES data

M(II)/MIII) atomic ratio[1]	Elements	Calculated Weight %	Exp. Weight %	Molecular formula
Ni_2Al	Ni	35.3	34.1	$Ni_{0.67}Al_{0.33}(OH)_2(NO_3)_{0.20}(CO_3)_{0.07}\bullet 0.7H_2O$
	Al	8.09	7.87	
	H	3.09	3.10	
	N	2.51	2.60	
	C	0.72	0.75	
Ni_5Al	Ni	44.8	44.6	$Ni_{0.84}Al_{0.16}(OH)_2(NO_3)_{0.16}\bullet 0.6H_2O$
	Al	3.89	3.90	
	H	2.93	2.88	
	N	2.02	2.03	
Ni_9Al	Ni	51.6	45.7	$Ni_{0.90}Al_{0.10}(OH)_2(NO_3)_{0.02}(CO_3)_{0.04}\bullet 0.5H_2O$
	Al	2.64	2.40	
	H	2.90	2.27	
	C	0.48	1.01	
	N	0.24	0.51	
Ni_2V	Ni	29.9	28.7	$Ni_{0.69}V_{0.31}(OH)_2(CO_3)_{0.16}\bullet 2(H_2O)$
	V	11.6	11.2	
	H	4.46	3.64	
	C	1.37	0.74	
Ni_5V	Ni	37.3	39.0	$Ni_{0.84}V_{0.16}(OH)_2(CO_3)_{0.08}\bullet 2H_2O$
	V	6.16	6.62	
	H	4.57	2.91	
	C	0.76	1.64	

Note: 1 Ratios rounded to the first decimal

Table 2.5 shows the experimental and calculated results obtained for each synthesized layered double hydroxide. The molecular formulas were calculated by using the general LDH equation shown below:

$Ni_{1-x}M(III)_x(OH)_2(NO_3^-)_{x/2}\ (CO_3^{2-})_{x/4}\bullet yH_2O$

Where M(III) = Al or V

The value of x was calculated from the Ni/Al or Ni/V ratio determined by the ICP analysis of the metals. The small deviation between the calculated and experimental results show that LDHs have been obtained.

2.3.2 XRD Data

Table 2.6: X-ray powder diffraction data for NiAl LDHs

M(II)/MIII) atomic ratio	x = Al/Al+Ni	hkl	d observed	Lattice Parameters	Takovite
Ni_2Al	0.33	003	8.49	a = 3.03	7.54
		006	4.24	c = 25.47	3.77
		101	Not observable		2.61
		012	2.61		2.55
		015	2.24		2.27
		018	1.95		1.92
		110	1.51		1.51
		113	Not observable		1.48
Ni_5Al	0.16	003	8.01	a= 3.08	
		006	4.00	c = 24.03	
		101	2.66		
		012	2.61		
		015	2.32		
		018	2.00		
		110	1.53		
		113	1.51		
Ni_9Al	0.11	003	7.81	a = 3.10	
		006	3.99	c = 23.43	
		101	Not observable		
		012	2.68		
		015	2.33		
		018	1.83		
		110	1.55		
		113	1.50		

The X-ray patterns obtained for the NiAl LDHs are characteristic of takovite, which is a naturally occurring NiAl layered double hydroxide containing carbonate in the interlayers (Takovite JCPDS 15-87). The interlayer spacing of the synthesized NiAl LDHs are larger than that of takovite as expected. Carbonate containing LDHs have smaller interlayer distances, because of the stronger electrostatic interaction of the divalent carbonate versus the monovalent nitrate.

The synthesized NiAl LDHs crystallize with rhombohedral symmetry [2] and the lattice parameters are $c = 3c'$ (where c' is the thickness of one layer which comprises one brucite like layer and one interlayer) and a which was indexed with the d_{001} reflection ($a= 2d_{110}$). The layer thickness was calculated from the average of the 003 and 006 reflections. All of these parameters are included in Table 2.6. We can note that there is a decrease in the a parameter as the aluminum content increases. The a parameter is related to the mean radius of the metals found in the layers of the LDH, and as the substitution of a metal with a smaller radius inside the layers increase, the a parameter decreases.[19] Therefore, since the radius of Al^{3+} is smaller than the radius of Ni^{2+}, the a parameter decreases with increasing content of Al^{3+} (or an increase of x) and this agrees with Vergard's law.[2] In addition, the reflections of the Ni_2Al and Ni_9Al LDHs are broader and more asymmetrical than those of the Ni_5Al LDH (Figure 2.8). This indicates that the stacking sequence of the two former LDHs is more disordered. Some authors refer to these types of materials as being turbostratic [132:156] where the plates of the layers are equidistant in the c axis but are randomly oriented in the a and b planes.

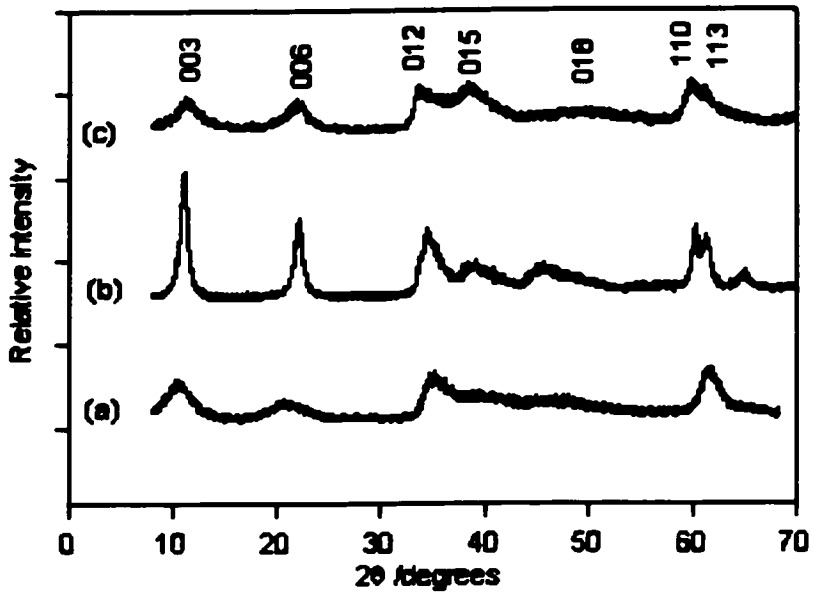

Figure 2.8 XRD patterns of a) Ni_2Al, b) Ni_5Al and c) Ni_9Al

The d spacing of the Ni_2Al and the Ni_5Al are similar to those quoted in the literature.[161] In addition, the c parameter increases with increasing aluminum content, which is also a trend, observed for nitrate containing LDHs.[161] This is due to the non-parallel orientation that the nitrates adopt as a result of the increased repulsion between anions as their quantity increases.[22] As for the Ni_9Al LDH, it has the smallest d spacing (7.81 Å). This sample was prepared using carbonates and therefore contains the highest carbonate concentration of all the NiAl LDHs. It is well known that carbonates have stronger electrostatic interaction than nitrates because of their higher negative charge, thus holding the positive metal layers closer together.

Table 2.7: X-ray powder diffraction data for NiV LDHs

Sample #/ M(II)/MIII) atomic ratio	X =V/V+Ni	Hkl	D observed	Lattice parameters
NiV02 Ni2V	0.310	003	7.58	a = 3.10 c = 22.74
		006	3.801	
		101	Not observable	
		012	2.57	
		015	2.35	
		018	1.96	
		110	1.55	
		113	1.50	
NiV04 Ni5V	0.164	003	7.76	a= 3.10 c = 24.03
		006	4.01	
		101	Not observable	
		012	2.65	
		015	2.32	
		018	Not observable	
		110	1.55	
		113	Not observable	

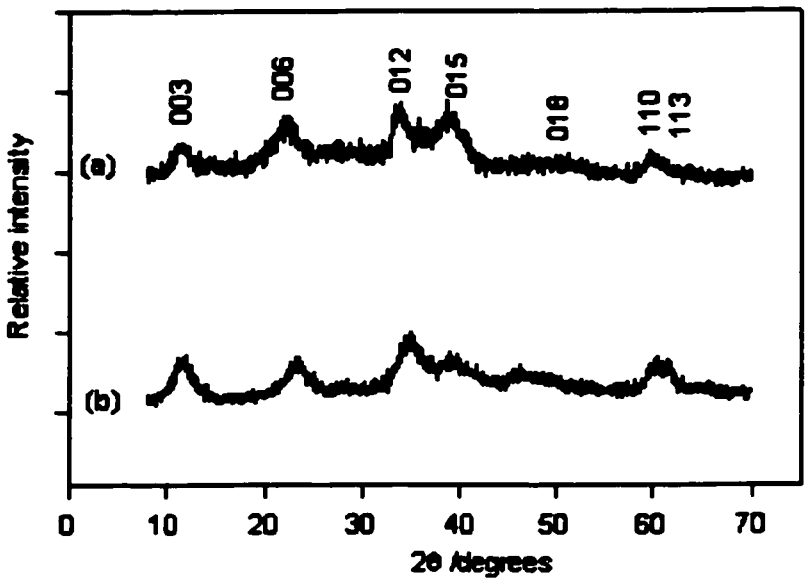

Figure 2.9 XRD patterns of a) Ni_2V and b) Ni_5V

The XRD reflections of both NiV LDHs are broad and asymmetrical indicating the turbostratic nature of these materials (Figure 2.9). These compounds were not hydrothermally treated for long periods of time, which resulted in lower crystallinity powders. The a and c parameters can be found in the last column of Table 2.7. These values were calculated in the same way as for the NiAl LDHs. In spite of the fact that the LDHs have different vanadium content, there is no observed difference for the a value. This is because the 110 peak is very broad for both samples and its exact value was difficult to determine. However, contrary to the NiAl LDHs, the d spacing decreases as the vanadium content increases as expected because there is higher carbonate content in the Ni_2V LDH. The higher carbonate content increases the electrostatic interaction between layers hence decreasing the spacing in between them.

2.3.3 IR Analysis

2.3.3.1 NiAl LDH

Figure 2.10 shows the infrared spectra of Ni_2Al, Ni_5Al and Ni_9Al. Each of these spectra are characteristic of layered double hydroxides compounds and contain the following absorption bands: [2] A broad peak centered at about 3500 cm^{-1} corresponding to the H bonding stretching vibrations of hydroxyl groups hydrogen bonded to water molecules. The H_2O bending vibration can be observed at 1630 cm^{-1}. The sharp and strong band at ~1380 cm^{-1} shows clearly the presence of the nitrate ion in a D_{3h} symmetry in each sample.[30] The shoulder at around 1360 cm^{-1} indicates the presence of carbonate ions (ν_3 CO_3^{2-}).

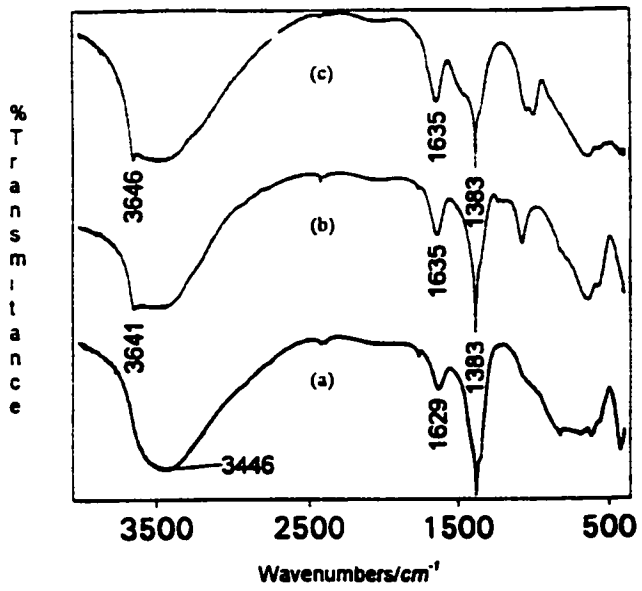

Figure 2.10 Infrared spectra of a) Ni_2Al, b) Ni_5Al and c) Ni_9Al

As shown by the elemental analyses and the sharp and strong band at ~1380 cm^{-1} in the IR spectrum, the predominant anion in the interlayer of the Ni_2Al LDH is the nitrate species. Despite the fact that the nitrate anion is the major interlayer species, there are still carbonate vibrations that are present in the infrared spectra such as the shoulder at 1360 cm^{-1} previously described and the small band at 692 cm^{-1} which is the ν_4 mode of the CO_3^{2-} anion.[27] In the range between 1200-400 cm^{-1} many structural lattice vibrations can be found. The sharp but small bands at 430 and 562 cm^{-1} are translational modes of oxygen in AlO_6 octahedra[162] and the band at 614 cm^{-1} is assigned to OH vibrations.[27] Finally, the sharp and small band at 825 cm^{-1} can be assigned to the ν_2 mode of the nitrate ion in a D_{3h} symmetry.[27]

For the Ni_5Al LDH, even if the carbonate concentration is small, the shoulder at ~1360 cm^{-1} indicates the presence of this ion and the band present at 1078 cm^{-1}, shows that carbonate is in a lower symmetry (C_{2v}). This band is normally inactive when the carbonate anion is in the D_{3h} symmetry.[2;27] Below 1200 cm^{-1} the AlO_6 translational modes of oxygen at 569 cm^{-1}, 430 cm^{-1} can be observed.[163] The band at 646 cm^{-1} has been assigned to the vibrations of OH groups. This band is normally observed at approximately 620 cm^{-1} but it has been known to shift to higher frequencies in NiAl LDHs.[163] The sharp band at 3641 cm^{-1} is characteristic of non hydrogen bound OH groups normally found in β-$Ni(OH)_2$.[140] This result signifies that there is a β-$Ni(OH)_2$ contamination in the sample. However, as the deviations between the experimental chemical analysis and the calculated values are low (<2%) the contamination is considered negligible (Table 2.5).

In the case of the Ni_9Al LDH the characteristic bands of nitrate in a C_{2v} symmetry are demonstrated by the shoulder at 1480 cm^{-1} and the band at 1001 cm^{-1}.[30] This LDH also

shows the carbonate ν_1 vibration mode at 1046 cm^{-1}.[27] The absorption bands observed in the region between 800 and 400 cm^{-1} can be assigned in the same manner as the previous LDHs. Furthermore, the sharp band at 3648 cm^{-1} associated to free OH groups of β-$Ni(OH)_2$ is larger than the one in Ni_5Al LDH thus indicating a larger amount of β-$Ni(OH)_2$ contamination in the sample. The larger discrepancy between the experimental and the chemical analysis corroborates this result (Table 1).

2.3.3.2 NiV LDH

The infrared spectra of the NiV LDH (Figure 2.11) are similar to the NiAl LDHs. However, the former were prepared from the metal chloride salts and precipitated in a bicarbonate solution. Therefore, only the carbonate anion can be found in the NiV LDHs since chloride was washed out of the precipitate during filtration. The elemental and the IR analysis both confirm this result (Table 2.5). In the spectra of Ni_5V LDH the ν_3 carbonate band at 1357 cm^{-1} can be observed, indicating the presence of only CO_3^{2-} anions in the interlayers with D_{3h} symmetry.[147] However in the spectra of Ni_5V the ν_3 mode exhibits a sharp band at 1360 cm^{-1} with a shoulder at ~1450 cm^{-1}. Furthermore, the carbonate ν_1 band at 1036 cm^{-1} is present. These bands are characteristic of carbonate with C_{2v} symmetry.[164] In addition, centred at approximately 3450 cm^{-1} the OH stretching band of hydrogen bonded hydroxyl groups and water molecules can be observed.[147] In the Ni_5V IR spectrum the sharp band at 3638 cm^{-1} can be observed and is due to non bonded OH groups and indicates the presence of β-$Ni(OH)_2$. The bands below 1000 cm^{-1} are associated with absorption bands due to metal oxygen vibrations and hydroxyl bending modes.

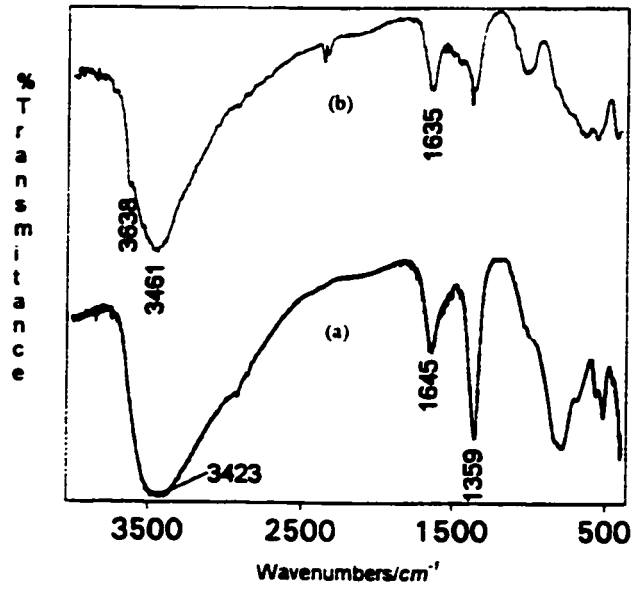

Figure 2.11 Infrared spectra of: a) Ni_2V and b) Ni_5V

2.3.4 Stability tests of the NiAl and NiV LDHs

To determine the stability of the NiAl and the NiV LDH in the caustic conditions found in alkaline batteries, the powders were immersed in KOH for varying amounts of time. They were analyzed to determine if any degradation occurred. The IR analysis was done to mainly determine if there was any change in the interlayer species. The XRD patterns of the LDHs are well established in the literature. Therefore, XRD analysis is a tool of choice to determine if there is any change in the crystalline structure of the material or if any degradation occurs.

2.3.4.1 NiAl LDH Stability Tests

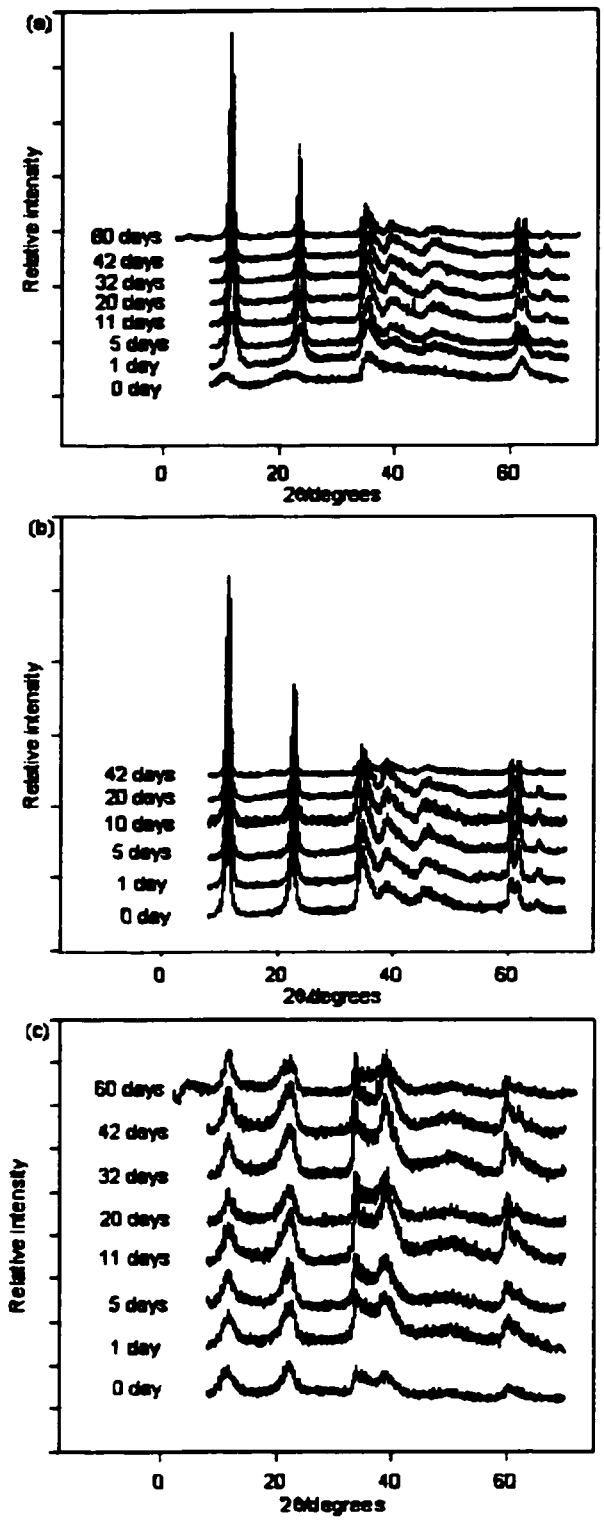

Figure 2.12 XRD patterns of the NiAl LDHs aged in 6M KOH: a) Ni_2Al, b) Ni_5Al and c) Ni_9Al

Figure 2.12 (a,b,c) shows the diffractograms obtained at different time intervals in KOH of the three different compositions of the NiAl LDHs (Ni_2Al, Ni_5Al, Ni_9Al). The broad lines of the XRD pattern of Ni_2Al at day 0 show that the original sample begins with a very low crystallinity. As immersion time in the KOH solution increases, the lines of the diffractograms become sharper. This indicates an increase in the crystallinity of the sample and confirms the results obtained by Elshissen *et al.*[30] where they reported that the LDHs become crystalline as they are aged in KOH. The increase in crystallinity can be explained by a mechanism involving dissolution and recrystallization processes. In addition, the d spacing is decreased from 8.48Å to 7.55Å, which is due to the replacement of the nitrate ions for the carbonate anions in the interlayer. This anion has stronger electrostatic interaction than the nitrate ion with the metal layers and hence reduces the interlayer spacing. The sample also shows no sign of degradation in KOH.

Figure 2.12 (b) shows the stability test of Ni_5Al. As the exposure time in the KOH solution progresses, the diffraction lines become sharper indicating an increase in the crystallinity of the LDH. However, this effect is not as pronounced as in the case of Ni_2Al LDH since the starting material is already more crystalline. Furthermore, with aging, the interlayer spacing does not decrease as much as the Ni_2Al LDH indicating that there is very little replacement of the interlayer nitrates by carbonates. Because Ni_5Al LDH has less aluminum than Ni_2Al LDH, the former has a lower positive charge in its hydroxide layers. Therefore, the carbonate anions would be less attracted inside the layers and this could possibly explain the slow replacement of the nitrate anions. For the length of the stability test there is also no apparent degradation of this compound.

Figure 2.12 (c) shows the stability test of the Ni_9Al LDH. Contrary to the literature there is seemingly no degradation of this compound even up to two months in the strong alkali (6M KOH). In addition, the peaks do not get sharper over time in the KOH indicating that there is no increase in crystallinity of the sample. It is stated that an aluminum content where $x>0.14$ is needed to stabilise the LDH in the alkali medium.[30;156] Otherwise, if the content is lower than this value, the LDHs are transformed into β-$Ni(OH)_2$ which is apparent by the appearance of a reflection at 4.6 Å after ageing. However, in the articles[30] where this is reported, the stability tests were done in 8 M KOH at 40°C and in 8 M KOH at room temperature (22°C to 28°C) respectively. In this study, as stated above, the LDHs were immersed in 6 M KOH. This condition is in line with the operating of practical sealed cells.

The comparison of the IR spectra of the non-aged Ni_2Al (Figure 2.13) to the aged material, reveals a change in the absorption bands of the anions. The disappearance of the nitrate band at 1380 cm^{-1}, which is replaced with the ν_3 absorption band of the carbonate ion at 1366 cm^{-1} clearly shows that there is the replacement of the nitrate ion for the carbonate ion even after only one day in the KOH solution. This result is consistent with those obtained in the literature for NiAl LDHs aged in KOH.[30] The appearance of the a shoulder at 3200 cm^{-1} further confirms this change as this is a result of hydrogen bonding between the carbonate ions and the interlayer water molecules.[31]

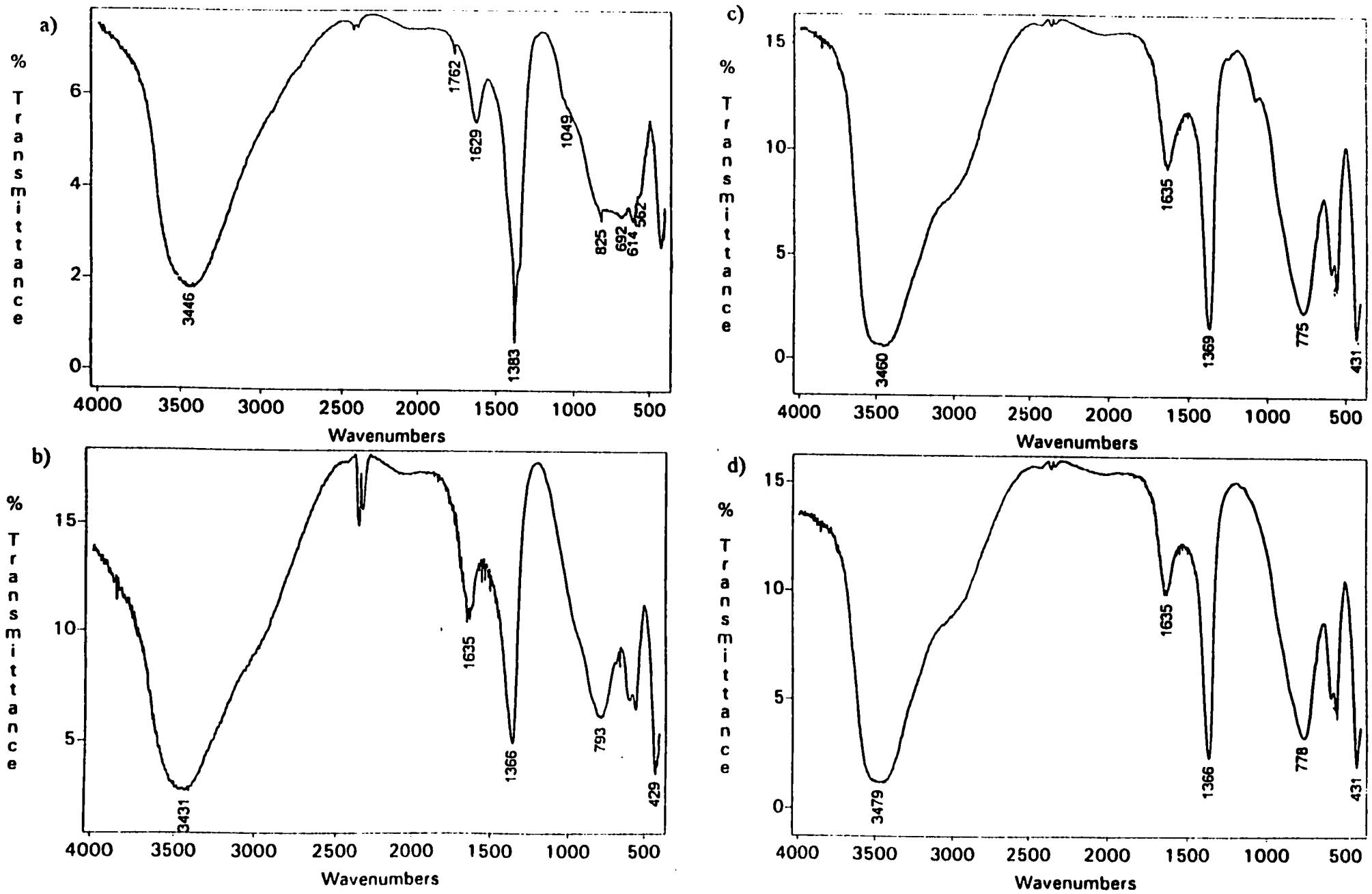

Figure 2.13 Infrared spectra of the Ni_2Al LDH aged in KOH a) 0 days, b) 1 day, c) 42 days and d) 60 days

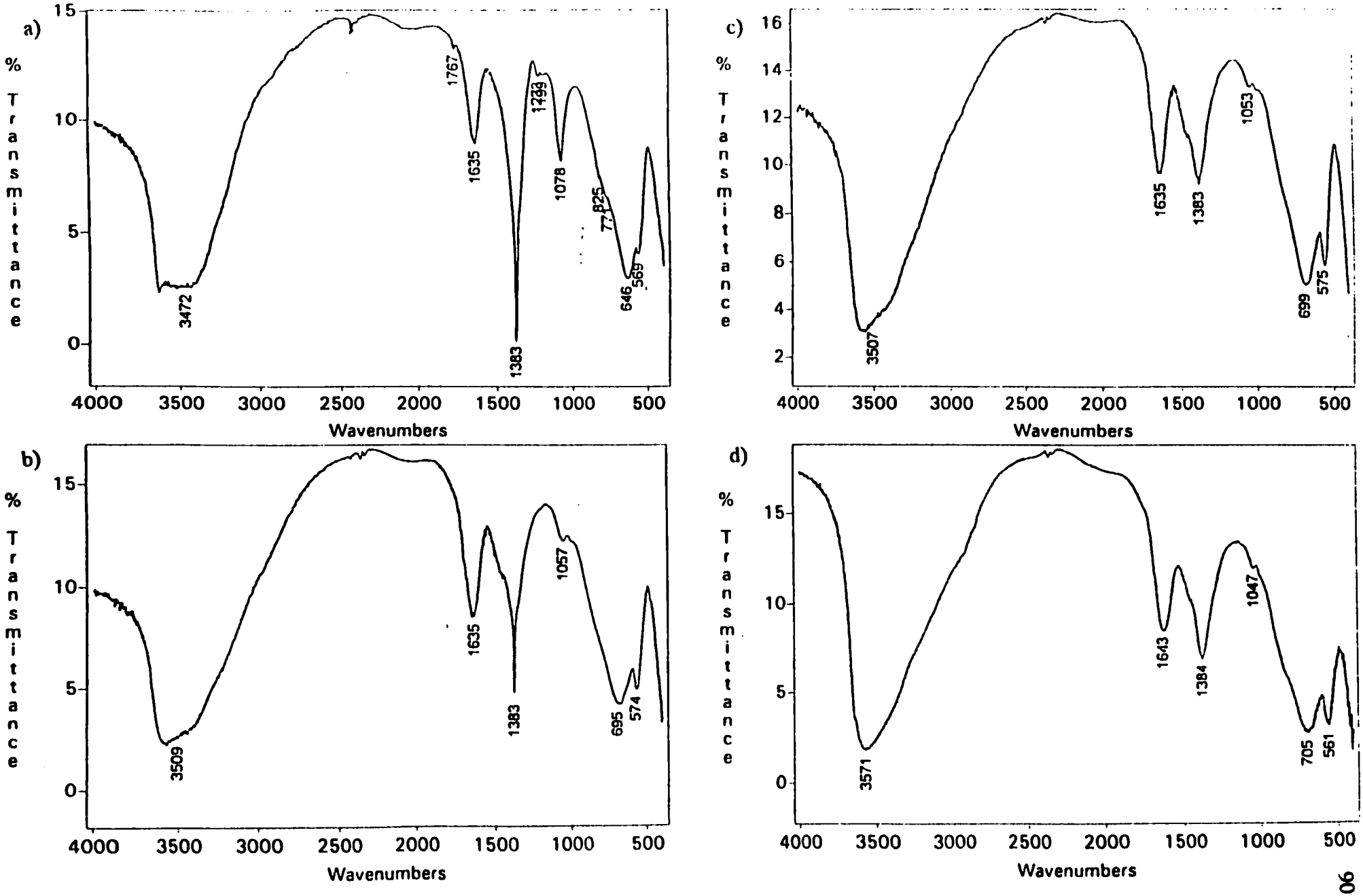

Figure 2.14 Infrared spectra of the Ni;Al LDH aged in KOH a) 0 days, b) 1 day, c) 42 days and d) 60 days

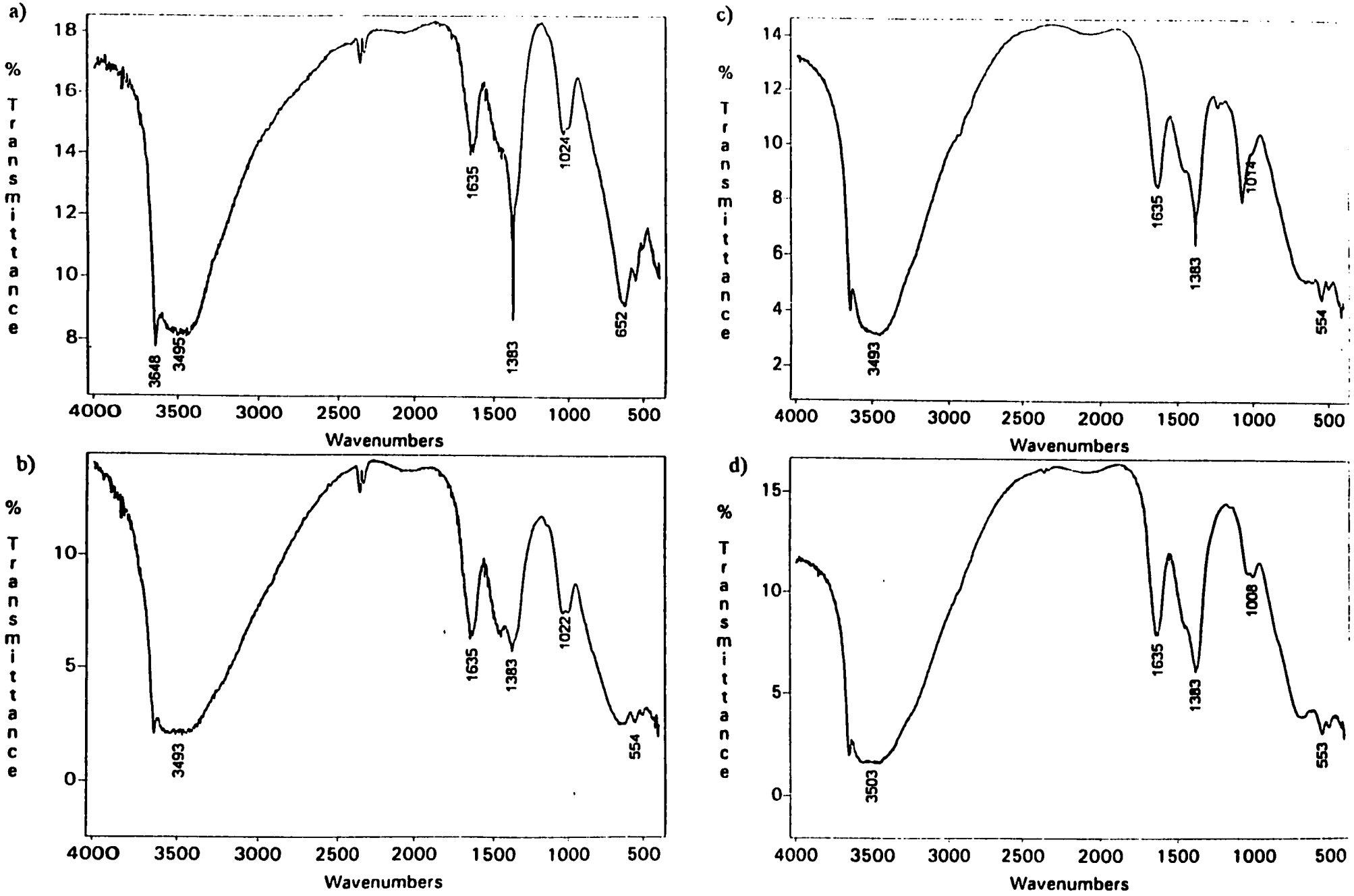

Figure 2.15 Infrared spectra of the Ni_6Al LDH aged in KOH a) 0 days, b) 1 day, c) 42 days and d) 60 days

Figure 2.14 shows the IR spectra of the Ni_5Al LDH before and after immersion in the KOH solution. The reduction of the band at 1383 cm^{-1} shows that carbonate is replacing nitrate in the interlayers. Nevertheless, the IR results obtained for the Ni_5Al LDH confirm those obtained by XRD. That is, the replacement of the nitrate ions by the carbonates is less pronounced than in the case of the Ni_2Al LDH. Even after 42 days of soaking in the KOH solution, the nitrate band at 1383 cm^{-1} is still apparent indicating the presence of this ion in the LDH.

The IR spectra of Ni_9Al LDH before and after ageing in the KOH solution are shown in Figure 2.15. The pattern of change in the absorption bands is similar to that observed in the Ni_5Al LDH. There is a reduction of the nitrate band after one day in the KOH solution signifying a replacement of the nitrate anions for the carbonate anions. However, the nitrate band is still apparent after 42 days in the KOH solution indicating the slow replacement of the nitrate ion. As previously mentioned, for both the Ni_5Al and The Ni_9Al LDHs the slow replacement of the nitrate anion in comparison to the fast replacement observed in the Ni_2Al LDH is plausibly due to the lower positive charge density in the layers of the former LDHs.

2.3.4.2 NiV LDHs Stability tests

The diffractograms of the stability test of Ni_2V are shown in Figure 2.16 (a). Contrary to the NiAl LDHs, Ni_2V is unstable after 14 days in the KOH solution. However, similarly to the NiAl LDHs, the vanadium containing LDHs also become more crystalline when immersed in KOH. This result is shown by the sharpening of the d_{003} and d_{006} reflections (Figure 2.16 (a)). Furthermore, between 14 and 34 days the XRD patterns reveal the appearance of two new reflections at 4.3Å and 2.7Å in addition to the disappearance of the d_{006} reflections of the LDH. This is an indication of the transformation of the LDH into β-$Ni(OH)_2$. The XRD pattern obtained after 40 days shows that the transformation can be considered complete, as the characteristic lines of the LDH have completely disappeared leaving behind the characteristic pattern of β-$Ni(OH)_2$. The β-$Ni(OH)_2$ phase was identified by comparing the diffractogram of the Ni_2V LDH exposed to KOH for 40 days with a diffractogram of β-$Ni(OH)_2$. We can conclude that the Ni_2V LDH is only stable up to 14 days in KOH 6M after which it starts to transform into β-$Ni(OH)_2$.

The diffractograms of Ni_5V LDH are found in Figure 2.16 (b). After only 5 days the diffraction lines of β-$Ni(OH)_2$ start appearing and the transformation is complete between 20 and 42 days. Since Ni_5V has less V^{3+} in the layers than Ni_2V there is less electrostatic interaction holding the layers together. Therefore, it was expected that Ni_5V LDH would be less stable than Ni_2V in KOH and the transformation into β-$Ni(OH)_2$ would be quicker.

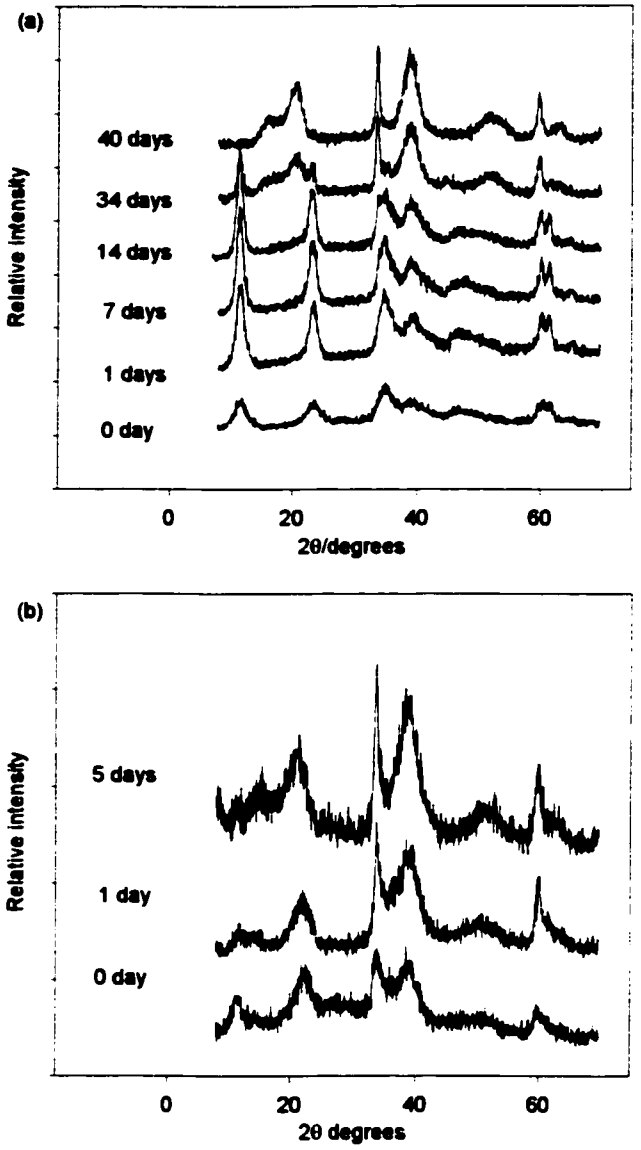

Figure 2.16 XRD patterns of the NiV LDHs aged in 6M KOH: a) Ni_2V and b) Ni_5V

The accrued stability of the NiAl LDH over the NiV LDH is most certainly because Al^{3+} has a larger charge over radius than V^{3+} (5.6 vs 4.7 respectively) allowing stronger electrostatic interaction in the layers.

2.3.5 Cycling Performance of the LDHs

2.3.5.1 Number of Exchanged Electrons (NEE)

Figures 2.17 and 2.18 show the number of exchanged electrons (NEE) per atom of nickel as a function of cycle number for the three NiAl LDHs and that of a commercial β-$Ni(OH)_2$ powder. Figure 2.17 shows 40 discharge/charge cycles of the electrodes and Figure 2.18 shows the long-term cycling of these electrodes (up to 500 cycles).

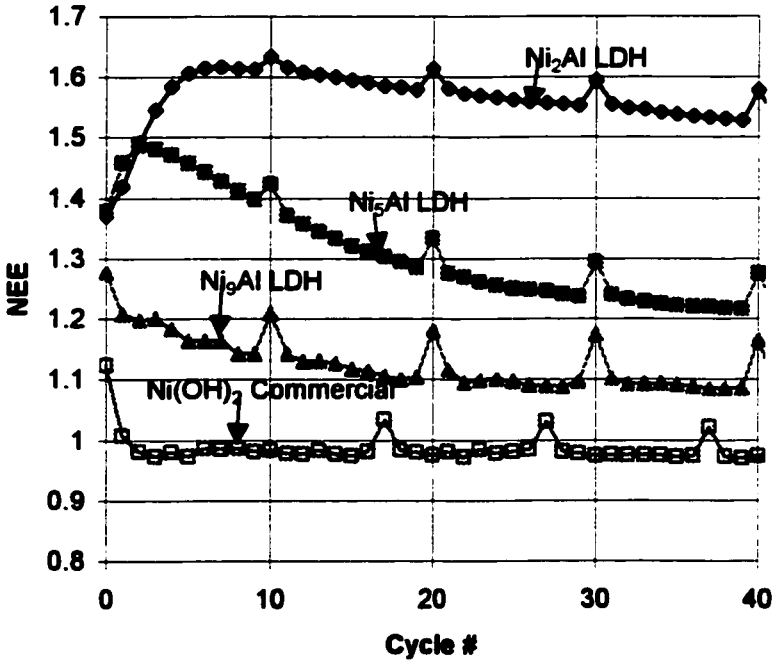

Figure 2.17 NEE of the NiAl LDHs and the commercial $Ni(OH)_2$ (short-term)

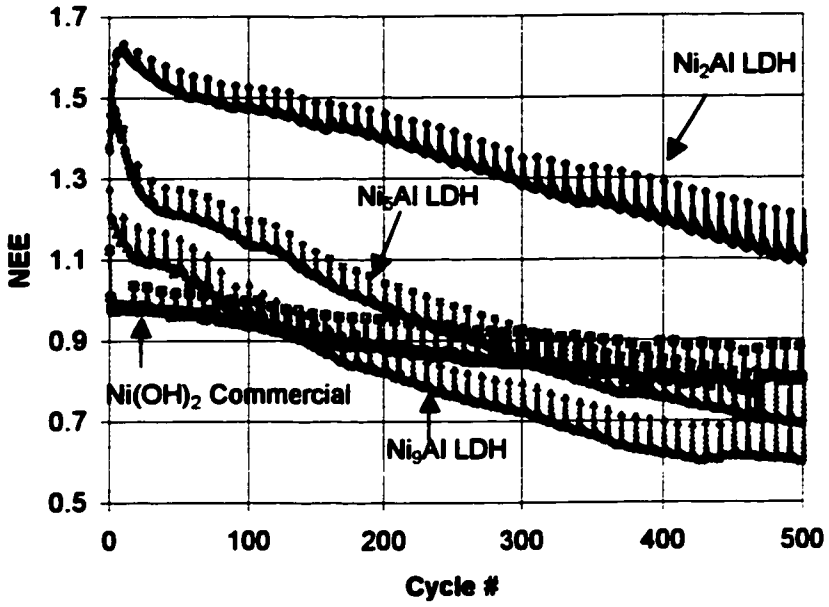

Figure 2.18 NEE of the NiAl LDHs and the commercial $Ni(OH)_2$ (long-term)

The NEE for each powder was calculated using the equations below:

$$nNi = (1g\ LDH\ X\ W\%\ Ni) / MM\ Ni$$

Where n is the number of moles of nickel per gram of LDH, W% is the weight percent of nickel in the LDH determined by ICP analysis and MM is the molecular mass of nickel. For a one electron process where nickel is cycled between the +2 and + 3 oxidation state the # moles Ni = # moles of electrons exchanged. Thus, the maximum gravimetric discharge capacity (C) in Ah per g LDH is equal to:

$$C = (n\ Ni\ X\ F) / 3600\ s\ h^{-1}$$

where F is Faradays constant 96485 C moles^{-1} , and the number of exchanged electrons (NEE) is equal to:

$$NEE = EC / C$$

Where EC are the experimental gravimetric discharge capacity taken from the measured values of current (in amperes) obtained from discharging the half-cells in the charge/discharge cycles, divided by the weight of the LDH in the electrode.

As shown in Figure 2.17, these electrodes reach their maximum discharge/charge capacity after 5 to 10 cycles. The NEE of Ni_2Al is higher than the NEE of both Ni_5Al and Ni_9Al LDHs. Furthermore, the NEE of Ni_5Al is higher than the NEE of the Ni_9Al and all three LDHs have higher NEE than the commercial $Ni(OH)_2$. It is known that on discharging from γ-$Ni(OH)_2$ to α-$Ni(OH)_2$ it is possible to exchange up to 1.6 electrons. This is because the nickel atoms in γ-$Ni(OH)_2$ have an average oxidation state of 3.6 due to some nickel atoms being in a +4 oxidation state.[138;165] Therefore since the LDHs stabilize the α–nickel hydroxide phase, cycling between the α-$Ni(OH)_2$ and the γ-$Ni(OH)_2$ can occur and more electrons can be exchanged. Since the Ni_2Al LDH has the highest NEE, this would indicate that on charging it is the material that is able to obtain the most nickel with the + 4 oxidation state. A study by Balej *et al.*[165] has shown that the nickel in the gamma phase with a + 4 oxidation state is most probably in the form of $NiO_2 \bullet xH_2O$. It is known that (M^{3+}) cations in the layers weaken the OH bond of the hydroxyl groups (increasing the Brønsted acidity) facilitating the release of protons in the layers.[154] The increased acidity of the hydroxyl

groups due to the aluminum cations near the vicinity of nickel atoms in the layers may thus help the formation of NiO_2.

On the long-term, shown in Figure 2.18, the NEE of Ni_9Al decreases rapidly, and at approximately 90 cycles reaches the NEE of the commercial β–nickel hydroxide. The same is observed for Ni_5Al after approximately 300 cycles. The Ni_2Al LDH always exhibits a higher NEE than all the materials up to the end of the test. The decrease of the NEE as a function of time may be due to a transformation of the LDHs into β-$Ni(OH)_2$. This would reduce the NEE because the material would be cycling between the β(II)/β(III) phases. Even though the stability test showed that the materials were stable in the harsh alkali conditions, it did not take into account the harshness of charging and discharging the materials. During the charge and discharge process, there is concomitant intercalation and deintercalation of protons and anions in the interlayers and the recurring change of the oxidation state of nickel. These events possibly transform the LDHs, at least partially, into β-$Ni(OH)_2$ or other undetermined, amorphous phases.

This interpretation is suggested by the XRD of the material after 445 cycles (Figure 2.19). The initial hypothesis is nevertheless in line with the trend observed for the reduction of the NEE, that is the Ni_9Al LDH has the quickest decrease of NEE as a function of time followed by the Ni_5Al and the Ni_2Al LDH. The Ni_9Al LDH with the lowest charge density has less carbonate in the interlayers and thus less electrostatic interaction holding the layers together. This material would then degrade quicker than both the Ni_2Al and Ni_5Al LDHs. Ni_2Al having the highest charge density is the most stable of the LDHs and lasts the longest.

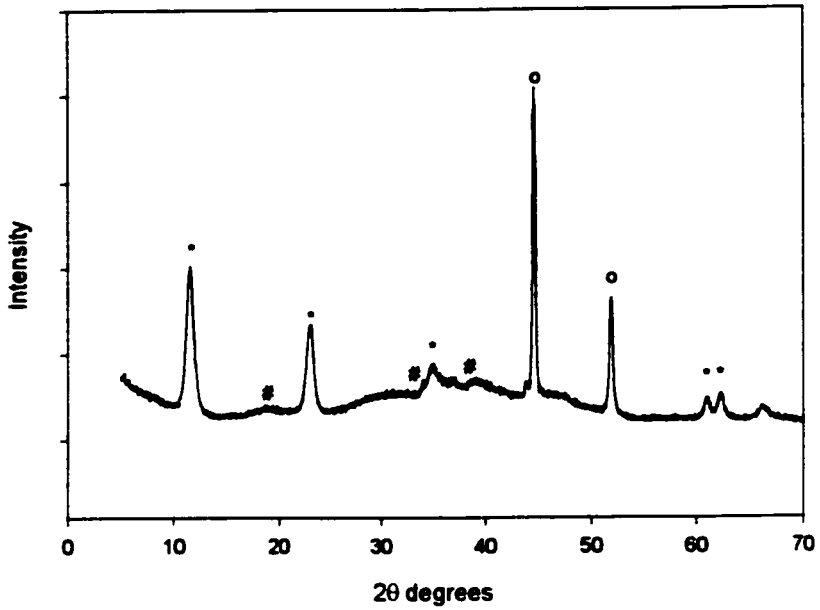

Figure 2.19 XRD pattern of the Ni_2Al LDH after 445 cycles

*: LDH; #: β-$Ni(OH)_2$; o Nickel powder

Figure 2.20 and 2.21 show the number of exchanged electrons (NEE) per atom of nickel as a function of cycle number for the two NiV LDHs and that of a commercial $Ni(OH)_2$ powder. These materials also level their discharge capacity at about 5 to 10 cycles. The trend of NEE is similar to that of NiAl LDHs. That is, Ni_2V containing the largest amount of vanadium has the highest NEE. Both NiV LDHs have higher NEE than the commercial β-$Ni(OH)_2$. However, the NEE of Ni_5V decreases quicker than that of Ni_5Al. The former reaches the NEE of the commercial powder at about 90 cycles which corresponds to approximately the same time as the complete transformation to β-$Ni(OH)_2$ as determined by the stability test (about 20 days). Ni_2V reaches the NEE of the beta nickel hydroxide at about 400 cycles (~80 days). This would then most likely correspond to the complete transformation of the LDH into β-$Ni(OH)_2$.

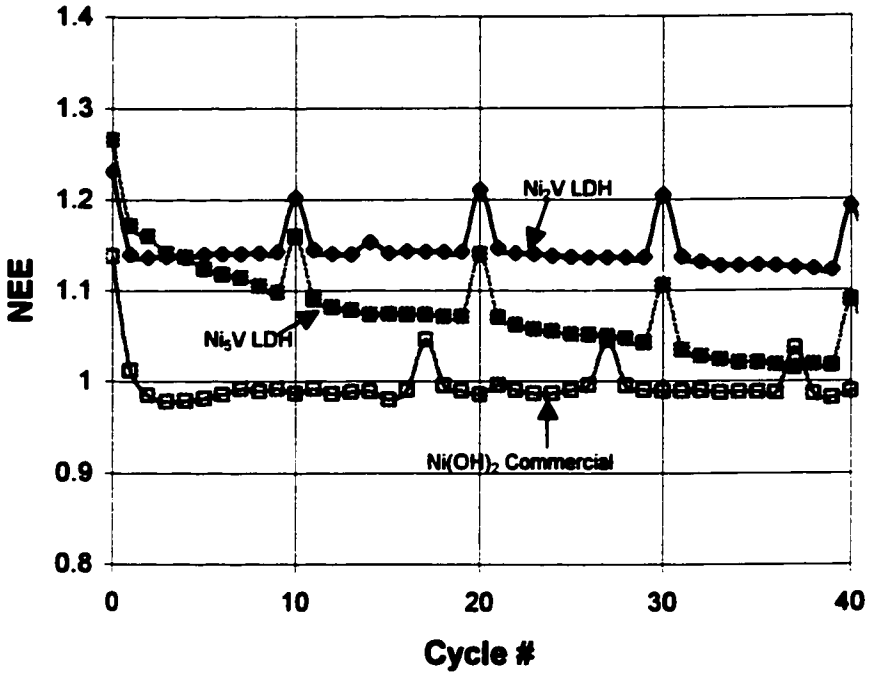

Figure 2.20 NEE of the NiV LDHs and the commercial $Ni(OH_2)$ (short-term)

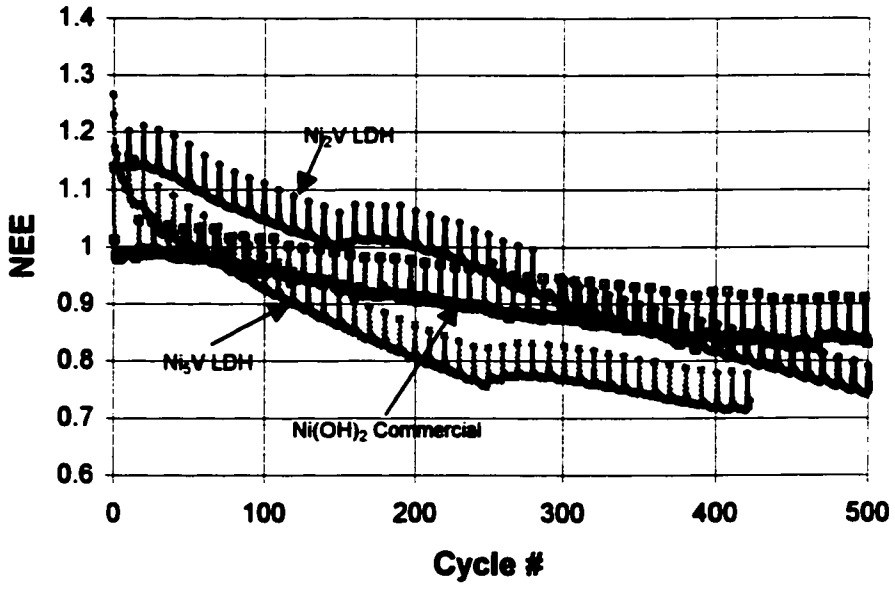

Figure 2.21 NEE of the NiV LDHs and the commercial $Ni(OH_2)$ (long-term)

2.3.5.2 LDH/commercial $Ni(OH)_2$ gravimetric capacity

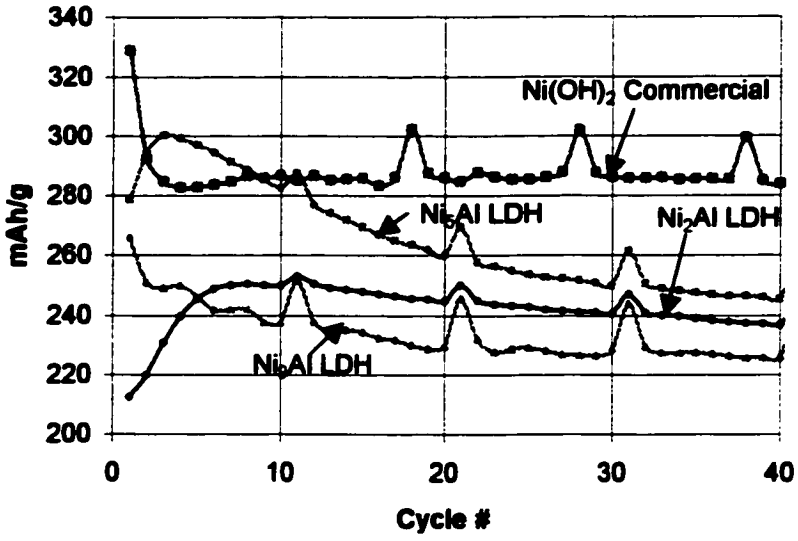

Figure 2.22 Gravimetric capacity of the NiAl LDHs and the commercial $Ni(OH)_2$ (short-term)

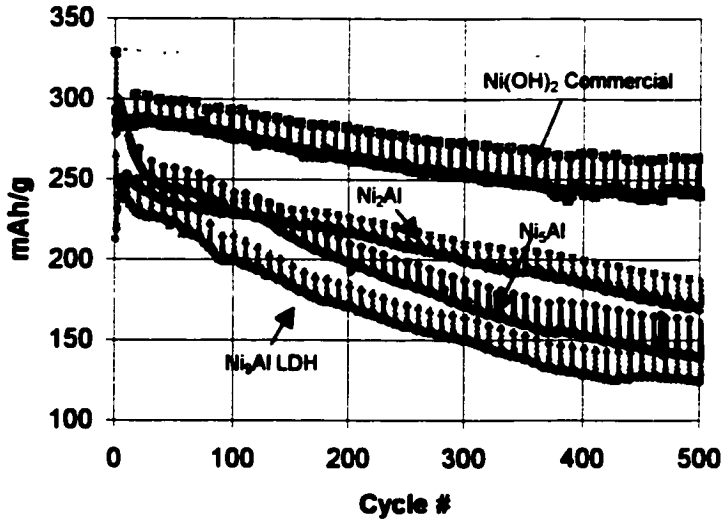

Figure 2.23 Gravimetric capacity of the NiAl LDHs and the commercial $Ni(OH)_2$ (long term)

Figure 2.22 shows the gravimetric capacity of the LDHs and $Ni(OH)_2$ as a function of cycles up to 50 cycles and Figure 2.23 up to 500 cycles . The gravimetric capacity is given as the number of mAh per gram of LDH or per gram of nickel hydroxide for the commercial powder. The Ni_5Al begins with the highest capacity but after 15 cycles goes below the commercial nickel hydroxide. It however keeps the highest capacity of all the LDHs in this cycling range. Ni_2Al LDH has the second highest capacity followed by Ni_9Al LDH. In spite of the fact that Ni_2Al has the highest NEE it does not have the highest gravimetric capacity. To understand these results one must not only take into account the number of exchanged electrons but also look at the quantity of LDH that was pasted inside the electrode. The electrodes pasted with the Ni_2Al LDH contain on average ~0.64g of LDH.(Table 2.1) On the other hand, approximately 0.82g of LDH of Ni_5Al LDH was pasted in the electrodes. There is 28% more Ni_5Al LDH pasted in the electrode than Ni_2Al. Therefore, when the capacity values of the electrodes containing Ni_2Al were corrected for the weight difference and for the difference in the number of exchanged electrons, gravimetric capacities similar to the electrodes containing Ni_5Al LDH were obtained (<2 % deviation). As for the electrodes containing Ni_9Al LDH, on average 0.91 g of LDH (42% more material) was pasted inside the electrode. When the capacity of the electrodes containing Ni_2Al were corrected for this weight difference and corrected for the difference in the number of exchanged electrons, the new values were similar to the Ni_9Al LDHs gravimetric capacities but larger by about ~5-8%. The difference may be due to the β-$Ni(OH)_2$ contamination in the Ni_9Al LDH that further lowers its gravimetric capacity. On the long-term, Ni_2Al keeps the highest capacity of all the LDHs, which is in agreement with the fact that it is the most stable LDH.

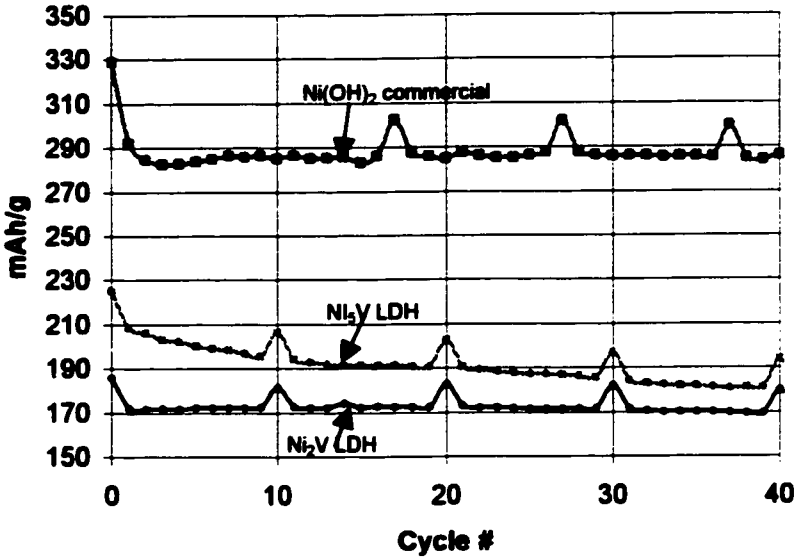

Figure 2.24 Gravimetric capacity of the NiV LDHs and the commercial nickel hydroxide (short-term)

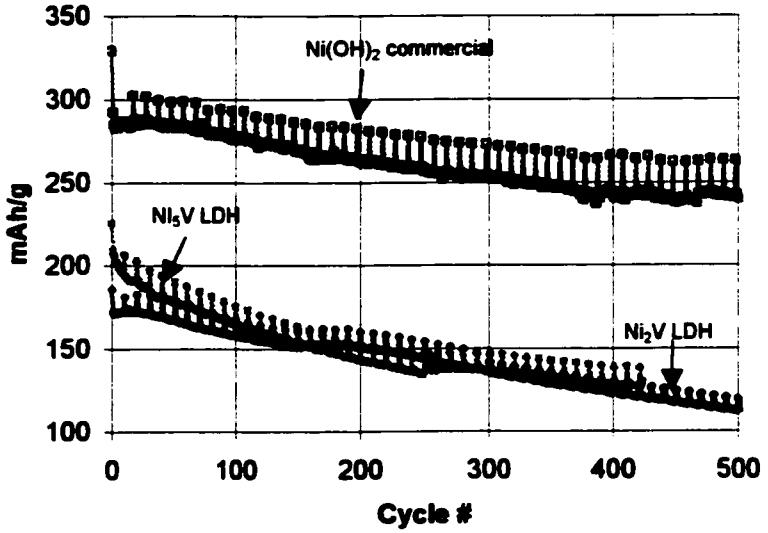

Figure 2.25 Gravimetric capacity of the NiV LDHs and the commercial nickel hydroxide (long-term)

Figure 2.24 and 2.25 show the gravimetric discharge capacity of the NiV LDH for the short-term (40 cycles) and long-term experiment respectively (500 cycles). The gravimetric capacities of the Ni_5V LDH are higher than that of the Ni_2V LDH up to about 150 cycles. The electrodes that contain the Ni_5V LDH have ~19% more material than the Ni_2V containing electrodes. When the gravimetric capacities of the Ni_2V containing electrodes are corrected for the difference in mass and for the NEE, similar gravimetric capacities to the Ni_5Al LDH are obtained.

The reason for the difference in the quantity of powder pasted in the electrode is most certainly due to the difference in densities of the materials. Ni_2Al with the smallest density (2.60g/mL) has less powder pasted in the electrode followed by Ni_5Al (2.97g/mL) and finally Ni_9Al (3.00 g/mL). The same can be said for the NiV LDHs since Ni_2V has a density of 2.38 g/mL and Ni_5V has a density of 2.66 g/mL. Knowing this, an increase of the density of the powders by milling them and making them finer would be a good way to maximize the LDHs properties as battery material. It has already been demonstrated by Wronski *et al.*[135] that β-$Ni(OH)_2$ powders when milled for several hours in a vibratory ball mill, exhibit improvement in the discharge capacity by 10% to 20% and outstanding stability up to at least 800 cycles.

2.3.6 Fast and slow discharge capacity

In the Figures 2.17 to 2.24, (excluding Figure 2.19) the observed repeating spikes are the result of the cells being discharged at a slower rate during these parts of these cycles than the rest of the cycles. During a slow discharge, more electrons are being extracted from the material than during a regular discharge. This is because during the regular discharge, there is apparently[166] the formation of a layer of a relatively non-conductive hydroxide phase near the surface of the particles that can force a large fraction of the discharge current to travel through alternative electrical paths, instead of reducing the oxyhydroxide material. The slow discharge allows more time for the current to access the core of the unreduced oxyhydroxide particulates and promotes a more homogeneous supply of electrons, thus giving a better utilization of the active mass and consequently higher discharge capacity of the electrode material.

Figure 2.26 shows the curves of the difference between the slow and fast discharge vs the number of cycles for the different powders. This data gives us some insight into the kinetic aspects of the cycling. The difference in the NEE between the slow and fast discharge increases from Ni_2Al, Ni_5Al, and Ni_9Al LDHs. A small difference between the slow and fast discharge indicates that not only the electrons but also the protons, which must accompany the redox electron exchange on cycling, become more available in the Ni_2Al structure. Consequently, the reduction of the more conductive active mass becomes less dependent on the discharge rate. This graph therefore indicates that the Ni_2Al LDHs has greater proton availability than Ni_5Al and Ni_9Al LDHs, and that this availability decreases as the cycle number increases. The increase in availability may be a result of an increase in Brønsted acidity of the hydroxyl groups attached to the aluminum atoms.[154] This may control the onset

of proton exchange between neighbouring OH groups. The decrease in availability of protons as shown by the increase in the difference between the fast and slow discharge as the cycle number increases could be an indication of the LDHs becoming β-$Ni(OH)_2$.

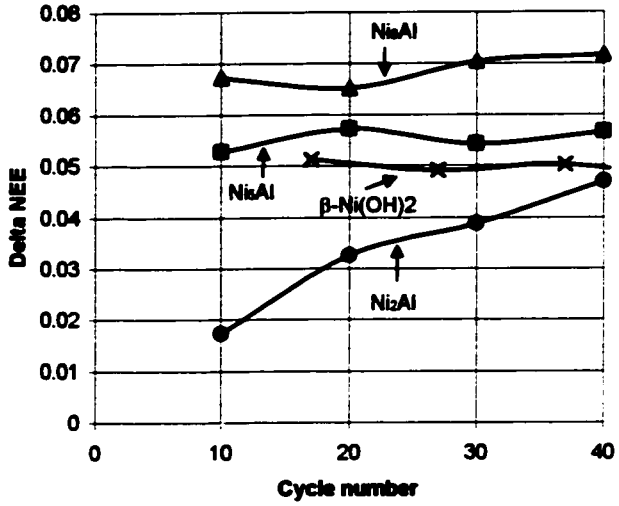

Figure 2.26 The difference between the NEE of the slow and fast discharges of the NiAl LDHs

Figure 2.27 shows the difference between the slow and fast discharge as a function of cycles for the NiV LDHs and the commercial powder. In this case, the differences between the slow and fast discharge for both the NiV LDHs and the commercial powder are very similar. This result indicates that the LDHs have been mostly transformed into β-$Ni(OH)_2$. Such an outcome is expected since both NiV LDHs transform very quickly into β-$Ni(OH)_2$ and at cycle 10, the electrodes have been put through the cycling process ten times (not counting the activation charge and discharge) and have been immersed in the KOH solution for at least five days.

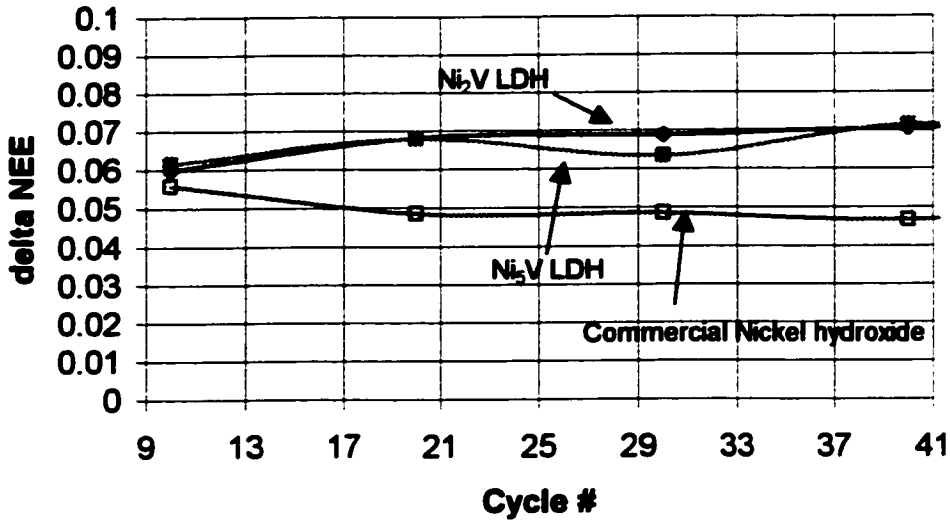

Figure 2.27 The difference between the NEE of the slow and fast discharges of the NiV LDHs

2.3.7 Charge and Discharge curves

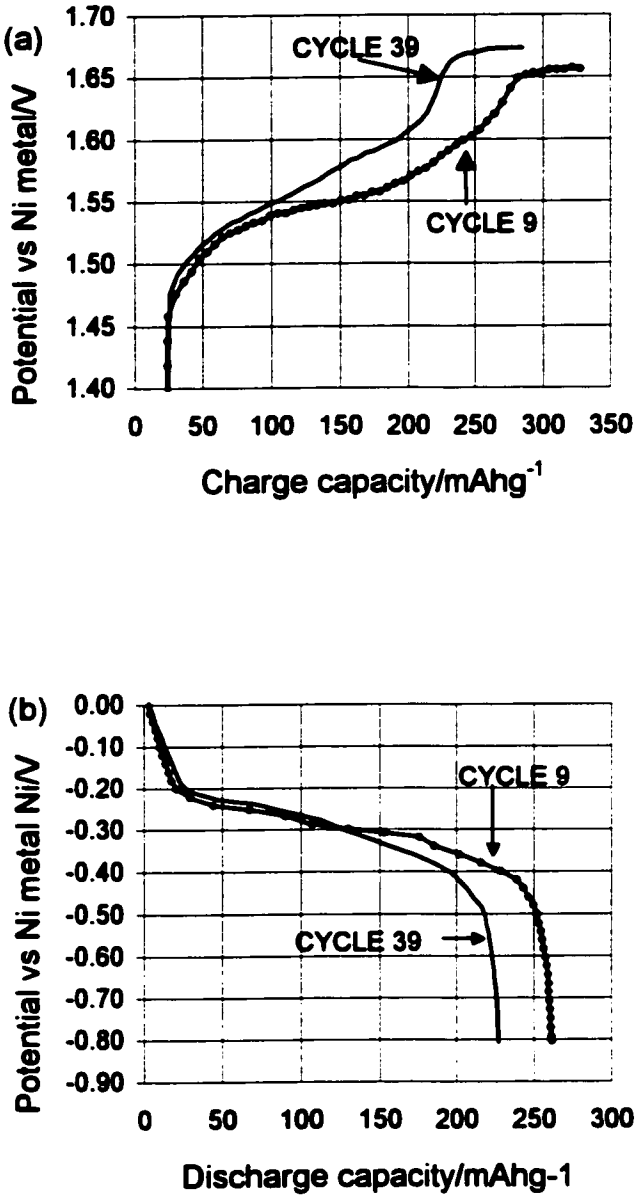

Figure 2.28 Potential curves of Ni_5Al LDH a) Charge Curve and b) Discharge Curve

Potential curves collected during charging and discharging of the Ni_5Al LDH are shown in Figure 2.28. These curves represent the general trend observed upon charging and discharging all the LDHs. The curves collected during charging at cycle and 9 and 39 are shown in Figure 2.28 (b). The first portion of the curve is the result of the oxidation of the LDH (up to approximately 250 mAh/g for cycle 9 and approximately 200 mAh/g for cycle 39) and the last and distinct part of the curve can clearly be related to oxygen evolution,[166] which results from the electrolyte decomposition. The curve at cycle 39 exhibits a higher potential and a shorter charging plateau before the oxygen evolution reaction begins compared to the curve at cycle 9. This indicates that as the cycling process progresses more current is being wasted for the oxygen evolution reaction and less is being used for the oxidation of the material. This result suggests that the material is becoming more difficult to charge as the cycle number increases and consequently there is less material being charged. The difficulty in charging the material as the number of cycles increase may be attributed to the reduction in proton mobility due to the formation of β-$Ni(OH)_2$, during the cycling process.[158] The lesser amount of material being charged at cycle 39 is reflected in the discharge curve at cycle 39 which exhibits a lower discharge capacity than the discharge curve at cycle 9.

2.4 CONCLUSION

The NiAl layered double hydroxides have shown stability in 6M KOH for at least two months whereas the NiV LDHs have demonstrated a maximum stability of 14 days (for the Ni_2V LDH) in the same alkali solution. The higher stability of the NiAl LDH versus the NiV LDHs was ascribed to the higher charge over radius ratio of the aluminum vs. vanadium. All the LDHs exchanged more electrons per nickel atom than the β-$Ni(OH)_2$ which was consistent with the materials cycling between the alpha-gamma phases. The Ni_2Al LDH obtained the highest NEE (maximum of 1.6 electrons per nickel atoms was exchanged) that was attributed to the increase in acidity of the hydroxyl groups as a result of the aluminum atoms in the layers. From the quantity of exchanged electrons obtained from the NiV LDH (maximum of 1.2 for Ni_2V) it is most unlikely that vanadium added to the exchange of electrons, however there was no direct evidence for this process. The Ni_2Al showed higher proton mobility than the commercial nickel hydroxide, which was also consistent with an increase in Brønsted acidity of the protons from the hydroxyl groups due to the presence of aluminum. From the results obtained, NiAl LDHs are extremely good candidates for the material of the positive electrode of nickel based batteries. Further studies could be done to optimize the gravimetric capacity of the NiAl powders using a milling process to increase their density. Increasing the capacity of the electrode could also be obtained by optimizing the cycling profile of the cells.

CHAPTER 3

The Intercalation of Phenylene Phosphonic Acid and 1,4-Phenylene Bis Phosphonic Acid in ZnAl Layered Double Hydroxide

3.1 INTRODUCTION

3.1.1 Microporosity

The domain of materials that exhibits microporosity is important in the field of chemistry, especially in the petroleum and pharmaceutical industries, and in the fields of catalysis, ion exchangers and separation technologies. Interestingly, these types of materials have had a very large influence on the economy as they had a return of 1000 billions dollars per year in the mid-1990s.[167] A microporous material is a compound that has pores smaller than 20Å. "Pores (from the Greek 'poros' = 'hole') can be defined as empty spaces in the internal structure of a solid."[168] The International Union of Pure and Applied Chemistry (IUPAC 1985)[169] has recommended the following terminology to describe the different categories of pores:

1) Micropores: pores of dimensions that are smaller than 20 Å
2) Mesopores: pores of dimensions between 20-500Å
3) Macropores: pores of dimensions that are larger than 500 Å.[169]

All these dimensions are considered of equivalent spherical diameter. Nanopore is another term that is becoming more frequently used in the literature to describe materials that also have pores of dimensions smaller than 20 Å.

3.1.2 Determination of microporosity

The determination of surface area and pore size can be achieved by using gas adsorption techniques such as the BET (Brunauer-Emmett-Teller) or the t method. Adsorption occurs when a gaseous phase encounters a solid one and gas molecules adhere to the surface of the solid. The substance or solid on which the adsorption occurs is called the adsorbent and the gas is called the adsorbate. Adsorption on solids is classified into physical (physisorption) and chemical (chemisorption) adsorption that is characterized by the strength of interaction with a solid. During physical adsorption, the molecules are held by weak van der Waal interactions with enthalpies in the range of -4 to –40 kJ/mol. On the other hand, chemical adsorption interactions are in the order of –40 to –800 kJ/mol.[170]

3.1.2.1 Adsorption Isotherms

Adsorption isotherms describe the relationship between the amount of molecules adsorbed on a surface of a solid and the concentration of the adsorbate at a given temperature. The majority of experimental isotherms can be grouped in six classifications (type I , II, III,... VI) that are shown in Figure 3.1

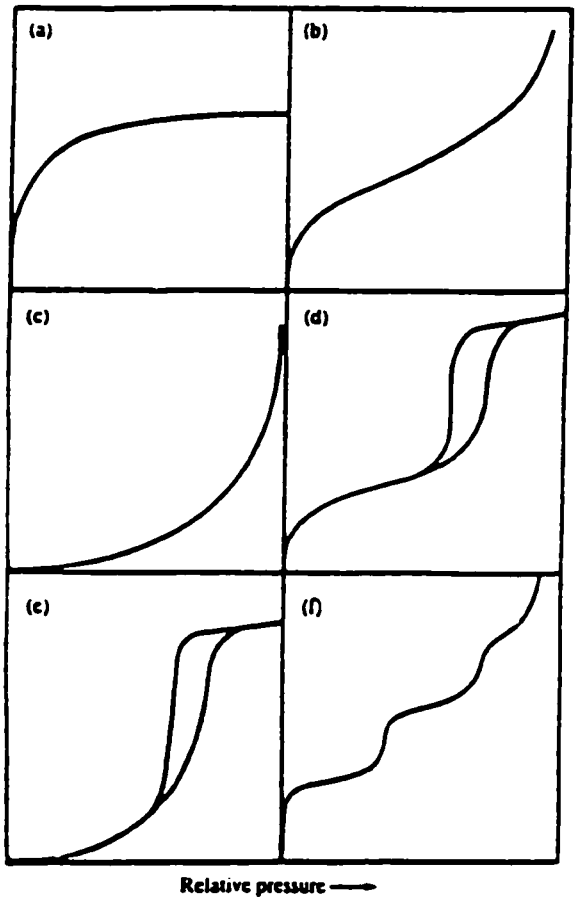

Figure 3.1 The 6 different types of adsorption Isotherms (a)-(f) (I-VI)[168]

Type I : Also called Langmuir isotherms, are typical of the adsorption curves obtained from microporous materials such as molecular sieves, zeolites and activated carbons.

Type II: Obtained from multilayer physisorption on flat non porous or microporous materials.

Type IV: Similar to multilayer adsorption isotherms accompanied with the capillary condensation in mesopores (indicative of the presence of mesopores).

Type III, and V: Characteristic of weak gas solid interactions such as water adsorption on gold.

Type VI: Characteristic of the adsorption isotherm obtained from krypton on graphite at 90 K.

3.1.2.2 The BET method

The BET method is one of the most widely used methods to determine surface area of materials. Nitrogen, krypton or CO_2 are normally used as the adsorbate in this technique. In this method, the amount of gas adsorbed is measured as a function of gas pressure at the liquid temperature of the adsorbate. By repeating the experiment with different initial pressures, a series of values of the number of moles of adsorbates versus the relative pressure is generated, giving an adsorption isotherm that can be expressed as:

$$n^a = (p/p^0) \quad (3.1)$$

Where n^a is the number of moles of gas adsorbed per g of adsorbate, p is the vapour pressure and p^0 the saturated vapor pressure. The BET method is based on the determination of the adsorption in the presence of multilayers and relates the amount of adsorbate to a monolayer capacity. It extends the pre-established Langmuir monolayer adsorption model. The BET model postulates that the adsorption rate of the gas onto the material is equal to the desorption rate, thus the BET adsorption can be derived.

$$p/[n^a(p^0-p)] = 1/n^a_mC + (C-1)p/n^a_mCp^0 \quad (3.2)$$

From a plot of $p/[n^a(p^0-p)]$ versus p/p^0 we can obtain a slope of $(C-1/\ n^a_mC)$ and a y intercept of $1/\ n^a_mC$. The surface area can be calculated with the following equation:

$$A_s = n^a_mLa_m \quad (3.3)$$

A_s is the specific area of the solid, a_m the average area occupied by the adsorbate molecule in the monolayer, L the Avogadro constant and n^a_m the monolayer capacity in moles of adsorbate per gram of solid.

The BET method has proven quite accurate to determine the surface areas of non porous, mesoporous and macroporous materials. However, the BET surface area of microporous materials must be taken only as an approximate surface area of the solid due to several limitations. The BET monolayer model is not applicable for the process of micropore filling at very low pressures (involving stronger adsorbate-adsorbent interactions). Furthermore, in

microporous materials molecules make contact with more than one surface and this phenomenon is not estimated in the BET model because it assumes that molecules have contact on only one surface.

3.1.2.3 The t method

The t plot method was developed by Lippens and De Boer in the 1960's. It is used to detect the presences of micropores, mesopores and to determine their respective surface areas. The t plot is represented by the curve obtained from the plot of the ratio V/V_m versus the relative pressure p/p^0 :

$$t= (V/V_m)\delta = f(p/p^0) \quad (3.4)$$

where t is the statistical thickness of the layer, V the volume of adsorbate, V_m the monolayer capacity and δ the thickness of a monolayer of gas (0.354 nm if nitrogen is used and assuming a hexagonal close packed configuration for the nitrogen molecules on the surface). When V_m is determined from the BET analysis of a known standard nonporous material, t can be related to a given value of p/p^0 by:

$$V= (V_m/\delta)t.= b_t t \quad (3.5)$$

For non-porous or microporous materials, there exists a linear relationship between V and t, with a slope b_t. The specific area of the solid is related to the quantity of adsorbed gas given by the BET equation:

$$A = V_m A_m N \quad (3.6)$$

and this equation is related to the slope b_t by the relationship:

$$A = a_m \delta N b_t \quad (3.7)$$

Deviation from linearity in equation (3.7) allows the nature of the pores to be deduced. For microporous materials a downward deviation from linearity is observed due to enhanced adsorption and for mesoporous materials, an upward deviation from linearity is observed due to capillary condensation occurring in the mesopores.

The t curve of a microporous material has two sections; the first one represents the filling of the micropores and the second represents the filling of the macropores. To calculate the micropore volume an extrapolation of the second part of the curve to the y-axis is done. The volume of the micropores in cm^3 is obtained by multiplying the extrapolated value by the ratios of the densities of the gas in the liquid and gaseous state. (0.00156 for nitrogen)

3.1.2.4 Pore size distribution (Horvarth Kawazoe)

The Horvarth Kawazoe[171] method was used to determine the pore size distribution in this study. It is based on the interaction between an adsorbate and the surface of a material in the shape of a slit like pore. The slit like pore shape is an appropriate model for the types of materials that were synthesized in the following research because this is the shape of the pores that should be formed when the organic molecules are intercalated in the layers of the LDHs. The potential function of the adsorbate and surface interaction are defined and based on statistical thermodynamic mathematical calculations and can be represented by the following equation:

$$RT\ln(p/p_0) = U_0 + P_a \quad (3.8)$$

where R is the gas constant, t is temperature, p/p_0 is the relative pressure as described earlier, U_0 is the function describing the adsorbate-adsorbent interaction and P_a defines the adsorbate-adsorbate-adsorbent interaction. Graphite and nitrogen are used as the adsorbate and adsorbent model respectively for the interaction that occurs in the slit pores. The equations defining this interaction energy are the following:

$$\phi = 3.06\,\phi^0\,[(\delta/\gamma)^4 + (\delta/\gamma)^{10}] \quad (3.9)$$

$$\phi^0 = N_a A_a/[3.06(2\delta^4)] \quad (3.10)$$

where δ is the distance between the gas atoms and the surface at zero energy, γ is the distance from the surface , N_a is the amount of atoms per unit area of surface and A_a is a constant.

The function that gives the potential between 2 layers filled with adsorbate molecules is given by:

$$\phi = [(N_a A_a + N_A A_A/2\gamma^4]\{-(\delta/\gamma)^4 + (\delta/\gamma)^{10} - [\delta/(1-\rho)]^4 + [\delta/(1-\rho)]^{10}\} \quad (3.11)$$

where N_A is the number of molecules per unit area of the adsorbate, A_a and A_A are defined as:

$$A_a = 6mc^2\alpha_a\alpha_A/(\alpha_a/\chi_a + /(\alpha_A/\chi_A) \quad (3.12)$$

$$A_A = 3mc^2\alpha_A/\chi_A/2 \quad (3.13)$$

M is the mass of an electron, c is the speed of light, α_a and χ_a are the polarizability and magnetic susceptibility of the adsorbent atom respectively and α_A and χ_A are the polarizability and magnetic susceptibility of the adsorbate atom respectively.

Equation 3.11 describes the two types of interactions defined by P_a ,U_a and from these 2 parts, a potential can be calculated as :

$$RT\ln(p/p_0) = K(N_a A_a + N_A A_A)/2\delta^4(1-d)\int_{d/2}^{1-d/2}\{-(\delta/\gamma)^4 + (\delta/\gamma)^{10} - [\delta/(l-r)]^4 + [\delta/(l-r)^{10}\}dr \quad (3.14)$$

and

$$d = d_a + d_A \quad (3.15)$$

Where K is Avogadro number, d, d_a and d_A are the diameter of an adsorbent, adsorbate atom and molecule respectively.

By integrating (3.14) the function of p vs. l can be obtained

$$RT\ln(p/p_0) = K(N_aA_a = N_AA_A)/2\delta^4(l-d) \times [\delta^4/3(1-d/2)^3 - \delta^{10}/9(1-d/2)^9 - \delta^4/3(d/2)^3 + \delta^{10}/9(d/2)^9] \quad (3.16)$$

and a relationship between the pore size and the amount of molecules can be determined by using the results of the N_2 isotherm obtained at the temperature of liquid nitrogen given by:

$$W/W_\infty = f(l-d_a) \quad (3.17)$$

where W is the mass of adsorbate molecule, W_∞ is the maximum amount of molecules that can be adsorbed, l is the distance between the atoms in the layers and d_a is the diameter of the adsorbent atoms.

To obtain the pore size distribution, W_∞ is determined at $p/p_0 = 0.998$, the values in the range of 3.5 and 14 Å are substituted in equation (3.17) and from the adsorption data W values corresponding to chosen values of $(l-d_a)$ pore sizes can be calculated.

3.1.3 Microporous materials

Many different types of materials exhibit porous properties but stilbite, (which is a natural zeolite like material) discovered in the 18th century, was the first material that gave way to

the idea of solid porous materials.[172] Zeolites are naturally occurring or synthetic microporous crystalline solids composed of mostly aluminum, silicon and oxygen atoms that are arranged in a framework that consists of interlocking tetrahedrons of SiO_4 and AlO_4. Below is a figure showing the framework topology of a typical zeolite (Gmelinite)

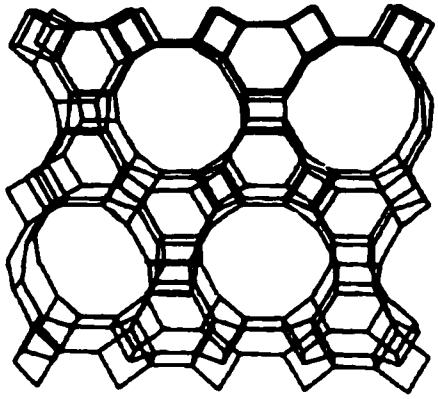

Figure 3.2 Framework topology of Gmelinite $[Na_8(AlO_2)_8(SiO_2)_{16}]$ [173]

The first successful zeolite synthesis was reported in 1862[172] and now chemists have synthesized over 100 types of these materials. Synthetic zeolites have the important trait of exhibiting homogeneous pore sizes in the range of 3-12 Å.[174] They are used as catalysts, ion exchangers, molecular sieves and in other important applications. Besides zeolites, other compounds that are considered as classical porous materials are active carbon, silicon, and aluminum oxides.[175;176] However, these materials have the drawback of exhibiting a large distribution of pore sizes. Later on, microporous zeolite like materials composed of aluminum and phosphates were synthesized and were denominated as AlPO[177] type compounds. Soon after, zeolite like gallophosphates[178], vanadium phosphate[179] and zinc phosphates[180] were synthesized. Although very useful, all of these materials were inconvenienced because of their limited pore sizes. Extensive research was therefore

expended in synthesizing microporous compounds that were different from zeolites and would not be limited in pore sizes. The research expanded into the area of pillared layered materials. Pillared cationic and anionic clays (LDHs) are such a group of materials and there is extensive literature on the pillaring of these materials. Because of the variety of clays and pillars, these materials offer the possibility of creating microporous solids that are not limited in pore sizes. Pillaring of layered materials is achieved by intercalating a host molecule in the interlayers of a guest molecule. The concept is to prop the layers of the lamellar material apart with pillars thus creating microporous cavities between the pillars and the layers.

3.1.4 Intercalation and pillaring

There are 4 types of reactions that can occur during the intercalation process: [181]

a) Brønsted acid-base reactions

b) Lewis acid base reactions

c) Redox reactions

d) Ion exchange reactions

The important characteristic of intercalation is the change in geometrical, chemical, electronic or optical properties of the host or the guest molecules that occurs upon intercalation. These changes can be minor or large depending on the interaction between the host and the guest. The interesting aspect of intercalation lies in the scope of parameters that can be changed to obtain the desired property of the material.

3.1.4.1 Definitions

The guidelines for the nomenclature and terminology associated with intercalation and pillared compounds were given in a technical report in 1999 by IUPAC.[182] In the next section the terminology and definitions from this report that are considered the most important for this study will be given.

According to the technical report on pillared clays and pillared layered solids given in 1999 by IUPAC, the first group to convey the idea of pillars to prop apart layered materials was given by Barrer and Macleod[183] in 1955. In their study, they reported the use of molecules to prop apart the layers of smectite clays. Furthermore, the term pillaring stemmed from the work of Brindley & Semples[184] and Vaughan & Lussier[185]in the late 70s on smectite clays. The work involved the intercalation of organic molecules in the layers of the clays followed by the calcination of the products that gave way to materials with increased interlayer spacing and microporosity.

A layered material is considered a crystalline material that has chemicals bonds between the atoms in the layers and the adjacent layers are held together by physical interactions. A single layer is called *lamella, slab* or *sheet* and the layered structure must have a well-defined X-ray diffraction (XRD) pattern, which demonstrates its lamellar structure.

Intercalation can be defined as the reversible insertion of a host inside a guest lamellar species without changing the main structural features of the guest. The proof of intercalation must be given unambiguously by the increase in interlayer spacing as determined by the XRD pattern of the intercalated compound.

Pillaring is achieved by intercalation of a host compound into a guest. However, the term "pillaring" should only be applied when certain criteria are met. After the pillaring process has occurred, the material must be transformed into a thermally stable micro- and/or mesoporous materials with retention of the layer structure. The pillared derivative is distinguished from an intercalated one by the virtue of intracrystalline porosity made possible by the lateral separation of the intercalated guest. To obtain a "pillared layered solids" or "pillared compounds", a "pillaring agent" must be used. The pillaring agent is defined as any compound that can be intercalated in a layered material, which maintains the spacing between the layers upon removal of the solvent, and which induces an observable pore structure between the layers. In addition to the above criteria, "pillared layered solids" and "pillared compounds" when synthesized have the following characteristics:

1) The minimum increase in basal spacing is the diameter of the N_2 molecule, which is commonly used to measure surface areas and pore volumes (0.315-0.353 nm.)
2) The pillaring agent has molecular dimensions and is laterally spaced in the interlamellar space on a molecular length scale.
3) The interlamellar space is porous and at least accessible to molecules as large as N_2; there is no limit to the size of the pores.

Furthermore, for a compound to be called pillared, the following minimum requirements must be met:

1) The material must be chemically and thermally stable and have a molecular distribution of pillars but no order of the pillars is required.
2) The lamellae of the layered compound must be ordered to give an XRD pattern that allows the determination of the d_{001} spacing.
3) The interlayer region must be accessible to molecules at least as large as N_2

The characterization guidelines of pillared materials were also given by the IUPAC report and these will be given in the following paragraph.

The main characterization techniques used on pillared compounds should follow the suggestions given in " Recommendations for characterization of porous solids" [186]
Nevertheless, the minimum characterization requirements to show that a pillared compound has been obtained are the following:

1) Powder XRD showing clearly the d_{001} line after removal of the solvent. (e.g. heating at 120°C in air or N_2 (Ar, He) for the removal of water)
2) t and α-plots analysis of N_2 adsorption isotherms must be done to determine porosity and surface area of the material. Pretreatment of the sample must be as described in 1)

In addition to the data given above, it was recommended to show the following data:

- Pillar to host ratio given either in an empirical formula or a unit cell formula.
- Comparison between the following data of the precursor and the pillared compound:

- Basal spacing from an XRD
- Surface area from samples that have undergone the same pretreatment, micropore obtained from t and α-plots and surface area outside micropores.

3.1.5 Review of the literature

The following review of literature will mostly focus on compounds that have been treated or intercalated with phenylphosphonic acid (PPA) and 1,4-phenylene bis phosphonic acid (b-PPA). Because of their shape (Figure 3.3 a and b) length and fairly rigid structure, these molecules offer the potential of being high quality pillars in layered materials.

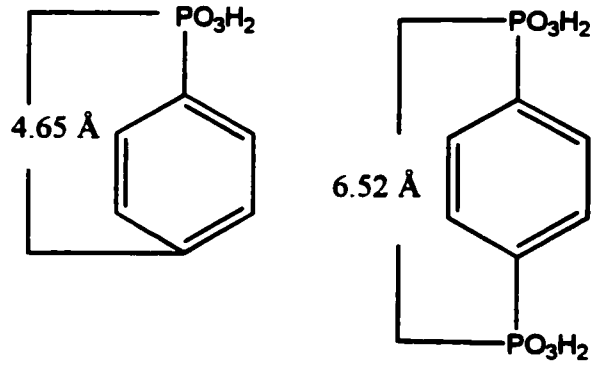

Figure 3.3: Structures of a) phenylphosphonic acid (PPA) and b) 1,4-phenylene bis phosphonic acid (B-PPA)

The values of bond length are taken from reference [187]

In the first portion of the review, studies on the reactions of zirconium with PPA and B-PPA will be discussed. The research on the reactions of these organic molecules with divalent and trivalent metals will then be explored and finally the research that has been done on the intercalation of PPA and B-PPA with LDHs will be reviewed.

3.1.5.1 Zr/PPA and Zr/B-PPA compounds

The interest in zirconium phosphonates derivatives stems from their high stability and their variety of possible uses in applications such as microporous materials for molecular sieves, catalysts,[188] ion exchange membranes, solid supports in gas chromatography as well as in thin layer chromatography. Upon review of the literature, it appears that researchers have mostly used three different precursors of zirconium to obtain microporous materials with the organic phosphonates as possible pillars: the α–$Zr(HPO_4)\bullet H_2O$, γ–$Zr(HPO_4)\bullet 2H_2O$ phase, or the tetravalent metal in the form of $ZrOCl_2$. The α–$Zr(HPO_4)\bullet H_2O$ phase was first synthesized in 1964 by Clearfield *et al.*[189] and it is formed of layers of zirconium atoms that are bridged by phosphate groups (three phosphate oxygen bridge across metal atoms.) above and below the layers and with the P-OH groups pointing inside the layers.[190] This gives a configuration in which zirconium octahedra are sandwiched between phosphate tetrahedra. (Figure 3.4a)

The γ–$Zr(HPO_4)\bullet 2H_2O$ phase on the other hand was first synthesized in 1968.[191] This compound was first thought to be a the di-hydrate polymorph of the alpha phase since it had the same chemical composition but a different interlayer spacing (7.5 Å and 9.4Å for the

alpha and gamma phase respectively.) The gamma phase was initially thought to simply have a different packing order but later was discovered to be a different material. This compound is different in that half of the phosphates are deprotonated (PO_4 groups) having all four oxygens bound to the zirconium layers while the other half of the phosphate groups are diprotonated and are bonded with only 2 oxygens (Figure 3.4b). [181;188]

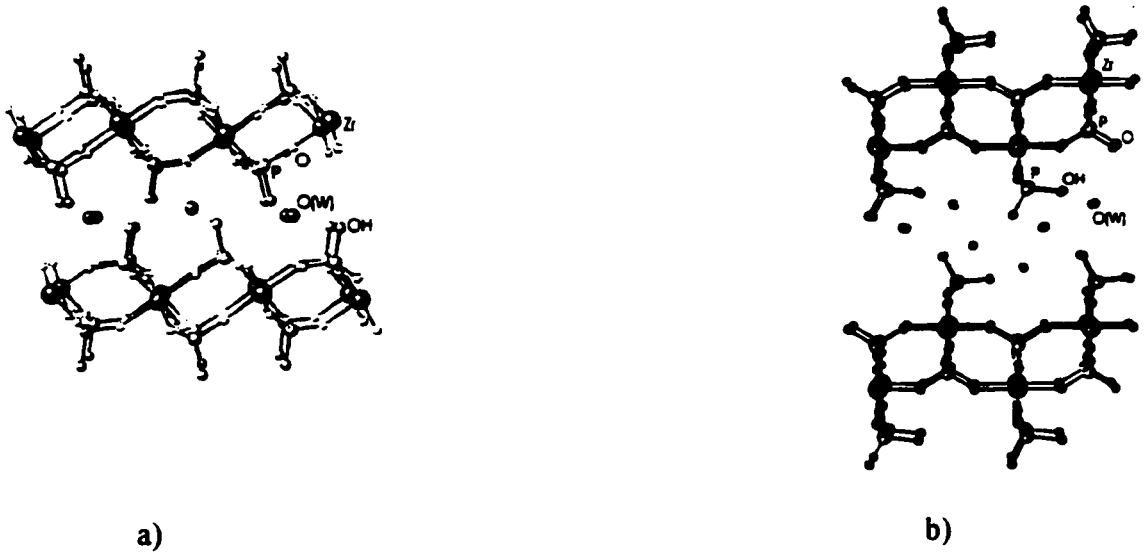

a) b)

Figure 3.4 Structure of a) α-$Zr(HPO_4)_2 \bullet H_2O$ and b) γ-$ZrPO_4(H_2PO_4) \bullet 2H_2O$ [192]

One of the first studies on the treatment zirconium with phenyl phosphonic acid was reported as early as 1978.[187] A layered material was obtained by the slow precipitation of $ZrOCl_2 \bullet 8H_2O$ in the presence of HF_{conc} and 1M ($C_6H_5PO_3H_2$).[187] However, due to the size of crystallites, it was impossible to determine the compound's crystal structure. This structure was only discovered in 1993 using modeling techniques from powdered diffraction data.[193] The layered material contained phenylphosphonate groups that were in between the layers with a 30° angle to the lamella and exhibited an interlayer distance of 14.7Å.

In 1993, Wang and Clearfield[194] completed a comprehensive research on a number of layered zirconium compounds. They experimented with the synthesis of mixtures of zirconium phosphonates, phosphates and phosphites. Three types of compounds were synthesized: Zr-PPA/phosphate, Zr-PPA/phosphite, and Zr-B-PPA/phosphate. The reaction of ZrF_6^{2-} in the presence of H_3PO_4 and PPA formed a compound with an interstratified structure where one layer of Zr PPA alternates with layers of Zr HPO_4. Combination of Zr PPA with phosphite formed compounds in which the phenylphosphonates groups were opposite to the phosphite group. The treatment of $ZrOCl_2$ with B-PPA and H_3PO_4 at different ratios ranging from 1:1 to 1:6, produced amorphous compounds that had interesting selective ion exchange capacities for Cs^+ and could possibly be used for separation and nuclear waste disposal.[194]

Other researchers also studied the reaction of B-PPA with γ-$ZrPO_4$ (H_2PO_4). Alberti *et al.* (1993),[188] attempted to synthesize, via a topotactic reaction (replacement of an interlayer H_2PO_4 moiety with B-PPA), a pillared $ZrPO_4$ (H_2PO_4) B-PPA compound. The reaction was completed in a water/acetone mixture to yield what they considered to be a pillared $ZrPO_4$ (H_2PO_4)B-PPA material. The compound was shown to be pillared using a sodium exchange procedure. It is unsure that this compound is truly pillared as no microporosity data was provided. However, the guidelines from IUPAC were not in place when these results were presented.

Hix *et al.* (1998)[195] treated α-zirconium phosphate with molten PPA and obtained the first reported topotactic reaction of phenyl phosphonate with alpha zirconium phosphate. Their objective was to eliminate the extreme and highly hazardous conditions (hydrothermal techniques, or refluxing of zirconium salts in the presence of HF and phosphonic acid)

normally used to obtain alpha zirconium phosphonate compounds. Their attempts were unfortunately not completely successful in that they obtained a mixture of alpha zirconium phosphonates and alpha zirconium phosphate phases.

3.1.5.2 M (II) and M(III) PPA

It is well known that to obtain group 4 phosphonates, reactions are often performed under dangerous conditions. Furthermore, the literature demonstrates that it is difficult to obtain highly crystalline materials with tetravalent metal precursors because of the poor solubility of these materials making them difficult to characterize.[196] On the other hand, since M(II) phosphonate derivatives are generally soluble in acids it is easier to obtain their single crystals and therefore they are easier to characterize.[196] Trivalent metal derivatives of phosphonates also appear to share the same characteristics as their divalent counterparts. Given the variety of M(II) and M(III) phosphonates derivatives that can be synthesized, the use of these metals offers the possibility of different chemical properties compared to using only zirconium atoms as the precursors. The above reasons have prompted further research for using M(II) and M(III) as precursors to phosphonates derivatives.

There has been extensive research on divalent metal phosphonates, [195;197-207] but research on trivalent metal phosphonates is not as exhaustive, however, lately these compounds are becoming a more frequent subject of study.[208-214] The following section of this review will focus on a few characteristic M(II) and M(III) PPA and B-PPA compounds that have been synthesized and investigated.

Mallouk *et al.* (1988)[197] prepared a large series of M(II) alkyl and aryl phosphonates; $M(O_3C_nH_{2n+1})\bullet H_2O$ (M = Mg, Mn, Zn n = 1-12; M = Ca, Cd, n = 1-4), $M(O_3PC_6H_5)\bullet H_2O$ (M = Mg, Mn, Zn), $Ca(HO_3PC_6H_5)_2$ and $Ca(HO_3PC_nH_{2n+1})_2$ ($n \geq 5$). In all these compounds, the divalent metal had octahedral coordination with a water molecule in the coordination sphere. The structure of the $Mn(O_3PC_6H_5)\bullet H_2O$ was solved from the X-ray diffraction data of its single crystal. Mn in this compound showed a distorted octahedral coordination structure with five chelating oxygens from the phosphonate groups and sixth oxygen coming from a coordinated water molecule. The phenyl groups were found to be perpendicular to the metal layers with van der Waals interactions between the phenyl groups from one layer to the other. They found disorder in the phenyl group orientation in the b direction. They discovered that the phenyl groups alternated regularly in the a and c directions but not in the b direction.

In 1990,[208] the synthesis of a new lamellar Fe(III) phenylphosphonate prepared from the treatment of iron(III) oxychloride (FeOCl) with phenylphosphonate acid was reported. Depending on the phosphonate to the metal (III) ratio different compounds were obtained. When the M(III)/phosphonate ratio was equal to 2, $HFe(C_6H_5PO_3)_2\bullet H_2O$ (1) was obtained. When the ratio was superior or equal to four, $HFe(C_6H_5PO_3H)_4$ (2) was obtained. Furthermore, (1) showed three different crystallographic phases denominated α, β and γ with identical composition but different XRD, IR and Mössbauer spectra. All of the compounds were formed of FeO_6 octahedra and the phenyl groups were arranged in infinite sheets running parallel to the b axis. Each of the oxygens bound to Fe originated from different phosphonate groups. The alpha, beta and gamma phases were attributed to materials having water molecules in different locations in the layered structures. [208]

In 1991,[215] Zn and Co phenylphosphonate were synthesized and the monohydrates were shown to be isomorphous to other divalent M(II) phosphonate. Both the Zn and Co were in an octahedral configuration with the water molecule in the sixth coordination site. These compounds were dehydrated then exposed to CO_2, CO, O_2, propylamine, ethylene and ammonia to test their intercalation properties. They showed selective intercalation to ammonia only. The ammonia molecule was found in the original location of the coordinated water molecule and the selectivity was attributed to the restriction imposed by the phenyl groups in the layers.

Clearfield *et al.* (1992)[214] synthesized interesting lanthanide aryl phosphonates. La, Ce, Sm, Yb phenyl phosphonates and La, Ce benzyl phosphonates were prepared in this study. These compounds are interesting as they formed layers of metals with dodecahedral distorted coordination spheres instead of the octahedral coordination spheres that are normally expected from divalent[197;200] and trivalent[209;210] metal phosphonates. All of the phenylphosphonate compounds were obtained by treating the metal salts to aqueous solutions of the appropriate acids but only single crystals of the lanthanide system were produced $(LaO_3PC_6H_5)(HO_3PC_6H_5)$ and its structure was fully described. This compound was layered and had eight oxygen atoms coordinated to lanthanum: six from phosphonate groups and two from water molecules. Two of the oxygens atoms of the phosphonate groups were chelated to one La atom and the third one bridged to an adjacent metal atom. Water molecules were coordinated to the other two sites finishing the dodecahedral structure. The phenyl rings pointed in the interlayer but were disordered. The disorder was described as: " phenyl rings being parallel to each other in the same row in the a direction but being inclined in adjacent rows in the c direction at an angle of 58°."

Another interesting series of divalent metal phosphonates due to their odd coordination sphere are the derivatives of copper phosphonates. These divalent metal compounds have a square pyramidal coordination sphere. Clearfield *et al.*[201] conducted a study on the intercalation of alkyl amines in a series of copper phosphonates ($Cu(O_3PR)\bullet H_2O$ R = CH_3, C_6H_5, $CH_2C_6H_5$). The structure of the methyl phosphonates was solved and showed that each copper atom was coordinated by five oxygen atoms forming a square pyramidal conformation. Four of the oxygens coordinated to the metal were from the phosphonate groups and a water molecule was coordinated in one of the equatorial sites of the pyramid. The structure of the copper phenylphosphonates was not fully solved due to the unresolved *hkl* reflection of the XRD powder pattern but the researchers were still able to determine that the material crystallized in an orthorhombic system with an interlayer distance of 13.99 Å. Clearfield *et al.* were also able to determine that the water molecule in the coordination sphere "lay in the equatorial plane and pointed in the interlayer space in a slightly slanted direction to that of the phenyl groups." This compound exhibited a layered structure as shown by the first, second and third order reflections of the powder XRD pattern. An intercalation study ensued and was performed on the synthesized compounds after they had been dehydrated by heating under vacuum at 180°C. The investigation of the intercalation of alkyl amines in the layered methylphosphonate[201] demonstrated an increase in the d spacing of the material proportional to the size of the alkyl amine chain. A plot of the interlayer distance versus the number of carbons in the alkyl amine chain revealed that the interlayer region was intercalated with a bilayer of alkyl amine chains angled 53° to the metal plane. The same investigation performed on the phenylphosphonate derivative, showed that the

interlayer spacing only increased when the length of the alkyl amine chain (i.e. four carbons or more) was longer than the length of the phenylphosphonic molecule.[201]

Poojary *et al.* (1996),[204] synthesized lamellar zinc bisphosphonates materials with the similar objective of Dines *et al.*[216] (i.e. to create pillared cross-linked compounds).[204] Two sets of zinc phosphonates compounds ($Zn_2[(O_3PC_6H_4PO_3)(H_2O)_2]$ and $Zn[HO_3P(C_6H_4)_2PO_3H]$) were synthesized from the treatment of the divalent metal with a solution of the respective acids (1,4-phenylene bis phosphonic acid and 4,4'-biphenylene bis phosphonic acid). The compounds were characterized by powder X-Ray diffraction, TGA, infrared analysis and their structures was determined *ab initio* from powder diffraction data and refined by the Rietveld methods. Both these compounds were layered with the phosphonate groups of the organic moieties crosslinking one layer to the other. The zinc atoms were coordinated in an octahedral fashion with five of the coordination sites occupied by oxygens of the phosphonates groups and the sixth by a water molecule, similarly to zinc phenylphosphonate.

Synthesis and characterization studies by other researchers have also been carried out on nickel phosphonates[217], aluminum phosphonates[209-211], lithium aluminum phosphonates[213], barium phosphonates[218], molybdenyl phosphonates[203] and other zinc[205:206], and copper phosphonates[202]showing the rich and vast chemistry of metal phosphonates.

3.1.5.3 Layered double hydroxides treated with PPA or B-PPA

It appears that Wang *et al.* (1995)[70] were the first to report the synthesis of layered double hydroxides with 1,4-phenylene bis phosphonic acid (B-PPA). They also synthesized a very

large series of other LDHs intercalated with polyoxometalates (POM) anions, which will not be described in this section of this review. They examined the effect of temperature on the reaction of the phosphonates with magnesium aluminum LDH. Three different reaction temperatures were tested. When the reaction was performed at 0°C, only one phase was obtained as demonstrated by the XRD pattern of the compound. An interlayer spacing of 14.7 Å was reported and this corresponded to the length of the bis-phosphonate molecule and the thickness of the brucite layer. This result indicated a complete intercalation of the phosphonates in the layers. The following reaction scheme was used to explain the results:

$$Mg_2Al(OH)_6X + 1/4C_6H_4(PO_3H_2)_2 \rightarrow Mg_2Al(OH)_6(O_3PC_6H_4PO_3)_{0.25} + HX$$

When the reaction was performed at room temperature, a mixture of two phases was obtained; one with a d spacing of 14.7Å corresponding to the fully intercalated compound and another with a d spacing of 9.6 Å. The latter composition corresponded to a material in which the phosphonate groups were directly connected to the metal atoms. When the reaction was performed at higher temperature (100-150°C), only one phase was obtained with the layer spacing of 9.6Å. They explained these results with a dehydration process of the material as shown by the following reaction:

$$Mg_2Al(OH)_6(O_3PC_6H_4PO_3)_{0.25} \rightarrow Mg_2Al(OH)_3O_{1.5}(O_3PC_6H_4PO_3)_{0.25} + 1.5H_2O$$ [70]

Carlino *et al.* (1996)[219] intercalated a melt of phenylphosphonic acid in a magnesium aluminum LDH. This was done to overcome incomplete reactions in aqueous solutions (observed by other researchers)[220] of organic moieties with preformed phosphate hosts. The

incomplete reaction was reported to be due to limited diffusion.[220] Two different types of reactions were attempted; one with the LDH and PPA and the other with the calcined oxyde of the LDH (named LDO) and PPA. The reactions were carried out by heating mixtures of the acid and the LDH or LDO to 175°C at a rate of 1°C/min and this temperature was held for 10 hours. The mixture was cooled to room temperature before being washed, filtered and dried. The treated LDH gave rise to two phases: one with and interlayer spacing of 14.7 Å and the other with 15.67 Å. The first material was attributed to a phase similar to α-$Zr(C_6H_5PO_3)_2$ obtained via a topotactic reaction. It was suggested that the second phase was due to the presence of PPA and water molecules in the interlayers and that the water molecules were produced from the dehydroxylation process of the LDHs hydroxyl groups during the reaction. Idealized structures of both phases are shown below.

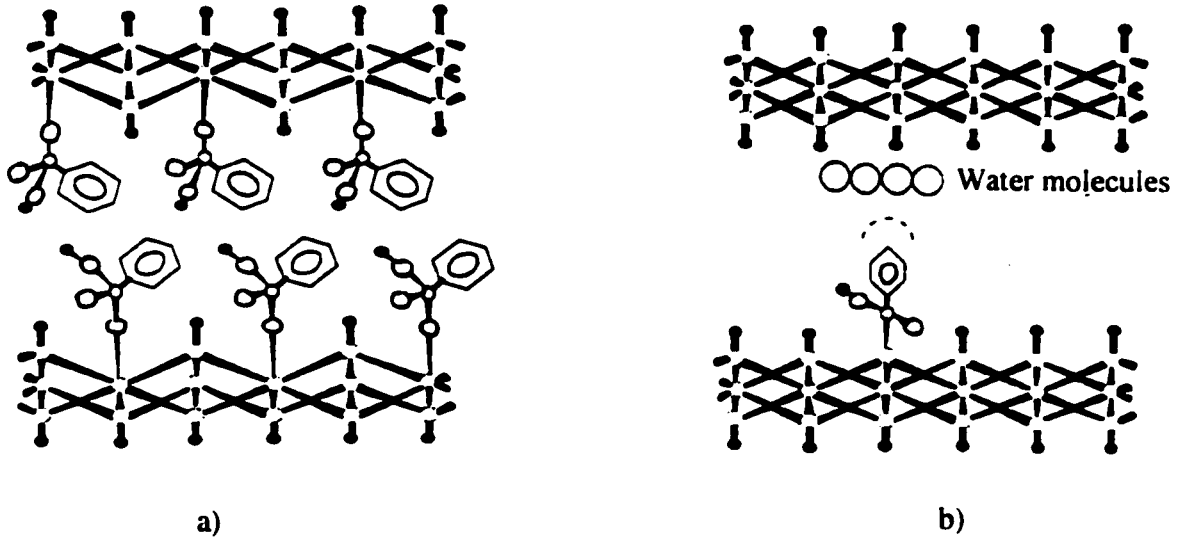

Figure 3.5 Idealized structure of the LDO and LDH/PPA thermal product

a) 14.7 Å phase b) 15.67 Å phase[219]

In 1997, Costantino *et al.*[221] studied the conductivity of so called grafted hydrogen phosphates, and PPA in ZnAl layered double hydroxides. The ZnAl LDH treated with PPA

gave a material with an interlayer spacing of 14.7 Å. They assumed that grafting of the PPA had occurred in the ZnAl LDH on the basis of the molecular formula determined by elemental analysis, TGA results and that the interlayer spacing was similar to that of layered $Zn(O_3PC_6H_5)$ The following molecular formula was proposed:

$$Zn_{0.67}Al_{0.33}(OH)_{1.65}(C_6H_5PO_3)_{0.35}\bullet 0.19H_2O$$

This formula shows evidence of grafting because there is an equal amount of PPA replacing hydroxyl groups. However, this formula is based on the assumption that PPA is monoprotonated and it may be possible that another form of PPA is present.

Nijs *et al.*[222] (1998) synthesized a series of MgAl and ZnAl LDHs with varying M (II) / M (III) ratios (in the range of 1/1, 2/1, 3/1, 4/1) and intercalated them with PPA. For the MgAl LDHs with a ratio of 2/1 the intercalation process was completed and they obtained a sample with a d spacing of 15.8 Å. It was noted that for the MgAl LDHs a 2/1 ratio or lower was needed to successfully complete an intercalation. Above this ratio, compounds with predominantly aluminum phenylphosphonate were obtained. On the other hand, the ZnAl LDHs treated with PPA gave rise to mixed ZnAl phenylphosphonic compounds. These materials showed surface areas between 1 and 25 m^2/g and displayed no microporosity. This was due to the large number of PPA molecules present inside the layers leading to a "stuffed" material with no spaces between the molecules.

Two very recent articles have been reported in the literature on the intercalation of PPA in LDHs.(Bonnet S. *et al.* in 1999[223] and Prévot *et al.* in 2001[224]). The first article described a

study conducted on intercalated MgAl (M(II)/M(III); 1:1, 2:1...5:1) LDHs with benzoate, benzenesulfonate or PPA. In all the cases of the LDHs treated with PPA, intercalated compounds were obtained. The samples with the ratio of M(II)/M(II) ratio of 3:1 or lower treated with PPA exhibited pure intercalated phases with a d spacing of 17.05 Å. However, when the ratio was above 3:1, biphasic materials were obtained one of which was identified as being $Mg(C_6H_5PO_3)\bullet H_2O$. In both cases, the structure of the compounds was not clearly defined. Interestingly, thermal treatment in a microwave of the Mg_3Al LDH intercalated with PPA gave a material with an interlayer spacing of 11.12 Å. The d spacing was attributed to a tilted monolayer of phenyl phosphonic molecules inside the layers.

The second article reported the grafting of PPA and other organic sulfonate and carboxylate moieties inside the layers of LDHs (CuAl and ZnAl). The LDHs were first intercalated via anion exchange or direct coprecipitation with the organic molecules and grafting was done by heating the intercalated LDHs (120°C in air during 4 to 12 hours). The bilayer inter-twined arrangement of the PPA molecules inside the ZnAl LDH was determined from the comparison of the gallery height of the intercalated LDH and the length of the anion. Grafting was confirmed from the reduction of the gallery spacing of the material. A topotactic reaction was proposed for the grafting mechanism (i.e. a substitution of the OH groups by the oxygen atoms of the organic anions).

3.1.6 Basis for research

Only recently have researchers started to experiment with layered double hydroxides (LDH) and phenylphosphonic acid (PPA) or 1,4-phenylene bis phosphonic acid (B-PPA) as possible pillars to obtain microporous materials. The successful pillaring of LDHs offers the possibility of obtaining microporous materials with enhanced reaction properties because of the large variety of metals available to them for their synthesis. Furthermore, LDHs have positive charge densities that can be controlled by changing the M(II)/M(III) ratio. This allows the introduction of another parameter to control the porosity of the materials, as the charge density can affect the quantity and position of the pillars. In the following study ZnAl LDHs were chosen as the precursors for the intercalated/grafted materials since these LDHs are stable in relatively low pH, and because of their range of M(II)/M(III) ratio allowing for possible tuneable microporisity. Furthermore, neither Zn nor Al is paramagnetic making the prepared materials amenable to solid state NMR analysis. This allows additional structural information to be collected.

3.2 EXPERIMENTAL

3.2.1 Synthesis of the LDHs and LDH/PPA compounds

3.2.1.1 Synthesis of Zn_2Al, Zn_3Al, Zn_4Al LDH

All LDHs were prepared using the method reported by Wang[81] *et al.* A mixture consisting of $Zn(NO_3)_2.6H_2O$ (29.7 g, 0.10 mol) and of $Al(NO_3)_3.9H_2O$ (18.89 g, 0.05 mol) in 300 mL of freshly boiled deionised water was added together with a 2 M NaOH solution (~200 mL), to a flask containing 150 mL of deionised water. Rapid stirring was kept throughout the addition and the rate of addition was such that the pH was kept at 10.0 ± 0.5. After the addition was completed, the mixture was heated at ~75-80°C for 16 hrs under N_2. It was then filtered, washed with water then dried at 70°C for 24hrs. Zn_3Al LDH and Zn_4Al LDH were prepared in a similar fashion but the zinc and aluminum nitrates were weighed to obtain the appropriate molecular ratios.

3.2.1.2 Synthesis of the LDH/PPA compounds

The LDH (1.00g) was dispersed in a 50 mL phenylphosphonic acid (0.1 M, Aldrich, 98%) solution, mixed and heated at 75°C for 48 hrs. The initial pH of this solution was originally at 2 and increased to approximately 5 to 8 depending on the LDH being intercalated. The mixture was filtered and the product was transferred to another phenylphosphonic acid solution (50 mL, 0.1 M, Aldrich, 98%), mixed and heated at 75°C for another 48 hrs. The

initial pH of this solution was also 2 and did not change after 48 hrs. The final product was filtered and dried for 18 hrs at 70°C.

3.2.2 Synthesis of the LDH, B-PPA and the LDH/B-PPA compounds

The LDH was prepared in the same fashion as in the previous section (3.2.1.1) except a pH of 8 was used for the coprecipitation instead of a pH of 10 to minimize the zinc oxide contamination in the LDH.

3.2.2.1 Synthesis of 1,4-phenylene bis phosphonic acid (B-PPA)

Many batches of the B-PPA were prepared. Table 3.1 shows a summary of the reactants and products obtained for each acid batch. The following preparation is a typical description of the synthesis of 1,4-phenylene bis phosphonic acid (Preparation of acid # 6). To a stirred mixture of diethylphosphate (2.3 mL, 18 mmol) , triethylamine (2.5 mL, 18 mmol) , and tetrakis(triphenylphosphine)palladium (0.47 g, 0.41 mmol) in toluene (8 mL), 1,4-dibromobenzene (1.888 g , 8.0 mmol) was added under a nitrogen atmosphere, and the resultant mixture was stirred at 90°C for 23 hrs. 1,4-phenylene bis (diethylphosphite) was obtained The compound was purified on a silica gel column with a mixture of ethanol:ethyl acetate 1:5 as the eluant. 1,4-phenylene bis (diethylphosphite) was finally obtained with a net yield of 69.5%.

The ester was hydrolyzed into the acid by mixing it with HCl (15 mL, 37% V/V) for ~24 hrs at 85° C. The mixture was then evaporated under reduced pressure to obtain 1,4-phenylene bis phosphonic acid. The acid was used without further purification for the

following reactions with the LDH.[225] The characterization of the esters and the acids can be found in section 3.2.3.8

Table 3.1: Summary of the reactants used and products obtained for 1,4-phenylene bis phosphonic acid

	Reactants				Products			
Acid Name	P-dibromo Benzene (g)	Catalyst[1] (g)	Triethyl Amine (mL)	Diethyl Phosphite (mL)	Ester (g)	Yield %	Acid (g)	Yield %
5	1.8874	0.47	2.5	2.3	2.1330	76.2	1.4202	98.0
6	1.8880	0.46	2.5	2.3	1.9477	69.5	1.2987	98.1
7	1.8923	0.32	2.5	2.3	0.9949	35.4	NA[2]	NA[2]
8	1.8832	0.32	2.5	2.3	0.9946	35.6	NA[2]	NA[2]
9	1.8909	0.31	2.5	2.3	0.4839	25.6	NA[2]	NA[2]
11	1.8911	0.41	2.5	2.3	2.4920	88.9	NA[2]	NA[2]
B[3]	-	-	-	-	4.9468	-	2.6197	77.9

Notes:

1) tetrakis(triphenylphosphine)palladium
2) Not available because the esters were combined to make one large batch of acid. (Acid B)

3) Acid B is the combination of the esters 7,8,9, and 11. Because of the larger batch size used, starting material remained after hydrolysis and was extracted with ethyl acetate (3X50 mL). Sodium hydroxide was added to the aqueous phase before the extraction to form the salt of the acid.

3.2.2.2 Synthesis of the LDH/B-PPA compounds

Table 3.2: Summary of the reactions of the LDHs treated with B-PPA

Sample Number	Time of reaction	pH of reaction	LDH:acid ratio	Acid Used
ZnAl35	48hrs[1]	5	4.38	5
ZnAl41	48hrs[2]	5	1.69	6
ZnAl54	48hrs[3]	No control of pH	1.69	6
ZnAl55	2X48hrs[4]	No control of pH	1.68	B

Notes:

1. ZnAl28 (0.50 g, 4.03 mmol) LDH was dispersed in 50 mL of freshly boiled deionized water. 1,4-phenylene bis phosphonic acid (B-PPA) (0.22 g, 0.92 mmol) dissolved in 25 mL of freshly boiled deionized water and sodium hydroxide (25 mL, 0.16 M) were added to the solution simultaneously at a rate to keep the pH of the solution at 5.0. The sample was filtered rinsed with water and dried at 70°C for 48 hrs

2. ZnAl28 (0.25 g, 2.13 mmol) was dispersed in 50 mL of freshly boiled deionized water. B-PPA (0.30 g, 1.26 mmol) dissolved in 25 mL of freshly boiled deionized

water and sodium hydroxide (25 mL, 0.30 M) were added to the solution simultaneously at a rate to keep the pH of the solution at 5.0. The sample was filtered rinsed with water and dried for 48 hours at 70°C

3. B-PPA (0.30 g, 1.26 mmol) was dissolved in 25 mL of freshly boiled water and added to ZnAL28 (0.25 g, 2.13 mmol) dispersed in 25 mL of freshly boiled deionized water. The mixture was stirred at 70°C for 48 hrs, filtered and the white gel was dried for 48 hours at 70° C.

4. B-PPA (0.198 g, 0.76 mmol) was dissolved in 7 mL of freshly boiled deionized water and ZnAl28 (0.15 g, 1.28 mmol) was added to the solution. The mixture was stirred at 70° C for 48 hrs, filtered and the white gel was transferred in 7 mL of a freshly prepared B-PPA (0.198 g, 0.76 mmol) solution. The sample was stirred for another 48 hrs at 70° C before it was filtered and rinsed with water. It was dried at 70° C for at least 24 hrs.

3.2.3 Characterisation

3.2.3.1 XRD

XRD patterns were obtained on the same apparatus as described in the Chapter 2. They were obtained using a Philips PW3710 diffractometer with Cu-Kα radiation at a wavelength of λ=1.54059 Å. A voltage of 45 kV and a current of 40 mA were used to record the patterns. The samples were run in a range from 2θ : 8° to 72° for the precursor LDHs and from 2θ: 2° to 72° for the LDH/PPA and LDH/B-PPA compounds. The preferred orientation samples were prepared in the following fashion: 50 mg of the sample was added to 1 mL of acetone. The mixture was sonicated for a ~ 30 seconds to form a slurry and was transferred, using a Pasteur pipette, on a zero background silicon disk and left to dry. The disk was mounted in the diffractometer and analysed.

Random orientation samples were prepared by transferring the powdered sample into a circular aluminum sample holder. The powder was pressed gently into place and care was taken not to disturb the surface to ensure random orientation of the particulates.

3.2.3.2 Elemental analysis

Elemental analyses of the samples were carried out in the same fashion as in the section 2.2.2.2 of Chapter 2.

3.2.3.3 Carbon, hydrogen and nitrogen analysis

C, H, and N elemental analysis were carried out in the same fashion as section 2.2.2.3 of Chapter 2

3.2.3.4 Fourier transform infrared spectra

Infrared spectra were recorded on the same apparatus and in the same fashion as in section 2.2.2.4 of Chapter 2

3.2.3.5 Solid state and solution NMR spectra

Solid state ^{13}C CPMAS-NMR and ^{31}P CPMAS-NMR spectra were recorded on a Bruker ASX-200 spectrometer at 50.3189 and 81.0021 MHz respectively. The rate of sample rotation was from 4 to 6 kHz. The ^{31}P chemical shifts were measured relative to H_3PO_4 85%. ^{31}P decoupling of the ^{13} C CPMAS spectra was performed with a 81 MHz band pass filter.

The ^{1}H and ^{13}C solution NMR were recorded on a Bruker AMX-500 spectrometer at 500.14 MHz and 125.04 MHz respectively with a ^{1}H decoupling frequency of 500.130 MHz, or a Varian Gemini 200 at 199.967 MHz and 50.2824 respectively with a ^{1}H decoupling frequency of 199.971 MHz.

3.2.3.6 BET Surface Area Determination

BET surface area and micropore determination experiments of the samples were performed on a micromeritics ASAP 2010 analyser.

The samples were heated at temperatures between 70 and 100°C under vacuum on the apparatus to eliminate adsorbed moisture that may have been present. The analyzer measured the pressure of the sample and when the pressure was constant, (indicating a completely dried sample) it could be analyzed for surface area and micropore determination (nitrogen adsorption). The drying process could sometimes take up to 3 days to be completed depending on the moisture content present in the sample.

3.2.3.7 TGA Analysis

Thermogravimetric Analysis (TGA) were performed on a Dupont 2100 series thermogravimetric analyser.

Approximately 15 mg of the sample was weighed and inserted on the TGAs microbalance. The samples were then heated from room temperature up to 1000°C in air at a rate of 20°C/min.

3.2.3.8 Characterization of the esters (1,4-phenylene bis (diethylphosphite)) and the B-PPA (1,4-phenylene bis phosphonic acid)

Ester 5

^{1}H NMR, (200 MHz, $CDCl_3$). δ = 7.88 (m,4 H), δ = 4.11(q, J = 8 Hz, 2H), δ = 1.31 (t, J = 8 Hz, 3H). ^{13}C NMR, (50 MHz), ($CDCl_3$), δ = 133.5 (d, ^{1}J = 200 Hz), δ = 132.3 (d, ^{2}J = 20Hz), δ = 132.5

IR (KBr), aromatic: 3071, Aliphatic 2986, P-OCH_2CH_3 between 1480-614

Acid 5

^{1}H NMR (500 MHz, D_2O) δ=7.82 (m, 4 H). ^{13}C NMR (125 MHz, D_2O) δ=135.34 (d, ^{1}J = 180 Hz), 130.08 (d, ^{2}J = 25 Hz), 130.08. ^{31}P NMR (202 MHz MHz, D_2O) δ = 15.56. EA: Calculated for $C_6H_4P_2O_6H_4$: C: 30.27, H: 3.39; Found: C: 30.35, H: 3.44

Acid 6

^{1}H NMR (500 MHz, D_2O) δ = 7.79 (m, 4 H). ^{13}C NMR (125 MHz, D_2O) δ = 134.23 (d, ^{1}J = 181 Hz), δ = 130.07 (d, ^{2}J = 25.0 Hz), δ = 130.07. ^{31}P NMR (202 MHz, D_2O) δ = 15.63. EA: Calculated for $C_6H_4P_2O_6H_4$: C: 30.27, H: 3.39; Found: C: 30.26, H: 3.35

Acid B

^{1}H NMR (500 MHz, D_2O) δ = 7.91 (m, 4 H). ^{13}C NMR (125 MHz, D_2O) δ = 137.32 (d, ^{1}J = 175 Hz), δ = 130.27 (d, ^{2}J = 23.8 Hz), δ = 130.27. ^{31}P NMR (202 MHz, D_2O) δ = 14.16. EA: Calculated for $C_6H_4P_2O_6H_3Na$ C: 27.70, H: 2.71; Found: C: 27.78, H: 3.03

3.2.3.9 Program used for the determination of the molecular formulas of the LDH/PPA and LDH/B-PPA compounds

An important part of the characterization of intercalated compounds is the determination of their molecular formula. In the case of this study the determination of the molecular formulas of the materials that were obtained was not trivial because it was unclear if the organic molecules simply replaced the interlayer anions via an ion exchange or if grafting had occurred (the oxygens atoms of the phosphonate groups had covalently bound directly to the metal atoms of the brucite like sheets). To determine the molecular formulas of the compounds, my colleague Arvin Moser and I developed a program in visual basic 6.0 to accomplish this task. A brief explanation of the operation of the program will be given in the following text. The input window and the code of the program will then be given and this will be followed by a step-by-step description of the operation of the program. The details of the actual function of every code line will not be given, as this is not necessary to understand how the program proceeds.

For the determination of the formulas of the LDH/PPA compounds, the program varied the coefficient "a", "z" and "y" in equation 1 below. On the other hand, for the determination of the B-PPA compounds these coefficients were varied in equation 2. The value of x in each equation was calculated from the Zn:Al ratio determined by the ICP analysis of the respective compounds.

$$Zn_{1-x}Al_x(OH)_a(C_6H_5PO_3H_z)^{2-z}_{((2-a)+x)/(2-z)} \bullet yH_2O \quad (1)$$

$$Zn_{1-x}Al_x(OH)_a(C_6H_4P_2O_6H_z)^{4-z}_{[(2-a)+x]/(4-z)} \bullet yH_2O \quad (2)$$

The coefficient "a" was varied from (0 to 2 for LDH/PPA and LDH/B-PPA compounds; the upper range represents the maximum number of OH groups possible in an LDH) and for each step, "z" was increased from (0 to 1.99 for LDH/PPA and 0 to 3.99 for LDH/B-PPA compounds; the upper values represent the maximum allowable number of protons on the acids). For each step of "z", "y" was varied from 0 to 2. By using these values all different valid possibilities of chemical formulas were considered. For each variation of the coefficients, the weight percent of the elements were calculated. The deviation between the calculated and experimental data as well as their sum was calculated. The molecular formulas having coefficients resulting in the lowest overall deviation between the experimental and the calculated data were kept.

3.2.3.9.1 Input window

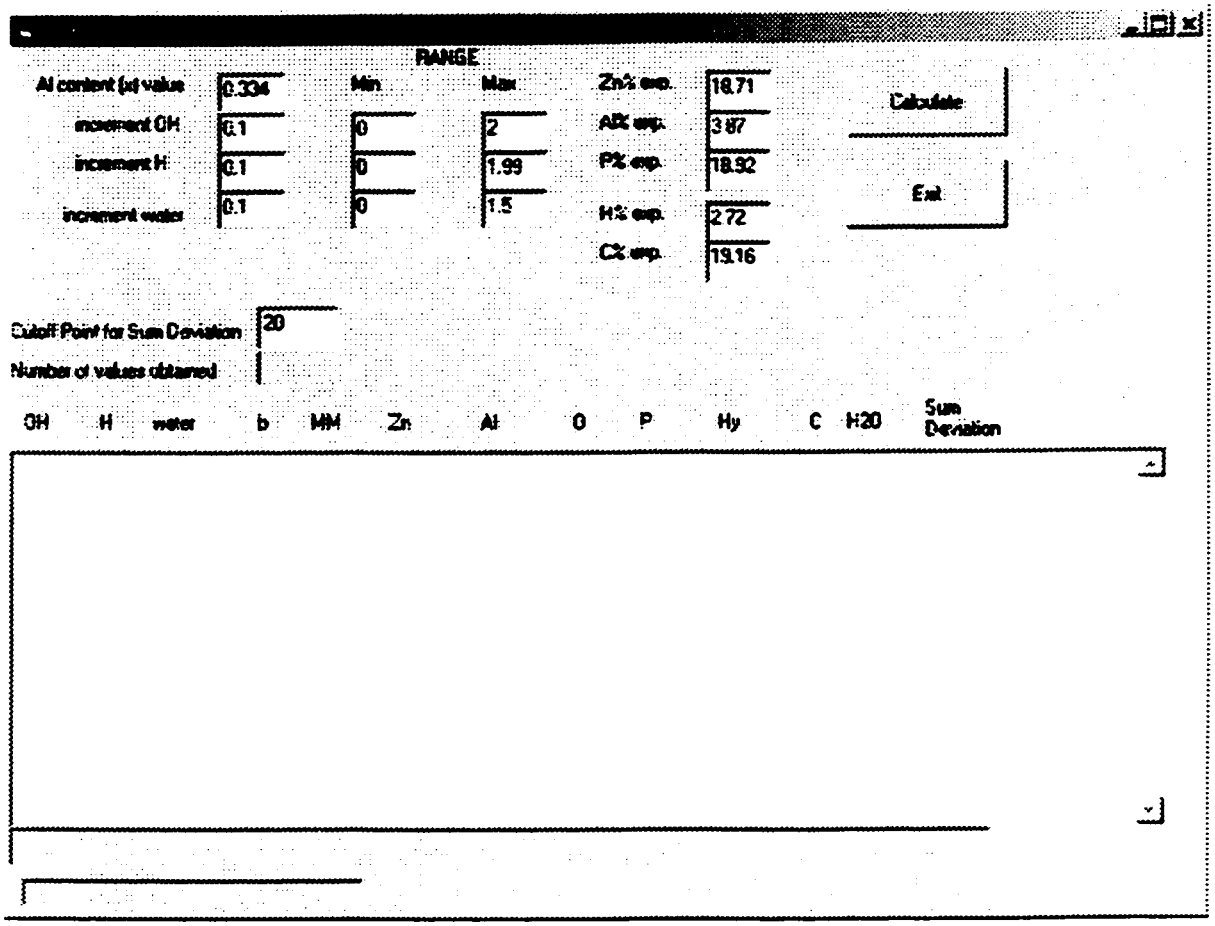

Figure 3.6 Input window of the visual basic program to determine the molecular formulas of the compounds

3.2.3.9.2 Program Code used to determine the molecular formulas of the LDH/PPA compounds

```
Private Sub Command1_Click()
Dim OH As Double
Dim OHb As Double
Dim H As Double
Dim Hb As Double
Dim x As Double
Dim water As Double, waterb As Double, calperwater As Double
Dim i As Integer
Dim b As Double
Dim MM As Double
Dim Zn As Double
Dim Al As Double
Dim O As Double
Dim P As Double, SumDev As Double
Dim Hy As Double
Dim C As Double
Dim minus As Double, minusaaa As Double
Dim sTitle As String
Dim sFinalValues As String, sTempContents As String
'FinalValues.Text = "" 'clear textbox
'sFinalValues = ""
```

```
OHb = incrementOH.Text
Hb = incrementH.Text
waterb = incwater.Text

x = All.Text
i = 0
' water = perwater.Text / 100 * mass.Text / 18.0152
DoEvents 'unknown function
sTitle = "OH" & vbTab & "H" & vbTab & "water" & vbTab & _
"b" & vbTab & "MM" & vbTab & "Zn" & vbTab & "Al" & _
vbTab & "O" & vbTab & "P" & vbTab & "Hy" & vbTab & "C" _
& vbTab & "H2O" & vbTab & "SumDev" & vbTab & "Dev H2O" & vbCrLf

For OH = OHmin.Text To OHmax.Text Step OHb          'INCREMENT OH BY "OHb"
ProgressBar1.Visible = True
ProgressBar1.Min = OHmin.Text
ProgressBar1.Max = OHmax.Text
ProgressBar1.Value = OH

For H = Hmin.Text To Hmax.Text Step Hb              'INCREMENT H BY "Hb"
ProgressBar2.Visible = True
ProgressBar2.Min = Hmin.Text
ProgressBar2.Max = Hmax.Text
ProgressBar2.Value = H
```

```
For water = watermin.Text To watermax.Text Step waterb 'INCREMENT water BY
"waterb"

b = ((2 - OH) + x) / (2 - H)                    ' COEFFICIENT OF PPA

MM = ((1 - x) * 65.38) + (x * 26.98154) +   'MOLECULAR MASS CALCULATION
((OH + (3 * b) + water) * 15.9994) _
+ (b * 30.97376) + ((OH + (5 * b) +
(2 * water) + H) * 1.0079) _
+ ((6 * b) * 12.011)

calperwater = (water * 18.0152 / MM * 100)      'DEVIATION % CALCULATION
Hy = ((OH + (5 * b) + (2 * water) + H) * 1.0079)_
 / MM * 100
Zn = ((1 - x) * 65.38) / MM * 100
Al = (x * 26.98154) / MM * 100
O = ((OH + (3 * b) + water) * 15.9994) / MM * 100
P = (b * 30.97376) / MM * 100
C = ((6 * b) * 12.011) / MM * 100
```

```
SumDev = Abs((Zn - ZnExp.Text) / ZnExp.Text) * 100 ' SUM DEVIATION
CALCULATION
+ Abs((Al - AlExp.Text) / AlExp) * 100
+ Abs((P - PExp.Text) / PExp.Text) * 100 _
+ Abs((Hy - HydrogenExp.Text) / HydrogenExp.Text) * 100
+ Abs((C - CExp.Text) / CExp.Text) * 100

If SumDev > Cutoff.Text Then GoTo ggg _          'CONDITION TO KEEP VALUES
Else i = i + 1: sFinalValues = sFinalValues & _

Round(OH, 3) & vbTab & Round(H, 3) & vbTab & Round(water, 3) & _
vbTab & Round(b, 2) & vbTab & Round(MM, 3) & vbTab & _
Round(Zn, 2) & vbTab & Round(Al, 2) & vbTab & Round(O, 2) & _
vbTab & Round(P, 2) & vbTab & Round(Hy, 3) & vbTab & Round(C, 2) _
& vbTab & Round(calperwater, 2) & vbTab & Round(SumDev, 2) & vbTab & _
Round(Abs(minusaaa), 1) & vbCrLf

'And Abs(minusaaa) > waterdev.Text
' If Abs(minus) < 1 Then

ggg:
Next water
Next H
```

```
Next OH
sTitle = sTitle & sFinalValues
FinalValues.Text = sTitle
i1.Caption = i
End Sub
Function Round(nValue As Double, nDigits As _    'SUBROUTINE TO ROUND VALUES
Integer) As Double
Round = Int(nValue * (10 ^ nDigits) + _
0.5) / (10 ^ nDigits)
End Function
Private Sub Command2_Click()
End
End Sub
```

3.2.3.9.3 Explanation of code

Visual Basic uses input/output windows that are associated to program code. The data is entered in the text boxes of the window then the program executes the desired tasks. Figure 3.6 shows the input/output window of the Molecular Determination Program henceforth called MDP. MDP is based on the use of three nested "For loops" that are used to vary the amount of OH, H and water in the molecular formula of the compounds in a given range inputted by the user in the appropriate text boxes. A "For loop" is a code line telling the computer to automatically increment a variable inside a given range by a certain amount. The

MDP, begins by executing the innermost "For loop" (which varies the quantity of water) through its full range which does the following:

1) Calculates the molecular formula and the weight percentages of each element using the quantities in the variables OH, H and water, which are the amounts, associated the coefficients of hydroxyl groups, hydrogen atoms in the acid and the amount of water in the molecule respectively.
2) Calculates the deviations between the experimental and computed values and sums them.
3) The sum of the deviations is compared to the value entered by the user in the "cut off point for sum deviation" text box and verifies the following conditions:
    a) If the sum of the deviations is higher than the % value inputted, these values are rejected, and the program performs the next iteration of the innermost "for loop"
    b) If the sum is lower, the values are kept, outputted and the program performs the next iteration of the innermost "for loop"
4) The program is completed when the upper bound values of each for loop is reached simultaneously.

3.3 RESULTS AND DISCUSSION OF THE ZnAl/PPA COMPOUNDS

3.3.1 Powder XRD analysis

Table 3.3: d spacing and "a" parameter of ZnAl LDHs

Sample name/ ZnAl LDH ratio	X = Al/(Al+Zn)	d spacing Å	a parameter
ZnAl09/Zn_2Al	0.33	8.77	3.06
ZnAl15/Zn_3Al	0.24	8.83	3.07
ZnAl14/Zn_4Al	0.19	8.89	3.08

Figures 3.7 a, b and c show the XRD patterns of the Zn_2Al, Zn_3Al, Zn_4Al LDHs, respectively. The d spacing and the "a" parameter of each compound are found in Table 3.3. The value of the d spacing of the Zn_2Al LDH was obtained by calculating the average of the first three reflections (003, 006 and 009 reflections) found in the compounds' diffractogram (Figure 3.7a). The d spacings of the Zn_3Al and Zn_4Al LDHs were obtained from the average of the first 2 reflections (003 and 006 reflections) of the materials diffractograms' (Figures 3.7b and 3.7c respectively).[81] The d spacings of these LDHs are similar to those found in the literature for ZnAl LDHs containing nitrates.[45;81] Furthermore, Table 3.3 shows that the a parameter decreases as the value of x of the LDHs increases. The a parameter is related to the

mean radius of the metals found in the layers of the LDH, and as the substitution of a metal with a smaller radius inside the layer increases, the a parameter decreases.[46] Therefore, since the radius of Al^{3+} is smaller than the radius of Zn^{2+}, the a parameter decreases with the increasing content of Al^{3+} (or an increase of x).

In the diffractogram of each LDH, extra reflections were noted and were labelled as ZnO in the Figure 3.7. These reflections were attributed to a zinc oxide contamination that was identified using the JCPDS database. However, this contamination was considered insignificant because the deviation between the calculated and experimental data of each LDH was small (Table 3.4). Finally, other important peaks that are indexed on the spectrum correspond to the ones found in the literature for ZnAl layered double hydroxides.[226]

The XRD patterns of the Zn_2Al, Zn_3Al, Zn_4Al LDHs that have been treated with phenyl phosphonic acid (PPA) are found in Figure 3.8 a, b and c respectively. The successful reactions can be noted by the disappearance of the original LDH patterns which were replaced with the patterns of new layered compounds that have 3 orders of (*00l*) reflections apparent at 2θ values of ~ 6.0°, 12.3° and 18.5°. The orders of reflections and the layered character of the compounds were confirmed by the enhancement of these reflections when the XRD was taken from the samples in preferred orientation. Figure 3.9 shows the enhancement of the *00l* lines of the Zn_2Al/PPA compound. The d spacing calculated from the average of the 3 orders of reflections corresponds to 14.5 Å. This value is very similar to the interlayer spacing of zirconium phenyl phosphonate (ca: 14.7 Å) reported by Alberti *et al.* [187] and Poojary *et al.* [193] In these materials, the three oxygens of the phosphonate group of the phenylphosphonic acid molecules are directly bound to the zirconium atoms. In addition, the

benzene rings are pointing inside the layers and form a bilayer arrangement that is perpendicular to the zirconium layers. The observed d spacing of the new materials are also comparable to the interlayer distance (ca: 14.7 Å) reported by Carlino *et al.* [219] for a product obtained from the thermal reaction of phenylphosphonic acid with a MgAl LDH. In the latter article the following structure was proposed for the product: one oxygen group of the phenylphosphonic acid is grafted to every second metal atom in the LDHs brucite-like sheets and the remaining metal atoms are bound to hydroxyl groups. Moreover, the phenyl groups are semi perpendicular to the metal layers. The structure proposed for the compounds in this study is a Zn/Al metal phosphonate where a double layer of phenyl groups is perpendicular to the metal layers, the oxygens of the phosphonate groups are bound to the metals and there are no hydroxyl groups present in the layers, similarly to the structure of a layered aluminum phosphonate compound reported by Raki *et al.*[209] or the structure of zirconium phenylphosphonate.[187;193]

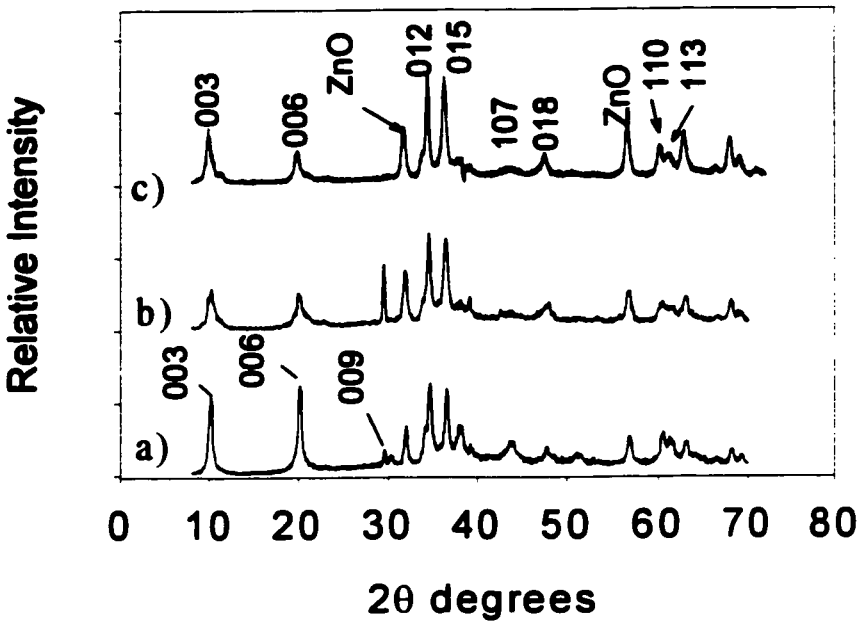

Figure 3.7 XRD patterns of a) Zn_2Al, b) Zn_3Al and c) Zn_4Al LDHs

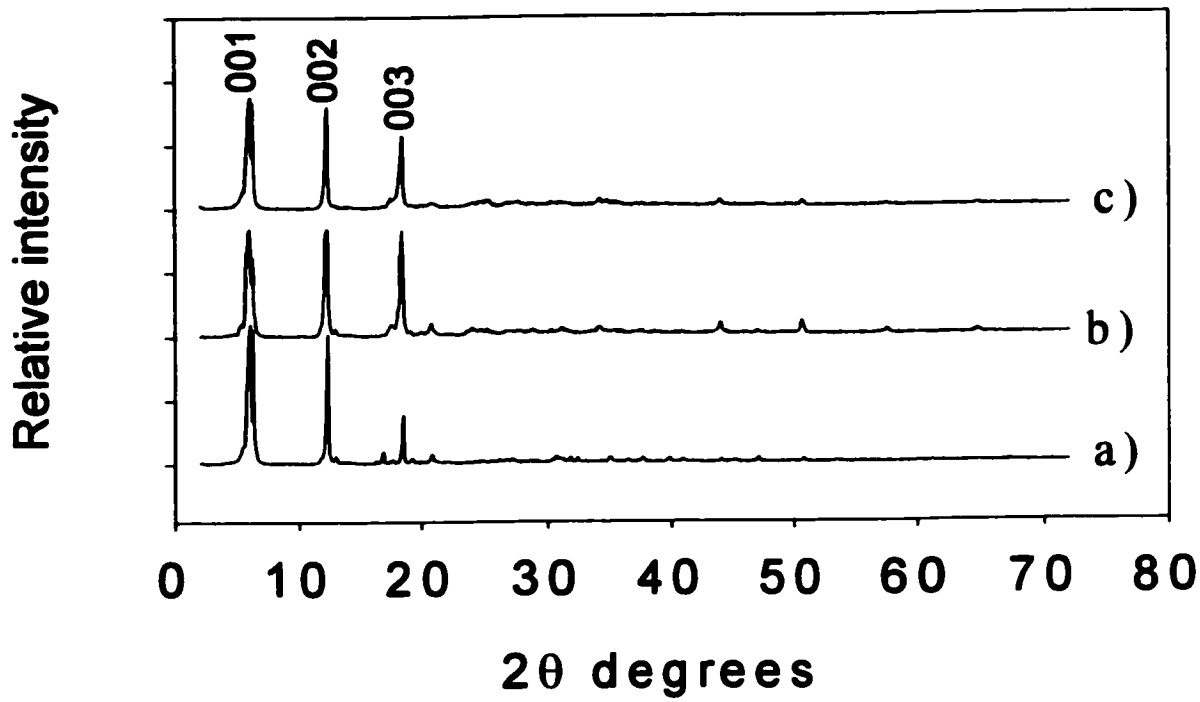

Figure 3.8 XRD patterns of the a) Zn_2Al/PPA, b) Zn_3Al/PPA and c) Zn_4Al/PPA compounds

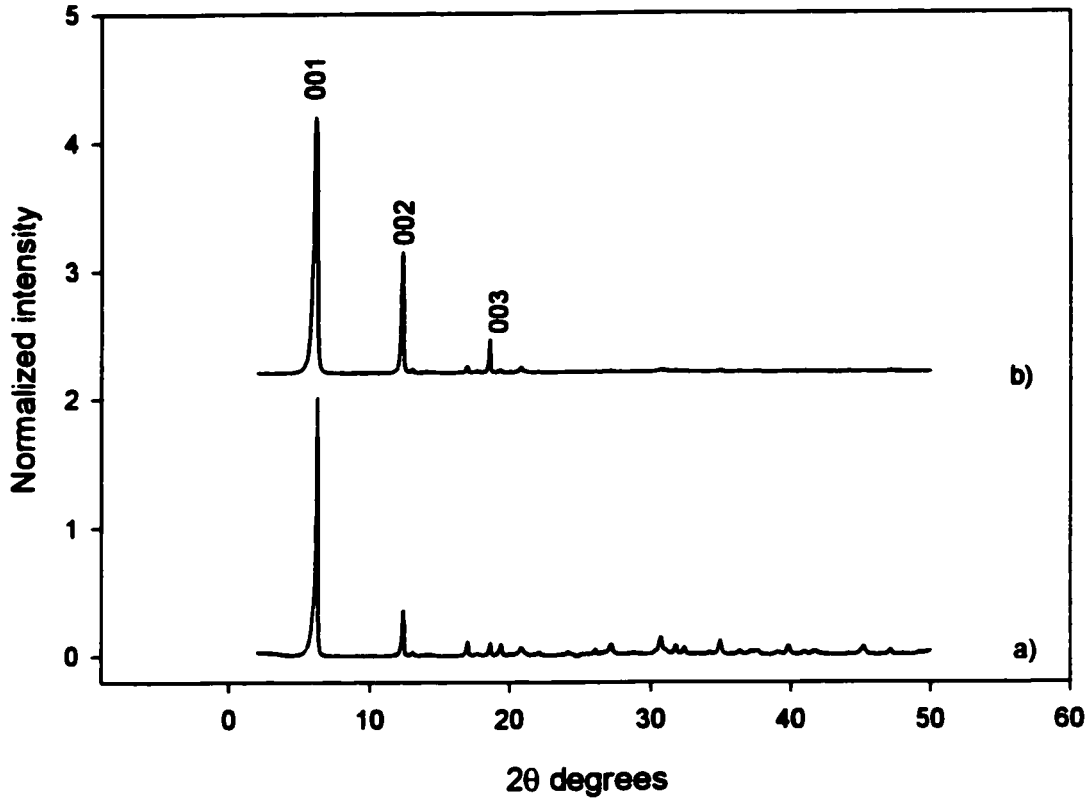

Figure 3.9 XRD patterns of Zn_2Al/PPA compound a) Random orientation and b) Preferred orientation

3.3.2 Chemical analysis of the LDHs and LDH/PPA compounds

3.3.2.1 Molecular formula determination of the LDHs

Table 3.4: ICP and elemental analysis of the ZnAl LDHs

M(II)/M(III ratio	Method of Analysis	Elements	Calculated Weight %	Exp. Weight %	Molecular Fomula
Zn_2Al	ICP[1]	Zn	39.2	39.0	
	ICP	Al	7.95	7.91	
	EA[2]	C	N C.[4]	0.17	$Zn_{0.67}Al_{0.33}(OH)_2(NO_3)_{0.33}\bullet 0.26H_2O$
	EA	H	2.27	1.90	
	ICP	N	4.13	4.39	
	TGA[3]	H_2O	4.19	4.00	
Zn_3Al	ICP[1]	Zn	44.2	42.1	
	ICP	Al	5.77	5.56	
	EA[2]	C	N.C.	0.21	$Zn_{0.76}Al_{0.24}(OH)_2(NO_3)_{0.24}\bullet 0.29H_2O$
	EA	H	2.32	1.87	
	ICP	N	4.78	3.90	
	TGA[3]	H_2O	4.65	4.72	
Zn_4Al	ICP[1]	Zn	46.6	52.4	
	ICP	Al	4.64	5.21	
	EA[2]	C	N.C.[4]	0.15	$Zn_{0.81}Al_{0.19}(OH)_2(NO_3)_{0.19}\bullet 0.25H_2O$
	EA	H	2.23	1.84	
	ICP	N	2.41	2.18	
	TGA[3]	H_2O	3.99	4.08	

Notes: 1) Inductively couple plasma, 2) Elemental analysis, 3) Thermogravimetric analysis, 4) Not calculated

Table 3.4 shows the results obtained from ICP and elemental analysis of the synthesized LDHs. The molecular formula of each compound was determined by calculating the value of x in the LDH type equation below using the molar zinc and aluminum ratio determined by the ICP analysis.

$$(1) \qquad Zn_{1-x}Al_x(OH)_2(NO_3)_x \bullet yH_2O$$

The experimental data shown in the table were obtained from the ICP and elemental analysis of the respective LDHs. These results coupled with the FT-IR and the powder XRD pattern confirm that LDHs were obtained. The deviation between the calculated and the experimental values is most likely due to the zinc oxide contamination that was identified in the powder XRD pattern.

3.3.3.2 Molecular formula determination of the LDH/PPA compounds

Table 3.5: Experimental and calculated data of the ZnAl/PPA materials.

M(II)/M(III) ratio	Method of analysis	Ele.	Calc. weight %	Exp. weight %	Dev. %	Molecular formula
Zn_2Al/PPA	ICP[1]	Zn	14.9	14.9	0.1	$Zn_{0.63}Al_{0.37}(OH)_{0.05}$
	ICP	Al	3.65	3.65	0.08	$(C_6H_5PO_3H_{0.23})_{1.32}\bullet$
	EA[2]	C	34.4	35.0	1.7	$0.99H_2O$
	EA	H	3.24	3.23	0.2	
	ICP	P	14.8	13.9	6.4	
	TGA[3]	H_2O	6.51	6.50	0.08	
Zn_3Al/PPA	ICP	Zn	18.4	18.4	0.2	$Zn_{0.72}Al_{0287}(OH)_{0.02}$
	ICP	Al	3.00	3.00	0.13	$(C_6H_5PO_3H_{0.01})_{1.16}\bullet$
	EA	C	32.8	35.3	7.1	$1.04H_2O$
	EA	H	3.14	2.89	8.7	
	ICP	P	14.1	13.9	1.5	
	TGA	H_2O	7.36	7.60	3.14	
Zn_4Al/PPA	ICP	Zn	20.7	20.8	0.5	$Zn_{0.78}Al_{0.22}(OH)_{0.03}$
	ICP	Al	2.40	2.40	0.2	$(C_6H_5PO_3H_{0.01})_{1.10}\bullet$
	EA	C	32.2	34.8	7.4	$0.95H_2O$
	EA	H	3.04	2.71	12.4	
	ICP	P	13.8	14.2	2.5	
	TGA	H_2O	6.95	7.00	0.8	

Notes: 1) Inductively coupled plasma 2) Elemental Analysis 3) Thermogravimetric analysis

The molecular formulas in table 3.5 were calculated from the program described in section 3.2.3.9 and the ones having coefficients resulting in the lowest overall deviation between the experimental and the calculated values were kept. They represent the best model for the ZnAl/PPA compounds. The molecular formulas have hydroxyl group coefficients that are lower than 0.05 and coefficients for the protons that are lower than 0.23. This demonstrates that the compounds are devoid of hydroxyl groups and that the great majority of interlayer acids are completely deprotonated. The absence of OH groups also indicates that the phenylphosphonic acid molecules are grafted directly to the metal layers of the material. This outcome has been described previously in the studies of the intercalation of different phosphonate molecules in LDHs.[70:222]

3.3.4 IR Analysis

Infrared spectra of the three non-treated LDHs are shown in Figure 3.10. These spectra are relatively simple and their general appearances are typical of LDHs.[27:227:228] A large absorption band is centered at ~3440 cm^{-1} corresponding to the stretching of hydroxyl groups present in the structure and the broadness of the band indicating a large number of hydrogen bonds. Another absorption band typical of these compounds is found at ~1630 cm^{-1} corresponding to the water molecule torsion. The nitrate interlamellar anions v_3 absorption mode is found at ~1383 cm^{-1}. A shoulder at 1360 cm^{-1} indicates residual carbonates in the LDHs and many of the bands below 1000 cm^{-1} are attributed to structural lattice and OH vibrations.[162]

Figure 3.11 shows the IR spectra of the ZnAl/PPA compounds. These patterns are definitely different than the original LDH spectra confirming a reaction of phenylphosphonic acid with the layered double hydroxide. In addition, the spectrum is almost identical to the one found in the article of Knight *et al.* where a layered zinc phenylphosphonate was synthesized via a sol gel method.[206] This change is especially noted in the region between 950cm^{-1} and 1200 cm^{-1}. This is the region of absorption of the P-O bonds. The bands at 1144,1080 and 986 cm^{-1} correspond to PO_3 stretching bonds.[206;222] The bands at 750, 720, 690 and 580 cm^{-1} correspond to bands associated to a monosubtituted phenyl ring.[206;222;229] At 1437 cm^{-1} the P-C (Phenyl) vibration can be observed[217;222]. Furthermore, in these compounds the bands at ~3400 cm^{-1} are due to OH stretching vibrations of water molecules.[206;217] The absorption at ~3057 cm^{-1} is due to the stretching of aromatic hydrogen atoms, and finally the water torsions can be observed at ~1630 cm^{-1}.

In the Figure 3.12 the IR spectra of a physical mixture of the acid and the Zn_2Al LDH and the Zn_2Al/PPA compound can be observed. The comparison of these spectra reveals that the ZnAl/PPA compound is different than the simple physical mixture. The bands in the mixture at 2800 and 2300 cm^{-1} are due to the intramolecular bonding of the P-OH groups of the phenyl phosphonic acid and are absent in the ZnAl/PPA compound because the acid has bound to the metal layers and can no longer form intramolecular hydrogen bonds.[55] The replacement of the interlayer anions by PPA can assuredly be confirmed because the nitrate and carbonate absorption at 1360 –1383 cm $^{-1}$ bands are present in the physical mixture and are almost absent in the ZnAl/PPA material. Finally the P=O band has moved from 1220 cm-^{1} in the mixture to 1205 cm^{-1} in the ZnAl/PPA compound that may be due to a decrease

in P=O bond strength after the reaction. This result suggests that the P=O may be interacting with the metal layers and may be losing its double bond characters.

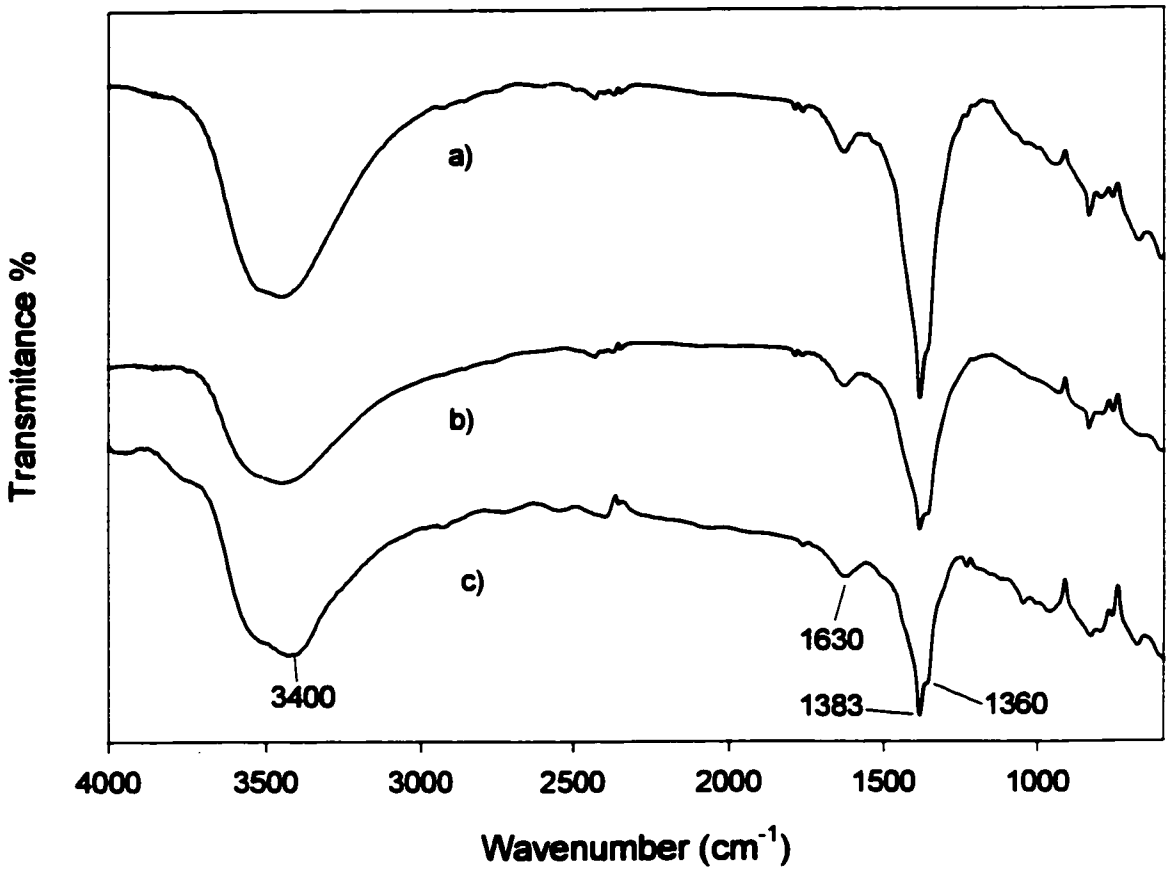

Figure 3.10 Infrared spectra of a) Zn_2Al, b) Zn_3Al and c) Zn_4Al LDH

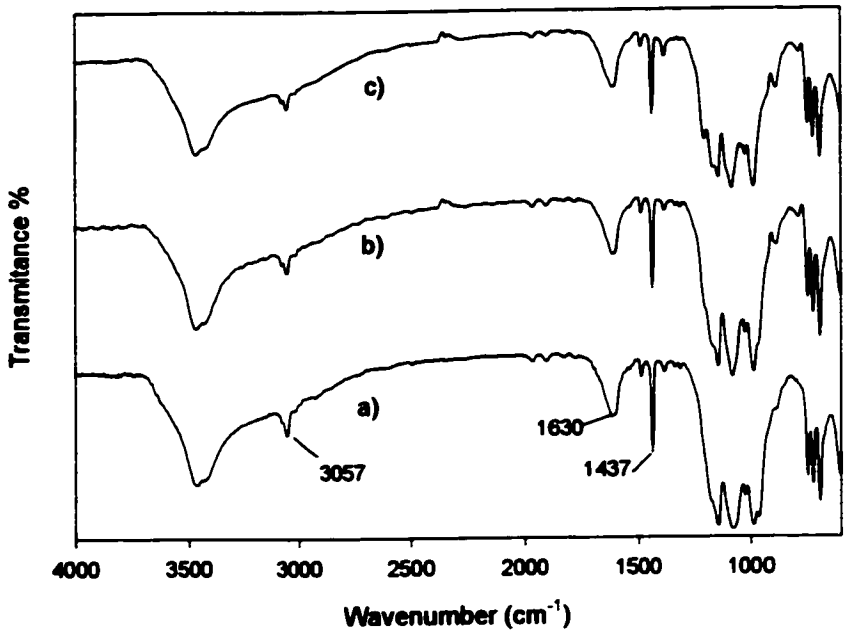

Figure 3.11 Infrared spectra of a) Zn_2Al/PPA, b) Zn_3Al/PPA and c) Zn_4Al/PPA compounds

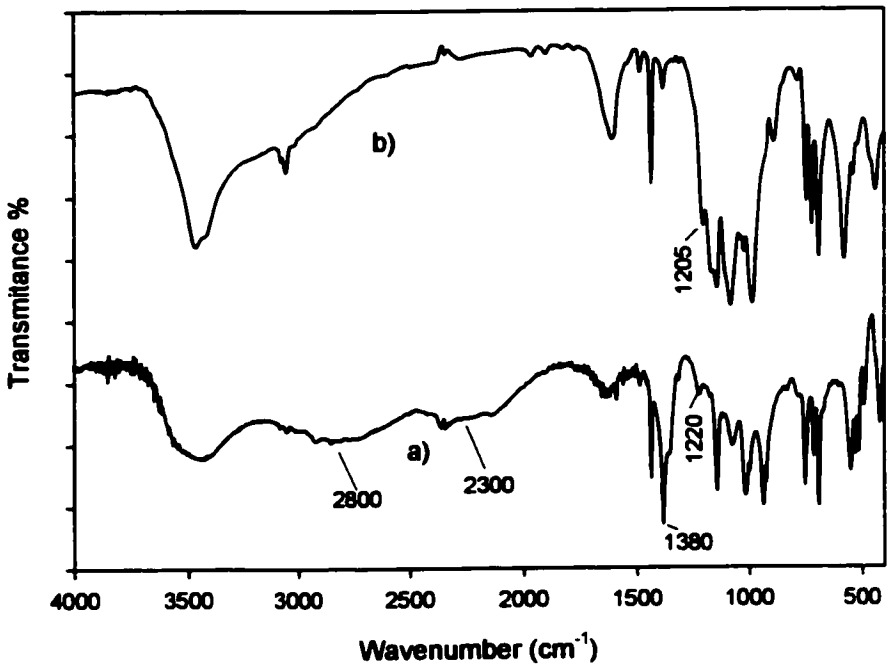

Figure 3.12 Infrared spectra of a physical mixture of the PPA and the Zn_2Al LDH and b) Zn_2Al/PPA compound

3.3.5 TGA Analysis

Figures 3.13a and 3.13b show the TGA curves of the Zn_4Al LDH before and after reacting with PPA respectively. These curves are similar to the TGA curves obtained for the Zn_2Al and Zn_3Al LDHs. The first weight loss found between 0 and approximately 100°C corresponded to the loss of interlayer water.[3] The losses between 200 and 1000°C corresponded to 31%, 27% and 22% of the total masses of the Zn_2Al, Zn_3Al and Zn_4Al LDHs respectively. These can be ascribed to the combined losses of the anions and to the dehydroxylation of the hydroxyl groups of the LDHs. The values were all within a 5 % deviation of the calculated losses that were determined from the LDHs molecular formulas (Table 3.3). Figure 3.13b shows the TGA of the Zn_4Al/PPA compound. The weight loss curve is similar to that of layered phosphonates found in the literature.[195;217;222] The first step between the ambient temperature and 150°C is attributed to the loss of water. The second mass loss of 31.8 % of the total mass that occurs between 500°C and 800°C was attributed to the loss of a phenyl ring. The theoretical weight loss of 31.3% for the phenyl ring, calculated by assuming the formula in Table 3.4, indicates an excellent agreement with the expected value. The same weight losses are observed for the Zn_2Al/PPA and Zn_3Al/PPA compounds. These results further support the formula obtained from the computer program in Table 3.4. In addition, these losses are similar to those observed in nickel phosphonate, zinc and cobalt phenylphosphonates.[215;217] The final □abeled□ions product was identified as being a mixture of zinc, aluminum and phosphorous oxides with the ratio of each element

shown in Table 3.6. The ratio of each element was determined by the chemical analysis of the calcined LDH/PPA compounds.

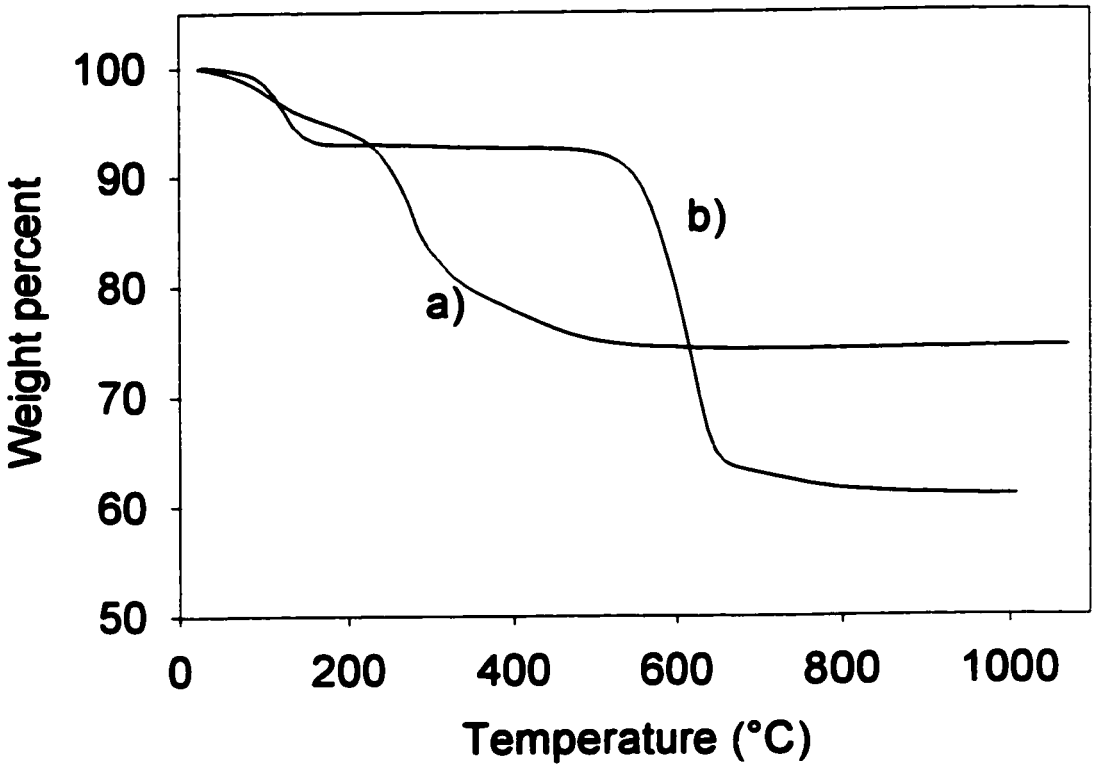

Figure 3.13 TGA of the a) Zn_4Al LDH and b) Zn_4Al/PPA compound

Table 3.6: Zn, Al and P weight% and ratios of the calcined ZnAl/PPA compounds.

#/M(II)/M(III) ratio	Elements	Calculated Weight %	Exp. Weight %	Molecular ratios
Zn_2Al / PPA	Zn	26.7	24.9	$Zn_{0.63}Al_{0.37}O_{4.15}P_{1.19}$
	Al	6.47	6.14	
	P	23.8	20.8	
Zn_3Al / PPA	Zn	30.5	32.1	$Zn_{0.72}Al_{0.28}O_4P_{1.14}$
	Al	4.90	4.93	
	P	22.9	25.7	
Zn_4Al / PPA	Zn	33.0	35.1	$Zn_{0.78}Al_{0.22}O_{3.88}P_{1.11}$
	Al	3.85	3.72	
	P	22.3	19.1	

3.3.6 Solid state NMR analysis

3.3.6.1 ^{13}C-MAS NMR

Figure 3.14a shows the ^{13}C NMR spectrum of the Zn_4Al/LDH compound. This is a representative spectrum of the three intercalated compounds. Using ^{31}P decoupling (Figure 3.14b) and a combination of ^{31}P decoupling and dipolar dephasing (Figure 3.14c) the ^{13}C resonances could almost all be unambiguously assigned. The resonances at 130.3 ppm and 134.3 ppm in Figure 3.14a are due to the ipso carbon coupled to the ^{31}P, which when decoupled, gives one resonance centered at 131.9 ppm. This is shown in Figure 3.14b. The

elimination of the doublet reveals the underlying peaks at 134 and 129 ppm. The dipolar dephasing experiment (Figure 3.14c) shows the disappearance of the resonance at 129 ppm, indicating that this peak is associated to the para carbons. The intensity of the resonances of 126.7 and 134 ppm do not diminish during the dipolar dephasing experiment. This indicates that these are either the meta or the ortho carbons and that the phenyl rings are rotating on their C2 axis. The rotation of the ring averages out the C-H dipolar coupling reducing the broadening effect of the dipolar dephasing experiment on resonances that are associated to carbons coupled to hydrogen.

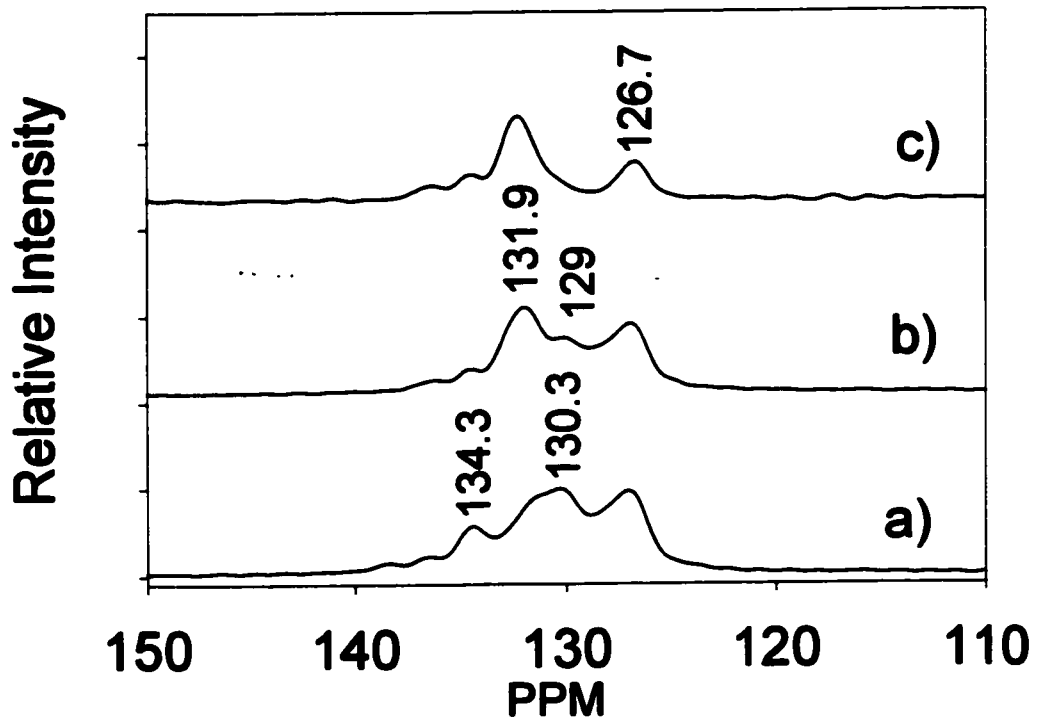

Figure 3.14 Solid state CPMAS NMR of Zn_3Al/PPA a) ^{13}C, b) ^{13}C with ^{31}P decoupling and c) ^{13}C with ^{31}P decoupling and dipolar dephasing 40 μs

3.3.6.2 ^{31}P-MAS NMR

The ^{31}P MAS NMR spectra of the 3 LDH/PPA compounds are shown in Figure 3.15. The phosphorous signal is much more complicated than expected. Since phenylphosphonic acid has only one phosphorous atom with no NMR active nuclei in its vicinity (or none in significant quantity), one would expect a single resonance indicative of phosphorous in a single environment. However, two groups of resonances (labeled A and B) can be observed in the spectra of each LDH/PPA compounds. The rather large difference in chemical shift between these sets of resonances, (~25 ppm) suggests phosphorus atoms that are chemically distinct.[190] Furthermore, to determine if the resonances between –6 to 3 ppm were individual signals or a result of splitting occurring from ^{31}P / ^{27}Al dipolar coupling, a ^{31}P NMR spectrum of Zn_2Al/LDH compound was taken on a 400 MHz spectrometer. If the phosphorus is coupled to aluminum a reduction in the broadness of the resonances is expected when the spectrum is taken at a higher magnetic field strength. This is due to the second order quadrupolar interactions being inversely proportional to the field strength.[230] Figure 3.16 shows the spectrum of Zn_2Al/LDH taken on a 200 MHz spectrometer after being electronically line broadened and the spectrum taken on a 400 MHz spectrometer. After line broadening is applied to the 200 MHz spectrum, the resonances shapes resemble that of the 400 MHz resonances. There is no decrease in the broadness of the resonances as the field strength increases. Therefore, the signals are different resonances and are not due to the dipolar coupling with ^{27}Al. In Figure 3.15, we can also note that there is a difference in relative intensity between the resonances found in the range of –6 to 3 ppm (labeled as B) and the resonances in the range of 21-24 ppm (labeled as A) for the 3 compounds. Table 3.7 below gives the A/B (calculated from the integration values) and Zn/Al ratio of each sample.

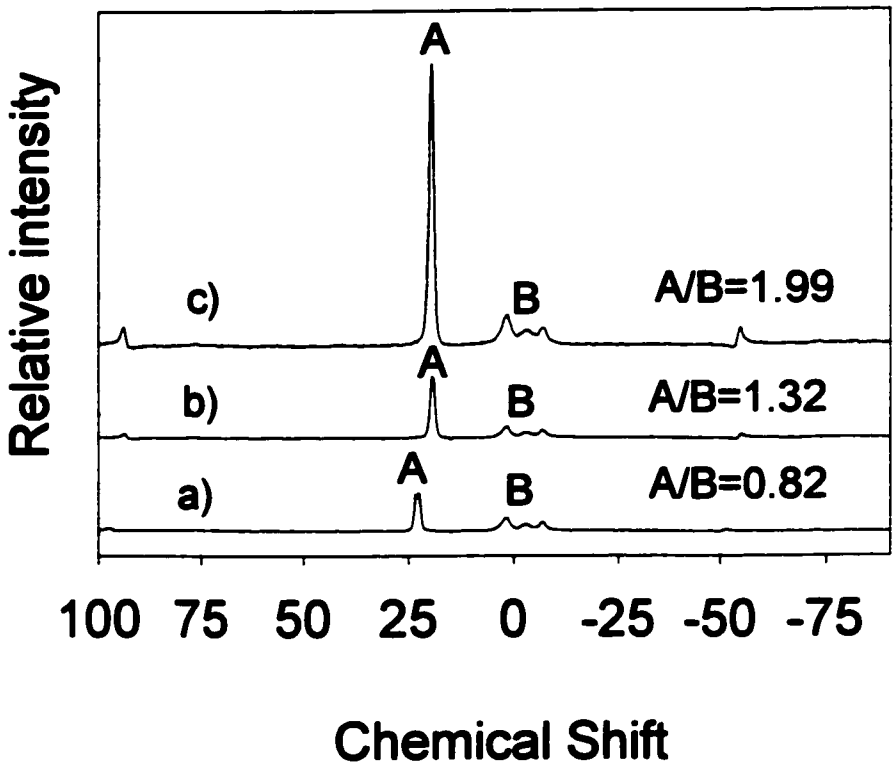

Figure 3.15 ^{31}P MAS quantitative spectra of a) Zn_2A/PPA, b) Zn_3Al/PPA and c) Zn_4Al/PPA compounds

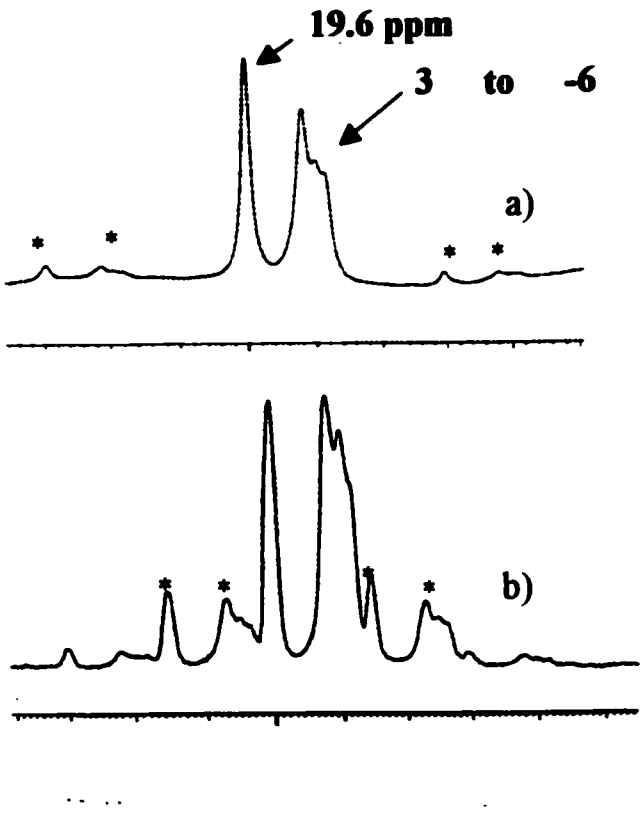

Figure 3.16 ^{31}P CPMAS spectra of Zn_2Al/PPA compound a) at 200 MHz with line broadening and b) at 400 MHz (*): spinning side bands

Table 3.7: Zn/Al ratio before and after reaction as a function of the relative intensity of the ^{31}P A/B resonances ratio

Zn/Al Ratio (before intercalation)	Zn/Al Ratio (after intercalation)	A/B Ratio
2.03	1.69	0.82
3.12	2.53	1.32
4.15	3.58	1.99

In addition, the A/B ratio increases proportionately with the Zn/Al ratio, which implies that the A signal is associated with a phosphorous in the vicinity of zinc and the B signal corresponds to a phosphorous in the vicinity of aluminum. The 3 resonances associated with aluminum which have a small difference in chemical shift, most likely represent chemically altered phosphonic acid in a range of crystallographically non equivalent sites.[219;231]

To ensure that the intensity ratio of the peaks was quantitative, a variable pulse delay time experiment was done on Zn_2Al/PPA LDH. The relative ratio of A/B was calculated as the pulse delay time was increased. The delay time used for the quantitative analysis was

determined when the A/B ratio did not significantly change from one pulse delay experiment to another (1200s). This is shown in Figure 3.17 where the A/B resonances ratio vs. the time of delay is plotted.

Finally, from the ratios obtained in the ^{31}P NMR study and from the molecular formula obtained from the program, the following (Table 3.8) molecular formulas were determined for the 3 LDH/PPA compounds.

Table 3.8: Molecular formula of the LDH/PPA compounds

LDH/PPA compound	Molecular Formula
(Zn_2Al/PPA)	$Zn_{0.63}Al_{0.37}(Pa)_{0.59}(Pb)_{0.73}\cdot 0.99H_2O$
(Zn_3Al/PPA)	$Zn_{0.72}Al_{0.28}(Pa)_{0.66}(Pb)_{0.50}\cdot 1.04H_2O$
(Zn_4Al/PPA)	$Zn_{0.78}Al_{0.22}(Pa)_{0.74}(Pb)_{0.37}\cdot 0.95H_2O$

Where Pa is the phenylphosphonic acid grafted to zinc and Pb is the phenylphosphonic acid grafted to aluminum.

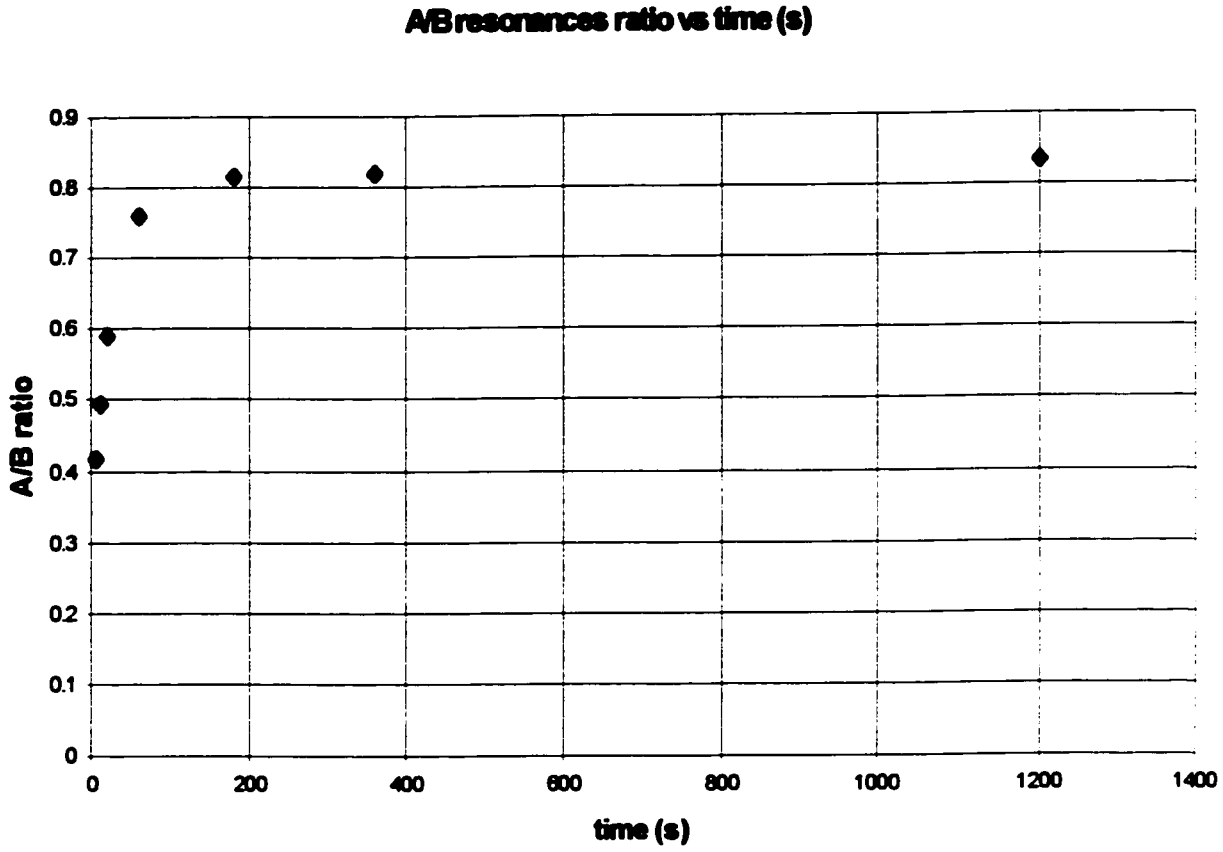

Figure 3.17 A/B ^{31}P resonances ratio vs the time of delay of the Zn_2Al/PPA compound

3.3.7 BET Surface Area

Table 3.9: BET surface area of the Zn_2Al/PPA compound

Sample	No treatment (m^2/g)	Calcined at 350°C for 1hr (m^2/g)	Calcined at 700°C for 1hr (m^2/g)
Zn_2Al LDH	1.72	9.79	14.5
Zn_2Al/PPA	32.0	9.25	2.00

Tables 3.9 shows the Bet surface areas of the original LDH and of the Zn_2Al/PPA compound before and after being heated at 350°C and 700°C. The heat treatment was done to eliminate a percentage of the organic moieties inside the layers in order to create micropores and increase the surface area of the sample.

The BET surface area before intercalation was 1.72 m^2/g and increased to 32 m^2/g after the intercalation. Despite this increase, the result is not indicative of microporosity, as a much larger surface area would be expected. Furthermore, the absence of microporosity was confirmed by the null value obtained for the micropore volume that was determined from the t-plot analysis of the adsorption data. After heating the sample at 350°C for 1 hr, the surface area of the Zn_2Al/PPA compound is almost the same as the original LDH. This is most likely because the interlayer PPA molecules are being released from the interlayers and the collapse

of the structure occurs. At 700° the structure is destroyed and most likely gives way to mixed metal and phosphate oxides as demonstrated in section 3.3.5.

3.4 RESULTS AND DISCUSSION OF THE ZnAl/B-PPA COMPOUNDS

3.4.1 Chemical analysis of the LDH and B-PPA/LDH compounds

3.4.1.2 Molecular formula determination of the LDH

Table 3.10: ICP and elemental analysis of the ZnAl LDH

Sample name	Method of Analysis	Elements	Calculated %	Experimental %	Formula
ZnAl28	ICP[1]	Zn	34.5	31.5	$Zn_{0.62}Al_{0.38}(OH)_2$
	ICP	Al	8.84	8.07	$(NO_3)_{0.38}{\cdot}0.47H_2O$
	EA[2]	H	2.53	3.23	
	EA	N	4.59	3.13	
	ICP	C	N.C.[4]	0.18	
	TGA[3]	H_2O	7.24	6.70	

Notes:

1. ICP: Inductively Coupled Plasma)
2. EA: Elemental Analysis
3. TGA: Thermogravimetric Analysis
4. N.C.: not calculated

Table 3.10 shows the results obtained from the ICP and elemental analysis of the synthesized LDH. The molecular formula was determined by initially calculating the value of x in the LDH type equation below with the molar zinc and aluminum ratio determined by the ICP analysis.

$$Zn_{(1-x)}Al_x(OH)_2(NO_3)_{2x} \bullet y\ H_2O \quad (1)$$

Subsequently the molar weight percent of each element could be calculated by dividing the amount of each element in the formula by the molecular mass of the LDH. The experimental data shown in table 3.10 were obtained from the ICP and elemental analysis of the samples. The small difference between the experimental and calculated data (except for nitrogen) coupled with the powder XRD and IR spectra of ZnAl28 (Zn_2Al LDH) indicate that an LDH has been successfully obtained. The relatively large deviation (>40%) between the experimental and calculated weight % of nitrogen is because the carbon content was not taken into account in the molecular formula calculation. The carbon content is due to carbonates that are difficult to remove from the layers of layered double hydroxide.[22;232] It was considered unnecessary to take the carbon content into account because it would not alter the molecular formula significantly.

3.4.1.2 Molecular formula determination of the LDH/B-PPA compounds

Table 3.11: Chemical analysis of the LDH/B-PPA compounds

Sample Name	Method of Analysis	Elements	Experimental %
ZnAl35	ICP[1]	Zn	22.6
	ICP	Al	5.52
	EA[2]	C	10.8
	EA	H	2.78
	ICP	P	10.44
ZnAl41	ICP[1]	Zn	21.5
	ICP	Al	4.96
	EA[2]	C	14.3
	EA	H	2.63
	ICP	P	11.3
ZnAl54	ICP[1]	Zn	16.8
	ICP	Al	4.26
	EA[2]	C	21.12
	EA	H	2.79
	ICP	P	17.9
	TGA[3]	H_2O	9.5
ZnAl55	ICP[1]	Zn	18.7
	ICP	Al	3.87
	EA[2]	C	19.2
	EA	H	2.72
	ICP	P	18.9
	TGA[3]	H_2O	9.5

Notes: 1) Inductively Coupled Plasma 2) Elemental Analysis 3) Thermogravimetric analysis

Table 3.11 shows the chemical analysis of ZnAl28 intercalated with different quantities of 1,4-phenylene bis phosphonic acid (B-PPA) under different reaction conditions. To determine the molecular formulas of the intercalated compounds three different methods were tested. A brief description of each one will be examined in the following text and the reason why the third one was chosen will be described.

In the first method, the x value in the LDH formula shown below was calculated with the Zn:Al ratio obtained by the ICP data.

$$Zn_{1-x}Al_x(OH)_a(C_6H_4P_2O_6H_Z)^{4-Z}_{[(2-a)+x]/(4-Z)} \bullet yH_2O$$

Subsequently, the values of "a", "z" and "y" in the formula above were manually varied to obtain diverse molecular formulas. For each new formula the weight percent of each element was determined and the deviation between the experimental and calculated data was found with the help of an electronic spreadsheet (Excel 2000). The value of "a" was varied in the range (a = 0, 1, 2) and for each value of "a", "z" was varied in the range of (z = 0,1,2,3,4) and "y" was adjusted to minimize the deviation between the experimental and calculated weight percentage of hydrogen. This method did not yield any conclusive results because none of the formulas gave a satisfactory fit (i.e. the overall deviation between the calculated and experimental data was not acceptable). It was quickly understood that this method could not efficiently calculate the intermediate possible ranges for "a","z" and "y" because these values were chosen manually, therefore another method was tested.

The second method consisted of using the 3 general formulas shown below as possible molecular formulas for the compounds.

(1) $Zn_{1-x}Al_x(OH)_2(C_6H_5P_2O_4H_z)_{(x/4-z)}\bullet yH_2O$

(2) $Zn_{1-x}Al_x(OH)_1(C_6H_5P_2O_4H_z)_{(1+x/4-z)}\bullet yH_2O$

(3) $Zn_{1-x}Al_x\ (C_6H_5P_2O_4H_z)_{(2+x/4-z)}\bullet yH_2O$

A system of 5 equations was used to resolve the values of "x", "y" and "z" of each formula. Each equation represented the weight % of Zn, Al, C, P, H, and was made equal to their respective experimental weight percentages. The equations were solved using an iterative Levenberg-Marquardt method (a nonlinear least-squares fit method) found in the Mathcad Professional 8 software. In this method initial "x", "y" and "z" values must be chosen to solve the equations (initial guesses). The initial values of "x", "y" and "z" were chosen with the following restrictions; $0 \leq x \leq 1$, $0 \leq y \leq 10$, $0 < z < 4$ with variable increments for each range. These ranges were chosen because they are the quantities of aluminum, water and hydrogen that are possible for the molecular formulas of each compound. Afterwards, for each initial guess, the software calculated "x", "y" and "z" values. With this data, the theoretical weight percentages of each element were calculated as well as the deviation between the experimental and theoretical values. The molecular formula with the lowest overall deviation would have been considered the most probable model. Again, this method like the one described previously had inherent limitations because the range of initial guesses

for "x", "y" and "z" had to be chosen manually. Therefore, it was impossible to efficiently determine all the intermediate possibilities in the given ranges.

A program developed in Visual Basic 6 was the 3rd method that was used to determine the molecular formulas of the compounds. This program is described in detail in the experimental section (3.2.3.9) and does not have the limitations of the two previous ones because the program is able to calculate all the intermediate ranges of the variables taking into account all the possible molecular formulas. The molecular formula determination was done on the samples ZnAl54 and ZnAl55 and the results are shown in table 3.12 but it was not done on the samples ZnAl35 and ZnAl41 because their reactions were not completed as judged by their low % of carbon (10.8, 14.3 % respectively) and their powder XRD pattern. (Figures 3.21 and 3.23 see discussion below).

Table 3.12: Molecular formulas of ZnAl54 and ZnAl55

Sample Name	Method of analysis	Elements	Calculated Weight %	Exp. Weight %	Dev %	Molecular Formula
ZnAl54	ICP[1]	Zn	16.6	16.8	1.3	$Zn_{0.62}Al_{0.38}$
	ICP	Al	4.22	4.26	0.95	$(OH)_{0.26}$
	EA[2]	C	20.8	21.12	1.6	$(C_6H_4P_2O_6H_{0.98})_{0.70}$
	EA	H	2.76	2.79	1.84	$\bullet 1.29H_2O$
	ICP	P	17.9	17.9	0.02	
	TGA[3]	H_2O	9.53	9.50	0.37	
ZnAl55	ICP[1]	Zn	18.7	18.7	0.10	$Zn_{0.67}Al_{0.33}(OH)_{0.33}$
	ICP	Al	3.88	3.87	0.16	$(C_6H_4P_2O_6H_{0.90})_{0.65}$
	EA[2]	C	20.3	19.2	5.7	$\bullet 1.23H_2O$
	EA	H	2.74	2.72	0.70	
	ICP	P	17.4	18.9	1.7	
	TGA[3]	H_2O	9.56	9.50	0.62	

Notes: 1) Inductively Coupled Plasma. 2) Elemental Analysis. 3) Thermal Gravimetric Analysis

The molecular formulas of ZnAl54 ad ZnAl55 (Table 3.12) were the ones obtained from the computer program that gave the smallest overall deviation between the experimental and calculated data and therefore represents the best model for these compounds. Both formulas exhibit small quantities of OH groups and approximately one proton per acid molecule. Similarly to the ZnAl/PPA compounds, these results imply that the B-PPA molecules are grafted to the metal layers. However, because the B-PPA is monoprotonated this suggests that one of the oxygen of the phosphonate groups is not coordinated to the metal layer.

3.4.2 XRD analysis

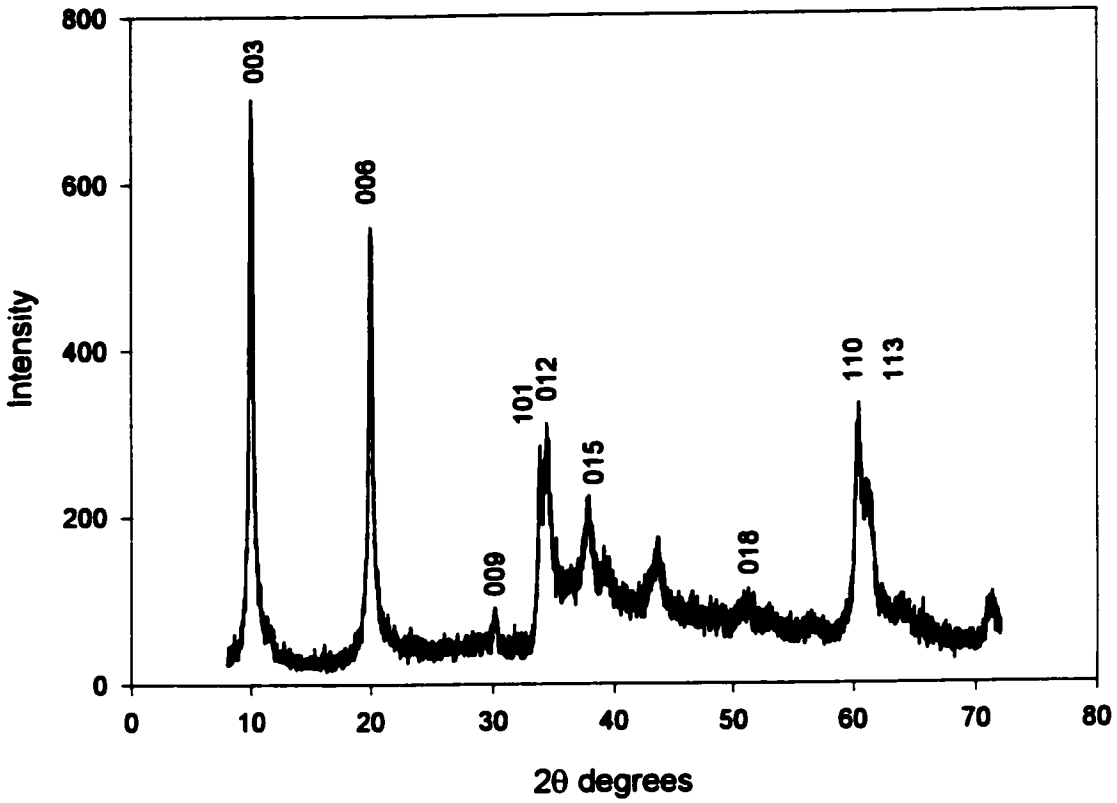

Figure 3.18 XRD pattern of ZnAl28 (Zn_2Al LDH)

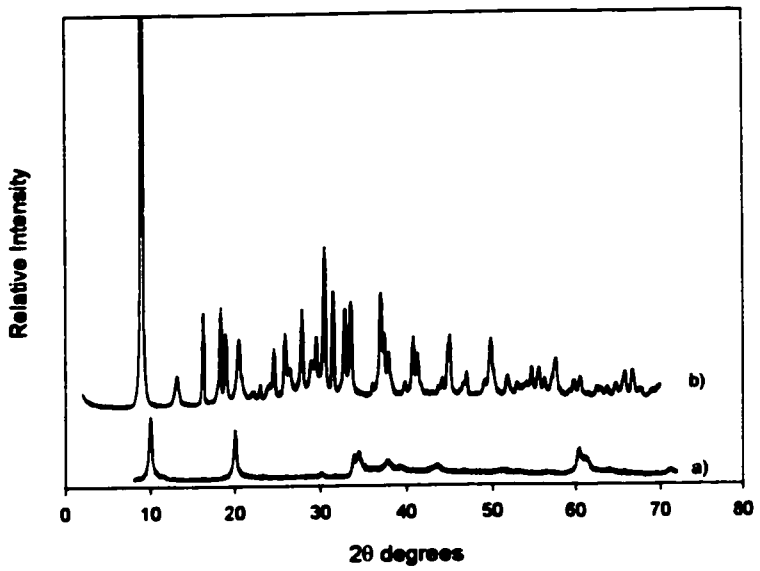

Figure 3.19 XRD patterns of a) ZnAl28 and b) ZnAl54

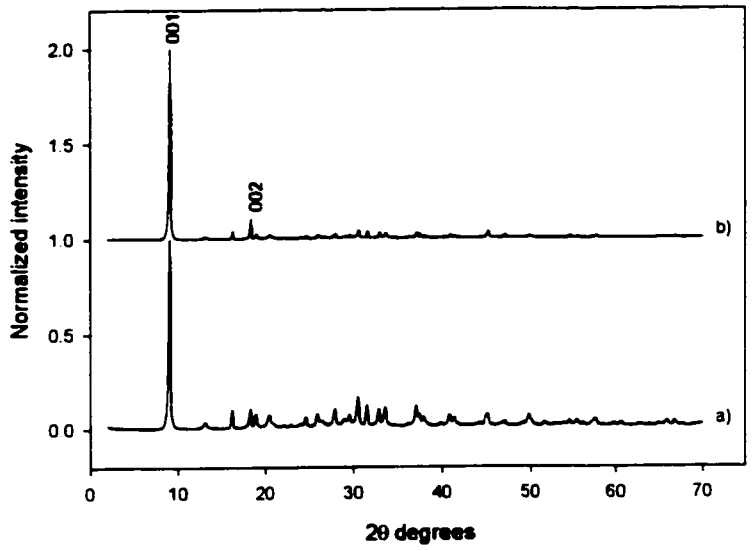

Figure 3.20 XRD patterns of ZnAl54 a) Random Orientation and b) Preferred orientation

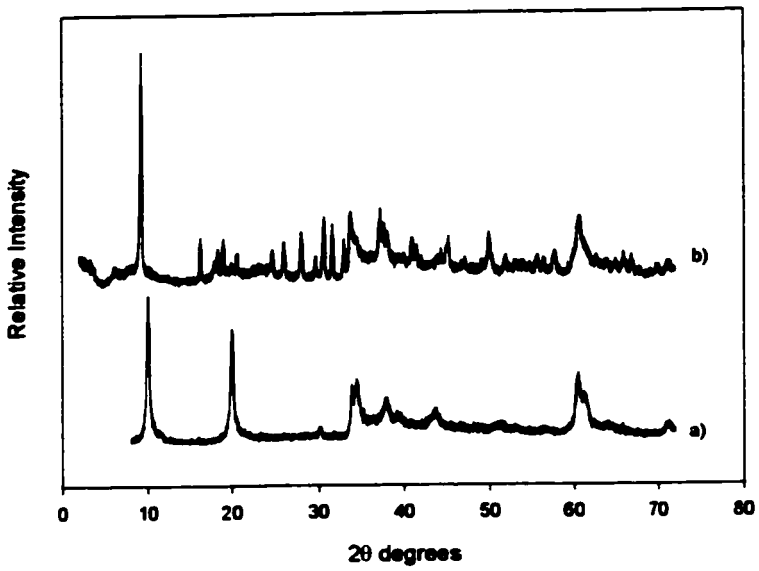

Figure 3.21 XRD patterns of a) ZnAl28 and b) ZnAl35

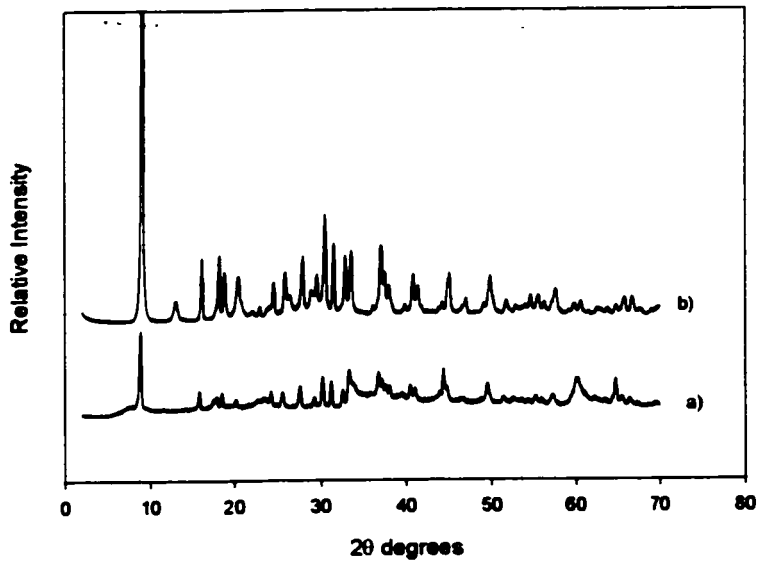

Figure 3.22 XRD patterns of a) ZnAl41 and b) ZnAl54

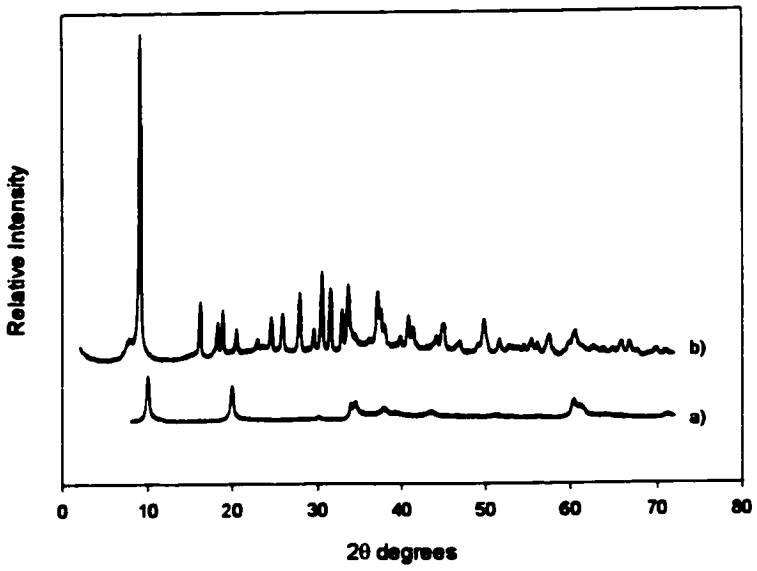

Figure 3.23 XRD patterns of a) ZnAl28 and b) ZnAl41

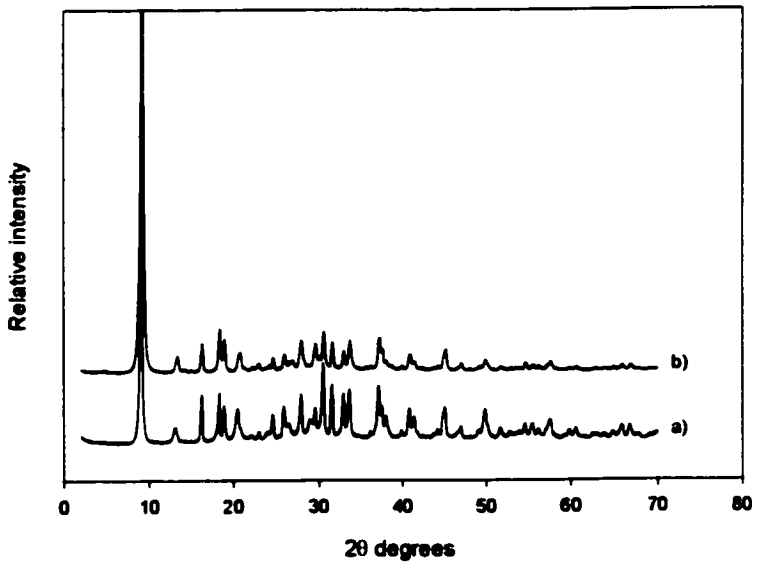

Figure 3.24 XRD patterns of a) ZnAl54 and b) ZnAl55

Figure 3.18 shows the XRD pattern of the Zn_2Al LDH (ZnAl28) and the main reflections are in the range found in the literature [45;64;233] for ZnAl LDHs with nitrates in the interlayers. Figure 3.19 shows the comparison between the XRD pattern of ZnAl28 and this LDH treated with B-PPA (denominated: ZnAl54). The diffractogram of ZnAl54 does not show the usual LDH pattern as demonstrated by the absence of the 012 and 110 reflections characteristic of an LDH. Similarly to the case of the ZnAl LDHs treated to PPA, the layered character of ZnAl54 can be confirmed by comparing its preferred orientation XRD pattern to its random orientation pattern that are shown in Figure 3.20. The enhancement of the first and second order diffraction lines in the preferred orientation XRD pattern is characteristic of a layered material.[201] Furthermore, the first (*00l*) reflection of the LDH/B-PPA compound appears at 9.14° 2θ (d spacing: 9.66 Å) and the second one at 18.43° 2θ. From the average value of these reflections, a d spacing of 9.66 Å was calculated. This distance was found to be the same as the one reported by Wang *et. al.*[70] for a MgAl LDH grafted with B-PPA. In the reported work, B-PPA was reacted with MgAl LDHs at different temperatures. When the LDH was heated with the acid or dried rigorously, they obtained a phase with an interlayer spacing of 9.647 Å. They proposed that the temperature dependence of the phases could be explained by a dehydration process:

$$Mg_2Al(OH)_6(O_3PC_6H_4PO_3)_{0.25} \xrightarrow{100\text{-}150^\circ C} Mg_2Al(OH)_3O_{1.5}(O_3PC_6H_4PO_3)_{0.25} + 1.5H_2O$$

and the loss of the hydroxyl groups led to a pillared product in which the organophosphorus molecules were connected directly to the metal cations in the LDH sheets and no longer

through the hydroxyl groups.[70] Figure 3.21 shows the XRD pattern of ZnAl28 (Zn_2Al LDH) and of ZnAl35 (LDH treated with B-PPA for 48 hrs with a controlled pH of 5 throughout the reaction). A comparison of these patterns reveals that ZnAl35 has remnant LDH reflections (012, 015,110 and 113) indicating that the reaction was not complete. Furthermore, comparison of the XRD pattern of ZnAl35 with the XRD pattern of ZnAl54 (Figure 3.22) shows that there is a mixture of the LDH and the LDH/B-PPA layered compound in the former sample. To determine if a larger quantity of B-PPA was needed to complete the reaction, ZnAl41 was prepared. This sample was synthesized under the same conditions as ZnAl35 except a larger quantity of B-PPA was added to the reaction mixture. The XRD pattern of the original LDH (ZnAl28) and ZnAl41 are shown in Figure 3.23. The characteristic LDH 012, 015, 110 and 113 diffraction lines are also apparent in the XRD pattern of ZnA41 indicating an incomplete reaction despite the increased quantity of B-PPA. Since the ratio of LDH to B-PPA for ZnAl41 and ZnAl54 are the same, this implies that the reaction in acidic medium facilitates the reaction. The pH of the reactions of ZnAl35 and ZnAl41 were adjusted with sodium hydroxide which most likely formed the partial sodium salt of the acid effectively hindering the completion of the reaction. This process has been reported in the literature.[70] Figure 3.24 shows the comparison between the diffractogram of the LDH treated two times with B-PPA (2 x 48 hrs) (denominated: ZnAl55) and ZnAl54. Both diffractograms are almost identical signifying that the reaction can be completed in only 48 hours.

3.4.3 IR analysis

Figure 3.25 shows the infrared spectrum of ZnAl28. The spectrum is characteristic of a layered double hydroxide. A broad band centred at about 3450 cm^{-1} corresponds to the OH vibration bands of hydrogen-bonded water molecules.[161:234] The H_2O bending vibration can be observed at 1627 cm^{-1}. The sharp and strong band at 1383 cm^{-1} (ν_3) and the small but sharp band at 826 cm^{-1} (ν_2) shows clearly the presence of the nitrate ion in the sample.[27] The shoulder at around 1360 cm^{-1} in addition to the band at 1017 cm^{-1} indicates the presence of carbonates ions (ν_3 and ν_1 of CO_3^{2-} respectively).[2:27]

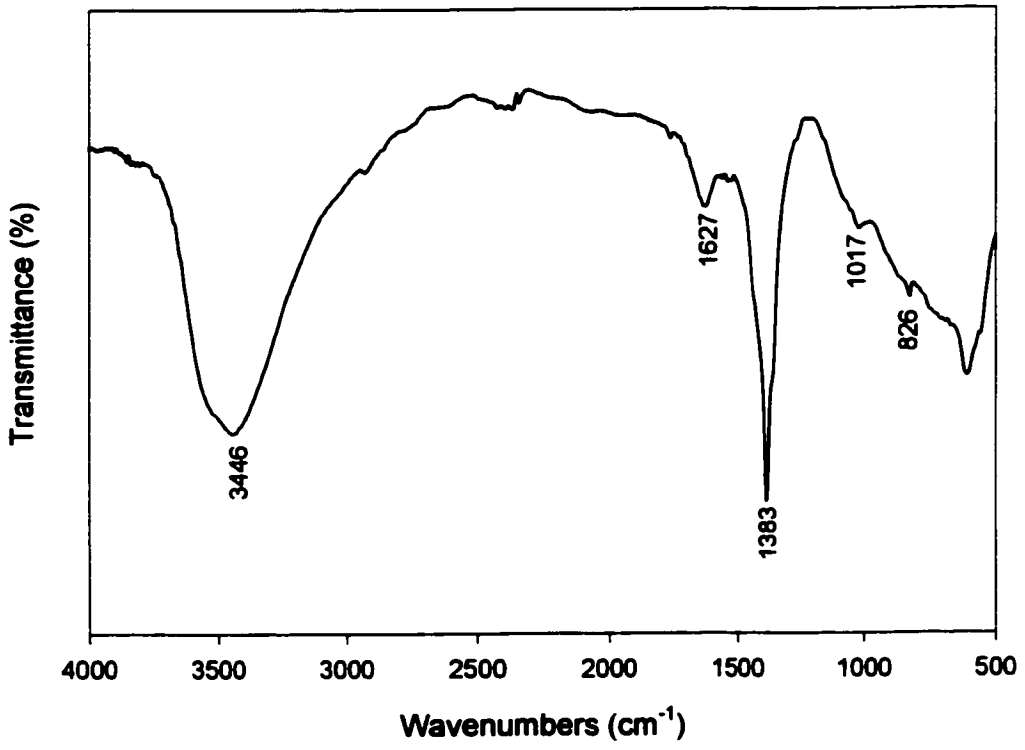

Figure 3.25 Infrared spectrum of ZnAl28

Figure 3.26 shows the infrared spectra of B-PPA, ZnAl54 and ZnAl55. The water absorption band at 1620 cm^{-1} can be observed indicating the presence of water in all the samples. The presence of water is also indicated by the broad absorption band at 3400 cm^{-1}. The $-PO_3$ vibration frequencies can be found between 980 cm^{-1} and 1200 cm^{-1} and the sharp band at ~824 cm^{-1} are attributed to out of plane vibrations for para-substituted phenylene rings.[204] The decrease in relative intensity of the band at 1386 cm^{-1} compared to the band found in the original LDH (see Figure 3.25) confirmed the replacement of the nitrate anion for the B-PPA molecules. The same band can be seen in the IR spectra of the acid and is associated to C-C stretching of the aromatic ring.[204] Furthermore, the comparison of the spectra of the ZnAl/B-PPA materials and B-PPA gives additional structural information. Similarly, to the ZnAl/PPA compounds, the large P-OH absorption bands at 2800 and 2300 cm^{-1} are no longer present in the ZnAl/B-PPA compounds because the phosphonate molecules are bound to the metals layers and intramolecular hydrogen bonding of the acid does not occur. The modifications of the bands between 500 to 600 cm^{-1} (δPO_3) region also show changes in the intramolecular hydrogen bonding system.[55]

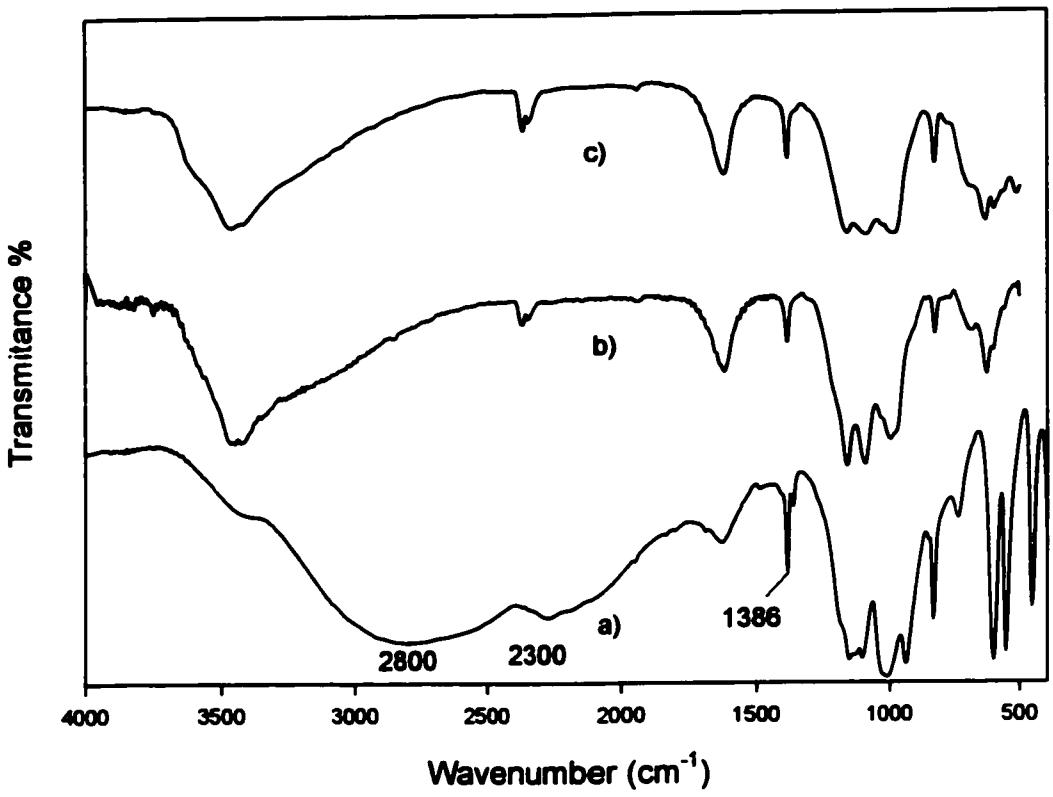

Figure 3.26 Infrared spectra of a) B-PPA, b) ZnAl54 and c) ZnAl55

3.4.4 NMR analysis

In the following section, the results obtained from ^{13}C CPMAS NMR experiments that were performed on B-PPA and on ZnAl54 as well as the ^{13}C solution NMR experiments on B-PPA will be described. The solution NMR results of B-PPA were used to help identify the resonances obtained from the CPMAS NMR experiment of this acid. The NMR experiments were conducted on the original acid and on the LDH/B-PPA compound to note any differences that would occur before and after intercalation.

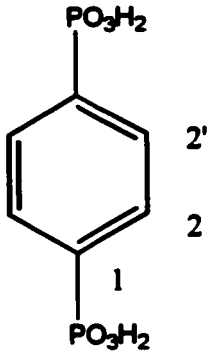

Figure 3.27 1,4-phenylene bis phosphonic acid B-PPA

3.4.4.1 ^{13}C-CPMAS and solution NMR

Table 3.13: ^{13}C Chemical shift of 1,4-phenylene bis phosphonic acid in solution (D_2O)

Carbon #	Chemical shift (ppm)	Coupling Constant (Hz)
1	Doublet: 134.9;133.4 Center of doublet: 134.2	J_1 : 182.4
2	Doublet: 130.2;130.0 Center of doublet: 130.05	J_2: 25.0
2'	Doublet: 130.0	ND[1]

Notes :

1. Not determined

The values of the chemical shifts in the NMR spectrum of B-PPA in solution are shown in Table 3.13. The doublet centered at 134.2 ppm occurs due to the coupling of the ipso carbons that are coupled to the phosphorus atoms of the molecule. The resonances of the doublet are separated by 182.4 Hz and this value is similar to literature ^{1}J coupling constants for ^{13}C-^{31}P coupled atoms that are found in phosphonates.[235] The second doublet centered at 130.1 ppm is due to the ^{2}J coupling of the ortho carbons identified as 2 on the figure 3.27. The third doublet centered at 130.0 ppm is due to the ^{3}J coupling of the carbons in position 2' with the phosphorus atom. The separation of the last doublet is not indicated because it was too small to be resolved by the spectrometer.

Table 3.14: ^{13}C CPMAS solid state NMR chemical shifts of 1,4-phenylene bis phosphonic acid

Experiment	Chemical shifts (ppm) / relative intensities					
CPMAS ^{1}H decoupling.	134.2	4.7	132.6	4.2	130.3	8.0
CPMAS ^{1}H decoupling, DD[1] (40 μs).	134.2	8.0			130.2	7.2
CPMAS ^{1}H & ^{31}P decoupling.			132.3	9.0	130.3	6.2
CPMAS ^{1}H & ^{31}P decoupling, DD[1] (40 μs).			132.1	9.0		

Notes DD: dipolar dephasing

Figure 3.28 shows the ^{13}C CPMAS and the CPMAS dipolar dephased (DD) proton decoupled spectra of the pure acid. The dipolar dephasing experiment gives information on the mobility of the carbons and on the C-H dipolar interactions. In the dipolar dephased spectrum, the resonance at 132.6 ppm disappears. This result indicates that there is an active line broadening mechanism causing this resonance to diminish due to ^{13}C-^{1}H dipolar interactions. For this process to occur the phenyl ring must be stationary so as not to average out the C-H dipolar interaction by rotation. This resonance is therefore associated with carbons bonded to protons in the phenyl ring. We can also note a reduction of the relative intensity of the resonance at 130.2 ppm in the dipolar dephased spectrum. This indicates that there are 2 resonances at this chemical shift and as a result of the elimination of the first resonance, the underlying resonance is revealed. The disappearance of the resonance at 130.2 ppm signifies that it is also associated with carbons coupled to protons. The resonances at 130.2 ppm and 132.6 ppm cannot be the result of a doublet that is caused by a ^{2}J coupling as they are separated by a larger amount than the associated ^{2}J coupling constant of a carbon coupled to a phosphorus atom (115 Hz vs. 25 Hz respectively). This shows that there are two crystallographic different sets of ortho carbons. In addition, the resonances at 134.2 and 130.2 are not affected by the dipolar dephasing experiment indicating that they are the resonances due to the ipso carbon coupled to the phosphorus. These peaks are separated by a value of 200 Hz, which is very similar to the coupling constants of the C-P atoms found in the solution NMR of B-PPA and is in the range of values of C-P coupling constants of phosphonates found in the literature.[235]

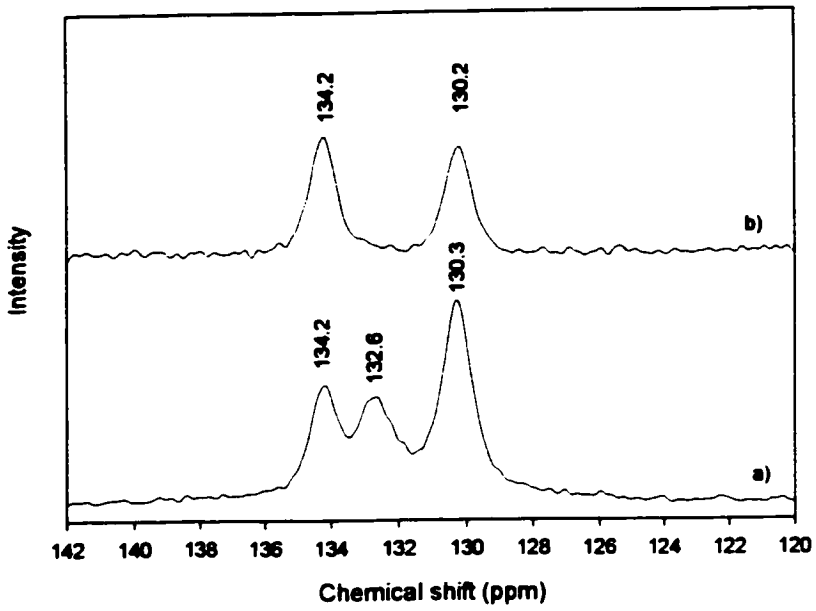

Figure 3.28 ^{13}C CPMAS spectra of B-PPA a) with ^{1}H decoupling and b) ^{1}H decoupling and dipolar dephasing (40 μs)

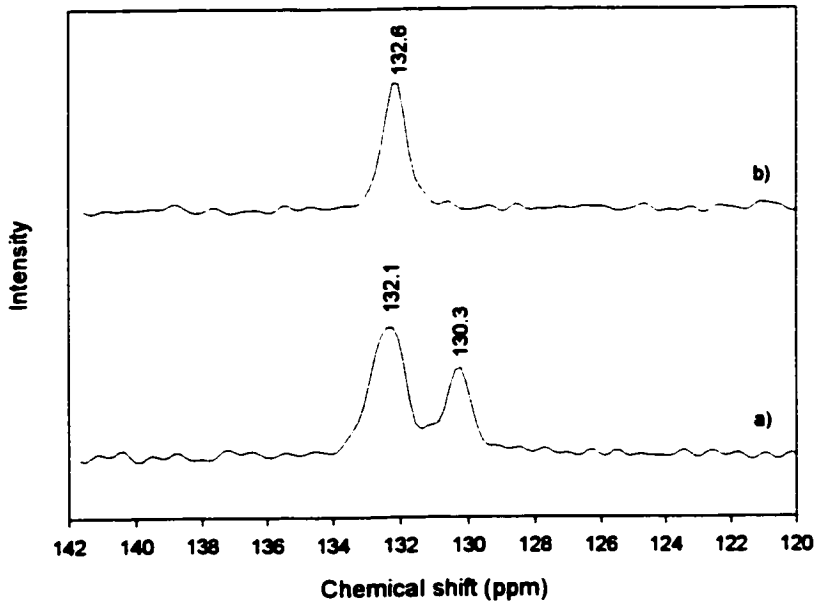

Figure 3.29 ^{13}C CPMAS NMR spectra of phenylene bis phosponic acid: a) ^{1}H & ^{31}P decoupling and b) ^{1}H and ^{31}P decoupling with dipolar dephasing (40 μs)

Finally, the value of the chemical shift of the ipso carbon was confirmed by performing an NMR experiment with proton and phosphorus decoupling showed in Figure 3.29. This spectrum showed a single resonance at 132.6 ppm, which is the center of the C-P doublet.

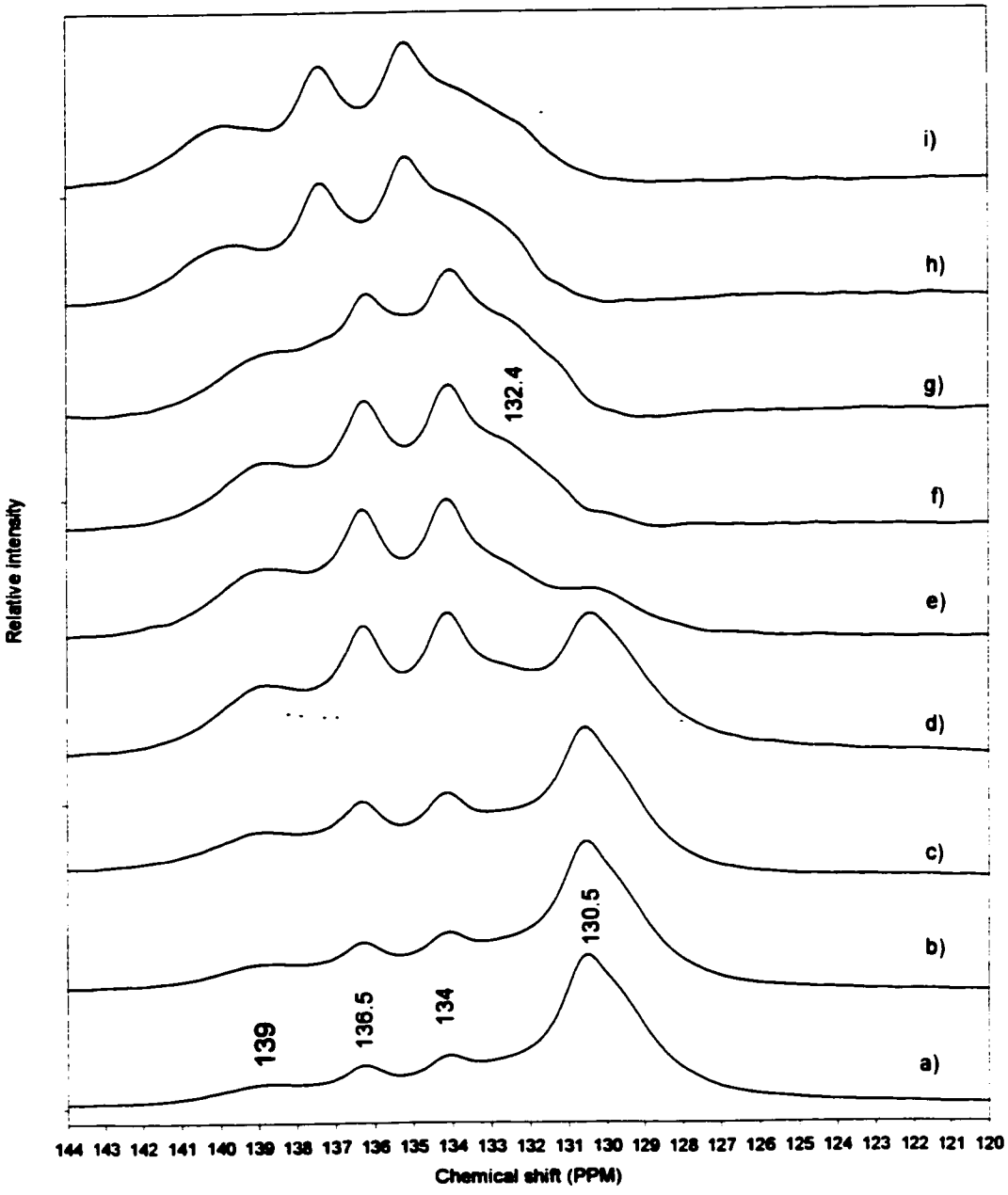

Figure 3.30 ^{13}C CPMAS with ^{31}P and ^{1}H decoupling NMR experiments on ZnAl54 using increasing dipolar dephasing times

a) 0 ms, b) 10 ms, c) 20 ms, d) 30 ms, e) 40 ms, f) 50 ms, g) 60 ms, h) 70 ms, i) 80 ms

Figure 3.30 shows the CPMAS ^{13}C spectra obtained with ^{1}H and ^{31}P decoupling at different dipolar dephasing times of ZnAl54. Deconvolution of all the spectra was completed to identify the chemical shifts of each resonance. The deconvolution of the spectra obtained with the dipolar dephasing times between 0 and 40 μs revealed 4 separate resonances at the following chemical shifts:

130.5 ppm,

134.0 ppm,

136.5 ppm

139.0 ppm

In addition, the resonance at 130.5 ppm reduced in intensity as the dipolar dephasing time increases and completely disappeared when the dipolar dephasing time was 50 μs. While this phenomenon was occurring, a hidden resonance was revealed when the dipolar dephasing time was 30 μs. The chemical shift of this resonance could then be assigned at 132.4 ppm. The reduction of the resonance at 130.5 ppm is an indication that the ^{13}C-^{1}H dipolar coupling is active, establishing the rigid character of the phenyl ring found inside the layers. Therefore, the resonance at 130.5 ppm is the one associated with the ortho carbons of the phenyl ring. Since the other resonances are not affected by the increase in the dipolar dephasing times, these can be associated with the carbons bound to the phosphonate groups. The four separate resonances are most likely due to molecules in four different crystallographic sites as the spectrum of the original acid only shows one resonance under the same experimental NMR conditions. Furthermore, two of these resonances exhibit a narrow line shape (134 ppm and 136.5 ppm) and the other two exhibit a broad character (130.5 ppm and 139.0 ppm). It is known that random motion of a molecule causes the signal to broaden

in MAS NMR, indicating that the latter resonances are associated with carbons that are more mobile.[236]

The intensity of all the resonances versus the dipolar dephasing times has been plotted in Figure 3.31. From these plots, it is clear that the only resonance that is diminishing is the one-labeled at 130.5 ppm.

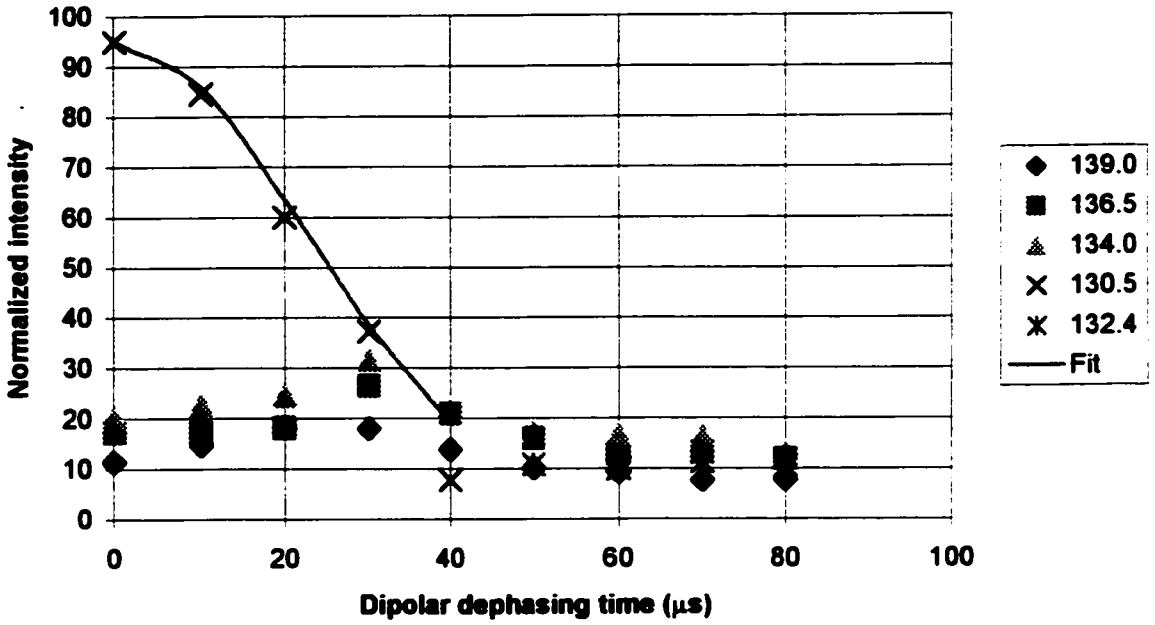

Figure 3.31 Normalized intensity of the resonances as a function of dipolar dephasing times of ZnAl54 CPMAS ^{13}C NMR ^{1}H & ^{31}P decoupling

Furthermore, from the plot of the intensity of the peak 130.5 ppm, it is possible to get semi-quantitative information on the molecular dynamics of the molecule.[237] The attenuation of a resonance during dipolar dephasing is described by the following equation:

$$I_{DD} = I_o e^{-\tau/(2T_2^2)}$$

Where I_{DD} is the attenuated dipolar dephased signal, I_o is the non-dipolar dephased signal, τ is the dipolar dephasing time and T_2 is the spin-spin relaxation time. In figure 3.31 the solid line (Fit) is a fitted line obtained by plotting a graph of $\ln(I_{DD}/I_o)$ vs. τ^2giving a slope of $-1/2T^2_2$. From this fit a T_2 of 16.8 μs was obtained.

3.4.6 Surface area and micropore analysis

Table 3.15: BET surface area, Micropore area and Pore diameter of the ZnAl/B-PPA compound

Treatment	BET surface area (m^2/g)	Micropore Surface area (m^2/g)	Micropore Diameter Å
None	40.1	4.12	9.6
Heated at 400°C for 1 hour	26.2	6.9	9.2

The data in table 3.15 are from micropore experiments performed on a new batch of ZnAl/B-PPA material that was synthesized, characterized and had the same characteristics as ZnAl54 and ZnAl55. The results in Table 3.15 show that the sample has micropores, however, none in significant quantity. The micropores are most likely found in between the B-PPA molecules and their pore diameter is in agreement with the interlayer spacing of the material.

After heating, the micropore surface area increases but not significantly. This suggests that there is the removal of B-PPA molecules from the interlayers, creating more micropores

however, the decrease in the total surface area implies there is a collapse of the structure of the material.

3.5 CONCLUSION

3.5.1 ZnAl/PPA compounds

ZnAl LDHs of varying ratios have been synthesized and reacted with phenyl phosphonic acid. The powder XRD pattern of each material shows a d spacing of 14.7 Å, which corresponds to the d spacing of pure zirconium phenyl phosphonates and other LDHs grafted with phenyl phosphonic acid. The results from the chemical analysis of the ZnAl/PPA compounds fit best with a molecular formula that contains mostly aprotic acid molecules and an absence of OH groups. Furthermore, calcination of the compounds resulted in mixed metal oxides and phosphates similar to those obtained by metal(II) phenyl phosphonates. The IR analysis also confirmed the presence of the phenyl phosphonic acid in the layers of the materials. Solid state NMR analysis proved to be a good probe of the structure as information on the interlayer species was gathered from the carbon and phosphorus NMR analysis of the solids.

From the results we can conclude that phenyl phosphonic acid moieties have been grafted inside the layers of the ZnAl layered double hydroxide. Furthermore, the material unfortunately exhibited no microporosity and this was attributed to the large quantity of PPA molecules allowing no space in the layers due to the high charge density of the LDH.

3.5.2 ZnAl/B-PPA compound

Zn_2Al LDH was treated with B-PPA under different reaction conditions revealing that an acidic medium was the optimum environment for reaction completion. The ZnAl/B-PPA material exhibited a d spacing of 9.6 Å, which was similar to other bis phosphonate grafted compounds. Similarly to the ZnAl/PPA compounds the molecular formula with the best fit was one that had no hydroxyl groups. However, the interlayer acids were found to be monoprotonated. The replacement of the interlayer anions by B-PPA was also confirmed by the IR analysis. Solid state ^{13}C NMR analysis also proved to be a good probe of the structure as information on the interlayer molecules was collected. The ZnAl/B-PPA exhibited microporosity but not in significant quantity.

Future work could involve the intercalation of a combination of PPA or B-PPA molecules with phosphates or phosphites in LDHs to create spaces between the organic phosphonates and obtain microporosity similarly to the zirconium phosphonate/phosphates-phosphites. Furthermore, PPA or B-PPA molecules with substituents on the phenyl ring acting as spacers to distance the phosphonate molecules could be intercalated in LDHs to obtain microporosity.

CHAPTER 4

The Attempt at the Formation of MCM/FSM Type Material from LDHs

4.1 INTRODUCTION

4.1.1 Surfactants

The word surfactant means surface active agent and can be defined by materials that are characterized by the tendency to absorb at interfaces rather than in the bulk of a solution. Surfactants are also sometimes called amphiphilic because the word amphiphilic has its origin from the Greek word amphi, meaning both. All surfactants contain at least 2 parts: a lyophilic part (that is soluble in a liquid) and a lyophobic part (that is insoluble in a liquid). When a surfactant is used in an aqueous solution, we can talk of a hydrophilic part (soluble water) and a hydrophobic part (insoluble in water). The hydrophobic section of many surfactants is composed of a hydrocarbon chain and the hydrophilic section is composed of a polar ionic headgroup.

4.1.1.1 Classification of surfactants

Surfactants are normally classified by their ionic nature and there are 4 classifications: Anionic, cationic, zwitterionic and non-ionic[91]

Anionic

Alkali alkanoates and soaps with carboxyl groups providing the negative charge are the most well known anionic surfactants. We can also find alkyl sulfates, alkyl ethers, sulfates, alkyl sulfonates, and secondary alkyl sulfonates in the family of anionic surfactants.

Cationic

The cationic surfactants have the quaternary nitrogen as the most common ionic species, alkyl ammonium bromides being the most common cationic surfactants.

Zwitterionic

Zwitterionic surfactants are formed when both a negative and a positive ionic species are found in an amphiphilic molecule. In this class we find betaines, including alkyl betaines, amidoalkylbetaines and heterocyclic betaines

Non-ionic

The non-ionic surfactants are similar to cationic and ionic surfactants but the head group is uncharged. Many of these are based on polyoxyethylene where the headgroup are oligomers of ethylene oxide.

The ethylene oxide surfactants can also be represented by C_nE_m where n is the length of the alkyl chain and m is the length of the ethylene oxide head group.

4.1.1.2 Raw materials to fabricate surfactants

The raw material used for the fabrication of the hydrophobic section of surfactants can come from either natural or synthetic sources. The surfactants based on natural products are fabricated from fatty acids triglycerides that come from both animal and vegetable sources. The main components of these acids are shown below

Saturated

Dodecanoic acid $C_{11}H_{23}COOH$

Tetradecanoic acid $C_{13}H_{27}COOH$

Hexadecanoic acid $C_{15}H_{31}COOH$

Octadecanoic acid $C_{17}H_{35}COOH$

Unsaturated:

8-octadecanoic acid $C_{17}H_{33}COOH$

8-11 octadecanoic acid $C_{17}H_{31}COOH$

Another natural source of materials for surfactants comes from the digestion of pulpwood with sodium hydroxide. From this process, polycyclic terpene carboxylic acids are obtained which need to be purified for further use as raw material for surfactant fabrication.

Byproducts of petrochemicals are also used as the raw material for the hydrophobic part of surfactants such as olefins, alcohols, paraffins and aromatic hydrophobes. For instance, ethylene is obtained by cracking of naphtha, linear alcohols can be obtained by the hydrogenation of the corresponding fatty acid methyl ester or by the Ziegler-Natta polymerization of ethylene.

4.1.1.3 Applications

The main application of surfactants is their use as detergents. They are also used in personal care (eg: soap bars for washing), household detergents, industrial laundries, pine oil disinfectants, cosmetics and shampoos. They can also be used as antifoam agents in coating applications, dispersing agents in paint, and in a wide variety of other applications.

4.1.1.4 Properties of surfactants

The main properties characterizing surfactants are the following:

Adsorption, micelle formation, solubilisation, microemulsion, wetting, foaming/defoaming, macro emulsions, dispersiong/aggregation of solids, detergency. [238] As mentioned above, surfactants adsorb more at the surface than in the bulk of the solution. This happens because it minimizes the contact of the hydrophobic part of the surfactant with the solution thereby reducing the free energy of the system. Another method by which this can happen is the formation of micelles. When a small quantity of surfactant is added to an aqueous solution, the surfactant aggregates near the surface in a flat position. As the concentration of the surfactant increases, there is less room for the surfactant at the interface and they start to orient themselves in a fashion determined by the nature of the hydrophobic group. As the concentration is increased furthermore, the surfactants form a monolayer across the whole interface of the solution until a critical concentration is achieved when there is not enough room for all the molecules at the interface. At this point, they start to form micelles and this concentration is called the critical micelle concentration (CMC). This particular concentration varies with each type of surfactant and varies with the temperature of the

solution. In solution, micelles can take many different shapes. They can be spherical, cylindrical, lamellar or cubic. The actual structure and shape of a micelle depends upon the temperature, type of surfactant and its concentration. It also depends on other factors such as the type of ions in solution and other water-soluble organic compounds. Generally, the diameter of the micelle is approximately twice the length of the hydrophobic group of the surfactant molecule, and the number of surfactant molecules in a micelle is known as the aggregation number, which is around 50 to 100 molecules for most ionic surfactants.

In the 1930's, the existence of micelles was generally accepted after McBain and co-workers[239] published their studies on different types of soaps. They showed that the abnormal behavior of aqueous soap solutions was due to the presence of micelles. A few years later, Tartar and co-workers [239;240] presented studies on the solubilities and micelle formation of some surfactants. For the following decades, investigators did much research on these molecules to determine their structure and studies on the concentration and the temperature at which micellar formation became significant.

4.1.2 MCM and FSM type materials

In 1992 Beck *et al.*[241] discovered a new family of mesoporous molecular sieves designated as M41S that were synthesized using aluminosilicate gels and micelles as templates. There are four main groups in the M41S family of materials designated as:[242]

MCM-48: displays a three dimensional cubic ordered pore structure

MCM-41: one-dimensional hexagonal pore structure

MCM-50: Unstable lamellar structure

Octamer: unstable surfactant-silica compound (surfactant-$(SiO_2)_8$)

The illustration of each structure are shown in the figure below (Figure 4.1)

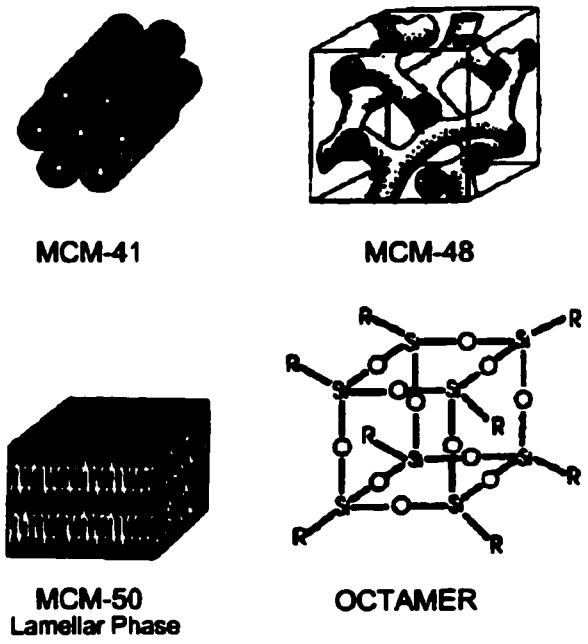

Figure 4.1 Structures of the different types of MCM materials[242]

MCM type materials exhibit high surface area (exceeding 1000 m^2/g) and high sorption capacities.[241;243] Because of these properties the materials have a great potential of being used as adsorption media, ion exchangers, molecular hosts and are currently being extensively

researched for these purposes.[207] In addition, researchers have recently been incorporating metals in their pore structures[243-250] that would also allow for applications as catalysts. The MCM-41 materials are the most researched compound of this family and exhibit a network of hexagonal array of uniform mesopores and channels varying in size between 15 Å to more than 100 Å that can be varied with the choice of surfactants.[241;251] A typical preparation involves the mixing of a surfactant solution (e.g.: hexadecyltrimethylammonium) with alumina, tetramethylammonium silicate solution and precipitated silica.[241] The mixture is normally placed in a static autoclave at a temperature over 100°C for 48 hours or more. The obtained material is filtered, rinsed and dried in air at ambient temperature. To open the mesopores the surfactants must be eliminated and this is done by calcining the material at a temperature of 540°C for 7 hours (1 hour in nitrogen, 6 hours in air.)

At approximately the same time that the MCM type materials were synthesized, another group of researchers had synthesized mesoporous hexagonal silicates and aluminosilicates prepared from kanemite, a layered polysilicate that were designated as FSM-16 materials.[207] These materials can be fabricated with channels that are in the range of 20 to 40Å with internal surface areas of ~900 m^2/g.[252] Two mechanisms have been proposed for the formation of the material. Inagaki *et al.*[253;254] proposed a two-step formation mechanism involving the intercalation of alkyltrimethyl ammonium cations and the subsequent folding of the intercalated kanemite layers to form the framework ("Folded sheet mechanism" hence the name FSM). The second mechanism proposed by Chen *et al.* [255] involves the same first step as the previous one but entails a reorganization of the kanemite layers in the second step. The driving force of the latter mechanism is the ability of the surfactant to form double layers

and then adopt cylindrical micelle shapes that rearrange the silicates around them. A silanol condensation then occurs to form the mesophase framework.

4.1.3 Basis for research

To date there has been no article reported in the literature concerning the formation of MCM or FSM type materials starting from LDHs. In a similar fashion to the formation of FSM materials, it was believed that it might be possible to transform LDHs into these types of compounds by using anionic instead of cationic surfactants.

The transformation of LDHs into FSM type materials could be an attractive method of forming mesophases incorporating a variety of metals that could be used for highly active catalytic mesoporous materials. In the following study, LDHs were used as starting material with hexadecanesulfonic acid or sodium dodecyl sulfate, to form FSM type compounds. The compounds were then characterized by XRD, IR and EA.

4.2 EXPERIMENTAL

4.2.1 LDH synthesis

The LDH was prepared using the same conditions as in the previous chapter.

A mixture consisting of $Zn(NO_3)_2 \cdot 6H_2O$ (29.7 g, 0.10 moles) and of $Al(NO_3)_3 \cdot 9H_2O$ (18.89 g, 0.05 moles) in 300 ml of freshly boiled deionised water was added together with a 2N NaOH solution (~200 ml), to a flask containing 150 ml of deionised water. Rapid stirring was continued throughout the addition and the rate of addition was such that the pH was kept at 8 ± 0.5. After the addition was completed, the mixture was heated at ~75-80°C for 16 hrs under N_2. It was then filtered, washed with water then dried at 70°C for 24hrs.

4.2.2 Synthesis of LDH/FSM type compounds

5 different synthesis routes were adopted to form the FSM type materials.

Anion exchange method: Direct treatment of the LDH with the surfactant at the critical micelle concentration.

Memory effect method: Calcined LDH treated with the surfactant at the critical micelle concentration.

Coprecipitation at constant pH method: Coprecipitation of a ZnAl LDH in the presence of the surfactant at the critical micelle concentration.

The first two methods were also performed in an autoclave. These reactions were tested in an autoclave because M41S type materials are normally formed using this apparatus. Hexadecanesulfonic acid (HDSA) and sodium dodecyl sulfate (SDS) were used as the surfactant because these compounds have been studied extensively in the literature and their properties are very well known. The reactions mixtures were kept at the temperatures of the CMC of the surfactant in question. All reactions were done using boiled distilled/deionized water and done under a nitrogen atmosphere unless stated otherwise, to minimize carbonate contamination.

4.2.2.1 Method 1: Anion exchange method

Surfactant: 1-hexadecane sodium sulfonate (ZnAl42)

1-hexadecane sodium sulfonate (0.1158 g, 0.353 mmol) was dissolved in freshly boiled deionized water (350 mL) and was kept at 55°C. Zn_2Al LDH (0.0234 g, 0.200 mmol) was added to the solution and the mixture was stirred for 48 hrs at 55°C. The solution was filtered rinsed with water and the compound was dried at 50°C for 24 hrs.

Surfactant: n-dodecyl sulphate (ZnAl49)

n-dodecyl sulphate (5.7691 g, 0.020 mol) was dissolved in 250 mL of freshly boiled deionized water and kept at 55°C. Zn_2Al LDH (1.2693 g, 0.011 mol) was added to the solution and the mixture was stirred for 48 hrs at 55°C. The solution was filtered rinsed with water and the compound was dried at 50°C for 24 hrs.

4.2.2.2 Method 1A: Anion exchange (in autoclave)

4.2.2.2.1 Surfactant: 1-hexadecane sodium sulfonate (ZnAl46)

1-hexadecane sodium sulfonate (0.4291 g, 1.31 mmol) was dissolved in freshly boiled deionized water (150 mL) and was kept at 55°C. Zn_2Al LDH (0.0828 g, 0.71 mmol) was added to the solution and the mixture was stirred for 30 minutes at 55°C before being transferred into an autoclave with a Teflon liner. The autoclave was heated at 56°C for 48 hrs. The mixture was filtered and the product was dried for 68 hrs at 50°C.

4.2.2.2.2 Surfactant: sodium dodecyl sulphate (ZnAl51)

Sodium dodecyl sulphate (2.3079 g, 8.00 mmol) was dissolved in freshly boiled deionized water (100 mL) and was kept at 55°C. Zn_2Al LDH (0.5096 g, 4.36 mmol) was added to the solution and the mixture was stirred for 30 minutes at 55°C before being transferred into an autoclave with a Teflon liner. The autoclave was heated at 56°C for 48 hrs. The mixture was filtered and the product was dried for 24 hrs at 50°C.

4.2.2.3 Method 2: Memory effect (ZnAl44)

A Zn_2Al LDH (0.1992 g, 1.70 mmol) was calcined at 450°C for 18 hrs. The calcined LDH was then added to a solution containing 1-hexadecane sodium sulfonate (1.0039 g, 3.06 mmol) in 350mL of water. The mixture was stirred for 48 hrs at 56°C. It was then filtered and the compound was dried at 50°C for 24hrs.

4.2.2.4 Method 2A: Memory effect (in autoclave) (ZnAl47)

1-hexadecane sodium sulfonate (0.4292 g, 1.31 mmol) was dissolved in freshly boiled deionized water (150 mL) and was kept at 55°C. The calcined Zn_2Al LDH (0.0828 g, 0.71 mmol)

(calcined at 450°C for 18 hrs) was then added to the solution and the mixture was stirred for 35 minutes at 58°C before being transferred into an autoclave with a Teflon liner. The autoclave was heated at 58°C for 48 hrs. The mixture was filtered and the product was dried for 24 hrs at 50°C.

4.2.2.5 Method 3: coprecipitation at constant pH (ZnAl48)

A mixture consisting of $Zn(NO_3)_2 \cdot 6H_2O$ (1.29 g, 4.3 mmol) and of $Al(NO_3)_3 \cdot 9H_2O$ (0.82 g, 2.2 mmol) in 50 mL of freshly boiled deionised water was added together with a 0.05 M NaOH solution (~50 mL), to a flask containing a solution of 1-hexadecane sodium sulfonate (1.4298, 4.4 mmol) in 425 mL of deionised water. Rapid stirring was kept throughout the addition and the rate of addition was such that the pH was kept at 8.0 ± 0.5. After the addition was completed, the mixture was heated at 56°C for 48 hrs under N_2. It was then filtered, washed with water then dried at 50°C for 24hrs.

Table 4.1: Summary of the reactions performed

Sample #	Type of reaction	Surfactant:LDH molar ratio
ZnAl42	ZnAl28[1] + HDSA[2] (Anion exchange)	1.8
Znal44	Calcined LDH[1] (ZnAl45) + HDSA (Memory effect)	1.3
ZnAl45	ZnAl28 calcined @ 450°C 18hrs (Calcined LDH)	
ZnAl46	ZnAl28[1] + HDSA (Anion exchange, in autoclave)	1.8
ZnAl47	ZnAl45 + HDSA (Memory effect, in autoclave)	1.8
ZnAl48	Coprecipitation of LDH with HDSA (Coprecipitation)	~2
ZnAl49	ZnAl28[1] + SDS[3] (Anion exchange)	1.8
ZnAl51	ZnAl28 + SDS in autoclave (Anion exchange, in autoclave)	2.0

Notes:

ZnAl28 = $Zn_{0.62}Al_{0.38}(OH)_2(NO_3)_{0.38}\bullet 0.47H_2O$

HDSA = Hexadecanesulfonic acid

SDS = Sodium dodecyl sulfate

4.3 RESULTS AND DISCUSSION

4.3.1 XRD Analysis

Table 4.2: XRD data summary

Sample name	d_{001} Å phase1	d_{001} Å phase 2	Notes
ZnAl42	27.5	NONE	1 phase
ZnAl44	35.7	NONE	1 phase
ZnAl46	27.9	NONE	1 phase
ZnAl47	N.A[1]	N.A	No reaction
ZnAl48	36.2	29.5	2 phases
ZnAl49	25.4	NONE	1 phase
ZnAl51	25.2	NONE	1 phase

Notes:

1. N.A.: Not applicable

4.3.1.1 ZnAl42 (Zn_2Al LDH treated with HDSA)

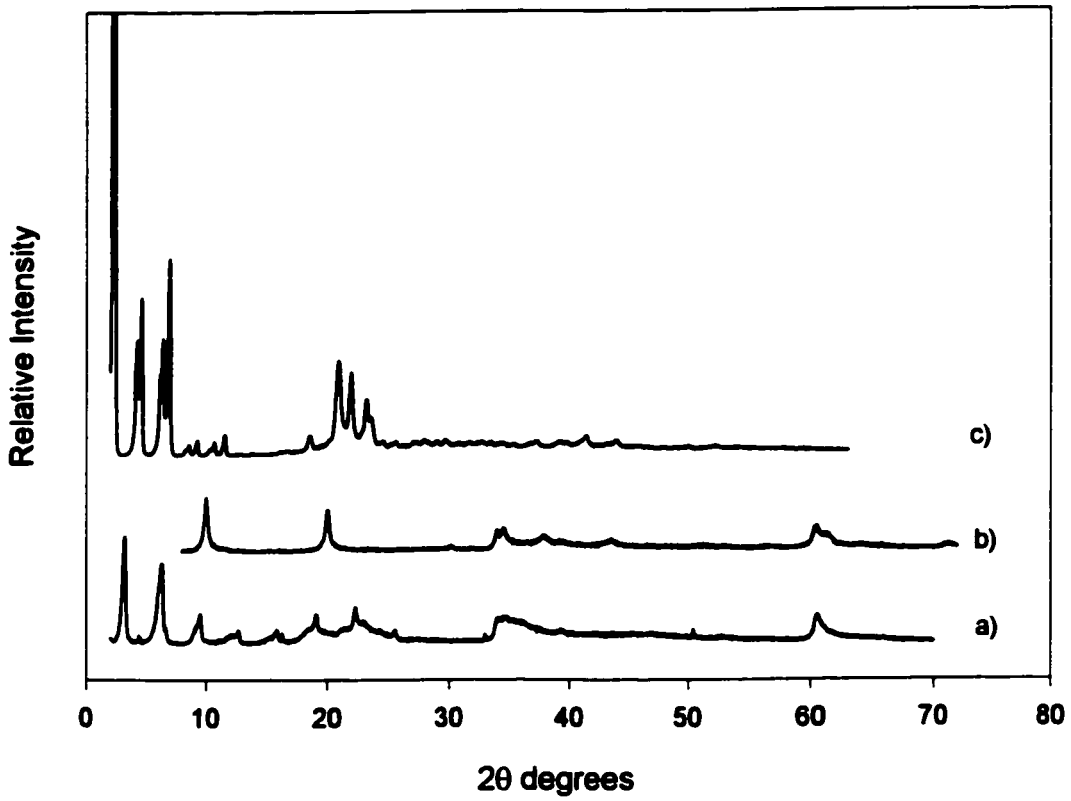

Figure 4.2 XRD patterns of a) ZnAl42, b) ZnAl28 and c) HDSA

Figure 4.2 shows the XRD patterns of the treated LDH (ZnAl42) with HDSA, the original LDH and HDSA. The comparison of these patterns show that the treated LDH is different from both starting materials. The pattern of ZnAl42 has three defined consecutive (*00l*) reflections characteristic of layered compounds that are found at 2ϴ: 3.26°, 6.41°and 9.28°. The average of the three reflections gives a d spacing of 27.5 Å. In addition, ZnAl42 XRD pattern shows characteristic LDH reflections above 2ϴ: 30° (i.e.: 015, 110 etc...). Subtracting the brucite layer length (4.8 Å) from the d spacing (27.5 Å) gives a gallery height of 22.7 Å,

which is similar to the length of the HDSA molecule (~24.5 Å). The above result suggests that HDSA molecules have been intercalated in monolayer configuration and are in a tilted configuration inside the layers of the LDH. This behavior has already been reported by Kopka et al.[66] on a study of ZnCr LDHs that were intercalated with sodium alkyl sulfate surfactants ($C_{nc}H_{2nc+1}SO_4^-Na^+$ where n_c ranged from 6 to 18). From their research, they were able to determine that the surfactants were tilted at an angle of 56° inside the layers using the following formula:

$d_L = 2.04 + 2.20 + 2.44 + 1.27n_c\sin\alpha + 3\ (Å) = 9.7 + 1.27n_c\sin\alpha\ (Å)$

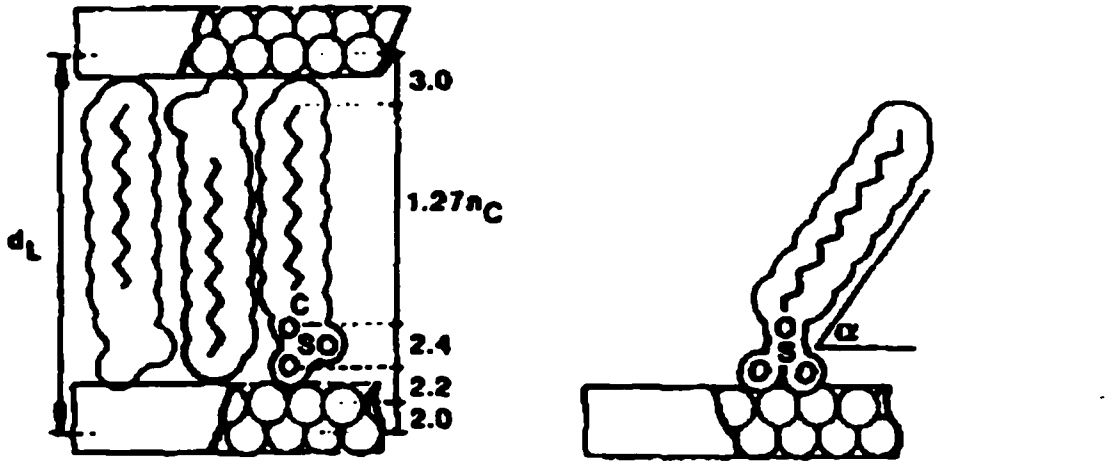

"It was assumed that one SO_4 oxygen had a van der Waals diameter of 2.8 Å and the terminal methyl group (van der Waals diameter of 4 Å) were in close proximity to the surface hydroxyl groups."[66]

4.3.1.2 ZnAl44: (Calcined LDH treated with HDSA)

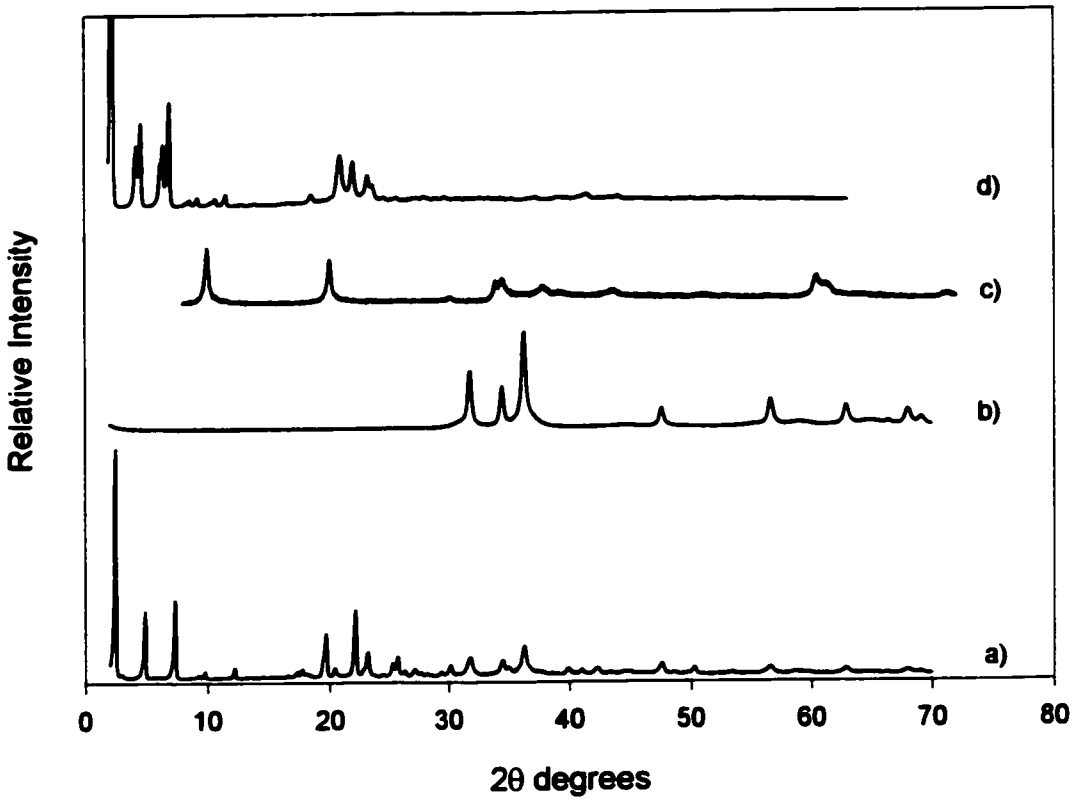

Figure 4.3 XRD patterns of a) ZnAl44, b) ZnAl45, c) ZnAl28 and d) HDSA

Figure 4.3 shows the XRD pattern of ZnAl44, the calcined precursor (ZnAl45), the original LDH and HDSA. The XRD pattern of ZnAl44 has three main reflections that are indicative of a layered compound and give an average d spacing of 35.7 Å. The XRD pattern is different from both the original LDH and the surfactant. There are however reflections of the calcined compound that can still be found in the pattern of ZnAl44 indicating an incomplete

reaction with HDSA. The large d spacing could be associated with a bilayer arrangement of HDSA molecules. Bilayer arrangements of sodium dodecyl sulfate molecules in layered double hydroxide have also been reported in the literature supporting the suggestion above.[66]

4.3.1.3 ZnAl46 (Zn_2Al LDH treated with HDSA in autoclave)

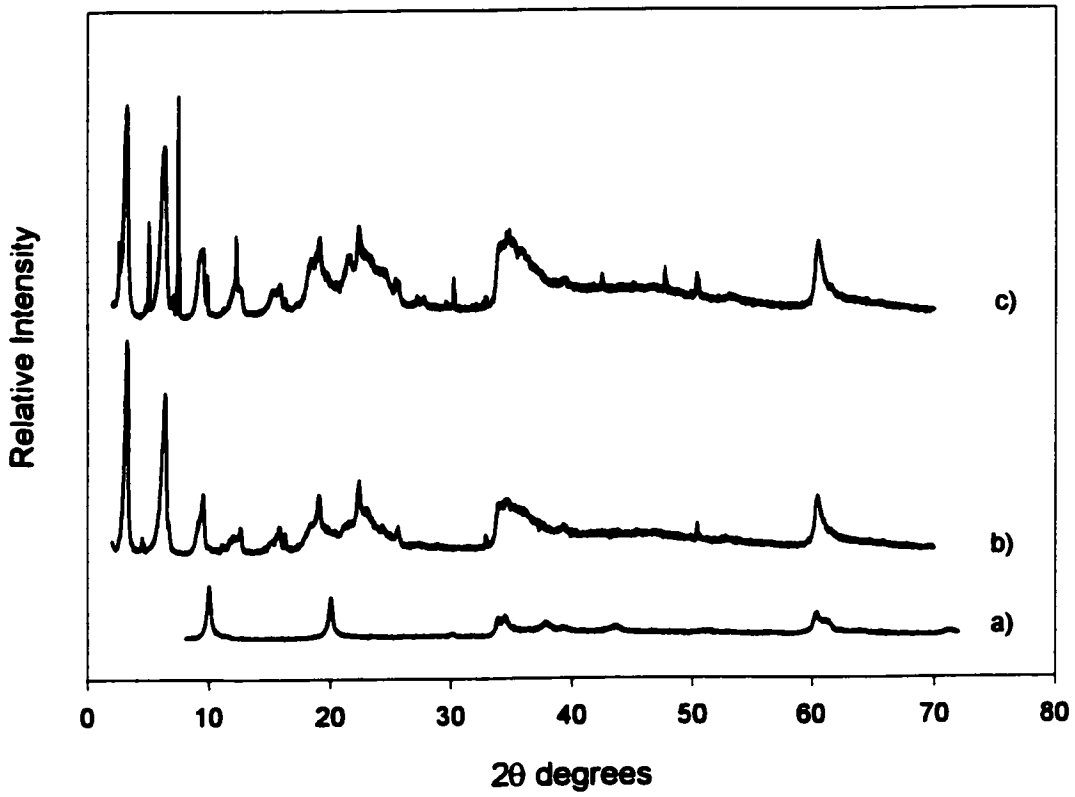

Figure 4.4 XRD patterns of a) ZnAl28, b) ZnAl42 and c) ZnAl46

Figure 4.4 shows the XRD patterns of ZnAl28 (Zn_2Al LDH) , ZnAl42 (Zn_2Al LDH+ HDSA) and ZnAl46 (Zn_2Al LDH +HDSA in autoclave).The XRD pattern of ZnAl46 is the same as the pattern of ZnAl42 except for extra reflection due to an unknown phase. This result demonstrates that ZnAl46 is the same type of material as a ZnAl42. It can be concluded that there is no difference between performing the reaction in the autoclave or in a round-bottomed flask as they both give rise to the same type of compound. The extra reflections are of unknown origin and it is unclear if the unknown phase is due to a contamination in the autoclave or due to the reaction conditions that are obtained when the reaction is performed inside an autoclave.

4.3.1.4 ZnAl47 (Calcined LDH treated with HDSA in autoclave)

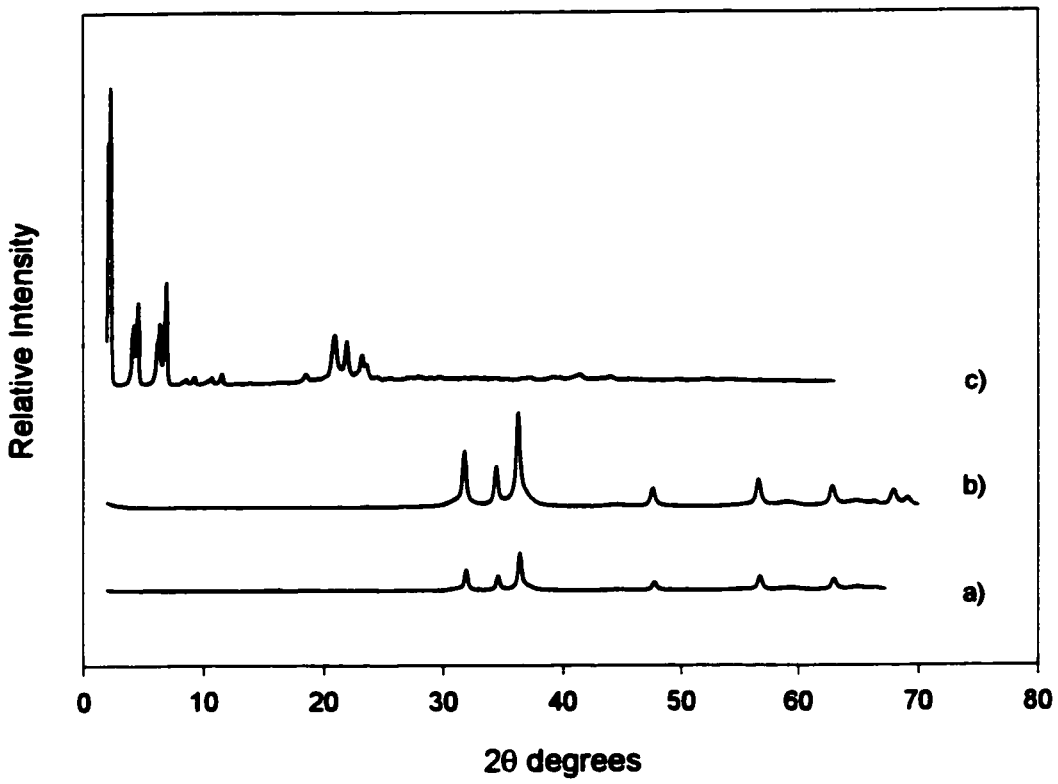

Figure 4.5 XRD patterns of a) ZnAl47, b) ZnAl45 and c) HDSA

Figure 4.5 shows the XRD spectrum of ZnAl47 (Zn_2Al LDH + HDSA in autoclave), of the calcined LDH and of HDSA. The pattern of ZnAl47 is identical to the one of the calcined LDH indicating that the mixture did not react and that only the calcined LDH remained after filtration and washing.

4.3.1.5 ZnAl48 (Coprecipitation of LDH with HDSA)

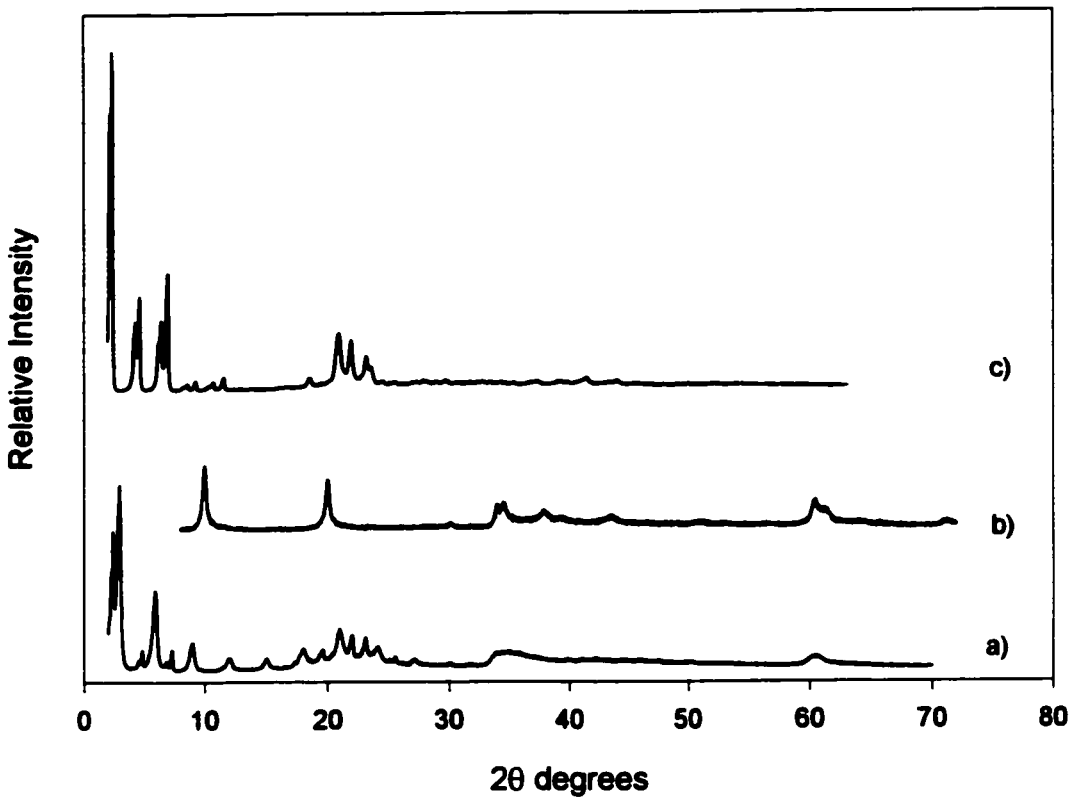

Figure 4.6 XRD patterns of a) ZnAl48, b) ZnAl28 and c) HDSA

Figure 4.6 shows the XRD pattern of ZnAl48 the original LDH and HDSA. This sample has (*00l*) reflections of 2 phases (d spacing: 29.5 Å and d spacing: 36.2 Å) in addition to having characteristic LDH reflections (015, 110). This result indicates an LDH intercalated with surfactant molecules in a monolayer and bilayer configuration within the layers. Subtracting the brucite thickness layer (4.8 Å) from the d spacing of the monolayer phase gives an interlayer spacing of 24.68 Å, which is approximately the physical length of the HDSA molecule (~24.5 Å). This would suggest that in this phase the HDSA molecules are perpendicular to the brucite like layers. The interlayer spacing of the second phase (31.4 Å)

is not twice the length of the HDSA molecules therefore to accommodate this gap the aliphatic chains must overlap each other inside the layer of the LDHs.

4.3.1.6 ZnAl49 (Zn_2Al LDH treated with SDS)

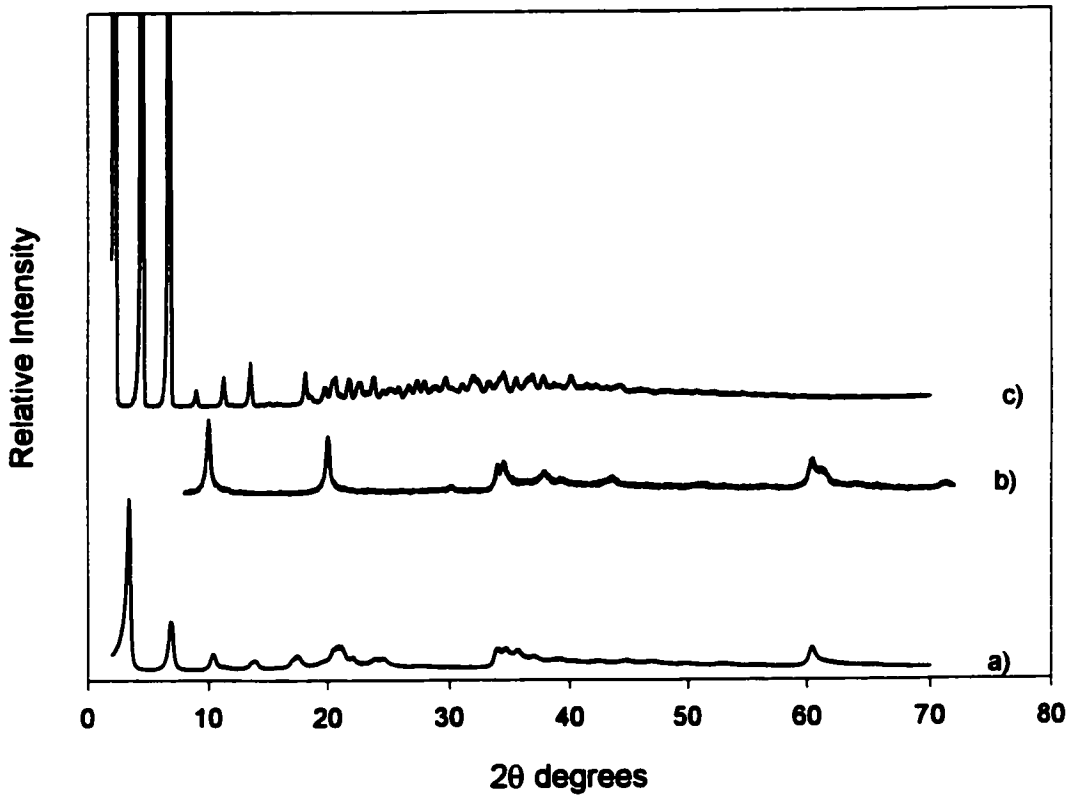

Figure 4.7 XRD patterns of a) ZnAl49, b) ZnAl28 and c) SDS

Figure 4.7 shows the XRD pattern of ZnAl49, the original Zn_2Al LDH and of SDS. The ZnAl49 pattern shows 3 main (*00l*) reflections at 2θ: 3.47°, 6.89° and 10.55° giving and average d spacing of 25.4 Å. In addition, there is the characteristic LDH reflections found between 2θ: 30 and 40°, and the characteristic 110 reflection can also be found. The d spacing is very similar to the one found by Clearfield [66] for SDS intercalated in NiAl, MgAl

and ZnCr LDHs. Clearfield attributed the d spacing to dodecyl sulfate anions that are in a perpendicular arrangement to the metal sheets. The same arrangement can be proposed for the ZnAl LDH intercalated with SDS.

4.3.1.7 ZnAl51 (Zn_2Al LDH treated with SDS in autoclave)

The results for this reaction are the same as those obtained for ZnAl49. Therefore, it can be concluded that the same type of material was obtained and that there is no difference between performing the reaction inside the autoclave or in a round bottomed flask.

4.3.2 Elemental analysis

Table 4.3: Elemental analysis of the samples

Sample name	%C		%H		Sample description
	Exp	Found	Exp	Found	
ZnAl42	26.48	26.48[a]	6.74	6.70	Zn_2Al LDH + HDSA
ZnAl44	45.83	45.76[b]	8.16	8.57	Calcined LDH + HDSA
ZnAl46	30.36	30.36[c]	7.28	7.27	Zn_2Al LDH + HDSA in autoclave
ZnAl48	40.60	40.57[d]	8.23	8.37	Coprecipitation LDH + HDSA
ZnAl49	24.29	24.24[e]	5.62	5.61	Zn_2Al LDH + SDS
ZnAl51	25.25	25.56[f]	6.24	6.26	Zn_2Al LDH + SDS in autoclave

Notes:

a. based on the formula $Zn_{0.67}Al_{0.38}(OH)_2(C_{16}H_{33}SO_3)_{0.235}\cdot 0.8H_2O$

b. based on the formula $Zn_{0.67}Al_{0.38}(OH)_2(C_{16}H_{33}SO_3)_{0.740}\cdot 0.8H_2O$

c. based on the formula $Zn_{0.67}Al_{0.38}(OH)_2(C_{16}H_{33}SO_3)_{0.310}\cdot 1.0H_2O$

d. based on the formula $Zn_{0.67}Al_{0.38}(OH)_2(C_{16}H_{33}SO_3)_{0.600}\bullet 0.9H_2O$

e. based on the formula $Zn_{0.67}Al_{0.38}(OH)_2(C_{12}H_{25}SO_4)_{0.260}\bullet 0.05H_2O$

f. based on the formula $Zn_{0.67}Al_{0.38}(OH)_2(C_{12}H_{25}SO_4)_{0.320}\bullet 0.60H_2O$

The molecular formulas are consistent with layered double hydroxides intercalated with the surfactants molecules found inside the layers. Furthermore, the elemental analyses of the samples corroborate the results obtained from the XRD study. In both cases where a bilayer arrangement of molecules is proposed (ZnAl44, ZnAl48) the quantity of carbon is approximately twice as high as the samples where a monolayer arrangement of surfactants was suggested (ZnAl42, ZnAl46). The largest quantity of intercalated surfactant was obtained from the coprecipitation and memory effect technique. This result is reasonable because when the anion exchange method was used, the intercalation must be more difficult because the surfactants must replace the anions that are already present in the LDH.

4.3.3 Infrared analysis

Figure 4.8 shows the FT-IR spectra of ZnAl46, which is a typical spectrum of the treated LDHs with HDSA. A large band centered at 3500 cm^{-1} is due to the metal hydroxyl stretch and water O-H stretch. The H_2O bending vibration can be observed at ~1635 cm^{-1}. The HDSA absorption bands were identified from the pure spectrum. CH_2 and CH_3 stretching bands can be found at 2917 and 2851 cm^{-1} respectively. CH_2 bends are found at 1466 cm^{-1} and S=O sulfates bands are found between 1200 and 1065 cm^{-1} Figure 4.9 shows the FT-IR spectrum of ZnAl49 which is also a typical spectra of the LDHs treated with SDS. As expected, the spectrum is very similar to the one shown in Figure 4.8. Centered at 3500 cm^{-1}

is the OH and H_2O stretching absorptions. Water bending is found at 1623 cm^{-1}. CH_2 stretching bands can be found at 2917 and CH_3 at 2960 and 2851 cm^{-1}. In addition, CH_2 bands are found at 1469 cm^{-1}.[67] Also, in both cases the nitrate band (1363 cm^{-1}) is almost non-existent confirming the replacement of the nitrate anions for the surfactants.

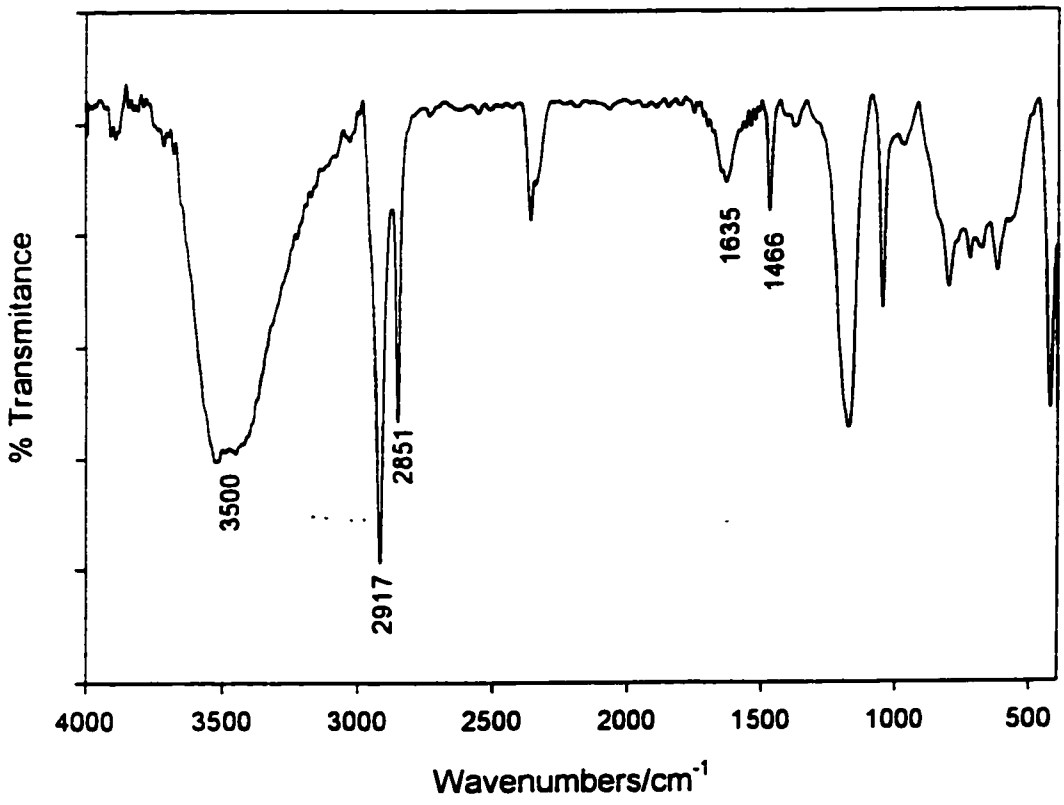

Figure 4.8 Infrared spectrum of ZnAl46

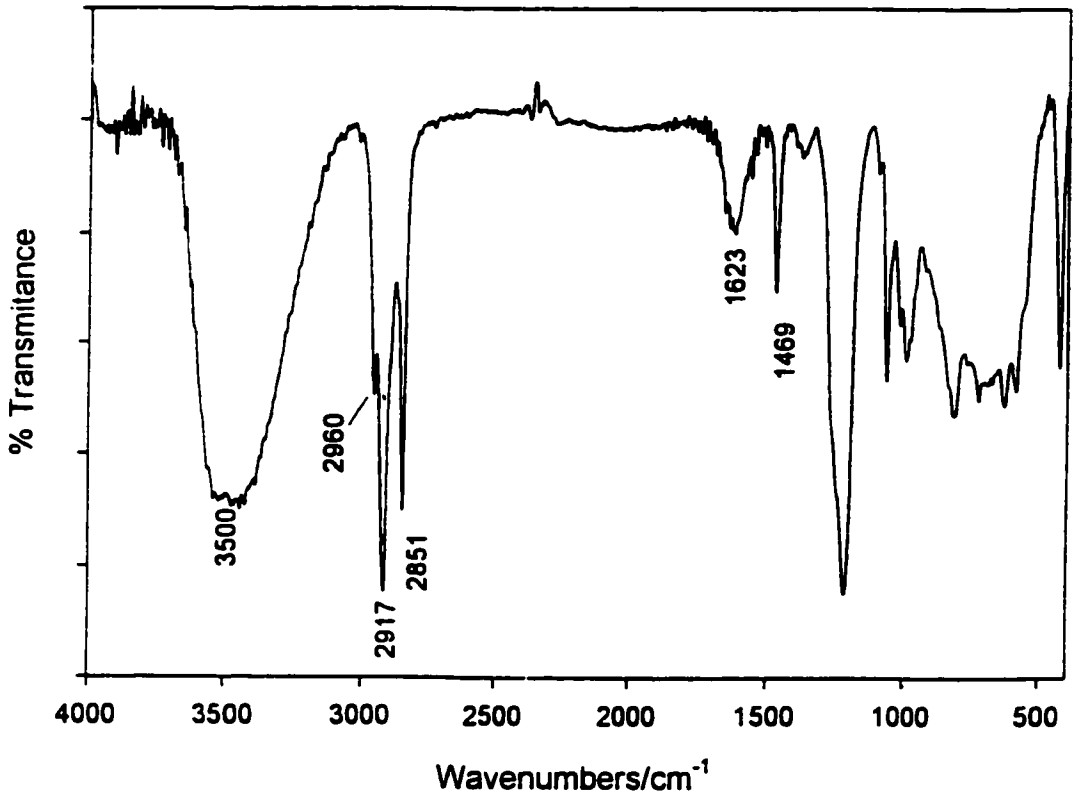

Figure 4.9 Infrared spectrum of ZnAl49

4.4 CONCLUSION

These preliminary results show that no matter what method was used, in most cases, HDSA and SDS have been intercalated inside the layers of the LDH and that there is no indication of the formation of mesoporous type materials. Future work could be undertaken to modify the reaction conditions or use another surfactant with stronger tendencies to from cylindrical micelles to help in the formation of the mesophase.

CHAPTER 5

General Conclusions

The research in this thesis involved the use of layered double hydroxides in two different fields of applications. The first involved the use of LDHs in the field of electrochemistry and the second in the field of microporous and mesoporous materials. In the first part of the thesis attention was given to Ni containing LDHs for the possible use as material for the positive electrode in Ni based batteries. The second and last part of the thesis involved the possible transformation of ZnAl LDHs into microporous or mesoporous materials via the intercalation of phosphonate or surfactants moieties respectively.

NiAl and NiV LDHs as material for the positive electrode in NiCd and NiMH batteries

NiAl and NiV LDHs of varying ratios were synthesized, characterized and electrochemically tested in half cells to determine their potential as the material for the positive electrode in nickel-cadmium (NiCd) and nickel metal hydride (NiMH) recheargable batteries. Nickel containing LDHs were used because they are isomorphous to α-$Ni(OH)_2$ and therefore offer the possibility of exchanging more electrons than the commercial $Ni(OH)_2$ now used in Ni based batteries. The NiAl LDHs were tested because they were promising candidates for the battery material and NiV was tested because vanadium has many oxidation states and it may have been possible to access these oxidation states to obtain more electrons during discharge.

Stability tests in KOH 6 M showed that all the NiAl LDHs were stable up to 2 months when immersed in the solution. On the other hand the Ni_5V LDHs was found to be only stable for 5

days and the Ni_2V LDH was stable only up to 14 days after which both materials were transformed into β-$Ni(OH)_2$. The accrued stability of the NiAl LDHs vs. the NiV was attributed to the higher charge over radius ratio of the Al vs. V. This allowed for stronger electrostatic interaction between the positively charged layers and the anions in the interlayers holding the material together. Furthermore, with the infrared study it was noted that during long exposure to the KOH solution, the nitrate anions of the NiAl LDHs were replaced by carbonate anions. The replacement of the anions was quicker in the Ni_2Al LDH than the other two NiAl LDHs and was attributed to the higher charge density of the Ni_2Al LDH. The short-term electrochemical testing of the LDHs showed that the highest number of exchanged electrons was attained by the Ni_2Al LDH with a maximum of 1.6 electrons per nickel atom. The Ni_5Al LDH and the Ni_9Al LDH attained a maximum of 1.5 and 1.3 electrons per nickel atom. The NiV LDH only attained a maximum of approximately 1.2 electrons. The higher number of electrons exchanged for the LDHs was attributed to the cycling between the alpha and the gamma phase in which nickel is cycling between the +2 and the +3.6 oxidation state. The 3.6 oxidation was due to the nickel found in the +3 and +4 valence states when in the charged state. The highest number of exchanged electrons attained by Ni_2Al was attributed to the presence of aluminum, which increased the Brønsted acidity of the hydroxyl groups and aided in the formation of the nickel in the +4 oxidation state. The low number of exchanged electrons of the NiV LDHs was most likely due to the quick transformation of the LDHs into β-$Ni(OH)_2$ during cycling. Furthermore, the low number of exchanged electrons for the NiV LDHs suggests that vanadium is not contributing to the electrons exchange as a larger quantity of electrons would have been expected during cycling. On the long-term the Ni_2Al LDH showed the highest stability of all the LDHs and the most number of exchanged electrons over time. The decrease in the number of exchanged

electrons as a function of time was attributed to the transformation of the LDHs into β-$Ni(OH)_2$. The difference in the slow and fast discharge showed that the proton mobility of the Ni_2Al LDH was greater than the commercial $Ni(OH)_2$ and this was also attributed to the increase in Brønsted acidity of the hydroxyl groups due to the aluminum in the layers. The NiV LDHs showed proton mobilities similar to the commercial powder and this was due to the degradation of the material into β-$Ni(OH)_2$. Gravimetric capacities of all the LDHs were lower than the commercial β-$Ni(OH)_2$. The lower density of the LDHs versus the commercial powder was determined to be the cause of the lower gravimetric capacity of the LDHs. The study of the charge and discharge curves of the LDHs showed that as the cycle number increased the LDHs became more difficult to charge and in consequence a lower discharge capacity was obtained after cycling. This was consistent with the material transforming into β-$Ni(OH)_2$ and reducing the proton mobility. Based on the long-term stability of the Ni_2Al LDH, this material may be a good candidate for the positive electrode of Ni based rechargeable batteries for an application where a long lasting battery is needed but the size of the battery is not an issue. Increased gravimetric capacity may be achieved by grinding the material to increase the density of the powder and allow more loading into the electrode. Furthermore, research to optimize the cycling profile may be conducted to increase the capacity of the electrode. Other important factors that can play a role in the capacity of the material is the particle size or the cristallinity of the LDHs that may be controlled and optimized to obtain a better electrode material.

ZnAl/PPA compounds

ZnAl LDHs with varying ratios were synthesized and intercalated with phenylphosphonic acid (PPA). ZnAl LDHs was chosen because they are less sensitive to acidic pH and have a large range of M(II)/M(III) ratio allowing for the possibility of fine tuning the microporosity of the material.

The treatment of the ZnAl LDHs with PPA resulted in layered materials with d spacing of 14.7 Å as determined by their XRD patterns. This spacing was similar to zirconium phosphonate and other LDHs grafted with PPA. The molecular formula of these compounds were determined by using a computer program (hereafter called MDP) that was developed during the course of the study. The value of x in the formula below was calculated from the Zn:Al ratio determined from the ICP analysis of the compounds. MDP then varied the coefficients of OH, H and water in the molecular formula below in a range and increment determined by the user.

$$Zn_{1-x}Al_x(OH)_a(C_6H_5PO_3H_z)^{2-z}_{((2-a)+x)/(2-z)} \bullet yH_2O$$

For each variation of the coefficients, the weight percentages of each element were calculated and the deviation between the experimental and the computed data was performed. The formula with the lowest overall deviation was kept and represented the best model for the molecular formula of the compounds. In the case of all the ZnAl/PPA materials the formula that were obtained had almost no hydroxyl groups and the acids were almost completely deprotonated. This result indicated that grafting of the oxygens of the phosphonate groups to

the metal layers had occurred. TGA of the compounds showed a weight loss between 500 and 700 °C that corresponded to the expected weight loss of a phenyl group. Furthermore, analysis of the calcined materials revealed that mixed metal and phosphorus oxides were obtained. The change in the IR spectra before and after intercalation was a clear indication that the ZnAl/PPA compounds were different from the original LDH. The comparison of the IR spectra of the ZnAl/PPA compounds and the physical mixture of the acid and the LDH confirmed that the LDH treated with PPA formed a new compound. Furthermore, the comparison of these spectra also revealed that the bonding of the PPA in the physical mixture was different than in the ZnAl/PPA materials. The solid state NMR analysis proved to be a good probe of the interlayer species as further information on the structure was gathered. The resonances of the ^{13}C CPMAS spectra were identified by using a combination of dipolar dephasing and phosphorous decoupling experiments and showed that the phenyl rings inside the layers were rotating. From the ^{31}P MAS solid state NMR, the ratio of PPA in the proximity to Zn and Al was determined. The Zn_2Al/PPA material was tested for microporosity but unfortunately exhibited none. This was attributed to the large quantity of PPA molecules in the layers due to the high charge density of the LDH thus not allowing space in between the molecules to form microporosity. The sample was then heated in the prospect of eliminating PPA molecules in the interlayer to create openings thus forming microporosity. After the heat treatment, the surface area of the material decreased and showed no microporosity. The destruction of the layered structure was the cause for the lower surface area after heating.

The overall results are consistent with PPA molecules grafted to the metal layers in a double layer configuration where the phenyl groups are pointing inside the layers in a head-to-head arrangement.

ZnAl/B-PPA compounds

In this part of the thesis, Zn_2Al LDH was treated with B-PPA under different reaction conditions. It was determined that an acidic medium was needed to complete the reaction of the acid with the LDH. The resulting product was a layered material that had a d- spacing of 9.6 Å. This d spacing was similar to MgAl LDHs that were treated with the same acid and resulted in cross-linked lamellar materials with the organic moieties fixed onto the layers through P-O-M bonds.[70] Moreover, the molecular formula of these compounds was also determined using MDP. The calculated formulas had almost no hydroxyl groups similarly to the ZnAl/PPA compounds, however the B-PPA molecules were found to be monoprotonated. This result was consistent with the grafting of the phosphonate groups directly to the metal layers but suggested that one oxygen of the phosphonate group was not bound to the layers. The infrared spectra of the ZnAl/B-PPA compounds showed that the acid was present in the LDH. Furthermore, the comparison of the infrared spectra of the ZnAl/B-PPA compound to the original acid revealed that the bonding occurring in the pure acid was different when inside the LDH. It also revealed that the nitrate anion of the original LDH had been replaced with the B-PPA molecules.

With the help of the ^{13}C CPMAS solid state of the pure acid, in addition to dipolar dephasing and ^{31}P decoupling experiments, the resonances of the intercalated/grafted B-PPA molecules

could be identified. The dipolar dephased and ^{31}P decoupled CPMAS ^{13}C showed four resonances that were associated to the carbons bound to the phosphorus groups. In addition, the four resonances suggested the presence of carbons in four different crystallographic sites. Micropore determination experiments performed on the material showed that it exhibited microporosity but in small quantity. The micropore diameter of 9.6 Å was consistent with the interlayer spacing of the material. After heat treatment, the surface area decreased which was consistent with the collapse of the structure.

Future work to form microporous materials from LDHs could involve the intercalation of two types of molecules such as a combination of phosphoric acid and PPA or B-PPA with the objectives of increasing the space between the phenyl containing acids and possibly creating micropores. Furthermore, adding substituents to the phenyl groups to increase the space between the molecules and form channels may be another method to pursue in order to form microporous materials from LDHs.

Attempts at forming MCM/FSM types of materials with ZnAl LDHs using surfactants as the templates

In this section of the thesis, Zn_2Al LDH was treated with hexadecanesulfonic acid or sodium dodecyl sulfate with the objective of forming FSM or MCM type materials. This project was undertaken because it may be a new way to form mesoporous materials with a variety of metals that could be used as catalysts and to date there has been no reports in the literature concerning the formation of these materials from LDHs.

Five different synthesis routes were tested in the attempt of achieving this objective: 1) anionic exchange method, where the LDH was dispersed in a solution containing an excess of the surfactant, 2) the memory effect method, which involved calcining the LDH then exposing the calcination products to a solution containing the surfactants, 3) the coprecipitation technique that entailed the coprecipitation of the metal salts in the presence of the surfactants, 4) anionic exchange in an autoclave (same procedure as in 1) except the reaction was performed in an autoclave), 5) memory effect in an autoclave (same procedure as in 2) except the reaction was performed in an autoclave). All the reactions were performed at the temperature and concentration of the CMC of the surfactants in question. The samples were subjected to XRD study, IR analysis and elemental analysis. The XRD patterns showed in all cases that layered materials were obtained with d spacings corresponding to surfactants inside the layers of the LDH either in a single or double layered arrangement. The molecular formulas of the compounds were calculated from the carbon and hydrogen analysis and corresponded to LDHs intercalated with the surfactants, corroborating the results obtained from the XRD patterns of the samples. Finally, the IR analysis showed that the interlayer species of the LDH were replaced with the surfactants in question. These preliminary results therefore showed that the surfactants have been intercalated in the layers of the layered double hydroxides and that no mesoporous phase has been formed.

Other research could involve the use of another micelle with a stronger tendency to form cylindrical micelles to help in the formation of the mesoporous framework or using different reactions conditions such as the changing the pH or reaction time.

Reference List

(1) *Chemistry of Clays and Clay Minerals*; Mineralogical Society: London, 1987.

(2) Cavani, F.; Trifiro, F.; Vaccari, A. *Catal.Today* **1991**, *11*, 173-301.

(3) Trifiro, F.; Vaccari, A. *Comprehensive Supramolecular Chemistry* **1996**, 1-41.

(4) Frondel, C. *Amer.Mineral.* **1941**, *26(5)*, 295-315.

(5) Feitknecht, W. *Helv.Chim.Acta.* **1942**, *25*, 131-137.

(6) Feitknecht, W. *Helv.Chim.Acta.* **1942**, *25*, 555-569.

(7) Brown, G.; Gastuche, M. C. *Clay Miner.* **1967**, *7*, 193-201.

(8) Allmann, R. *Acta.Cryst.* **1968**, *B24*, 972-977.

(9) Taylor, H. F. W. *Miner.Mag.* **1969**, *37(287)*, 338-342.

(10) Allmann, R.; Lohse, H. H. *N.Jhb.Miner.Mh.* **1966**, *6*, 161.

(11) Ingram, L.; Taylor, H. F. W. *Miner.Mag.* **1967**, *36(280)*, 465-479.

(12) Allmann, R.; Jespen, H. P. *Neues.Jahrb.Min.Monatsh* **1969**, 544-551.

(13) Taylor, H. F. W. *Miner.Mag.* **1973**, *39(304)*, 377-389.

(14) Velu, S.; Suzuki, K.; Okazaki, M.; Osaki, T.; Tomura, S.; Ohashi, F. *Chem.Mater.* **1999**, *11*, 2163-2172.

(15) Allmann, R. *CHIMI* **1970**, *24*, 99-104.

(16) Bish, D. L.; Brindley, G. W. *Amer.Mineral.* **1977**, *62*, 458-464.

(17) Gastuche, M. C.; Brown, G.; Mortland, M. M. *Clay Miner.* **1967**, *7*, 177-192.

(18) Miyata, S. *Clays Clay Miner.* **1975**, *23*, 369-375.

(19) Brindley, G. W.; Kikkawa, S. *Amer.Mineral.* **1979**, *64*, 836-843.

(20) Miyata, S. *Clays Clay Miner.* **1980**, *28*, 50-56.

(21) Pausch, I.; Lohse, H. H.; Schurmann, K.; Allmann, R. *Clays Clay Miner.* **1986**, *34(5)*, 507-510.

(22) Miyata, S. *Clays Clay Miner.* **1983**, *31*, 305-311.

(23) Mascolo, G.; Marino, O. *Miner.Mag.* **1980**, *43*, 619-621.

(24) Miyata, S.; Kumura, T. *Chem.Lett.* **1973**, 843-848.

(25) Besson, H.; Caillere, S.; Henin, S. *Bull.Groupe franç.argiles* **1973**, *XXVI*, 79.

(26) Bish, D. L. *Bull.Minéral.* **1980**, *103*, 170-175.

(27) Hernandez-Moreno, M. J.; Ulibarri, J. L.; Rendon, J. L.; Serna, C. L. *Phys.Chem.Miner.* **1985**, *12*, 34-38.

(28) Sato, T.; Fujita, H.; Endo, T.; Shimada, M. *React.Solids* **1988**, *5*, 219.

(29) Caravaggio, G. A.; Detellier, C.; Wronski, Z. S. *J.Mater.Chem.* **2001**, *11*, 912-921.

(30) Ehlsissen, K. T.; Delahayevidal, A.; Genin, P.; Figlarz, M.; Willmann, P. *J Mater.Chem* **1993**, *3*, 883-888.

(31) Labajos, F. M.; Sastre, M. D.; Trujillano, R.; Rives, V. *J.Mater.Chem.* **1999**, *9*, 1033-1039.

(32) Serna, C. J.; White, J. L. *Clays Clay Miner.* **1977**, *25*, 384-391.

(33) Sissoko, I.; Iyagba, E. T.; Sahai, R.; Biloen, P. *J.Solid State Chem.* **1985**, *60*, 283-288.

(34) Hernandez, M. J.; Ulibarri, J. L.; Cornejo, J.; Peña, M. J.; Serna, C. J. *Thermochim.Acta.* **1985**, *94*, 257.

(35) Mascolo, G. *Thermochim.Acta.* **1986**, *102*, 67.

(36) Reichle, W. T. *Solid State Ionics.* **1986**, *22*, 135-141.

(37) Gherardi, P.; Rugerri, O.; Trifirò, F.; Vaccari, A.; Del Piero, G.; Manara, G.; Notari, B. *Preparation of Catalysts III*; Elsevier: Amsterdam, 1983; p 723.

(38) Gusi, S.; Pizzoli, F.; Trifiro, F.; Vaccari, A.; Del Piero, G. *Prep.Cata* **1987**, 753-765.

(39) Busetto, c.; Del Piero, G.; Manara, G.; Trifirò, F.; Vaccari, A. *J.Catal.* **1984**, *85*, 260-266.

(40) Fornasari, G.; Gusi, S.; Trifirò, F.; Vaccari, A.; Del Piero, G. *Proc.VIth Int.Heterogeneous Catalysis, Bulg.Acad.Sciences, Sofia*; 1987; p 241.

(41) Szymanski, R.; Travers, P.; Chaumette, P.; Courty, Ph.; Durand, D. *Preparation of Catalysts IV*; Elsevier: Amsterdam, 1987; p 739.

(42) Herman, R. G.; Klier, K.; Simmons, G. W.; Finn, B. P.; Bulko, J. B. *J.Catal.* **1979**, *56*, 407.

(43) Trifirò, F.; Vaccari, A.; Del Piero, G. Elsevier: Amsterdam, 1988; p 571.

(44) Thevenot, F.; Szymanski, R.; Chaumette, P. *Clays Clay Miner.* **1989**, *37*, 396-402.

(45) Cervilla, A.; Llopis, E.; Ribera, A.; Corma, A.; Fornés, V.; Rey, F. *J.Chem.Soc.,Dalton Trans.* **1994**, 2953-2957.

(46) Kwon, T.; Pinnavaia, T. J. *Chem.Mater.* **1989**, *1*, 381-383.

(47) De Roy, A.; Besse, J. P.; Bondot, P. *J.Physique* **1986**, *47*, 713.

(48) De Roy, A.; Besse, J. P.; Bondot, P. *Mater.Res.Bull.* **1985**, *20*, 1091.

(49) Zhouri, E.; El Hajbi, A. *Annales de Chimie-Science des Materiaux* **1999**, *24*, 57-62.

(50) Aramendia, M. A.; Borau, V.; Jimenez, C.; Marinas, J. M.; Ruiz, J. R.; Urbano, F. J. *Appl.Catal.A-Gen.* **2001**, *206*, 95-101.

(51) Rousselot, I.; Taviot-Gueho, C.; Besse, J. P. *Int.J.Inorg.Mater.* **1999**, *1*, 165-174.

(52) Fernandez, J. M.; Barriga, C.; Ulibarri, M. A.; Labajos, F. M.; Rives, V. *Chem.Mater.* **1997**, *9*, 312-318.

(53) Aramendia, M. A.; Aviles, Y.; Borau, V.; Luque, J. M.; Marinas, J. M.; Ruiz, J. R.; Urbano, F. J. *J.Mater.Chem.* **1999**, *9*, 1603-1607.

(54) Weast, R. C.; Astle, M. J. *Handbook of Chemistry and physics 82nd edition*; CRC press: Boca Ratom, 1999.

(55) Vichi, F. M.; Alves, O. L. *J.Mater.Chem.* **1997**, *7*, 1631-1634.

(56) Rives, V.; Labajos, F. M.; Ulibarri, M. A.; Malet, P. *Inorg.Chem.* **1993**, *32*, 5000-5001.

(57) Del Piero, G.; Di Conca, M.; Trifirò, F.; Vaccari, A. Elsevier: Amsterdam, 1985; p 1029.

(58) Gusi, S.; Pizzoli, F.; Trifirò, F.; Vaccari, A.; Del Piero, G. Elsevier: Amsterdam, 1987.

(59) Busca, G.; Pattuelli, F.; Trifirò, F.; Vaccari, A. Elsevier: Amsterdam, 1989; p 239.

(60) Newman, S. P.; Jones, W. *New J.Chem.* **1998**, *22*, 105-115.

(61) Kooli, F.; Chisem, I. C.; Vucelic, M.; Jones, W. *Chem.Mater.* **1996**, *8*, 1969-1977.

(62) Kooli, F.; Jones, W. *Synthesis of Porous Materials. Zeolites,Clays, and Nanocomposites*; New York, 1996; pp 641-660.

(63) Moggridge, G. D.; Parent, P.; Tourillon, G. *Clays Clay Miner.* **1994**, *42*, 462.

(64) Meyn, M.; Beneke, K.; Lagaly, G. *Inorg.Chem.* **1990**, *29*, 5201-5207.

(65) Raki, L.; Rancourt, D. G.; Detellier, C. *Chem.Mater.* **1995**, *7*, 221-224.

(66) Kopka, H.; Beneke, K.; Lagaly, G. *J.Colloid Interf.Sci.* **1988**, *123*, 427-436.

(67) Clearfield, A.; Kieke, M.; Kwan, J.; Colon, J. L.; Wang, R. C. *J.Incl.Phen.Molec.Recog.Chem.* **1991**, *11*, 361-378.

(68) Boehm, H. P.; Steinle, J.; Vieweger, C. *Angew.Chem.Int.Ed.Engl.* **1977**, *16(4)*, 265-266.

(69) Drezdon, M. A. *Inorg.Chem.* **1988**, *27*, 4628-4632.

(70) Don Wang, J.; Serrette, G.; Tian, Y.; Clearfield, A. *Appl.Clay Sci.* **1995**, *10*, 103-115.

(71) Tanaka, M.; Park, I. Y.; Kuroda, K.; Kato, C. *Bull.Chem.Soc.Jpn.* **1989**, *62*, 3442-3445.

(72) Challier, T.; Slade, R. C. T. *J Mater.Chem* **1994**, *4*, 367-371.

(73) Oriakhi, C. O.; Farr, I. V.; Lerner, M. M. *J.Mater.Chem.* **1996**, *6(1)*, 103-107.

(74) Sugahara, Y.; Yokoyama, N.; Kuroda, K.; Kato, C. *Cerami.Inter.* **1988**, *14*, 163-167.

(75) Whilton, N. T.; Vickers, P. J.; Mann, S. *J.Mater.Chem.* **1997**, *7*, 1623.

(76) Occelli, M. L.; Robson, R. *Expanded Clays and OtherMicroporous Solids (Volume II)*; Van Nostrand Reinhold: New York, 1992.

(77) Twu, J.; Dutta, P. K. *J.Phys.Chem.* **1989**, *93*, 7863-7868.

(78) Hashimoto, K.; Matsumura, Y.; Fukuchi, M.; Kera, Y. *Catal.Lett.* **1993**, *19*, 375.

(79) Chibwe, K.; Valim, J. B.; Jones, W. *ACS Prepr.Symp.* **1989**, *34*, 507.

(80) Kwon, T.; Tsigdinos, G. A.; Pinnavaia, T. J. *J.Amer.Chem.Soc.* **1988**, *110*, 3653-3654.

(81) Wang, J. D.; Tian, Y.; Wang, R. C.; Clearfield, A. *Chem.Mater.* **1992**, *4*, 1276-1282.

(82) Park, Y.; Kuroda, K.; Kato, C. *Chem.Lett.* **1989**, 2057.

(83) Ulibarri, M. A.; Luque, J. M.; Cornejo, J. *Mater.Chem Phys.* **1990**, *25*, 81.

(84) Ulibarri, M. A.; Hernandez, M. J.; Cornejo, J. *J.Mater.Sci.* **1991**, *26*, 1512.

(85) Sato, T.; Wakabayashi, T.; Shimada, M. *Ind.Eng.Chem.Prod.Res.Dev.* **1986**, *25*, 89.

(86) Misra, C.; Perrotta, J. *Clays Clay Miner.* **1992**, *40*, 145-150.

(87) Chibwe, K.; Jones, W. *Chem.Mater.* **1989**, *1*, 489-490.

(88) Chibwe, K.; Jones, W. *J.Chem.Soc., Chem.Commun.* **1989**, 926-927.

(89) Sato, T.; Okuwaki, A. *Solid State Ionics* **1991**, *45*, 43.

(90) Narita, E.; Yamagishi, T. *Proceedings of the 9th International Clay Conference, Strasbourg*; 1990; p 145.

(91) Perez-Bernal, M. E.; Ruano-Casero, R.; Pinnavaia, T. J. *Catalysis.Lett.* **1991**, *11*, 55-62.

(92) Chibwe, M.; Pinnavaia, T. J *J.Chem.Soc., Chem.Commun.* **1993**, 278-280.

(93) Narita, E.; Kaviratna, P. D.; Pinnavaia, T. J. *Chem Lett.* **1991**, 805.

(94) Portemer, F.; Delahaye-Vidal, A.; Figlarz, M. *J.Electrochem.Soc.* **1992**, *139*, 671-678.

(95) Kamath, V. P.; Indira, L. *J.Mater.Chem.* **1994**, *4*, 1487-1490.

(96) Indira, L.; Dixit, M.; Kamath, V. P. *J.Power Sources* **1994**, *52*, 93-97.

(97) Mckenzie, A. L.; Fishel, C. T.; Davis, R. J. *J.Catal.* **1992**, *138*, 547-561.

(98) Reichle, W. T. *J.Catal.* **1985**, *94*, 547-557.

(99) Caldararu, H.; Caragheorgheopol, A.; Corma, A.; Rey, F.; Fornes, V. *J.Chem.Soc., Faraday Trans.* **1994**, *90*, 213-218.

(100) Li, Z.; Giese, R. F.; Vanoss, C. J. *Langmuir.* **1994**, *10*, 330-333.

(101) Malinowski, S. T.; Szcepanska, S.; Stoczynski, J. *J.Catal.* **1967**, *7*, 76-84.

(102) Ross, J. R. H.; Roberts, M. W.; Thomas, J. M. Royal Society of Chemistry: London, 1975; p 34.

(103) Herman, R. G.; Bogdan, C. E.; Kumler, P. L.; Nuszkowski, D. M. *Mater.Chem Phys.* **1993**, *35*, 233-239.

(104) Müller-Tamm, H., Frielingsdorf, G., Schweier, G., and Reuter, L. (2,163,851,-2). 1973. Germany, Basf AG.

(105) Parker, L. M.; Milestone, N. B.; Newman, R. H. *Ind.Eng.Chem.Res.* **1995**, *34*, 1196-1202.

(106) Houri, B.; Legrouri, A.; Barroug, C.; Forano, C.; Besse, J. P. *Collect.Czech.Chem.Commun.* **1998**, *63*, 732.

(107) Amin, S.; Jayson, G. G. *Water Res.* **1996**, *30*, 299.

(108) Ulibarri, M. A.; Pavlovic, I.; Hermosin, M. C.; Cornejo, J. *Appl.Clay Sci.* **1995**, *10*, 131.

(109) Hermosin, M. C.; Pavlovic, I.; Ulibarri, M. A.; Cornejo, J. *Fresenius Environ.Bull.* **1995**, *4*, 41.

(110) Trujillano, R., Vicente, M. A., and Rives, V. The Use of Anionic Clays for Extraction of Sulphate From the Pore Network of Aged Building Stones. 1-16. 2001.

(111) Faure, C.; Delmas, C.; Willmann, P. *J.Power Sources* **1991**, *36*, 497-506.

(112) König W. *Neun Jahre Iraq-Im verlorenen Paradies*; 1940.

(113) Kanani, N. *Oberflaechen Werkst.* **1996**, *37*, 6-14.

(114) Mantell, C. L. *Batteries and Energy Systems*; McGraw-Hill Book Company: 1983.

(115) Al-Haik, A. *Sumer* **1964**, *XX*.

(116) Jansen, W.; Fickenfrerichs, H.; Peper, R.; Flintjer, B. *CLB Chem.Labor Biotech.* **1993**, *44*, 128-133.

(117) Jansen, W.; Fickenfrerichs, H.; Peper, R.; Flintjer, B. *CLB, Chem.Labor Betr.* **1987** , *38*, 586, 588, 591-586, 588, 592.

(118) Jansen, W.; Fickenfrerichs, H.; Peper, R.; Flintjer, B. *CLB, Chem.Labor Betr.* **1987** , *38*, 528-30, 533.

(119) Volta, A. *Le Opere di Alessandro Volta*; Milano, 1968.

(120) Dibner, B. *Luigi Galvani*; Benton, W.: Norwalk , Connecticut, 1971.

(121) Wronski, Z. S. *Int.Mater.Rev.* **2001**, *46*, 1-52.

(122) Linden, D. *Handbook of Batteries*; McGraw-Hill, Inc.: 1995.

(123) Miller, S.; Holzer, F.; Haas, O. *J.Appl.Electrochem.* **1998**, *28*, 895.

(124) Bode, H.; Dehmelt, K.; Witte, J. *Electrochim.* **1966**, *11*, 1079.

(125) Rajamathi, M.; Subbanna, G. N.; Kamath, V. P. *J.Mater.Chem.* **1997**, *7*, 22963-22962.

(126) Delmas, C. *Mater.Sci.Forum* **1994**, *152-153*, 131-136.

(127) Szytula, A.; Murasik, A.; Balanda, M. *Phys.Status Solidi B* **1971**, *43*, 125.

(128) Greaves, C.; Thomas, M. A. *Acta.Cryst.* **1986**, *B42*, 51.

(129) Eckert, J.; Varma, R.; Diebolt, L.; Reid, M. *J.Electrochem.Soc.* **1997**, *144*, 1895-1899.

(130) Demourgues, A.; Gautier, L.; Chadwick, A. V.; Delmas, C. *Nucl.Instrum.Methods Phys.Res., Sect.B* **1997**, *133*, 39-44.

(131) Singh, D. *J.Electrochem.Soc.* **1998**, *142*, 116-120.

(132) Vidal delahaye; Figlarz, M. *J.Appl.Electrochem.* **1987**, *17* , 589-599.

(133) Wronski, Z. S.; Carpenter, G. J. C. *Electrochem.Soc.Proc.* **1996**, *96-14*, 177-188.

(134) Wronski, Z. S.; Carpenter, G. J. C.; Martineau, D. *Electrochem.Soc.Proc.* **1997**, *97-18*, 804-811.

(135) Wronski, Z. S. *Symposium of Electrochemical Power Sources after 200 Years , 50th ISE Mtg., Pavia,Italy,5-10 sep* **1999**.

(136) Delmas, C.; Tessier, C. *J.Mater.Chem.* **1997**, *7*, 1439-1443.

(137) Tessier, C.; Haumesser, P. H.; Bernard, P.; Delmas, C. *J.Electrochem.Soc.* **1999**, *146*, 2059-2067.

(138) O'Grady, W. E.; Pandya, K. I.; Swider, K. E.; Corrigan D.A. *J.Electrochem.Soc.* **1996**, *143*, 1613-1616.

(139) Faure C.; Delmas, C.; Fouassier M. *J.Power Sources* **1991**, *35*, 279-290.

(140) Bihan S.; Figlarz, M. *J.Crystal Growth* **1972**, *13/14*, 458-461.

(141) Audemere, A.; Delahaye, A.; Farhi, R.; Sac-Epée, N.; Tarascon, J. M. *J.Electrochem.Soc.* **1997**, *144*, 2614-2620.

(142) Ho, K. C. *J.Electrochem.Soc.:Rev.News* **1980**, *134*, 53C-55C.

(143) Mani, B.; Neufville, J. P. *J.Electrochem.Soc.* **1988**, *135*, 800-803.

(144) Ho, K. C.; Jorné, J. *J.Electrochem.Soc.* **1990**, *137*, 149-158.

(145) Shamina, I. S.; Maladin, O. G.; Rakhovskaya, S. M.; Sal'kova, L. N.; Vassev, A. V.; Vereschagina, L. A. *Elektrokhimiya* **1976**, *12*, 573.

(146) Oliva, P.; Leonardi, J.; Laurent, J. F.; Delmas, C.; Braconnier, J. J.; Figlarz, M.; Fievet, F.; de Guilbert, A. *J.Power Sources* **1982**, *8* , 229.

(147) Faure, C.; Borthomieu, Y.; Delmas, C. *J.Power Sources* **1991**, *36*, 113-125.

(148) Demourgues-Guerlou, L.; Delmas, C. *J.Electrochem.Soc.* **1994**, *141*, 713-717.

(149) Delmas, C.; Braconnier, J. J.; Borthomieu, Y.; Hagenmuller, P. *Mater.Res.Bull.* **1987**, *22*, 741.

(150) Delmas, C.; Braconnier, J. J.; Borthomieu, Y.; Figlarz, M. *Solid State Ionics* **1988** , *28-30*, 1132.

(151) Faure C.; Delmas, C.; Willmann, P. *J.Power Sources* **1991**, *35*, 263-277.

(152) Braconnier, J. J. 1983. Bordeaux. Ref Type: Thesis/Dissertation

(153) Delmas, C.; Faure, C.; Borthomieu, Y. *Mater.Sci.Eng.* **1992**, *B13*, 89-96.

(154) Bauer, J.; Buss, D. H.; Harms, H. J.; Glemser, O. *J.Electrochem.Soc.* **1990**, *137*, 173-178.

(155) Guerlou-Demourgues, L.; Delmas, C. *J.Electrochem.Soc.* **1996**, *143*, 561-566.

(156) Kamath, V. P.; Dixit, M.; Indira, L.; Hukla, A. K.; Kumar, V. G.; Nichandraiah, N. *J Electrochem Soc* **1994**, *141*, 2956-2959.

(157) Liu, B.; Wang, X. Y.; Yuan, H. T.; Zhang, Y. S.; Song, D. Y.; Zhou, Z. X. *J.Appl.Electrochem.* **1999**, *29*, 860.

(158) Sugimoto, A.; Ishida, S.; Hanawa, K. *J.Electrochem.Soc.* **1999**, *146*, 1251-1255.

(159) *Instruction manual multivolume pycnometer*; Micromeritics: 1987.

(160) Martineau, D. and Wronski, Z. S. Performance Evaluation of Fine Powders in Pasted Nickel Electrodes Using CANMET's Multichannel Battery Cycler and Microstructural Characterization Facilities. 225-239. 1997. Proceedings of the International Symposium on Materials Solutions for Environmental Problems. 8-17-1997.

(161) Kruissink E.C.; Van Reijen L.L. *J.Chem.Soc.Faraday Trans.* **1981**, *77*, 649-663.

(162) Serna, C. J.; Rendon, J. L.; Iglesias, J. E. *Clays Clay Miner.* **1982**, *30(3)*, 180-184.

(163) d'Espinose de la Caillerie, J.-B.; Kermarec, M.; Clause, O. *J.Amer.Chem.Soc.* **1995**, *117*, 11471-11481.

(164) Kannan, S.; Narayanan, A.; Swamy, C. S. *J.Mater.Sci.* **1996**, *31*, 2353-2360.

(165) Balej, J.; Divisek, J. *Ber.Bunsenges.Phys.Chem.* **1993**, *97* , 929-932.

(166) Corrigan D.A.; Knight S.L. *J Electrochem Soc* **1989**, *136*, 613-619.

(167) Clearfield, A. *Chem.Mater.* **1998**, 2801-2810.

(168) Lao, H. and Detellier, C. Microporosimetry. 8. 1996. Compr. Supramol. Chem.

(169) Sing, K. S. W.; Everett, D. H.; Haul, R. A. W.; Moscou, L.; Pierotti, R. A.; Rouquerol, J.; Siemieniewska, T. *Pure & Appl.Chem.* **1985**, *57* , 603-619.

(170) Levine, I. N. *Physical Chemistry 3rd edition*; McGraw-hill: 1988.

(171) Horvath, G.; Kawazoe, K. *J.Chem.Eng.Comm.* **1983**, *16*, 470-473.

(172) Ferey, G. *Chem.Mater.* **2001**, *13*, 3084-3098.

(173) Szostak, R. *Handbook of Molecular Sieves*; van Nostrand Reinhold: New York, 1992.

(174) *Zeolites and Related Microporous Materials: State of the Art 1994*; Elsevier: Amsterdam, 1994.

(175) Iler, R. K. *The Chemistry of Silica*; John Wiley: New-York, 1979.

(176) Bansal, R. C.; Donnet, J. B.; Stoekli, H. F. *Active Carbon*; Dekker: New York, 1988.

(177) Wilson, S. T.; Lok, B. M.; Messina, C. A.; Cannon, T. R.; Flanigan, E. M. *J.Am.Chem.Soc.* **1982**, *104*, 1146.

(178) Estermann, M.; McCusker, L. B.; Baerlocher, C.; Merrouche, A.; Kessler, H. *Nature* **1991**, *352*, 320-323.

(179) Soghomonian, V.; Qin, C. H.; Haushalter, R.; Zubieta, J. *J.Angew.Chem., Int.Ed.Engl.* **1993**, *32*, 610.

(180) Harrison, W. T. A.; Broach, R. W.; Bedard, R. A.; Gier, T. E.; Bu, X.; Stucky, G. D. *Chem.Mater.* **1996**, *8*, 691.

(181) Clearfield, A. *Prog.Interc.Res.* **1994**, 223-271.

(182) Schoonheydt, R. A.; Pinnavaia, T.; Lagaly, G.; Gangas, N. *Pure Appl.Chem.* **1999**, *71*, 2367-2371.

(183) Barrer, R. M.; MacLeod, D. M. *Trans.Farad.Soc.* **1955**, 1290-1300.

(184) Brindley, G. W.; Semples, R. E. *Clay Min.* **1977**, *23*, 229-237.

(185) Vaughan, D. E. W. and Lussier, R. 94-101. 1980. London. Proc. 5th Int. Zeolite Conf. Rees, L. V.

(186) Rouquerol, J.; Avnir, D.; Fairbridge, C. W.; Everett, D. H.; Haynes, J. H.; Pernicone, N.; Ramsay, J. D. F.; Sing, K. S. W.; Unger, K. K. *Pure & Appl.Chem.* **1994**, *66*, 1739-1758.

(187) Alberti, G.; Costantino, U. *J.Inorg.Nucl.Chem.* **1978**, *40*, 1113-1117.

(188) Alberti, G.; Murciamascaros, S.; Vivani, R. *Mater.Chem.Phys.* **1993**, *35*, 187-192.

(189) Clearfield, A.; Stynes, J. A. *J.Inorg.Nucl.Chem.* **1964**, *26*, 117-129.

(190) Clayden, N. J. *J.Chem.Soc.,Dalton Trans.* **1987**, 1877-1881.

(191) Clearfield, A.; Blessing, R. H.; Stynes, J. A. *J.Inorg.Nucl.Chem.* **1968**, *30*, 2249.

(192) Alberti, G.; Vivani, R.; Marmottini, F.; Zappelli, P. *J.Porous Mater.* **1998**, *5*, 205-220.

(193) Poojary, D. M.; Hu, H. L.; Campbell III, F. L.; Clearfield, A. *Acta.Cryst.* **2000**, *b49*, 996-1001.

(194) Wang, D. J.; Clearfield, A.; Peng, G. Z. *Mater.Chem.Phys.* **1993**, *35*, 208-216.

(195) Hix, G. B.; Kitchin, S. J.; Harris, K. D. M. *J.Chem.Soc., Dalton Trans.* **1998**, 2315-2319.

(196) Lin, H. P.; Cheng, Y. R.; Lin, C. R.; Li, F. Y.; Chen, C. L.; Wong, S. T.; Cheng, S.; Liu, S. B.; Wan, B. Z.; Mou, C. Y.; Tang, C. Y.; Lin, C. Y. *J.Chin.Chem.Soc.(Taipei)* **1999**, *46*, 495-507.

(197) Cao, G.; Lee, H.; Lynch, V. M.; Mallouk, T. E. *Inorg.Chem* **1988**, *27*, 2781-2785.

(198) Cao, G.; Lynch, V. M.; Steven S.J.; Mallouk, T. E. *Inorg.Chem.* **1990**, *29*, 2112-2117.

(199) Clearfield, A. *Design of New Materials*; New York, 1987; pp 121-134.

(200) Cao, G.; Mallouk, T. E. *Inorg.Chem.* **1991**, *30*, 1434-1438.

(201) Zhang, Y. P.; Scott, K. J.; Clearfield, A. *Chem.Mater.* **1993**, *5*, 495-499.

(202) Le Bideau, J.; Payen, C.; Palvadeau, P.; Bujoli, B. *Inorg.Chem.* **1994**, *33*, 4885-4890.

(203) Poojary, D. M.; Zhang, Y.; Zhang, B.; Clearfield, A. *Chem.Mater.* **1995**, *7*, 822-827.

(204) Poojary, D. M.; Zhang, B.; Bellinghausen, P.; Clearfield, A. *Inorg.Chem* **1996**, *35*, 5254-5263.

(205) Zhang B.; Poojary, D. M.; Clearfield, A. *Inorg.Chem* **1998**, *37*, 1844-1852.

(206) Deemie, R. W.; Knight, M. R. D. A. *J.Organomet.Chem.* **1999**, *585*, 162-166.

(207) Oye, G.; Sjoblom, J.; Stocker, M. *Adv.Coll.Interf.Sci.* **2001**, *89-90*, 439-466.

(208) Bujoli, B.; Palvadeau, P.; Rouxel, J. *Chem.Mater.* **1990**, *2*, 582-589.

(209) Raki, L.; Detellier, C. *Chem.Commun.* **1996**, 2475-2476.

(210) Hix, G. B.; Carter, V. J.; Wragg, D. S.; Morris, R. E.; Wright, P. A. *J.Mater.Chem.* **1999**, *9*, 179-185.

(211) Hix, G. B.; Wragg, D. S.; Wright, P. A.; Morris, R. E. *Journal of the Chemical Society-Dalton Transactions* **1998**, 3359-3361.

(212) Gao, Q.; Chen, J.; Xu, R.; Yue, Y. *Chem.Mater.* **1997**, *9*, 457-462.

(213) Hix, G. B.; Wragg, D. S.; Bull, I.; Morris, R. E.; Wright, P. A. *Chem.Commun.* **1999** , 2421-2422.

(214) Wang, R. C.; Zhang, Y.; Hu, H.; Frausto, R. R.; Clearfield, A. *Chem.Mater.* **1992**, *4*, 864-871.

(215) Frink, K. J.; Wang, R.-C.; COLON, J. L.; Clearfield, A. *Inorg.Chem.* **1991**, *30*, 1438-1441.

(216) Dines, M. B.; Cooksey, R. E.; Griffith, P. C.; Lane, R. H. *Inorg.Chem.* **1983**, *22*, 1003-1004.

(217) Hix, G. B.; Harris, D. M. *J.Mater.Chem.* **1998**, *8*, 579-584.

(218) Poojary, D. M.; Zhang B.; Clearfield, A. *Anal.Quim.Int.Ed.* **1998**, *94*, 401-405.

(219) Carlino, S.; Hudson, M. J.; Husain, S. W.; Knowles, J. A. *Solid State Ionics* **1996**, *84*, 117-129.

(220) Yamanaka, S.; Hattori, M. *Inorg.Chem.* **1981**, *20*, 1929.

(221) Costantino, U.; Casciola, M.; Massinelli, L.; Nocchetti, M.; Vivani, R. *Solid State Ionics* **1997**, *97*, 203-212.

(222) Nijs, H.; Clearfield, A.; Vansant, E. F. *Microp.Mesop.Mater.* **1998**, *23*, 97-108.

(223) Bonnet, S.; Jones, W. *Spec.Publ.- R.Soc.Chem.* **1999**, *239*, 166-175.

(224) Prevot, V.; Forano, C.; Besse, J. P. *Appl.Clay Sci.* **2001**, *18*, 3-15.

(225) Hirao, T.; Masunaga, T.; Yamada, N.; Ohshiro, Y.; Agawa, T. *Bull.Chem.Soc.Jpn.* **1982**, *55*, 909-913.

(226) Badreddine, M.; Legrouri, A.; Barroug, A.; De Roy, A.; Besse, J. P. *Collect.Czech.Chem.Commun.* **1998**, *63*, 741-748.

(227) Rey, F.; Fornes, V.; Rojo, J. M. *J.Chem.Soc., Faraday Trans.* **1992**, *88*, 2233-2238.

(228) Hashi, K.; Kikkawa, S.; Koizumi, M. *Clays Clay Miner.* **1983**, *31(2)*, 152-154.

(229) Clearfield, A.; Don Wang, J.; Tian, Y.; Stein, E.; Bhardwaj, C. *J.Solid State Chem.* **1995**, *117*, 275-289.

(230) Fyfe, C. A. *Solid State NMR for Chemists*; Ampersand Printing, 123 Woolwoch St.: Guelph, 1983.

(231) Maeda, K.; Kiyozumi, Y.; Mizukami, F. *Angew.Chem.Int.Ed.* **1994**, *33*, 2335-2337.

(232) Wang, J.; Tian, Y.; Wang, R. C.; COLON, J. L.; Clearfield, A. *Mat.Res.Soc.Symp.Proc.* **1991**, *233*, 63-80.

(233) Depege, C.; El Metoui, F. Z.; Forano, C.; De Roy, A.; Dupuis, J.; Besse, J. P. *Chem.Mater.* **1996**, *8*, 952-960.

(234) Bish, D. L.; Brindley, G. W. *American Mineralogist* **1977**, *62*, 458-464.

(235) Kalinowski, H.-O.; Berger, S.; Braun, S. *Carbon-13 NMR Spectroscopy*; John Wiley & Sons: Chichester, 1988.

(236) Raban, Morton, Kost, Daniel, and Carlson, Eric H. Validity of approximate equations for kc in dynamic nuclear magnetic resonance. J.Chem.Soc.D. (13), 656-657. 1971.

(237) Alemany, L. B.; Grant, D. M.; Alger, T. D.; Pugmire, R. J. *J.Am.Chem.Soc.* **1983**, *105*, 6697-6704.

(238) Porter, M. R. *Handbook of Surfactants*; 1991; p 227.

(239) Tartar, H. V.; Wright, K. A. *J.Amer.Chem.Soc.* **1939**, *61*, 539-544.

(240) Wright, K. A.; Abbott, A. D.; Sivertz, V.; Tartar, H. V. *J.Amer.Chem.Soc.* **1939**, *61*, 549-554.

(241) Kresge, C. T.; Leonowicz, M. E.; Roth, W. J.; Vartuli, J. C.; Beck, J. S. *Nature* **1992**, *359*, 710-712.

(242) Selvam, P.; Bhatia, S. K.; Sonwane, C. G. *Ind.Eng.Chem.Res.* **2001**, *40*, 3237-3261.

(243) Schmidt, R.; Akporiaye, D.; Stocker, M.; Ellestad, O. H. *J.Chem.Soc., Chem.Commun.* **1994**, 1493-1494.

(244) Reddy, K. M.; Moudrakovski, I.; Sayari, A. *J.Chem.Soc., Chem.Commun.* **1994**, 1059-1060.

(245) Sayari, A.; Danumah, C.; Moudrakovski, I. L. *Chem.Mater.* **1995**, *7*, 813-815.

(246) Yuan, Z. Y.; Liu, S. Q.; Chen, T. H.; Wang, J. Z.; Li, H. X. *J.Chem.Soc., Chem.Commun.* **1995**, 973-974.

(247) Maschmeyer, T.; Rey, F.; Sankar, G.; Thomas, J. M. *Nature (London)* **1995**, *378*, 159-162.

(248) Ulagappan, N.; Rao, C. N. R. *Chem.Commun.(Cambridge)* **1996**, 1047-1048.

(249) Jun, S.; Ryoo, R. *J.Catal.* **2000**, *195*, 237-243.

(250) Mathieu, M.; van der Voort, P.; Weckhuysen, B. M.; Rao, R. R.; Catana, G.; Schoonheydt, R. A.; Vansant, E. F. *J.Phys.Chem.B* **2001**, *105*, 3393-3399.

(251) Beck, J. S.; Vartuli, J. C.; Roth, W. J.; Leonowicz, M. E.; Kresge, C. T.; Schmitt, K. D.; Chu, C. T.-W.; Olson, D. H.; Sheppard, E. W.; McCullen, S. B.; Higgins, J. B.; Schlenker, J. L. *J.Amer.Chem.Soc.* **1992**, *114*, 10834-10843.

(252) O'brien, S.; Francis, R. J.; Fogg, A.; O'Hare, D.; Okazaki, N.; Kuroda, K. *Chem.Mater.* **1999**, *11*, 1822-1832.

(253) Inagaki, S.; Koiwai, A.; Suzuki, N.; Fukushima, Y.; Kuroda, K. *Bull.Chem.Soc.Jpn.* **1996**, *69*, 1449-1457.

(254) Inagaki, S.; Fukushima, Y.; Kuroda, K. *Stud.Surf.Sci.Catal.* **1994**, *84*, 125-132.

(255) Chen, C. Y.; Xiao, S. Q.; Davis, M. E. *Micropor.Mater.* **1995**, *4*, 1.